1985

Origin and Sedimentary Characteristics of Discrete Sand Beds in Modern Sediments of the Central Texas Continental Shelf (Storm, Hurricane, Geostrophic, Waves, Turbidities).

John William Snedden
Louisiana State University and Agricultural & Mechanical College

INFORMATION TO USERS

This reproduction was made from a copy of a manuscript sent to us for publication and microfilming. While the most advanced technology has been used to photograph and reproduce this manuscript, the quality of the reproduction is heavily dependent upon the quality of the material submitted. Pages in any manuscript may have indistinct print. In all cases the best available copy has been filmed.

The following explanation of techniques is provided to help clarify notations which may appear on this reproduction.

1. Manuscripts may not always be complete. When it is not possible to obtain missing pages, a note appears to indicate this.

2. When copyrighted materials are removed from the manuscript, a note appears to indicate this.

3. Oversize materials (maps, drawings, and charts) are photographed by sectioning the original, beginning at the upper left hand corner and continuing from left to right in equal sections with small overlaps. Each oversize page is also filmed as one exposure and is available, for an additional charge, as a standard 35mm slide or in black and white paper format.*

4. Most photographs reproduce acceptably on positive microfilm or microfiche but lack clarity on xerographic copies made from the microfilm. For an additional charge, all photographs are available in black and white standard 35mm slide format.*

*For more information about black and white slides or enlarged paper reproductions, please contact the Dissertations Customer Services Department.

Snedden, John William

ORIGIN AND SEDIMENTARY CHARACTERISTICS OF DISCRETE SAND BEDS IN MODERN SEDIMENTS OF THE CENTRAL TEXAS CONTINENTAL SHELF

The Louisiana State University and Agricultural and Mechanical Col. PH.D. 1985

PLEASE NOTE:

In all cases this material has been filmed in the best possible way from the available copy. Problems encountered with this document have been identified here with a check mark ✓.

1. Glossy photographs or pages ✓
2. Colored illustrations, paper or print _____
3. Photographs with dark background ✓
4. Illustrations are poor copy _____
5. Pages with black marks, not original copy _____
6. Print shows through as there is text on both sides of page _____
7. Indistinct, broken or small print on several pages ✓
8. Print exceeds margin requirements _____
9. Tightly bound copy with print lost in spine _____
10. Computer printout pages with indistinct print _____
11. Page(s) _____ lacking when material received, and not available from school or author.
12. Page(s) _____ seem to be missing in numbering only as text follows.
13. Two pages numbered _____. Text follows.
14. Curling and wrinkled pages _____
15. Dissertation contains pages with print at a slant, filmed as received _____
16. Other _____

_____

_____

ORIGIN AND SEDIMENTARY CHARACTERISTICS OF DISCRETE SAND BEDS IN MODERN SEDIMENTS OF THE CENTRAL TEXAS CONTINENTAL SHELF

A Dissertation

Submitted to the Graduate Faculty of the
Louisiana State University and
Agricultural and Mechanical College
in partial fulfillment of the
requirements for the degree of
Doctor of Philosophy

in

The Department of Geology

by
John William Snedden
B.A., Trinity University, 1977
M.S., Texas A&M University, 1979
December 1985

ACKNOWLEDGEMENTS

I would like to sincerely thank the companies and agencies which provided financial support for this project: ARCO Oil and Gas Company; Cities Service Oil and Gas Company; Marathon Oil and Gas Company; Sohio Petroleum Company; Chevron Oil Field Research Company; Science Applications, Inc; The U. S. Minerals Management Survey; and the Gulf Coast Association of Geological Societies. The Louisiana State University (LSU) Alumni Federation was responsible for the fellowship which facilitated this research effort.

I would also like to acknowledge the assistance of numerous individuals and companies: Dr. Alan Hart, Continental Shelf Associates, Inc., Tequesta, Florida; Conoco, Inc., Houston, Texas; Dr. Charles Nittrouer, North Carolina State University, Raleigh, North Carolina; Dr. Curtis Olsen, Oakridge, Tennessee; Henry Berryhill, U. S. Geological Survey, Corpus Christi, Texas; Dr. Robert Morton, University of Texas Bureau of Economic Geology, Austin, Texas; Dr. James Mazzullo, Texas A&M University, College Station, Texas; Dr. Evans Waddell and Mr. Robert Wayland, Science Applications, Inc., Raleigh, North Carolina; Dr. William Wiseman and Mr. Scott Dinnel of LSU; Dr. David Gilhousen, National Oceanographic Data Center, NTSL, Mississippi; Mr. James Hubbard, National Ocean Service, Rockville, Maryland; Mr. Linwood Weiss, U.S. Army Corps of Engineers, Galveston, Texas; Dr. Robyn Wright, University of New Mexico, Albuquerque, New Mexico; Dr. David Kersey, Core Laboratories, Inc., Dallas, Texas; and Dr. Edward Roy, Trinity University, San Antonio, Texas.

I also owe a debt of gratitude to several individuals with the

University of Texas Marine Science Institute, Port Aransas, Texas: Mr. Anthony Amos, Ms. Lynne Amos, Mr. Rick Kalke, Captain Don Gibson and the crew of the R/V Longhorn, Noe Cantu, Hayden Abel, and Billy Slingerland.

All the members of my dissertation committee have contributed in their various ways to the completion of this dissertation: Dr. Charles Adams, Dr. Robert Desbrandes, Dr. Jeffrey Hanor, Dr. Clyde Moore, Dr. Thomas Moslow, Dr. Donald Swift, and especially my committee chairman, Dr. Dag Nummedal.

In addition, I would like to express my appreciation to other individuals presently or formerly associated with LSU for their efforts with regards to this project: Dr. Lyle McGinnis; Mr. Bruce Kofron; Mr. Robert Cuomo; Mr. Stephen Moshier; Mr. Ken Hayes, Mr. Danny Peace; Mr. Terry Angelich; Ms. Cathy Duncan; Ms. Mary Lee Eggart; Mr. Lewis Nichols; Dr. Indira Singh; Mr. Brian Carter; Mr. Lonn Hamp; and Ms. Anne Prior.

Finally, I would like to sincerely thank my wife Peggy, for without her support and encouragement this dissertation would not have been possible.

TABLE OF CONTENTS

TABLE OF CONTENTS (CON'T)

LIST OF TABLES

LIST OF FIGURES

LIST OF FIGURES (CON'T)

LIST OF FIGURES (CON'T)

LIST OF FIGURES (CON'T)

LIST OF FIGURES (CON'T)

ABSTRACT

Thin (1-9 cm) discrete beds of sand and silt are present in the clayey modern sediments of the Texas shelf. Observation of seaward size-grading within the beds indicates that the source of the clastics is the adjacent coastal zone. Consideration of the nature of wave and current processes during storms and the dimensions of possible coastal sub-environment sources suggests that the shoreface supplied the sand found in the discrete sand beds. The seaward fining and along-shelf continuity of a correlative horizon dated as having been deposited during the passage of Hurricane Carla in 1961 imply that transport was along-shelf but also obliquely offshore.

The upward fining grain-size trends and vertical sequence of sedimentary structures within the beds point to deposition during the waning phase of an impulsive event such as a turbidity current, a simple wind-forced current motion, or the near-bottom interaction of a geostrophically balanced steady current and oscillatory wave orbital motion. However, the along-shelf continuity of the Carla bed precludes the turbidity current hypothesis.

Analysis of records of fluid motion and boundary shear stress during storm events in the Texas shelf area leads to the conclusion that bottom currents responsible for sand transport are not just a simple result of wind-forcing. Storm flows represent a complex interaction between the wind stress (both orientation and magnitude), regional pressure gradients induced by wind set-up, and wave orbital motion. Forcing occurs in different dynamic zones, each with an individual response, all of which converge to produce net sand transport.

Absolute dating of selected cores reveals that in the mid-shelf (20-50 m water depths) area of the central Texas continental shelf, the sand bed deposited during Hurricane Carla in 1961 has survived over twenty years of physical and biological reworking. Here the Carla bed, and other discrete sand layers like it, stand an excellent chance of becoming a permanent part of the sedimentary record of the Texas shelf. For this reason, the discrete sand beds represent viable modern analogs to thin bedded sandstones present in ancient shelf sequences.

CHAPTER 1

INTRODUCTION

The continental shelf off Texas represents an offshore extension of the gently seaward dipping coastal plain. It is bounded on the west by a linear trend of barrier islands and on the east by a change in slope from 0.08^{o} to 1.0^{o} at 180 m, marking the shelf break (Curray, 1960; Fig. 1). Berryhill et al., (1976) divided the Texas shelf into three sectors: a northern sector comprising the wide shelf offshore from the Brazos, Colorado, and Trinity river deltas, a narrow central sector seaward from the coastal bend region, and a southern sector adjacent to the Rio Grande River delta. Analysis of high resolution seismic reflection data collected by the USGS indicates that during the late Wisconsinian sea level lowstand, deltaic environments prograded across the shelf to the shelf break in the northern and southern sectors (Suter and Berryhill, 1985). However, the narrow central sector stood as a clastic-free embayment as terrigenous sediments bypassed the area in fluvial systems flowing to the south.

This study is concerned with this central sector, which will henceforth be referred to as the central Texas continental shelf (CTCS). It has become a depocenter for Holocene (18,000 to 4,500 y B.P.) and Modern (<4,500 y B.P.) sedimentation (Fisher et al., 1973). Post-Pleistocene thicknesses range from 20 m in the center of the shelf to 5 m on the nearshore and outer shelf (Fig. 2). There is an obvious thinning over the buried shelf-margin deltas in the southern and northern sectors. In fact, analysis of the size fraction of surficial sediments in these sectors suggests that these relict deltas still

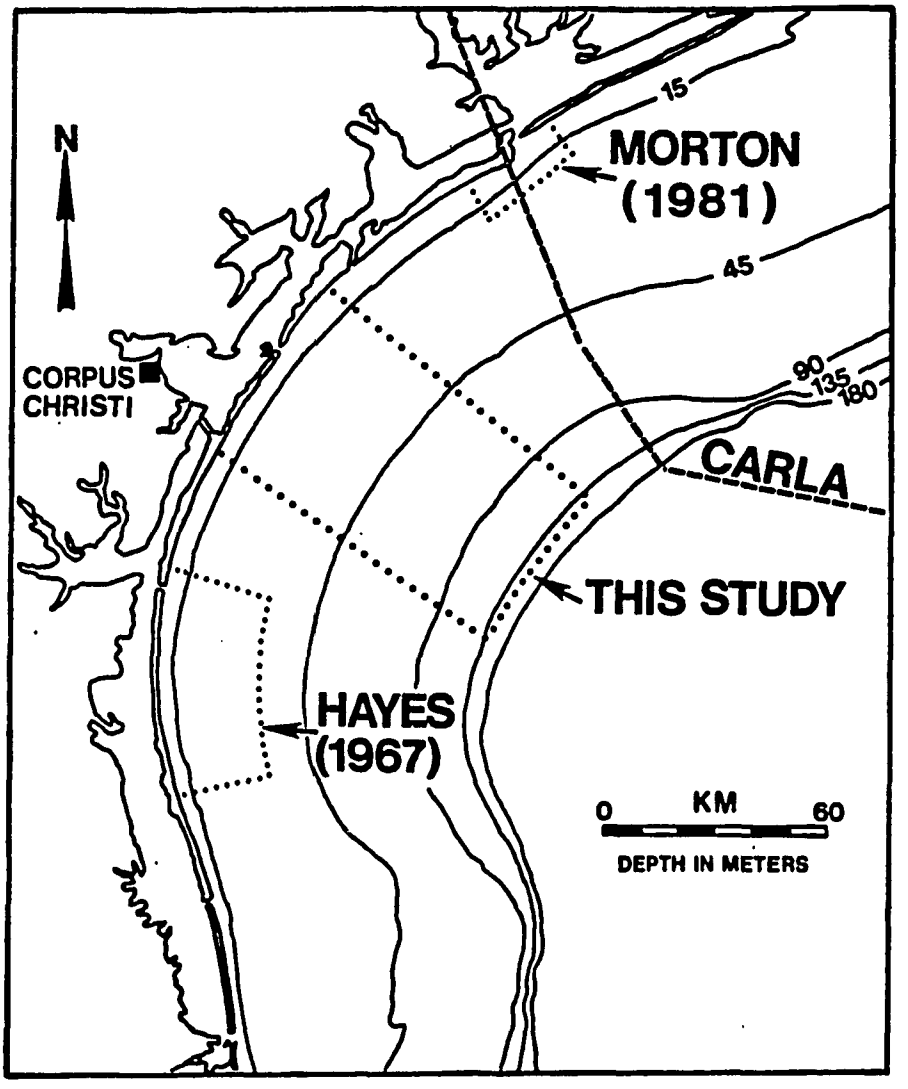

Fig. 1.--Location of study area and investigation sites of Hayes (1967) and Morton (1981). Dashed line is track taken by eye of Hurricane Carla in September of 1961.

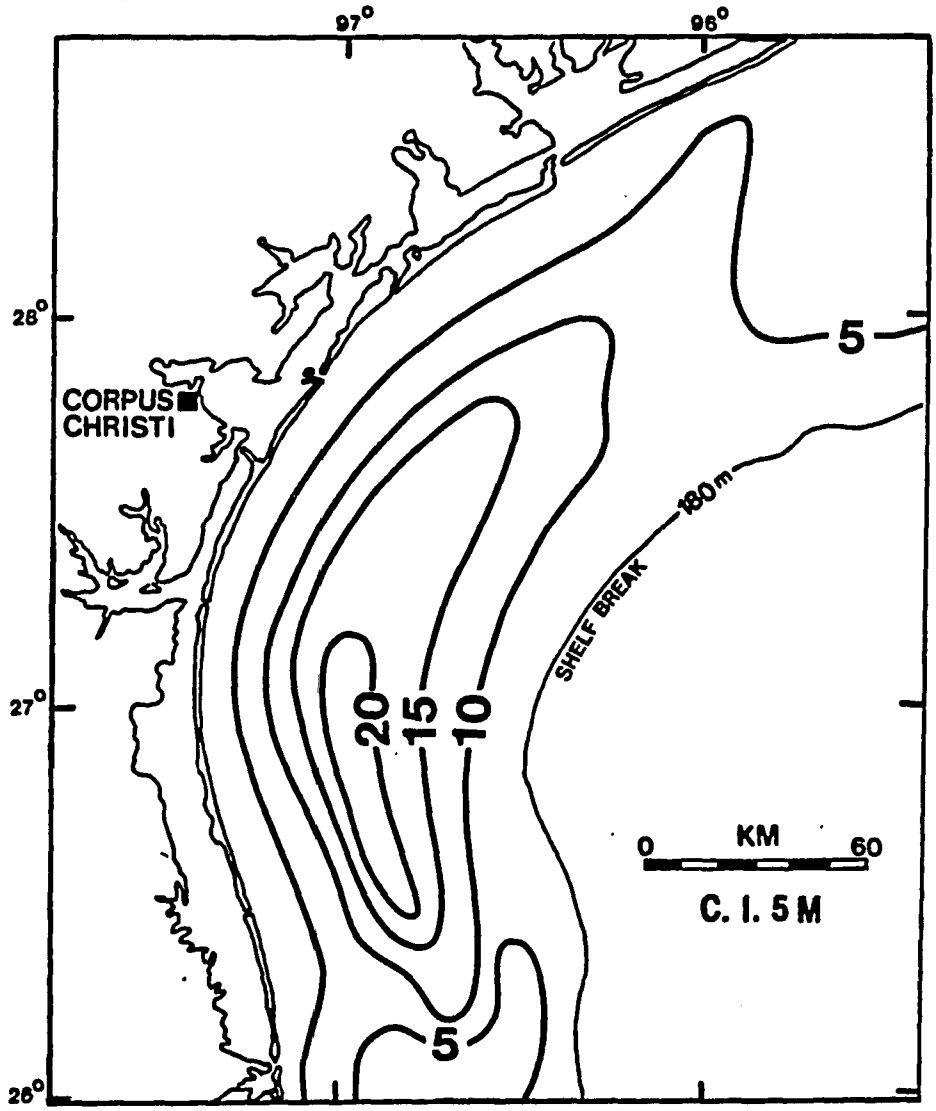

Fig. 2.--Isopach map of post-Pleistocene sediments. Contour interval equals 5 meters. Modified from Berryhill et al., (1976).

contribute sand to modern sediments. However, modern sediments of the CTCS area have received very little of this palimpsest material (Mazzullo and Withers, 1984; Shideler, 1978). The central Texas shelf surface shows an clear sediment size grading from sand nearshore to clay offshore (Hill, 1985). During fairweather periods, sand-sized surficial material is confined to water depths of less than 12 m (White et al., 1983). Thus, the CTCS can be considered to be a muddy shelf.

Cores of modern sediments of the CTCS area contain fine sand and silt in the form of discrete sand beds separated by thicker sections of clay (Fig. 3). These were first recognized in short gravity cores taken on the Texas shelf as part of API Project 51 (Curray, 1960). Described as "regular to irregular layers", the sand beds were most abundant in water depths of 15 to 30 m. None of the sand beds were located in the top 5 cm of sediment. Curray (1960) speculated that the beds were related to bottom currents associated with hurricanes or other storms.

Hayes (1967) took Phleger cores and grab samples in water depths of 18 to 36 m offshore from central Padre Island in the spring of 1962 (Fig. 1). He discovered thin (1-9 cm), graded sand deposits in the top of the cores which had not been present in coring surveys prior to the landfall of Hurricane Carla in September of 1961. Carla was an exceptionally large storm, its radius of hurricane-force winds (> 33 m/sec) stretching nearly 500 km from Brownsville to Port Arthur. In addition, Carla produced a large storm-tide, ranging from 1.0 m on the fringe of the storm to over 3 m just to the northeast of the landfall point of its eye (Nummedal, 1982).

In surveys following the storm, Hayes (1967) noted the occurrence of

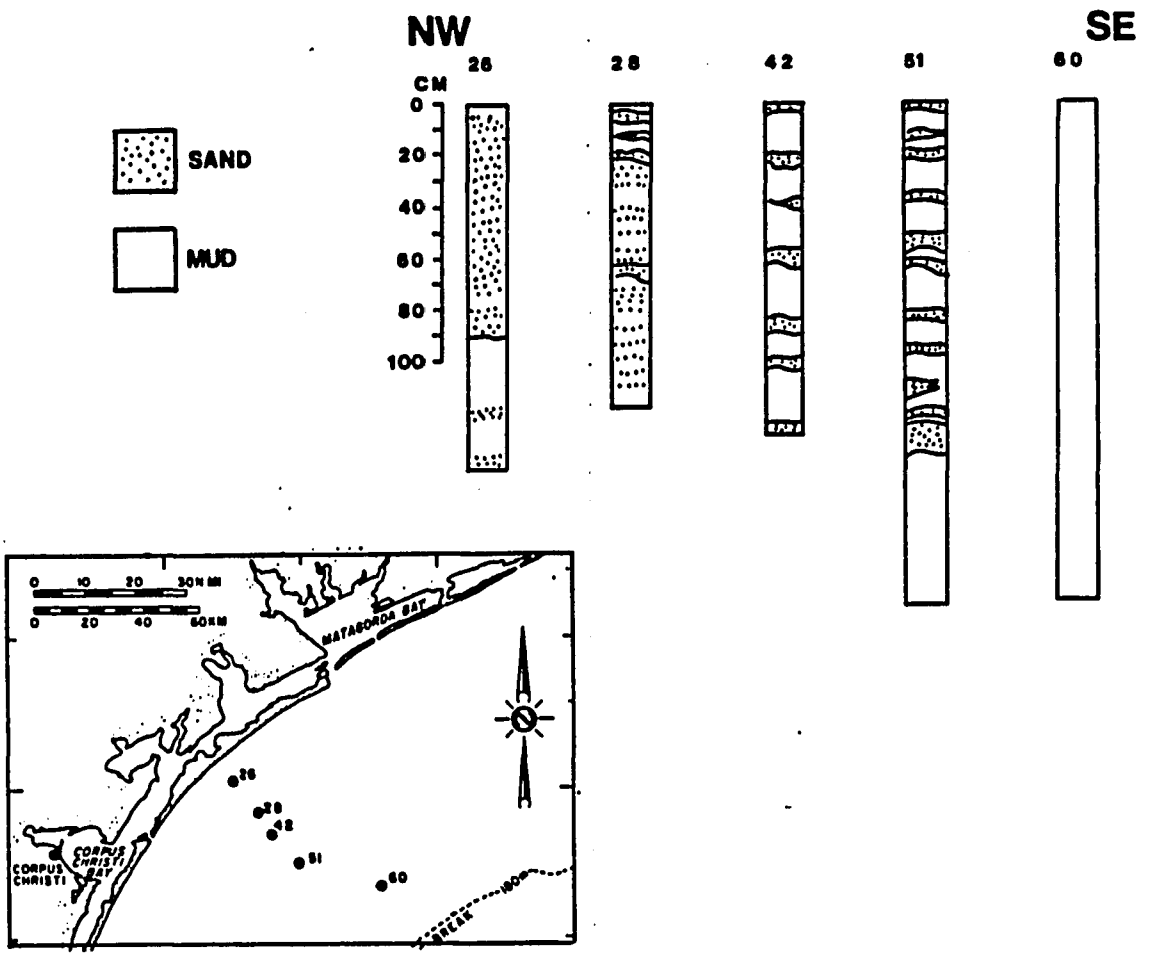

Fig. 3.--Gravity core transect across the northern portion of study area. Modified from Berryhill et al., (1976).

numerous shore-normal channels in the beach and foredune area (Fig. 4). He hypothesized that much of the storm-surge tide produced by Carla returned to the Gulf through these hurricane-cut channels. Further. he theorized that this "storm-surge ebb", once upon the shelf, became a turbidity current, transporting barrier island clastics into the Gulf. Hayes (1967) speculated that the turbidity currents were diverted to the north by shelf currents and by submarine topographic features.

Morton (1981) later challenged this "storm-surge ebb" mechanism of sand transport. First, he noted that the storm runoff from Laguna Madre was negligible, most of the excess water passing out Brazos-Santiago Pass to the south. Secondly, he observed that most of the washover deposits at Padre Island displayed flood-oriented features, suggesting a rather limited ebb transport through the storm-cut channels. And third, he pointed out that the thickest and most extensive deposits were located offshore from barrier segments with very few storm-cut channels. In fact, Morton (1981) demonstrated this point quite clearly by taking vibracores off Matagorda Island, a barrier island with few storm-cut channels (Fig. 1). There he found a large number of sand beds in four cores taken in water depths of 12 to 18 m, including some sand units at the top of the core which he related to Hurricane Carla. Citing published studies from other parts of the Gulf of Mexico (e.g. Forristall et al., 1977), Morton (1981) proposed that wind-forced currents, currents in a single layer driven solely by the wind, were responsible for erosion, transportation, and deposition of the clastics in the discrete beds.

The areal extent of these sand beds in the near-surface modern sedi-

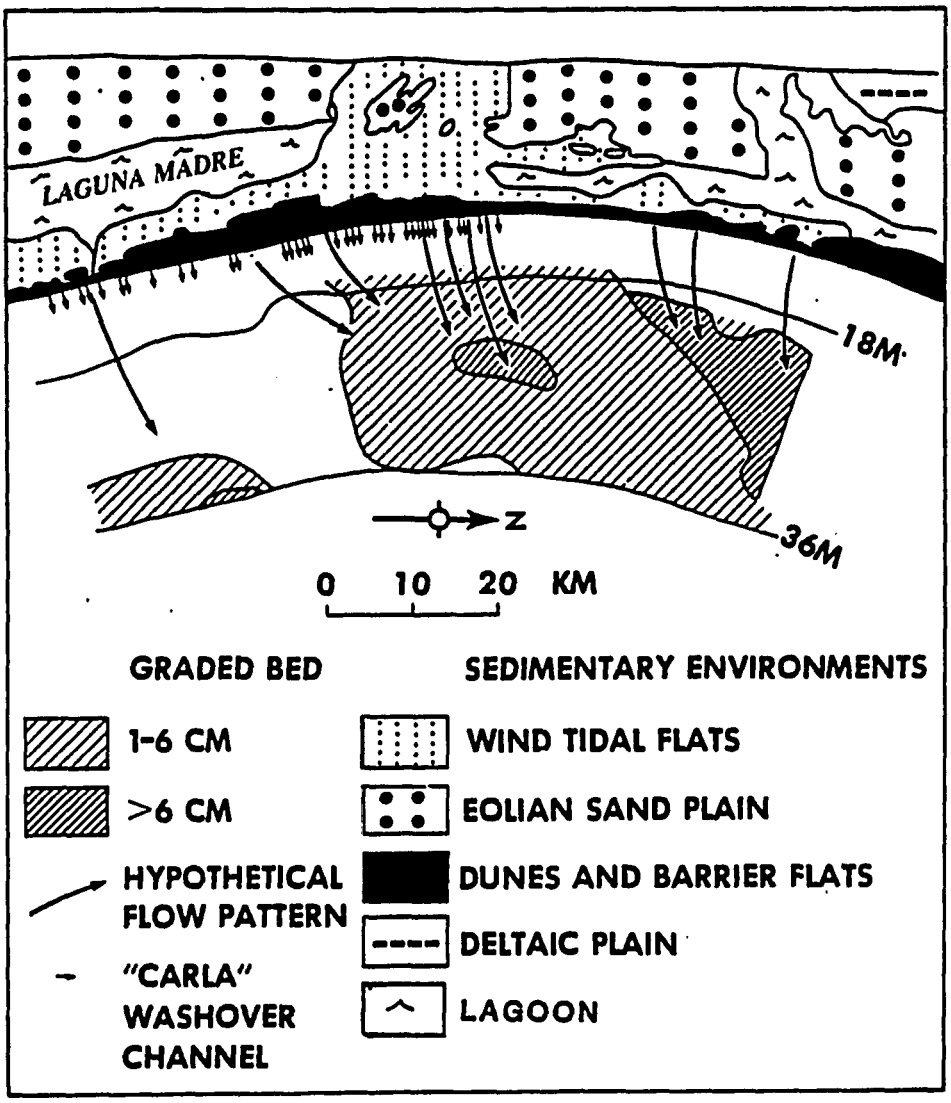

Fig. 4.--Hypothetical sand transport by storm-surge ebb following Hurricane Carla in 1961. Small arrows represent seaward terminus of hurricane-cut channels and large arrows the path of turbidity currents upon shelf. Modified from Hayes (1967).

ments of the Texas shelf was firmly established by the work of Berryhill et al., (1976; 1977). Discrete sand beds were present in 98 of 139 gravity cores recovered from the shelf, particularly in the CTCS area (Fig. 5). Incremental analysis suggested a tendency for the number of sand layers to increase toward shore and to the northeast. The sand beds in the cores often displayed ripples, cut-and-fill structures, and grading. On the basis of these observations, Berryhill et al., (1976;1977) speculated that hurricane-generated turbidity currents were responsible for the transport and deposition of the sand beds.

It is clear that there is no consensus as to the origin of the discrete sand beds present in near-surface modern sediments of the CTCS area. Several specific questions remain unanswered: 1) what is (are) the source(s) of the sand found in the discrete sand beds? 2) what is the transport pathway taken by these clastics? 3) what is the exact transport mechanism? In addressing these questions, previous studies have concentrated on characteristics of the sands themselves (Berryhill et al., 1976), shoreline processes (Hayes, 1967) or data from other parts of the Gulf of Mexico (Morton, 1981). No study conducted in the Texas shelf area has hitherto combined analysis of sedimentological data with actual measurements of the bottom current field from that same area. However, it is clear that any scientific inquiry directed toward these problems must include information on the processes operative upon the shelf as well as the products of those processes.

Another question relates to the preservation potential of the discrete sand beds found in modern sediments of the Texas shelf. This aspect is pertinent because of the geological importance of relating modern deposits to possible ancient analogs. A number of workers

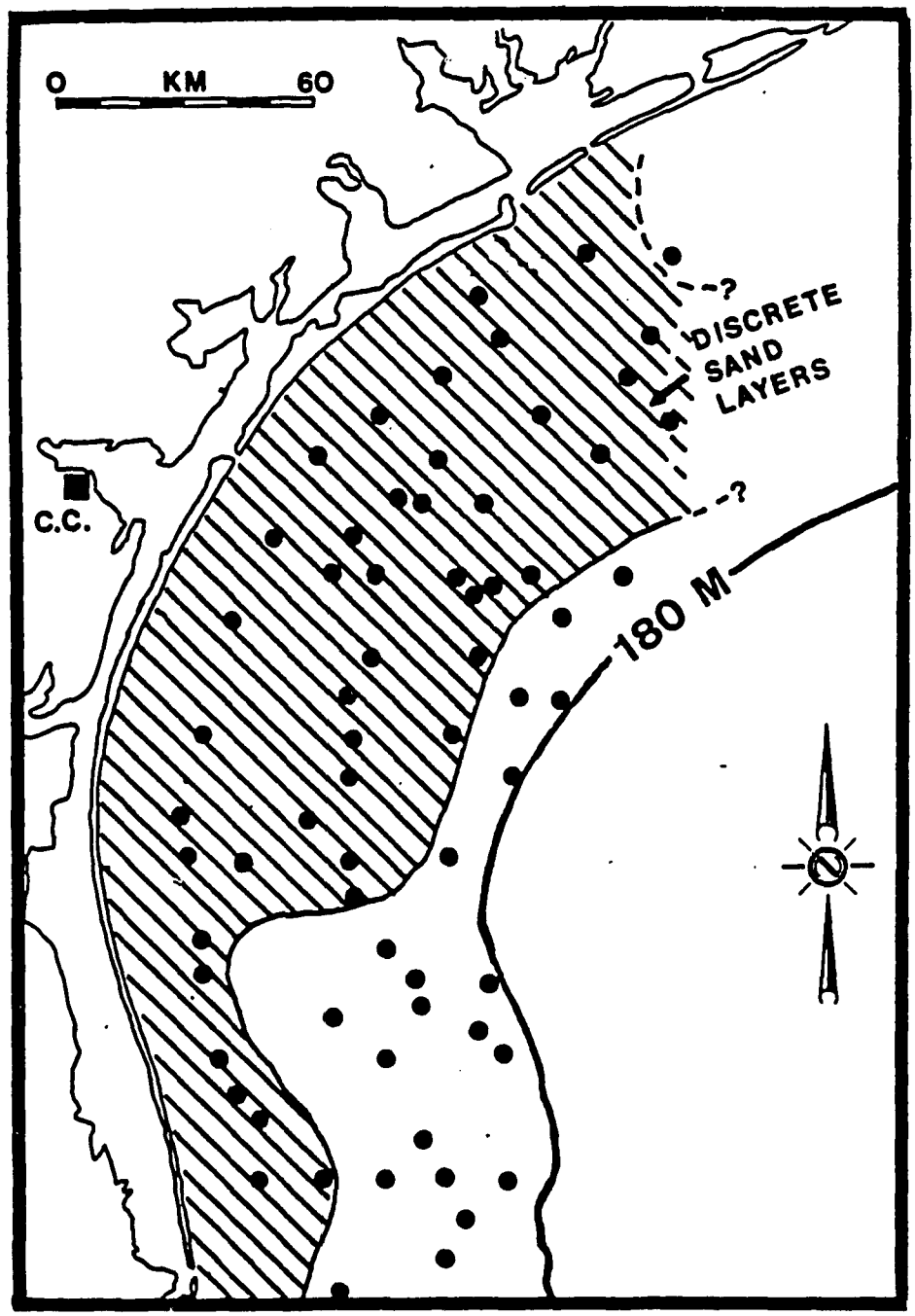

Fig. 5.--Distribution of discrete sand layers in modern sediments of the Texas shelf. Solid circles represent gravity core locations of Berryhill et al., (1976). C.C is Corpus Christi, Texas.

have reported thin, discrete sandstone beds of inferred marine origin similar to those described from cores of the Texas shelf (Berg and Powell, 1976; Brenchley et al., 1979; Snedden and Kersey, 1982; Eriksson and Soegaard, 1983; Montz et al., 1985). Recently, Dott (1983) suggested that the sand deposits associated with Hurricane Carla were completely obliterated by burrowing organisms. If so, the results of one of the most significant hurricanes of the century (Nummedal, 1982) will not become part of the sedimentary record of the Texas shelf. It has been argued that the geological record of ancient continental shelves is composed largely of "rare" events such as deposits associated with storms having a periodicity of 1,000 to 10,000 years (Walker, 1984). The geologic relevance of the answers to the first three questions to be addressed by this study is tied in some fashion to the response to the latter question.

Studies of sediment transport associated with storm events on other continental shelves have demonstrated the importance of analysis of the wave and current field near the sea bottom (Adams et al., 1982; Lavelle et al., 1978; Cacchione and Drake, 1982). Boundary shear stress generated by oscillatory wave motion is often superimposed upon the tangential stress associated with the steady unidirectional currents. The two interact in a non-linear fashion to produce a total shear stress which can be numerically greater than the simple sum of the the respective stresses (Grant and Madsen, 1979). This wave-current interaction during storm events has been termed "combined flow" (Harms, 1969; Swift et al., 1983). It is the contention of this study that such combined flow episodes are responsible for the erosion of coastal

sand sources, and the transport and deposition of siliclastic sediments in the CTCS area.

Studies on other shelves have also demonstrated that wind-induced hydrostatic pressure gradients contribute to flow during storm events (e.g. Beardsley and Butman, 1974). Flows with time scales on the order of a day or more must come into geostrophic balance with the rotation of the earth and the Coriolis force (Csanady, 1982). During storms, these "geostrophic currents" can be quite large, often with velocities in excess of 50 cm/sec or more (Swift and Niedoroda, 1984). Thus, any working hypothesis on the nature of sediment transport in the CTCS area should take this concept into consideration.

To test these hypotheses, a two-phased approach was used. First, core samples of surface and near-surface modern sediments were obtained from the CTCS area. Sampling was concentrated in a 50 X 90 km area offshore from Mustang Island, Texas (Fig. 6). This facilitated direct comparison and correlation of the cores. In addition, this sampling strategy allowed analysis of along-shelf and cross-shelf patterns in composition, texture and sedimentary structures of the discrete sand beds.

The second portion of this study involved the collection of Eulerian measurements of the near-bottom velocity field during selected periods in the CTCS area. This included deployment of current meters as well as the acquisition of previously-recorded, unpublished current meter data. The analysis of Eulerian measurements (measurements of fluid motions at fixed points in space) permitted an understanding of the kinematics and dynamics of shelf sediment transport during storms in the CTCS area.

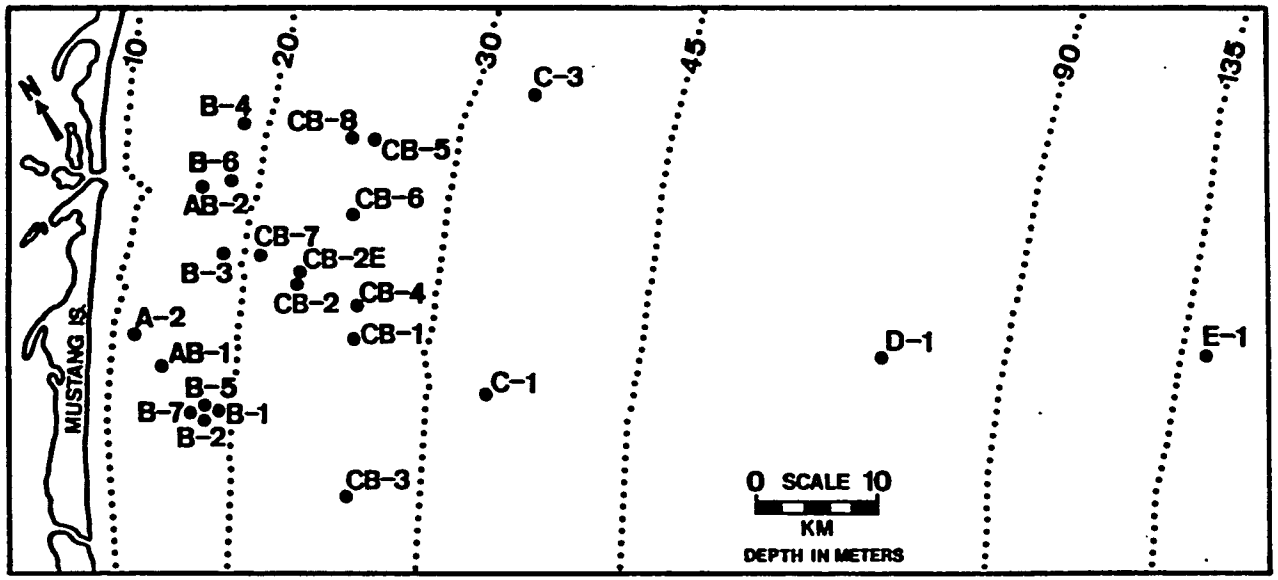

Fig. 6.--Location of boxcores taken in 1984. For study area location see Fig. 1.

In the last part of the study, comparison is made between the sedimentological data derived from the core samples and Eulerian data collected during periods of peak combined flow. This approach, the study of both product and process in the CTCS area, facilitated hypothesis-testing, particularly with regards to the questions of the transport mechanism and pathway, and preservation potential of the discrete sand beds. Conclusions about the origin of these discrete sand beds based on this combination of geology and oceanography certainly stand on firmer scientific ground than those based on one or the other alone.

CHAPTER 2

SEDIMENTARY CHARACTERISTICS OF THE DISCRETE SAND BEDS

Methods

All offshore operations performed as part of this study were conducted aboard the University of Texas R/V Longhorn, whose home port is Port Aransas, Texas. Relatively wide, undisturbed core samples of modern sediments in the study area were obtained using a conventional boxcoring device mounted on the Longhorn. Fig. 7 illustrates the relevant components of the device and the method used in coring. The box itself has dimensions of 20 X 30 X 60 cm. Once onboard, the boxcores were subsampled into plexiglass trays with a similar width but a thickness of 2 cm. The samples were then treated with acetone to prevent any further burrowing activity by organisms which were trapped by the coring operation. The plexiglass trays were then taped shut and stored upright in coolers. The samples were kept cool but were not frozen.

The samples were then taken to LSU where they were radiographed using a standard medical x-ray machine. X-ray radiography is a common technique used in the analysis of modern and ancient sediments (e.g. Coleman, 1966; Hamblin, 1962). After some experimentation, it was determined that a setting of 10 milliamps and 40 kilovolts and a duration of 2.2 minutes yielded the best quality radiographs. Radiography permitted identification of biogenic and physical sedimentary structures in the boxcore samples. In addition, delineation of discrete sedimentary units was made on the basis of the radiograph, once the x-ray response was calibrated against sand-silt-clay content determined by the sieve-and-pipette method described below (e.g. Fig. 8).

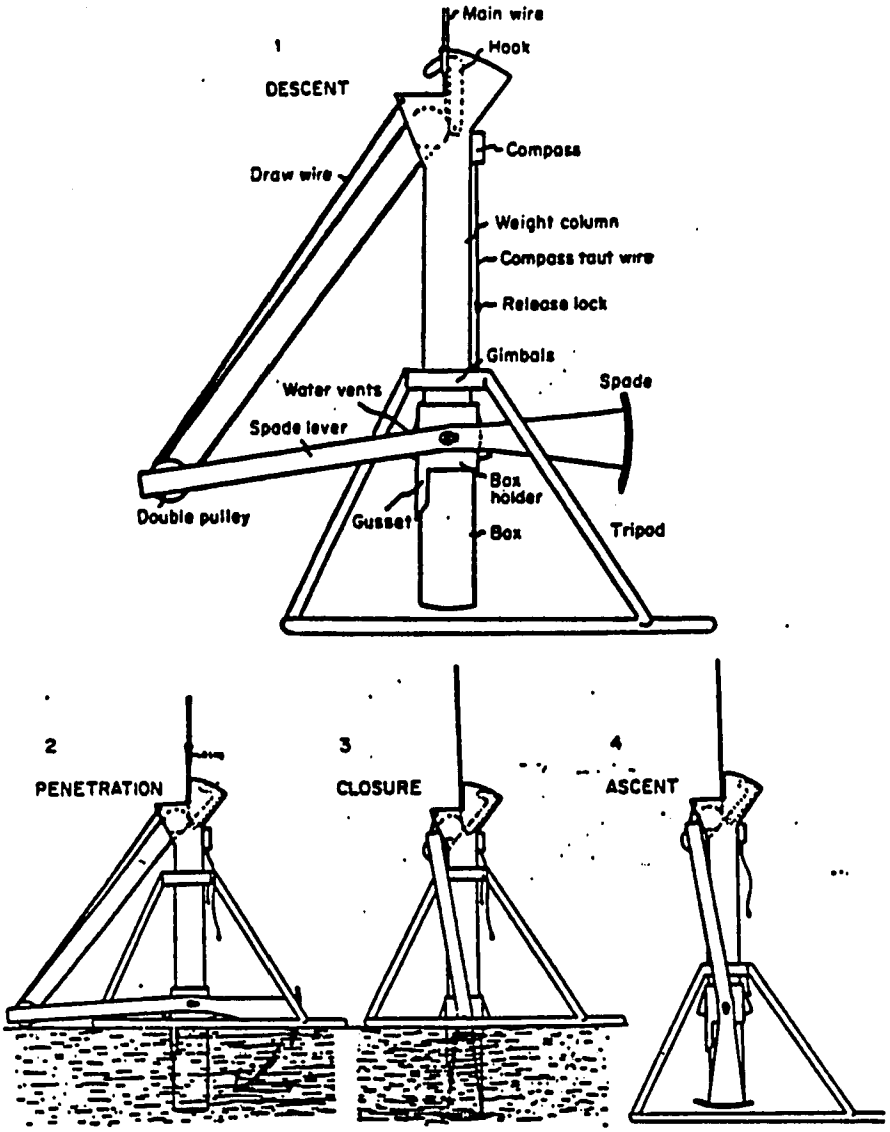

Fig. 7.--Diagram of boxcoring device and method of operation. From Shepard (1948).

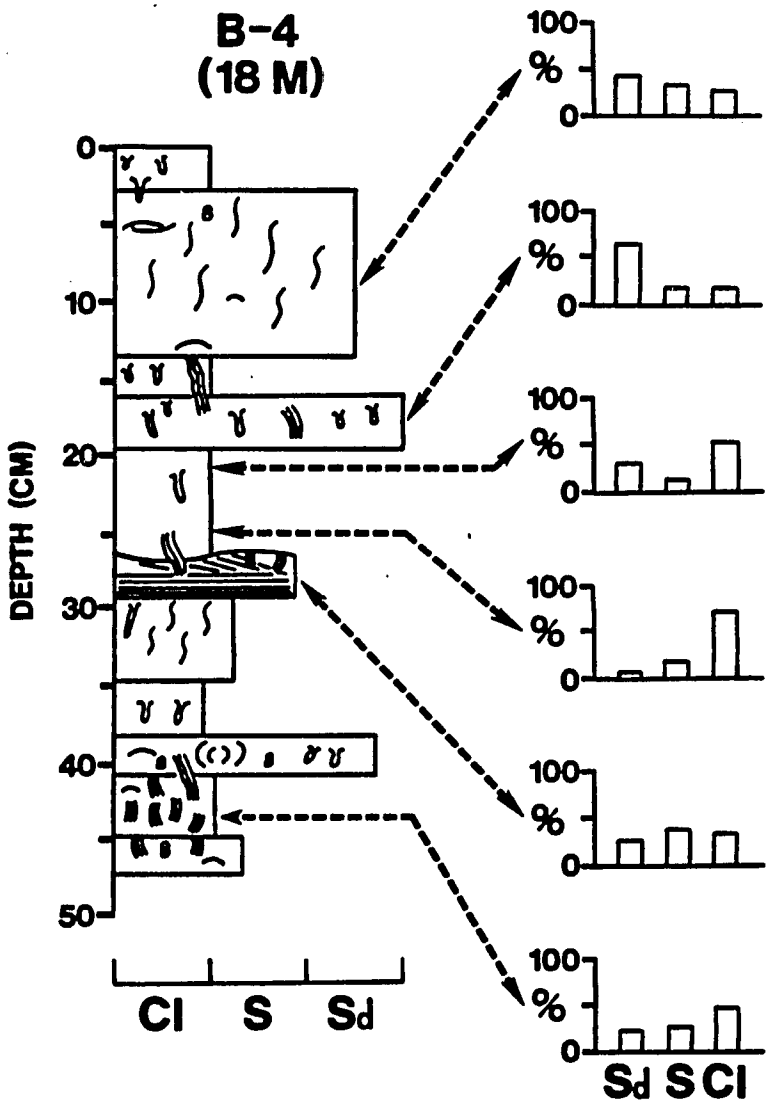

Fig. 8.--Columnar section of a typical boxcore from the CTCS area (Core B-4, water depth 18 m). Sand-silt-clay percentages of selected beds shown on right.

Textural analysis was performed using several different methods. The relative percentages of sand, silt, and clay were determined using the sieve-and-pipette technique described by Folk (1968). The size-frequency distribution of silt-sized material was delineated using a Model T Coulter Counter (see Sheldon and Parsons, 1967). Determination of the sand-size distribution proved to be somewhat difficult due to the fine size of the majority of the sand population and the angular nature of many of the grains. Sieve analysis did provide a general breakdown which was further defined by settling velocity analysis using an automated settling tube (see Anderson et al., 1982). Although through-out the text the discrete beds will be referred to as "sand" beds, it should be remembered that in some cases these units have a higher percentage of silt than sand.

The grain composition of selected samples was analyzed using grain mounts and standard petrographic techniques (Kerr, 1977). The thin sections were stained for potassium feldspar with sodium cobaltinitrate using the procedure described by Friedman (1971). Over 85 % of the detrital grains were quartz (Table 1). For this reason, 2.65 gm/cm^3 (the density of quartz) was used in the conversion of the fall velocity measurements from the automated settling tube to an equivalent grain size measurement from the automated settling tube.

Sedimentary Structures

Boxcores were collected during three cruises of the R/V Longhorn in 1984 (Table 2). After analysis of widely spaced cores taken during the September cruise, it was decided to concentrate coring effort on the next cruises in the area of 12 to 30 m. This was the area of the

TABLE 1.--Composition of selected sand samples

Boxcore	Depth in Core	Composition				
		Quartz	Feldspar	Rock Frags.	Carb. Frags.[1]	Other[2]
CB-7	9-16 cm	87%	3%	1%	8%	1%
CB-1	12-13 cm	85%	2%	--	13%	--
CB-8	12-13 cm	88%	1%	1%	10%	--
B-4	28-30 cm	89%	1%	2%	8%	--
Beach[3]	Mustang Is.	92%	2%	2%	5%	--

[1]Largely shell fragments and occasional whole forams.

[2]Mainly opaque grains.

[3]Sample taken six miles southeast of Horace Caldwell Pier, 25 m landward of the berm, 10 cm below surface on June 29, 1984.

TABLE 2.--Boxcore locations

Boxcore	Water Depth	Cruise[1]	Latitude	Longitude
E-1	140 m	J	27° 12.18' N	96° 23.61' W
D-1	74 m	J	27° 22.70' N	96° 34.80' W
C-1	34 m	J	27° 32.90' N	96° 51.70' W
C-3	34 m	D	27° 43.97' N	96° 42.78' W
CB-1	26 m	J	27° 37.00' N	96° 56.80' W
CB-3	26 m	N	27° 34.30' N	96° 59.50' W
CB-4	26 m	N	27° 39.50' N	96° 56.30' W
CB-5	25 m	D	27° 45.50' N	96° 50.10' W
CB-6	25 m	D	27° 42.30' N	96° 54.80' W
CB-8	24 m	D	27° 46.80' N	96° 50.10' W
CB-2	24 m	J	27° 40.00' N	96° 58.10' W
CB-7	21 m	D	27° 41.35' N	97° 00.00' W
B-1	18 m	J	27° 38.05' N	97° 04.08' W
B-2	18 m	J	27° 38.05' N	97° 04.08' W
B-3	18 m	J	27° 42.00' N	97° 01.20' W
B-4	18 m	J	27° 48.60' N	96° 56.00' W
B-5	18 m	N	27° 37.81' N	97° 04.12' W
B-6	18 m	N	27° 46.90' N	96° 57.50' W
B-7	18 m	D	27° 37.81' N	97° 04.12' W
AB-2	16 m	D	27° 47.80' N	96° 58.55' W
AB-1	15 m	D	27° 40.35' N	97° 05.65' W
A-2	12 m	N	27° 42.52' N	97° 06.20' W

[1] J= July 16-17, 1984; N=November 5, 1984; D=December 9, 1984.

greatest amount of variability in the sedimentary characteristics of the discrete sand beds (Fig. 6). Examination of the 23 boxcores taken in the CTCS indicated that the near-surface sedimentary section is composed of a variable number of discrete beds of sand, silt, and clay (Fig. 8). Within individual beds there are a variety of physical and biogenic sedimentary structures. Study of the physical structures in the discrete sand beds provided information which was relevant to the question of the transport mechanism. Analysis of the biogenic structures was useful in pursuit of the problem of preservability of these sand beds and their physical sedimentary structures. Appendix A contains the columnar sections constructed from the radiographs of the cored sediments. Fig. 9 is the legend of symbols used.

Physical Sedimentary Structures

Bedding contacts--Three types of bedding contacts are present in the cored sequences. These are described as flat, undulatory, and irregular (Fig. 9). These can either be sharp or gradual. Most of the thicker discrete sand beds possess flat and sharp basal contacts with underlying clays (Fig. 10). Upper contacts tend to be gradational due to a size grading into the overlying section or due to burrowing activity. However, sharp upper contacts also exist, particularly in the cores taken in 12 to 20 m water depths. Fig. 11 shows an example where a sand bed is truncated at the top by a clay unit in core B-4 (18 m). Many of the units in this cored sequence possess sharp upper and lower contacts reflective of the episodic nature of sediment accumulation. Fig. 12 displays core AB-2 (16 m) which is an extreme example of this phenomenon; Truncations are so numerous that it becomes difficult to separate-out individual stratification units (see also Fig.

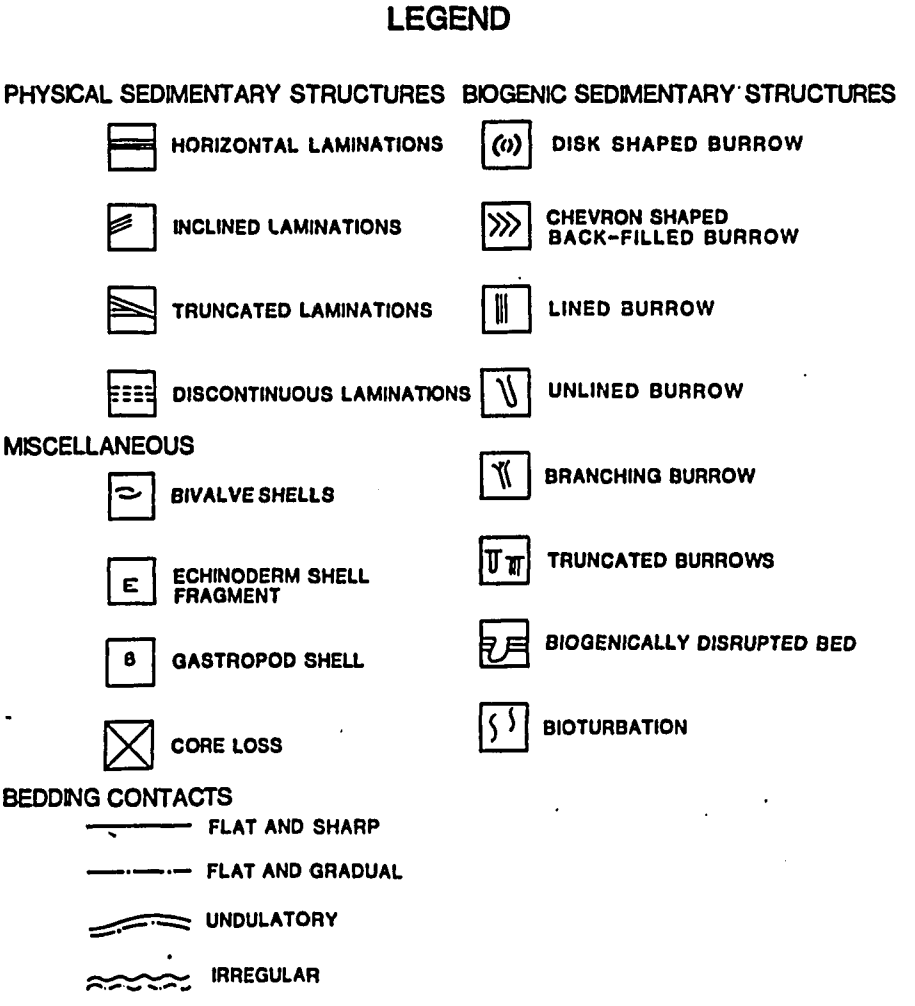

Fig. 9.--Legend of symbols. Symbols partly from Busby-Spera (1985).

Fig. 10.--Radiograph (negative) of boxcore CB-1 (26 m water depth). Note sharp lower contact and gradational upper contact of discrete sand bed at 7-15 cm core depth. See Fig. 6 and Table 2 for exact location.

(next page)

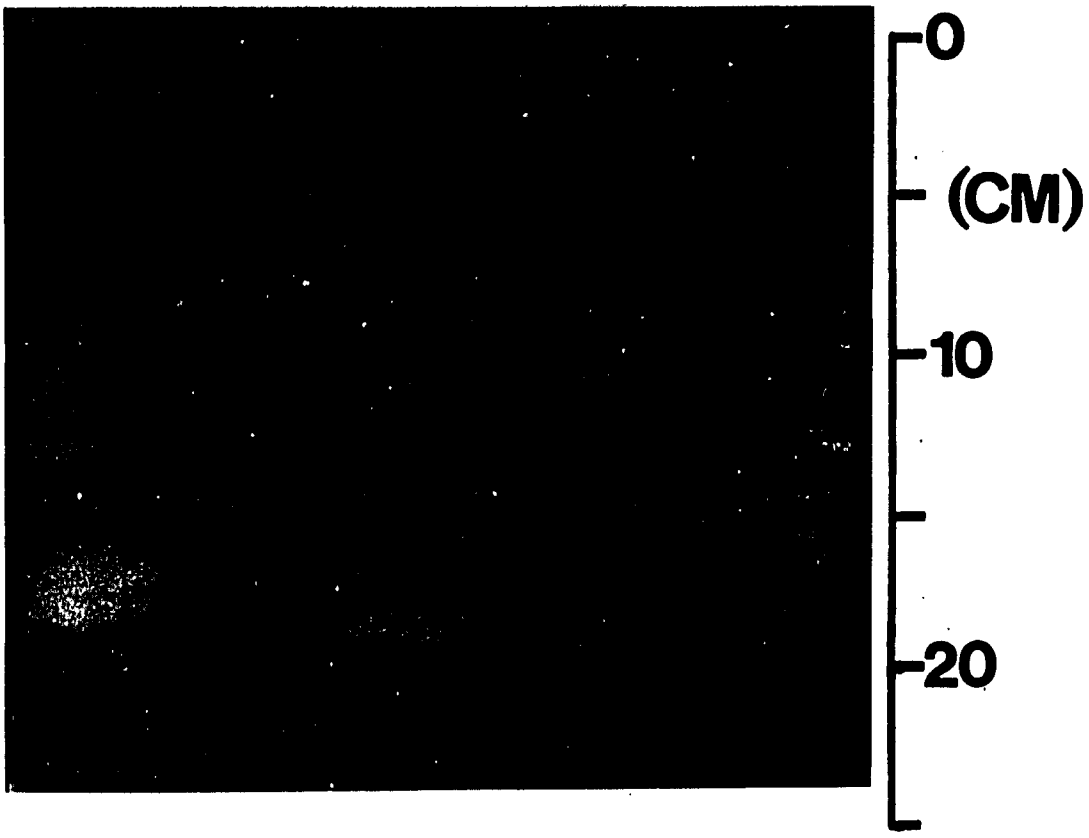
0
(CM)
10
20

Fig. 11.--Radiograph of boxcore B-4 (18 m). Arrow shows location of lined trace referred to in text.

(next page)

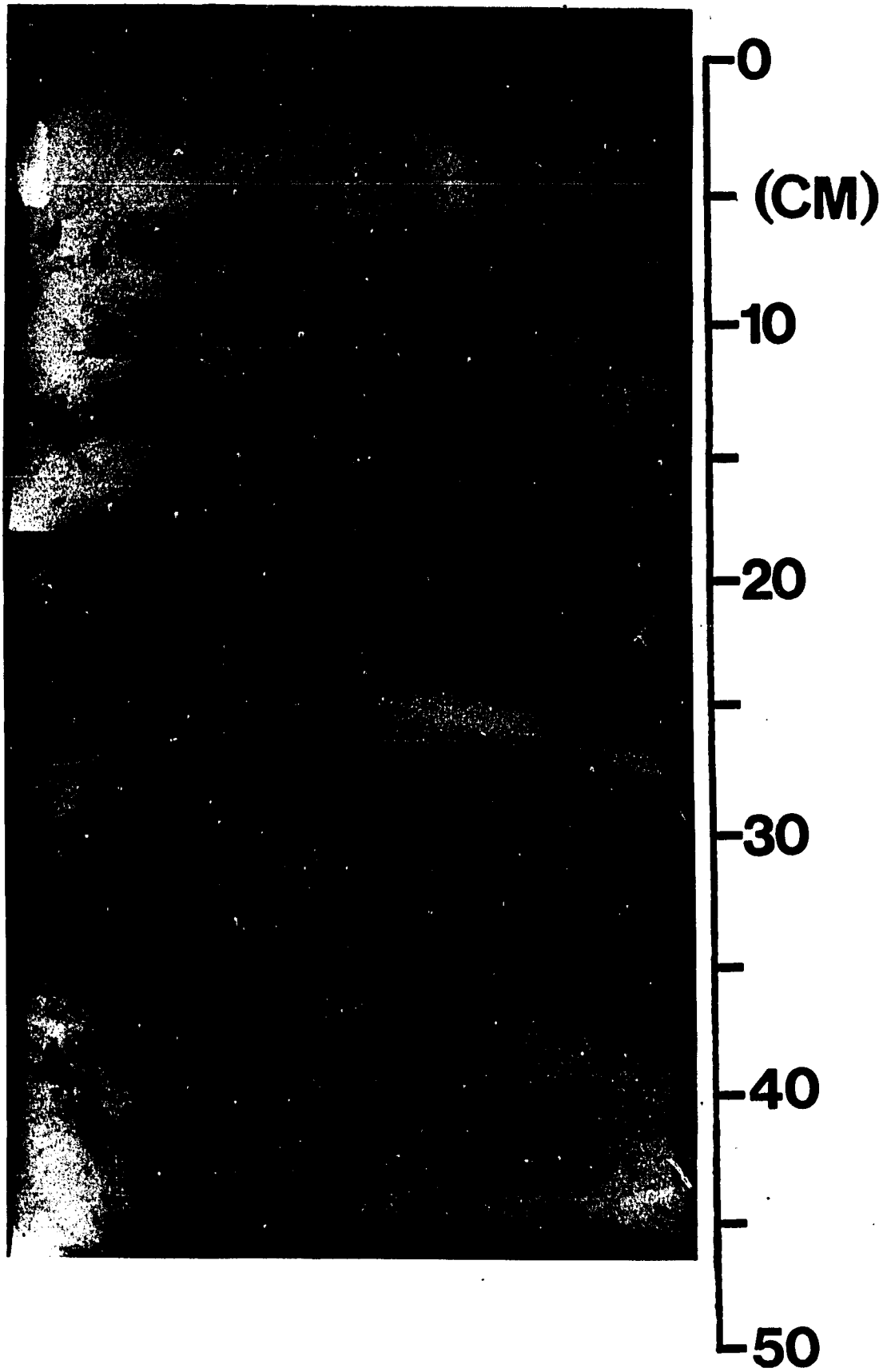
0
(CM)
10
20
30
40
50

Fig. 12.--Radiograph of boxcore AB-2 (16 m).

(next page)

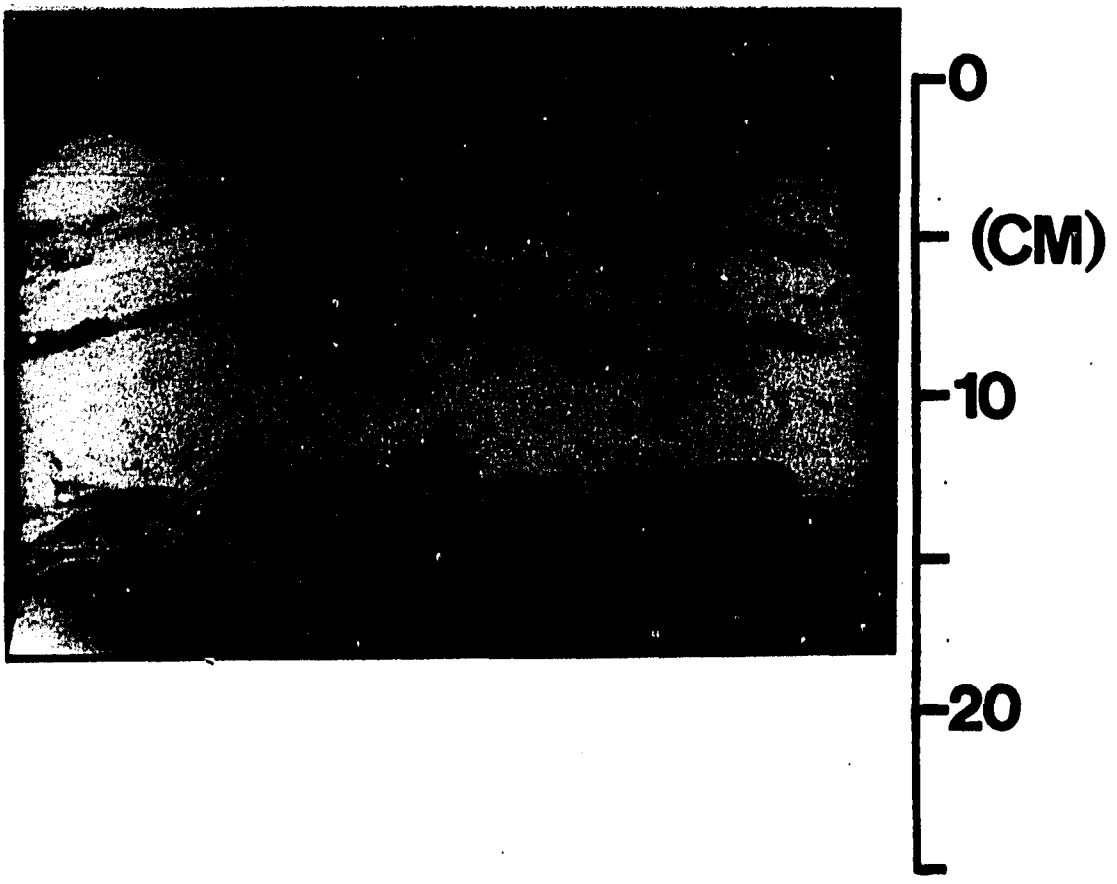
0
(CM)
10
20

17). In effect, the sequence has become amalgamated. Bioturbation also serves to blur unit contacts.

Horizontal Laminations--These are the most common form of lamination present in the sand beds (Figs. 13 & 14). These are typically parellel, even, continuous to discontinuous. In a few cases, the discrete sand beds appear massive (unlaminated) (Fig. 10). The horizontal laminations could have originated in a number of different ways. They are visible on the x-ray radiograph due to differential absorption of the radiation (Hamblin, 1962). In these uncemented, mono-mineralic sediments, this differential absorption is probably due to subtle differences in the texture, or more likely, in the relative amounts of sand, silt and clay. The presence of distinct laminations in a graded sequence such as these is not straight-forward. For example, how does one explain the deposition of clay during a period of waning flow when the boundary shear stress is such that only silt is settling out of suspension ?

A number of mechanisms have been proposed to explain the occurrence of horizontal laminations in a graded sequence, including variations in external forcing (Reineck and Singh, 1975), saltation sorting (Kuenen, 1966), boundary layer bursting (Bridge, 1978; Allen, 1984), and depositional sorting in a boundary layer (Stow and Bowen, 1980). Plane bed laminations are found to be associated with virtually any type of shear flow, be it a sediment gravity flow such as a turbidity current or a fluid gravity flow such as a decelerating bottom current (Reineck and Singh, 1972; Sanders, 1977).

"Plane-bed" bed phases are also common configurations found in laboratory flume experiments with unidirectional flow (Simons, Richard-

Fig. 13.—Radiograph of boxcore CB-3 (26 m). Slight tilt of laminations is due to subsampling. Arrow shows single-walled trace referred to in text. Note disk shaped traces in sand bed at 35 cm.

(next page)

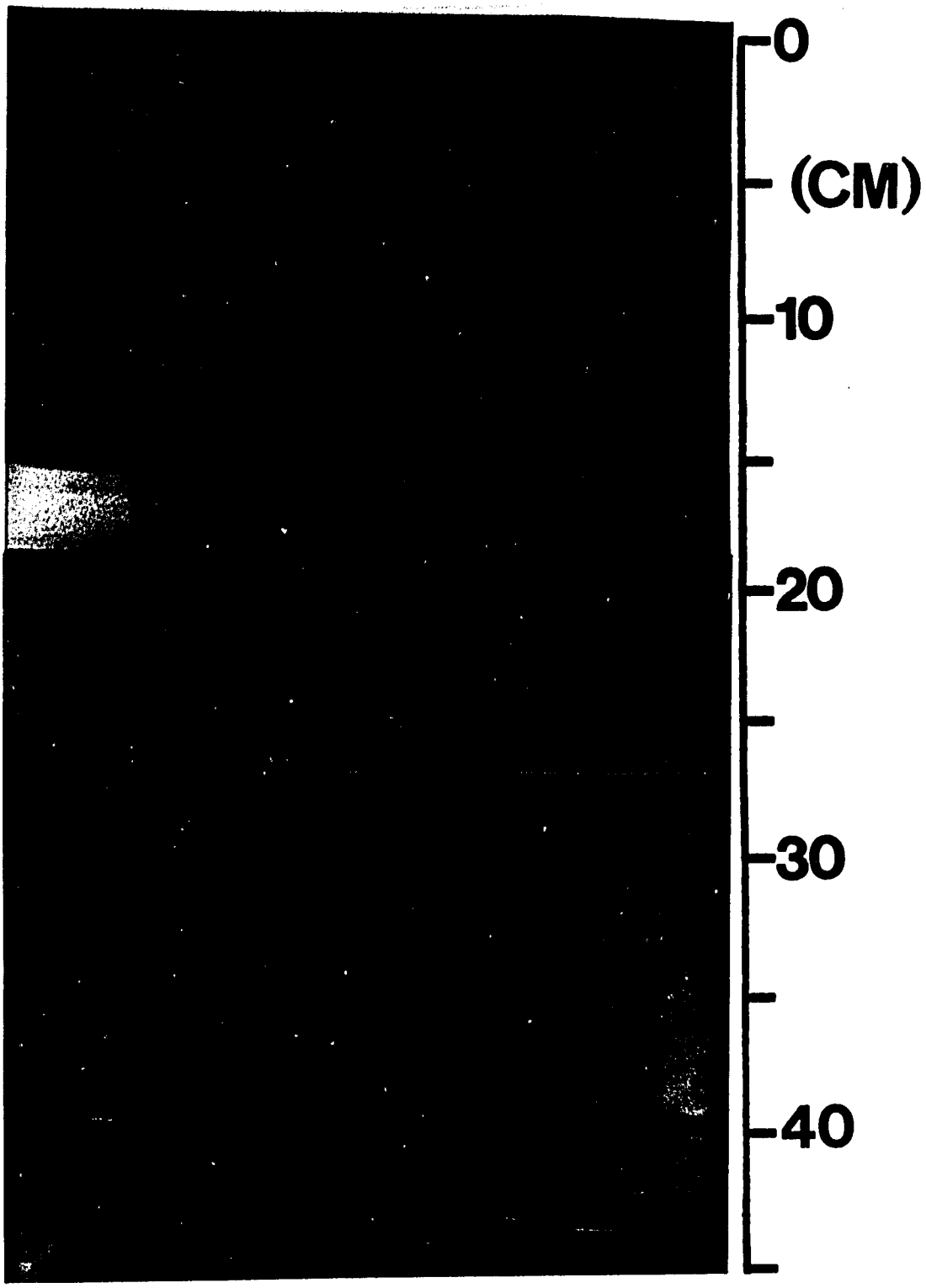
0
(CM)
10
20
30
40

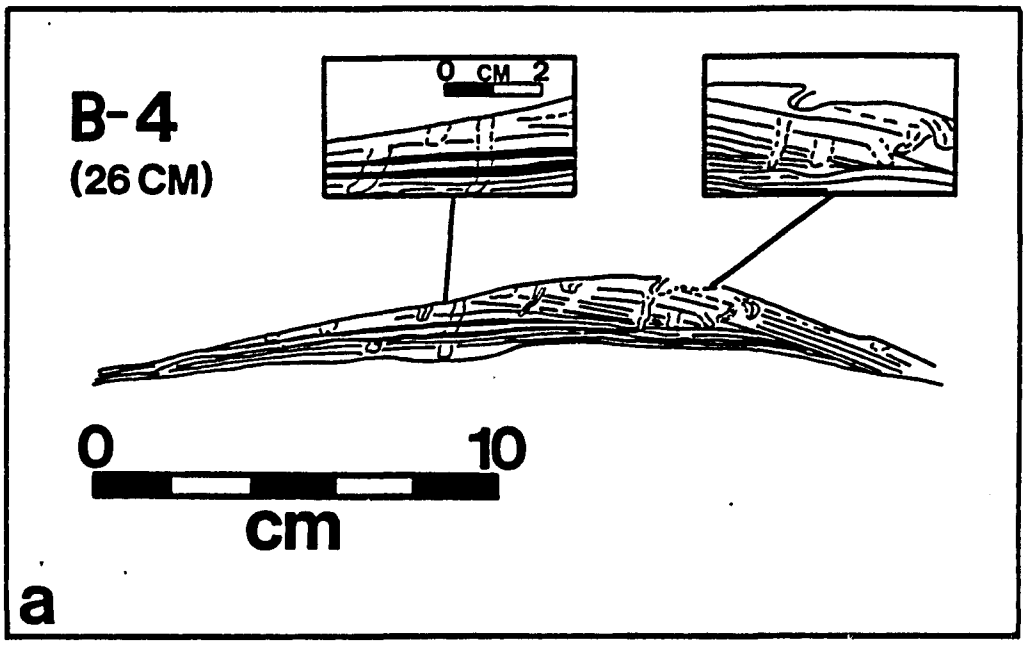

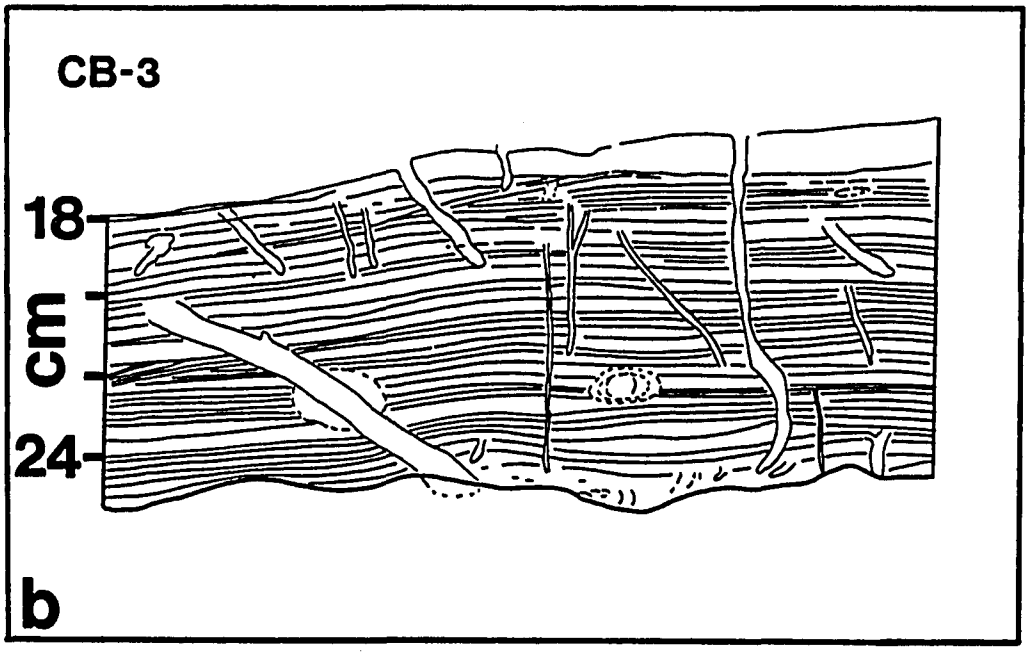

Fig. 14.--a) Tracing of an x-ray radiograph of a discrete sand bed at 26 cm core depth in boxcore B-4 (18 m water depth). Insets show pinch-and-swell structure, left, and inclined laminations showing tangential contacts with bottom-set laminations, right. b) Tracing of discrete sand at 18-25 cm depth in boxcore CB-3 (26 m water depth).

son, and Nordin, 1977). They occur at the beginning of lower and upper flow regime stages, as defined by the Froude number. The Froude number (F) is a dimensionless ratio of the inertial forces (such as flow velocity) and gravity forces:

$$F = U/(gL)^{1/2}$$

where U is the stream or flow velocity, g the gravitational acceleration, and L is the length scale of the flow. The Froude number describes the phase relationship between bedforms and fluid interfaces (such as the sea surface). At a Froude number of significantly less than 1.0, the fluid interface is out of phase with bedforms and flow is said to be subcritical. At a Froude number of close to and greater than 1.0, bedforms and the fluid interface are in phase and flow is supercritical (Friedman and Sanders, 1978).

Unfortunately, no flume experiments have yet been run under combined wave and current flow conditions. It is possible that the upper flow regime plane bed phase, recognized in the unidirectional current flume studies, may occur during lower flow regime conditions in the combined flow setting of a continental shelf. Some experiments suggest that with fine grain sizes the plane bed field does indeed expand into the lower flow regime, down to Froude numbers of 0.5 (Engelund, 1970). Such physical conditions are possible on the continental shelf with flow velocities of 100 cm/sec or greater and scaling lengths for wave boundary layers on the order of 5-50 cm.

For fine grain sizes, flume experiments indicate that this plane bed phase occurs at the highest flow rates under both unidirectional and oscillatory current conditions (Harms, Southard, and Walker, 1982).

Thus the supposition could be made that the horizontal laminations recognized at the base of the discrete sand beds also formed during such periods of relatively high velocity. However, the interpretation of flow velocities from sedimentary structures such as this is hampered by the lack of experimental evidence upon the relationship of sedimentary bedforms to flow intensity under conditions of combined flow, high sediment concentrations, and large water depths (Komar, 1985).

Inclined Laminations--When present, these occur near the top of the discrete sand beds. Inclinations of are of a low angle and appear to have tangential contacts with bottomset bedding (Fig. 14a). In controlled flume experiments, Jopling (1965) found that these types of contacts were associated with relatively high stream flow velocities, fine sediment sizes, and a predominance of suspension transport. As will be shown in later sections, the fine-size of quartz grains in the discrete sand beds (modal size 68 microns) suggests that suspended load transport is most typical of the fully developed flow (McCave, 1971).

The incipient development of bedforms on the sea floor is suggested by the bed depicted by Fig. 14a. Although the bed shows evidence of erosion at its upper contact and is probably form-discordant, bottomset and foreset (stoss side) laminations are apparent. It is possible that the sequence is related to the migration of a flow-transverse bedform such as a ripple. Development of ripple-like bedforms from initial perturbations during flows possessing a low (<1.0) Froude number has been demonstrated both numerically (Smith, 1970) and experimentally (Mantz, 1978). Early bedform growth appears to be related to a phase lag between topography and the boundary shear stress (Swift and

Rice, 1984). However, very high levels of shear-generated turbulence tend to inhibit further development, suggesting that a large portion of bedform growth takes place during current deceleration (Yalin, 1977). Thus, it is possible that the inclined laminations present in the tops of many of the discrete sand beds represent the migration of ripple bedforms during the waning phase of a impulsive flow event (such as a decelerating bottom current or a turbidity current).

Other Structures--Three of the primary sedimentary structures recognized in the boxcores from the CTCS area may be related to hummocky cross-stratification (HCS). Originally recognized in ancient shelf to shoreface sediments (Campbell, 1966; Harms, 1975), HCS is believed to be similar in form and origin to hummocky mega-ripples found on the inner Atlantic shelf (Swift et al., 1983). HCS appears to be a ubiquitous structure in marine environments, having now been identified in the shoreface, inner and outer shelf and deep sea sedimentary environments. However, most agree that it is intimately associated with storm processes (Dott and Bourgeois, 1982).

The inclined laminations mentioned in the preceding section are probably related to the growth of bedforms on the sea floor during the waning stages of a flow event. Indeed, it is possible that these inclined laminations are part of a larger scale bedform such as a hummock. Unfortunately, the boxcore width is at least an order of magnitude smaller than the wavelength of the hummocks recognized in both the modern and ancient. However, some criteria has been formulated for the identification of HCS in narrow cores. One is the presence of inclined laminations which thicken downwards (Dag Nummedal, pers. comm., 1985). This feature was not observed in the radiographs

of the boxcores taken in the CTCS area.

Another structure associated with HCS is the truncation of laminations by overlying laminae within a sequence. This is known as a second-order bounding surface in contrast to the first-order bounding surfaces at the top and base of a HCS sequence (Boyles, 1982). Microtruncations, such as the feature at 21.8 cm depth in Fig. 14b, are present within the thicker discrete beds. They sometimes pass laterally into third-order bounding surfaces (laminations), also a characteristic of HCS.

The third phenomenon which may be related to HCS is the presence of isolated undulations and irregularities in the lamination sets similar to what Kreisa (1981) termed "gentle pinch-and-swell" (Fig. 14a). These features are an order of magnitude smaller than the thickening and thinning commonly observed in hummocky strata in outcrops or in boxcores from the Atlantic shelf (e.g. Swift et al., 1983). Kreisa (1983) interpreted these pinch-and-swell structures to be wave-generated features which are transitional to symmetrical wave-ripple lamination. However, this conclusion was based solely on study of ancient sedimentary sequences in the Martinsberg Formation (Ordovician) of southwestern Virginia. In the Texas shelf boxcores, there are few distinct wave-formed features. It is possible that the pinch-and-swell structures are in some way related to HCS, possibly having been formed by the same set of processes. Although the origin is still controversial, HCS is thought to form in the intensified wave-current fields on continental shelves during storms (Swift et al., 1983).

Discussion--Other than those which might be ascribed to HCS, none of the sedimentary structures present in the discrete sand beds are unique

to the transport mechanisms being considered in this study. Plane-bed laminations and ripples are characteristic of deposition from both turbidity flows (Bouma, 1962) and unidirectional currents (Reineck and Singh, 1972). Massive, graded beds can also be formed by both processes (Sanders, 1977; Reineck and Singh, 1975). The absence of obvious symmetrical wave ripples suggests that either wave orbital motion was negligible or it acted in combination with unidirectional currents. Bed configurations formed under combined flow conditions are similar to those found in the case of steady unidirectional flow (Harms, Southard, and Walker, 1982).

Although there are some exceptions, the typical bedding sequence in the thicker discrete sand beds consists of, in ascending order, a sharp basal contact, horizontal laminations (or often a massive, unlaminated division), inclined laminations (often subtle) and a gradational (often bioturbated) upper surface (e.g. Fig. 14b). The thicker beds appear most often in 20-30 m of water. In shallower water (12-20 m), the beds are thinner and often structureless (e.g. sand at 15 cm in Fig. 11). However, a thin sand at 26 cm depth in core B-4 (18 m) shows a very clear sequence grading from flat to inclined laminations (Fig. 14a). Like the individual sedimentary structures, the sequence of structures is not exclusive to one process or the other. Both Aigner and Reineck (1982) and Nelson (1982) observed sedimentary sequences similar to these in discrete sand beds of modern shelf sediments of the Helgoland Bight (Germany) and the Norton Sound (Alaska),respectively, yet proposed different transport mechanisms (offshore flowing gradient currents vs. broad wave-induced liquefaction and storm-surge ebb flow). The least that can be derived from observation of these vertical

sequences is the interpretation that the discrete beds were deposited under conditions of decreasing energy.

Biogenic Sedimentary Structures

Specific Structures--Several types of burrow structures are present in radiographs of boxcores taken in the CTCS area (Fig. 9). One of the most ubiquitous is a double-walled lined burrow which looks similar to what Hill (1985) called "trace B" . The mucus-agglutinated outer wall appears light on x-ray, contrasting sharply with the dark-shaded inner wall (arrow. Fig. 11). The lining is probably due to a sequence beginning with burrowing followed by later active backfilling by the organism responsible for the burrow. The double-walled shaft is typically vertical in orientation and does not appear to branch. Boxcore C-3 shows one continuous burrow of 17 cm length (Appendix A). Although Hill (1985) was not able to identify the specific tracemaker, the burrow is probably the dwelling trace of some type of polychaete worm (I.B. Singh, pers. comm., 1985). The trace is evident in boxcores from nearly every water depth but is particularly abundant in the 18 to 20 m depth range.

Another abundant biogenic structure is a unlined, unbranched trace similar to Hill's (1985) "trace C" (arrow, Fig. 13). Vertical in orientation, it has a highly variable length and width. The traces are commonly straight, but some branching and horizontal portions are present. The lack of lining is suggestive of a more passive filling of the burrow following later sedimentation. Hill (1985) theorized that this burrow represented the dwelling trace of Glycera sp., a polychaete worm. However, the diverse morphology and variable dimensions taken on by this trace imply that more than one of type of organism can create

this type of structure.

Two biogenic structures in the cored sequences may be related to the feeding traces of the heart urchin. A disk-shaped burrow (Fig. 13) and a chevron-shaped back-fill trace (arrow, Fig. 15) are common. The former probably represents a cross-sectional view, the latter a longitudinal section (Howard et al., 1974). The disk shaped trace is much more prevalent than the back-fill structure. However, Hill (1985) only notes the latter trace. By itself, the trace is easily the most destructive of the biogenic structures in the cored sequences; in some sands, the physical sedimentary structures are completely obliterated by the burrow (e.g. the sand at 35 cm depth in CB-3, Fig. 13). As for the depth distribution, the heart urchin traces are widespread but are most abundant in 20 to 34 m. Hill (1985) noted that the burrow was less common in the sandier substrates close to shore. No whole urchins were obtained in the boxcores; yet the most abundant shell fragment in sieved samples was that of the spine-bearing echiniods.

Trends and Patterns--The degree of bioturbation decreases in an offshore direction from the 20 m water depth (Fig. 16a). This pattern was observed by Berryhill et al., (1976) and is confirmed by this study. However, analysis of boxcore radiographs suggests that there is a decrease in the observed bioturbation between 12 and 16 m water depth, an area not extensively sampled by Berryhill et al., (1976). Burrowing activity also varies vertically in the cores, with a general downward increase in bioturbation.

The apparent relationship between the amount of bioturbation and the water depth parallels shore-normal trends in the number and diversity of live macrobenthic organisms present in surficial sediments (Fig.

Fig. 15.--Radiograph of boxcore CB-2 (18-46 cm core depths) taken in 24 m of water. Arrow points out chevron-shaped burrow referred to in text.

(next page)

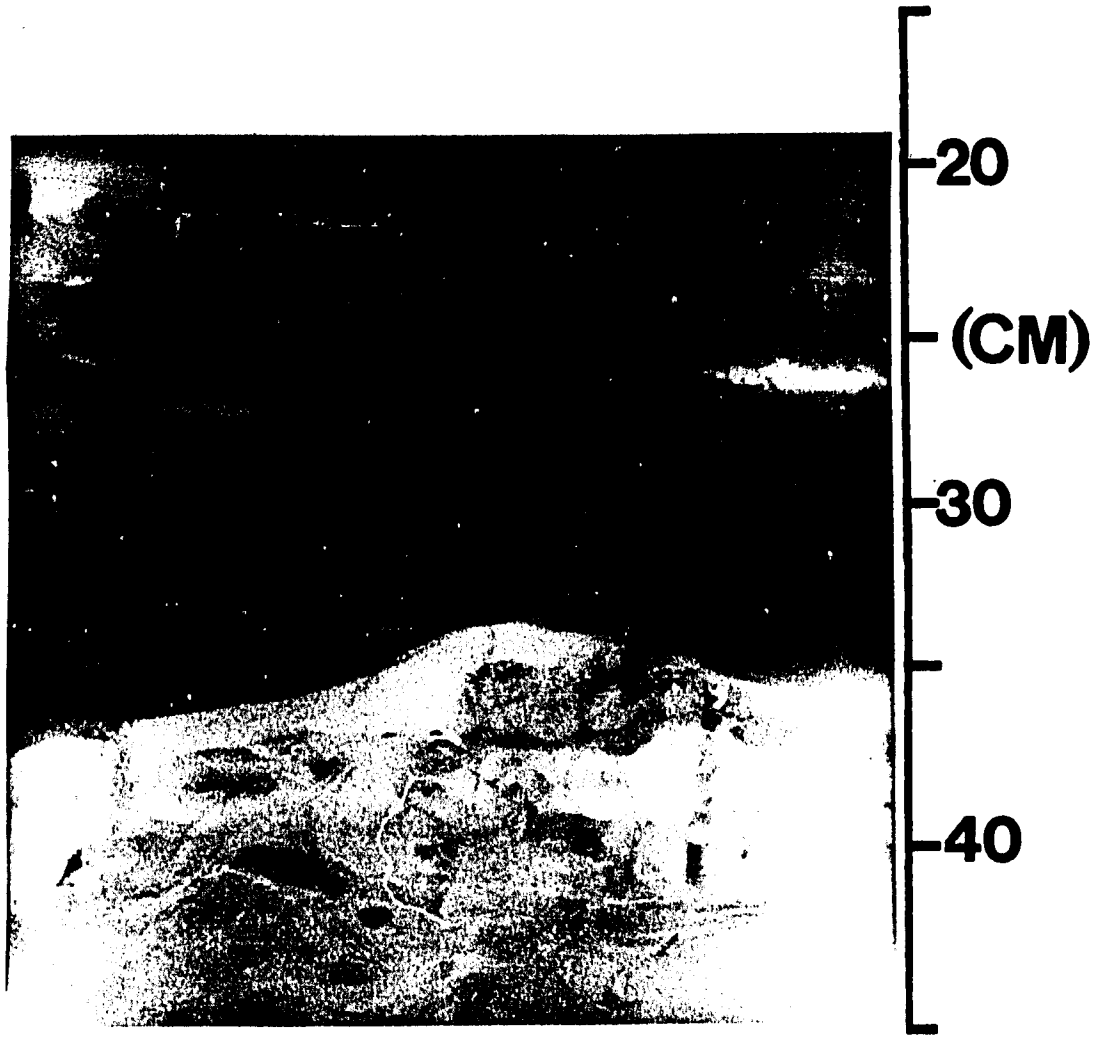
20
(CM)
30
40

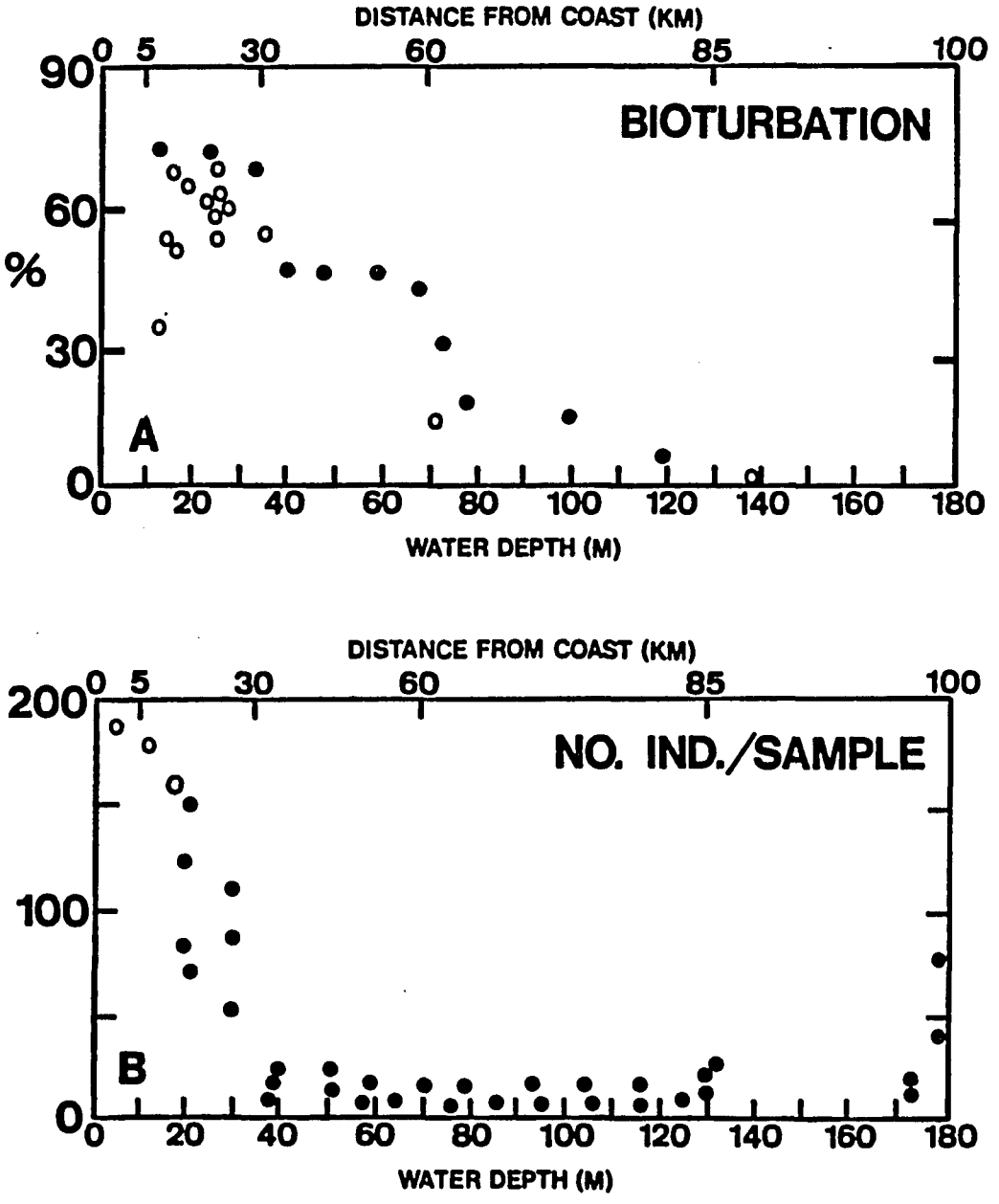

Fig. 16.--Shore-normal trends in A) percentage of core bioturbated (solid circles data of Berryhill et al., 1976 and open circles this study) and B) Number of live individuals per grab sample (solid circles data of Hill, 1985 and open circles data of White et al., 1983).

16b). Grab samples taken across an area just south of the study area show significant decreases in the species density (number of live individuals/sample) and species richness (number of live species/sample) from the shoreline to 30 m (White et al, 1983; Hill, 1985). The two parameters remain approximately constant to 130 m, where they increase slightly. These cross-shelf patterns in biologic parameters were attributed by Hill (1985) to shore-normal gradients in bottom water temperature variability and the type of surficial sediment.

However, there are significant departures between the trends in the degree of bioturbation and infaunal numbers. Hill (1985) attributed this to differences in sedimentation rates across the shelf. However, as will be shown in a later section, the rates calculated by Holmes and Martin (1977) and used by Hill (1985) are somewhat questionable in the inner shelf (10-20 m) depth range. Recently acquired data, which will be presented as part of this study, indicates less cross-shelf variability in sedimentation rates. Two other factors, not mentioned by Hill (1985), appear to be related to this difference in bioturbation and infaunal numbers. One is a change in the type of trace which is involved in the bioturbation. For example, the high rates of biogenic reworking in water depths of 17 to 20 m correlate well with the high density of polychaete worms in this area. The radiographs show that the majority of the burrows in these depths are the dwelling traces of the polychaete worm. However, in mid-shelf waters (20 to 40 m), the dominant burrow structure is the feeding trace of the heart urchin. Sampling by Hill (1985) indicates that the heart urchin, and echinoids in general, represent less than 10 % of the of the total number of individuals. But the heart urchin is an active infaunal feeder,

injesting a disproportionally large amount of sediment in relation to its numbers (Howard et al., 1974).

Secondly, the apparent decrease in bioturbation from 18 to 12 m, can be related to physical processes of wave and current activity. As will be shown later, the frequency of wave resuspension in this area is much higher than in greater water depths. The numerous truncations and erosional surfaces tend to yield a highly amalgamated sequence (Figs. 12 & 17). The frequent reworking may limit infaunal activity to the surficial sediments and hence less overlap of burrowing episodes. Burrows also appear to be less distinct in these sandy sequences.

Discussion--Analysis of the cored sequences from the CTCS suggests that the preservability of the discrete sand beds is dependent upon the frequency and intensity of physical and biological processes. The optimum case is where the individual deposit of sand is preserved intact and eventually becomes a permanent part of the sedimentary record of the shelf. The worst case scenario is represented by a sand bed which loses its coherence, sedimentary structures are destroyed, bedding contacts are blurred, and it becomes impossible to distinguish the bed from the over- and underlying sediments. Both extremes occur in the modern strata of the Texas shelf as well as cases intermediate to the two.

In shallow parts of the CTCS (12-16 m), the high frequency of resuspension by wave and current activity leads to the amalgamation of beds (Figs. 12 & 17). It becomes difficult to separate out individual "events". Each sand deposit is susceptible to erosion associated with successive storm events. The amount and frequency of truncation appear

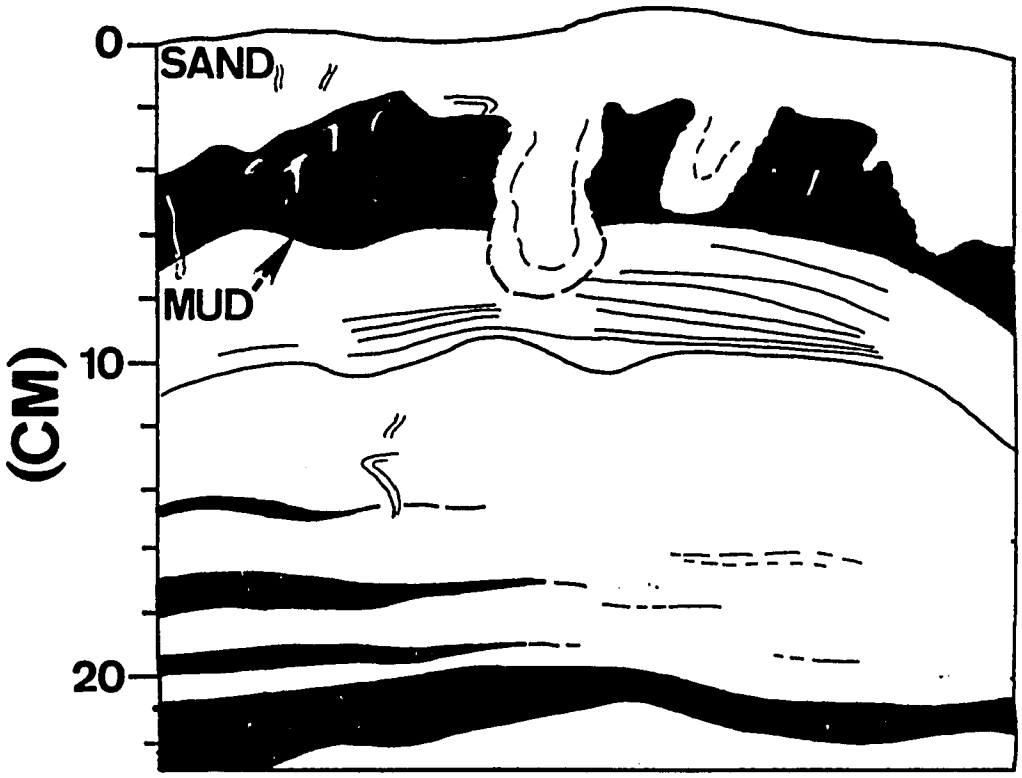

Fig. 17.--Tracing of an x-ray radiograph of boxcore AB-1 (water depth 15 m). Note apparent amalgamation of beds from core depth of 13 to 23 cm.

to diminish with increasing water depth, in accordance with decrease in the frequency of storm events capable of resuspending sand. This notion is consistent with the conceptual model for shelf sediment accumulation presented by Nittrouer and Sternberg (1981). This model implies that, given a fairly constant sedimentation rate, the degree of amalgamation is proportional to the frequency of storm-related resuspension.

Further offshore (16-20 m), the intensity of physical processes lessens while the biologic activity becomes more important. Bioturbation may be thought of as a process which tends to produce progressively greater degrees of disorder in unconsolidated sediments (Hanor and Marshall, 1971). The exception is where preferential concentration of sedimentary components occurs (e.g., sand grains packed in a burrow). Hanor and Marshall (1971) give a systematic framework for classifying the relative amounts of order and disorder caused by infaunal organisms. Particularly applicable to the CTCS boxcores is the notion of the scale and intensity of segregation (Fig. 18). The scale of segregation is related to the relative sizes of the undisturbed portions of sediments. The intensity of segregation describes the relative difference between the composition of discrete regions and the bulk composition. Sediments which have been completely homogenized by biologic activity have a low intensity of segregation--there are no undisturbed regions. This is certainly the case in the 18 to 20 m depth region where polychaete burrows dominate the biogenic structures. The high density of polychaetes and other worm-like creatures has resulted in sequences which have a small scale and low intensity of segregation: they are well-mixed and nearly homogeneous. Fig. 19 shows

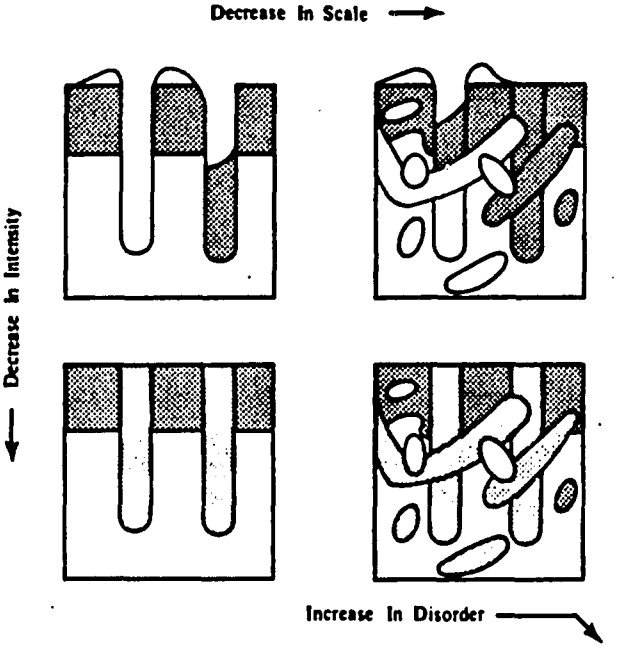

Fig. 18.--Schematic representation of how biological mixing can lead to a decrease in the scale of segregation (size of discrete volumes in the sediment) and decrease in the intensity of segregation (difference in composition of discrete volumes) (from Hapor and Marshall, 1971). Blank = unmixed, light shade = partial mixing, dark shade = highly mixed

Fig. 19.--Radiograph of boxcore B-1 (16-44 cm core depth) taken in a water depth of 18 m.

(next page)

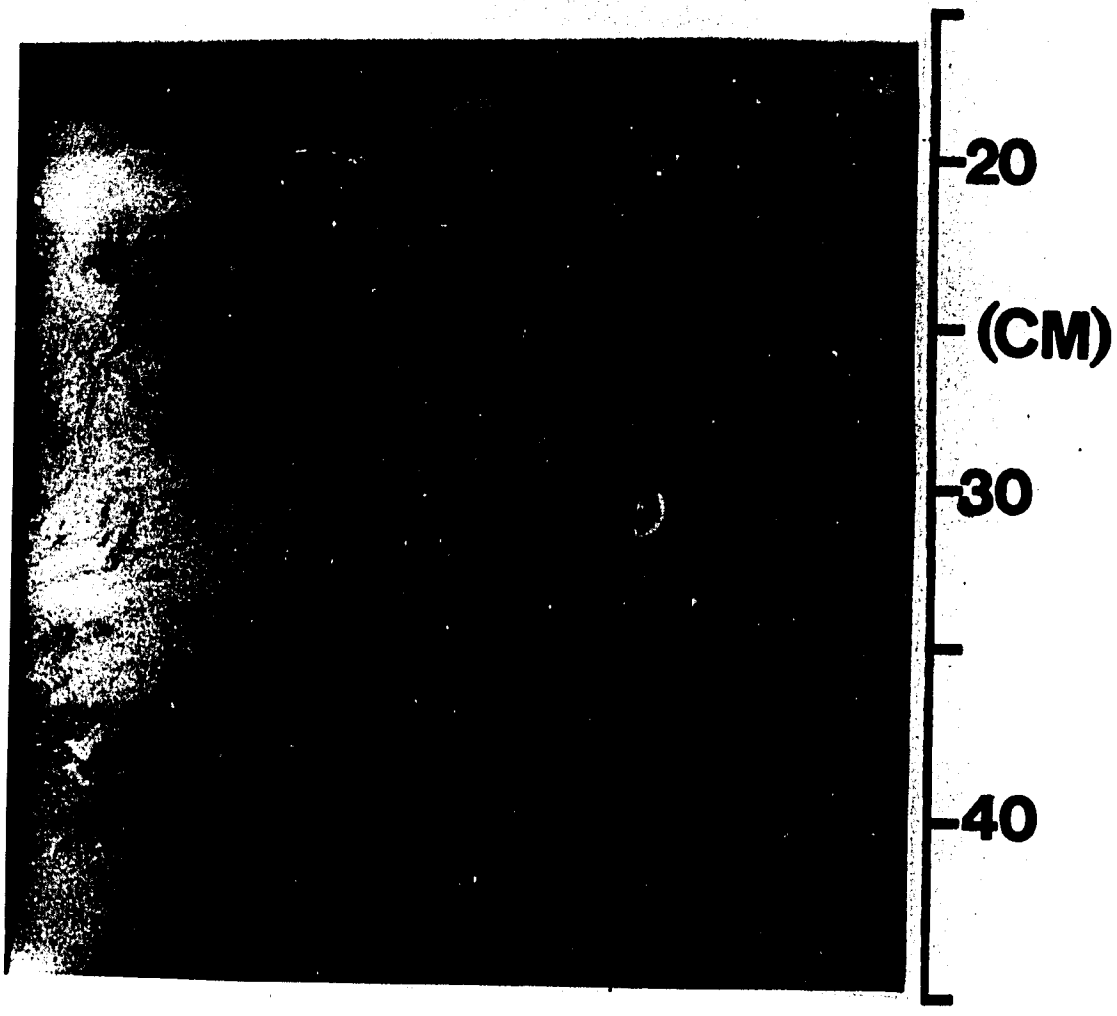
20
(CM)
30
40

an example of a bed at 18 to 30 cm which has just such an appearance. It is possible that the unit was originally two discrete sand beds separated by a clay layer. Presently the unit is considered a "muddy, bioturbated sand". In this case, the discrete sand beds are not preserved and may not be recognizable as such in the future sedimentary record.

In somewhat deeper water (20-34 m), the density of polychaetes decreases and the heart urchin feeding traces become more prevalent. Unlike the polychaetes, the heart urchin trace distribution is sporadic: some sands are completely obliterated by its distinctive burrow (e.g. the sand at 35 cm in CB-1, Fig. 13). In other places, the sands are virtually undisturbed (Fig. 10). Another feature is the complete disruption of a bed (e.g. a sand at 10 cm in Fig. 20). Although the assignment of culpability is uncertain, the size of the disrupted zone is on the order of the heart urchin shell. This is an example of mixing with a large scale and high intensity of segregation--the sands flanking the gap are virtually undisturbed (compare with upper left of Fig. 18). The laminations and bedding contacts are still visible. Should this unit become part of the sedimentary record, it could be recognized as a discrete sand bed.

Another factor to consider in these waters is the maximum depth of biologic and physical reworking. Although a few organisms can burrow from the surface to 30 cm depth in sediments, most confine their activity to the top 5 cm or so (e.g. Table 13 in Reineck and Singh, 1975). Thus the discrete beds located at 10 cm depth or more probably will not be further bioturbated. As for physical processes, it is likely that the 6-8 cm clay layer overlying the uppermost discrete sand beds in 20

Fig. 20.--Radiograph of boxcore CB-5 (water depth 25 m).

(next page)

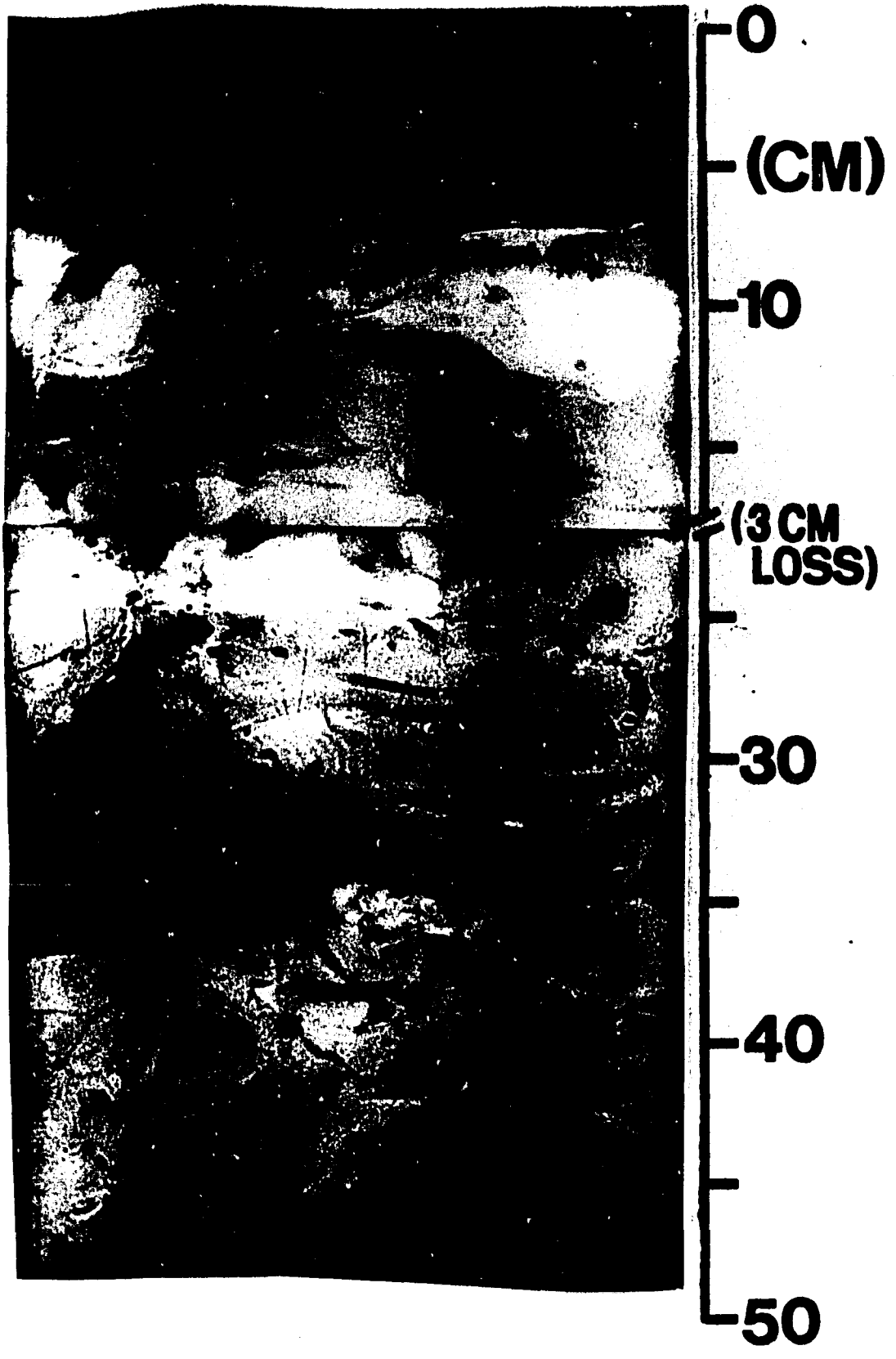
0
(CM)
10
(3 CM
LOSS)
30
40
50

to 30 m water depth may act to dampen wave and current effects during future storms. Kreisa (1981) proposed that just such an effect was responsible for the preservation of the storm-deposits in the Martinsberg Formation (Ordovician). Nelson (1982) felt the higher preservability of discrete sand beds in parts of the Norton Sound (Alaska) was due to the high rates of fairweather clay deposition from suspension in the vicinity of the Yukon delta. Further, Swift and Rice (1984) argue that on muddy shelves, storm-related erosion does not procede throughout an event but ceases once the sediment-carrying capacity of a flow has been attained (assuming there are no large spatial gradients in the flow dynamics). For this reason, even large storms may not erode more than a few centimeters of surficial sediment.

Another matter of note is the relationship between the thickness of a sand bed and the degree of bioturbation. In the 25-30 m water depth range, the thickest beds are sometimes the least bioturbated. In some cases, thick, unbioturbated sand beds cap intensely bioturbated intervals (Fig. 10). This suggests that there may be some decimation of the infaunal population during the impulsive events responsible for the deposition of the sand. Or, by contrast, the thick sand bed may be considered less than a favorable habitat or source of food by the infaunal organism. In either case, it seems that the preservation potential of thick discrete sand beds is much higher than thin beds.

Texture and Composition

The hydrodynamic properties of detrital grains are a function of their size, shape, and density (Anderson et al., 1982). Textural analysis reveals information about the size and shape of the grains,

while compositional analysis sheds light on the type of grain and thus its density. Comparison of the textural trends in a vertical and lateral sense also aid in making inferences about temporal and spatial gradients in the competency of a shear flow.

Composition--The detrital grains in samples from the discrete sand beds are dominantly quartz, paralleling the composition of a representative sample from the beach at Mustang Island, which is shown for comparison (Table 1). These are expected results, considering the provenance and multi-cyclic nature of the sands present along the Texas coast (Bullard, 1942; Mazzullo and Withers, 1984). In fact, some of the quartz grains show silica overgrowths which could only have originated during prior history as a framework grain in a cemented sandstone (Fig. 21a).

Grain-Size Frequency Distributions--Fig. 22 shows a comparison of the of the size frequency distributions of the silt and sand fraction of discrete sand beds in cores from 24 m and 74 m water depths, as well as a sample from the surf zone at adjacent Mustang Island. It is apparent that there is a steady depletion in the coarser particles moving into deeper water. This is reflected both in the shift of the curves toward the fine end of the grain size spectrum and the transition from the negatively (coarse) skewed distribution of the surf zone samples to the positively skewed shelf samples. Such a pattern has been termed "progressive sorting" (Russell, 1939). Progressive sorting, the steady depletion of coarse grains down a transport pathway, will result in fine-skewed grain-size frequency distributions regardless of the shape of the input population and is especially well-pronounced when there is a decrease in the intensity of the flow field down the transport pathway (Swift and Ludwick, 1976). In fact, the beach-shoreface-shelf

Fig. 21.--Scanning electron micrographs of A) quartz grain showing probable quartz overgrowth from sample of discrete sand bed in boxcore CB-1 (core depth 11 cm) and B) numerous quartz grains from same sample. Note echinoid spine upper left. Bar represents 10 microns in A and 100 microns in B.

(next page)

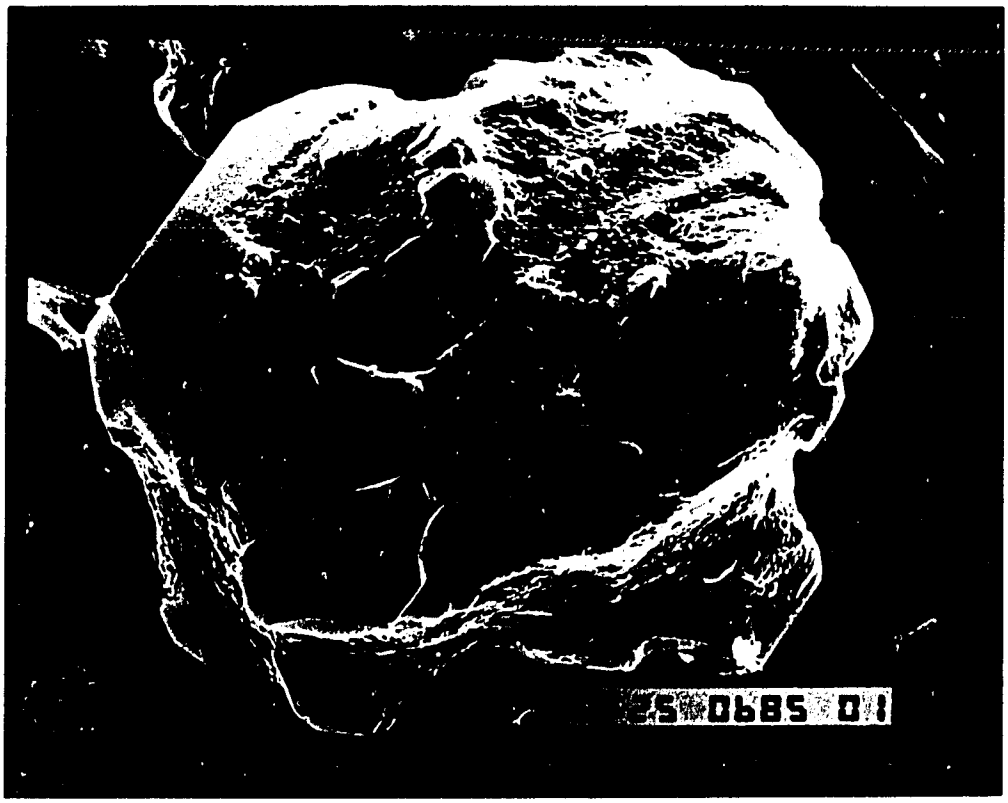

A

B

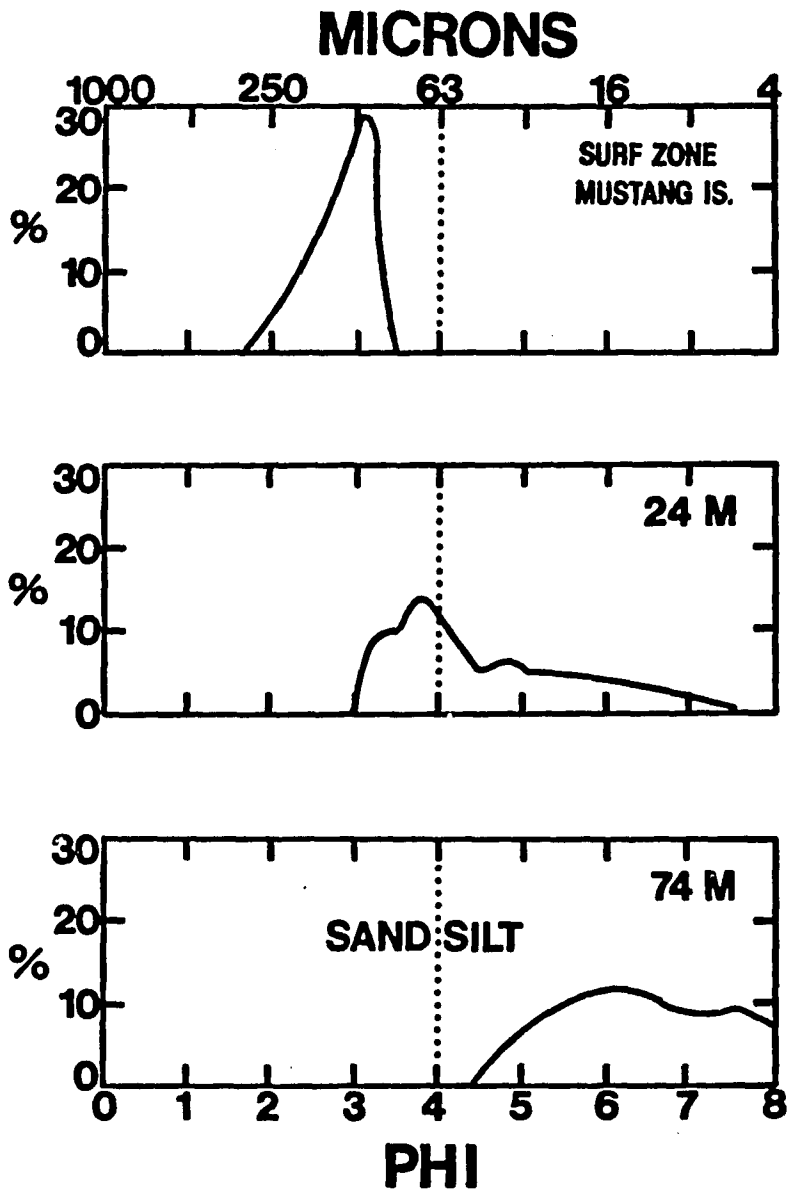

Fig. 22.--Grain size frequency distributions of sand and silt from surf zone at Mustang Island, Texas, a discrete sand bed in a boxcore taken in 24 m of water, and a discrete bed in a boxcore from 74 m of water in the CTCS area.

transect may be regarded as one of the more spectacular examples of the influence of progressive sorting upon grain size frequency distributions (D. Swift, pers. comm., 1985).

Grain Shape--As shown by Fig. 22, the modal class of the sand and silt fraction straddles the sand-silt boundary. Grains of this size range are quite angular (Pettijohn et al., 1973; Fig. 21b). Silt grains, in particular, are poorly rounded. This is related to the transport mode. Studies by Bagnold (1966) and McCave (1971) indicate that the sand-sizes which are typical of the discrete sand beds are transported entirely in suspension (Fig. 23). During suspension transport, the grains are insulated from inertial impacts against other grains and there is less tendency for rounding. This conclusion is supported by evidence of delicate features which are preserved upon the surfaces of the grains from the discrete sand beds (Fig. 21a).

Vertical Grain Size Trends--Settling velocity analysis, which can discriminate grain sizes to tenth of a phi, reveals that the majority of the variability in sand sizes in a typical vertical sequence occurs within a fraction of a phi interval (Fig. 24). Closely-spaced sampling through a discrete sand bed at 10 cm depth in boxcore CB-1 shows only very subtle upward fining in equivalent sand grain diameters. However, there is a clear increase in clay and silt relative to the proportion of sand. Coulter Counter measurements of the silt sizes also show clear upward fining trends (Fig. 25).

The lack of upward variability in the sand sizes as measured by the automated settling tube can be attributed to the progressive sorting process. The steady depletion of the coarser particles will tend to produce a very peaked (leptokurtic) sand-size frequency distribution.

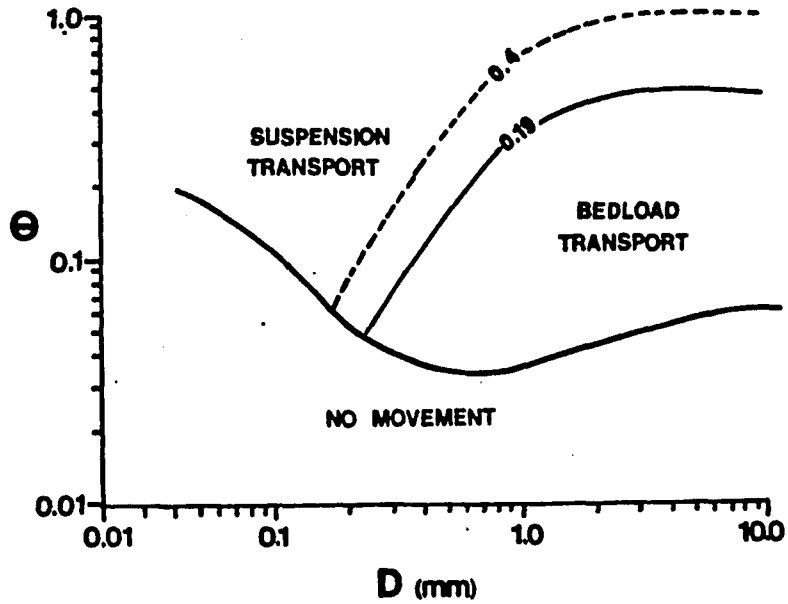

Fig. 23.--Modified Shield's diagram. Dashed line is critical suspension criteria of Bagnold (1966), solid line is that of McCave (1971). D is the grain size in mm. Modified from McCave (1971).

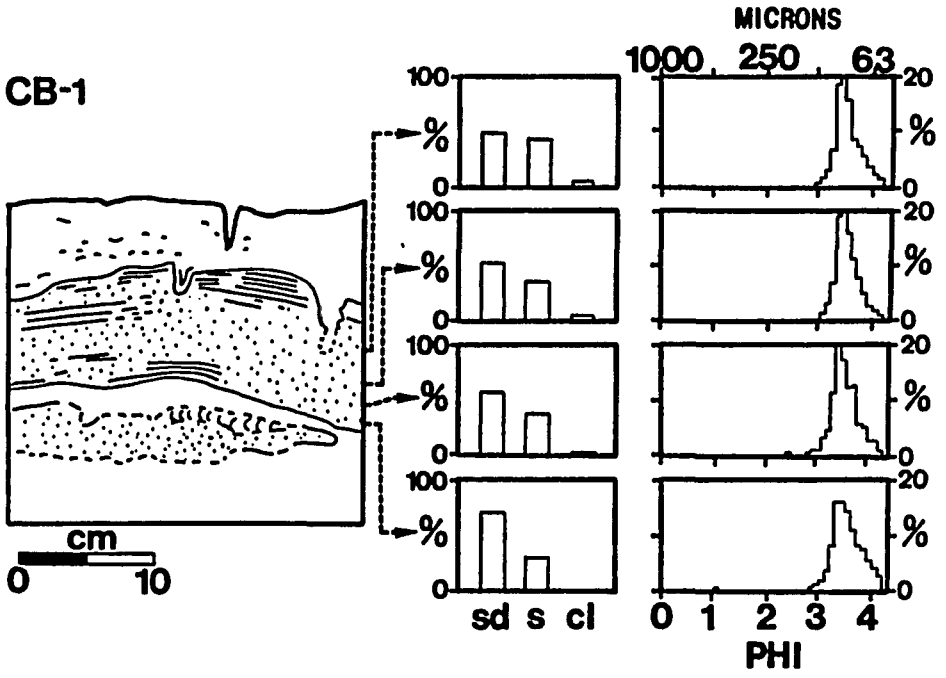

Fig. 24.--Vertical trends of sand-silt-clay percentages and equivalent sand size (from settling velocity measurements) in a discrete sand bed of boxcore CB-1 (26 m water depth).

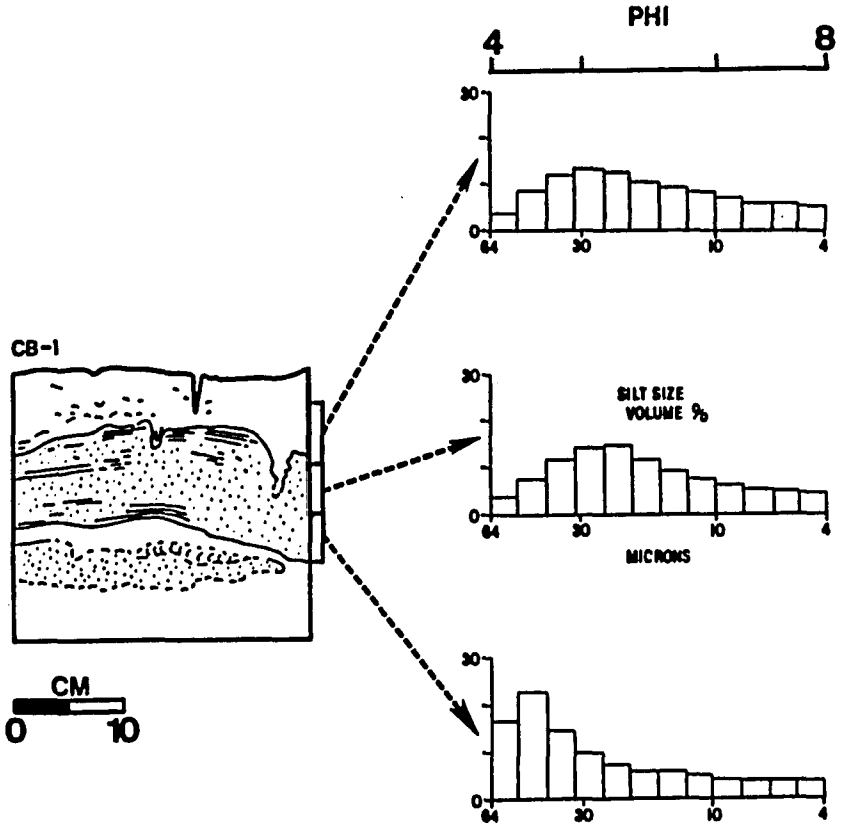

Fig. 25.--Vertical trend of silt sizes (from Coulter Counter measurements) from three samples of boxcore CB-1 (26 m water depth).

As the available size range is quite narrow, vertical trends in the sand sizes are quite subtle, due to the lack of variability. However, the availability problem is not so critical in the silt and clay range, which display quite distinctive upward fining trends.

This normal (fine) grading indicates that deposition of the discrete sand beds proceeded as an orderly settling of grains as the levels of shear-generated turbulence decreased. In other words, those grains which had higher settling velocities fell out of suspension prior to those with lower velocities. This undoubtedly occurred during the waning energy phase of an impulsive event.

This finding contrasts with the suggestion of Allen (1984) that some sand is deposited at the height of a storm. According to Allen's (1984) hypothesis, storm-deposited beds should show first a vertical progression in which sand and silt sizes and the percentages of sand, silt, and clay remain constant up through the major portion of the bed. The waning energy portion of a storm would then be represented by a short fining interval at the very top of the bed. The lack of such a pattern in the discrete sand beds of the CTCS area indicates that the phase lag between inner-, mid- and outer shelf stations during a storm, deemed so important by Allen (1984), is less critical than the temporal changes in the levels of shear-generated turbulence. The vertical grain size trends are more consistent with the "temporal acceleration" model proposed by Swift and Rice (1984): 1) erosion and transport occur during flow acceleration; 2) erosion ceases once the sediment-carrying capacity is reached; 3) deposition procedes as the flow decelerates, turbulence levels fall and the grains settle out of suspension.

Lateral Grain Size Trends--Spatial trends in the grain size present in discrete sand beds are also apparent (Fig. 26). Two points should be mentioned with regard to this figure. First, the samples were taken from a correlative horizon, a bed which absolute dating (next section) suggests was deposited within the time period 1961-2. This time-equivalence is crucial to the interpretation of the cross-shelf competency of a single flow event. Secondly, comparison of the grain sizes at each station could only be done within the silt range, as sand-sized material was not present at the 74 m site. Seaward fining is indicated by the shifts in silt-sizes and in the sand-silt-clay ratios within this bed. This seaward fining again may be related to progressive sorting, where a deposit becomes increasingly finer down the transport path due to a gradient of decreasing shear stress and consequent depletion of the coarser grains (Russell, 1939; Swift and Ludwick, 1976).

Discussion--Again, neither the vertical or lateral fining shown by the discrete sand beds are unique to the turbidity current (Stow and Bowen, 1980) nor the current transport mechanism (Swift and Ludwick, 1976). However, Fig. 26 does bring to light some points relevant to questions of source and pathway. The seaward fining is consistent with the concept of a transport pathway oriented at some angle (not necessarily perpendicular) to the trend of the isobaths across the shelf. It also fits with the idea of a coastal source for these clastics. In fact, this seaward fining parallels the size-grading shown by the surficial sediments of this area (Fig. 27). The similarity between the trend of surficial sediment sizes and bathymetric contours is thought to be a result of the offshore decrease in wave orbital bottom velocities (Curray, 1960). It is possible that mechanism responsible for the

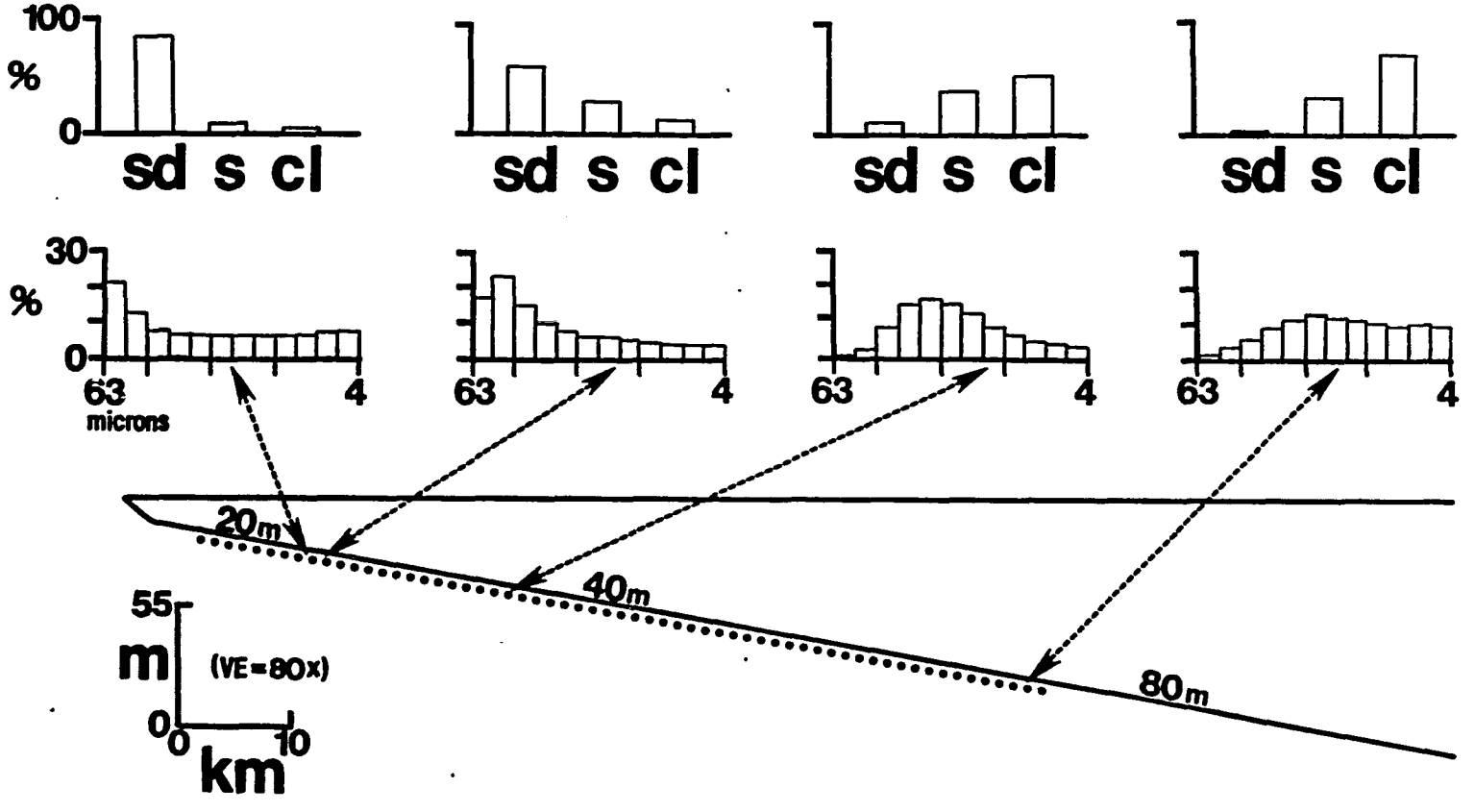

Fig. 26.--Shore-normal trends of silt sizes and sand-silt-clay ratios within a single correlative horizon across the CTCS area.

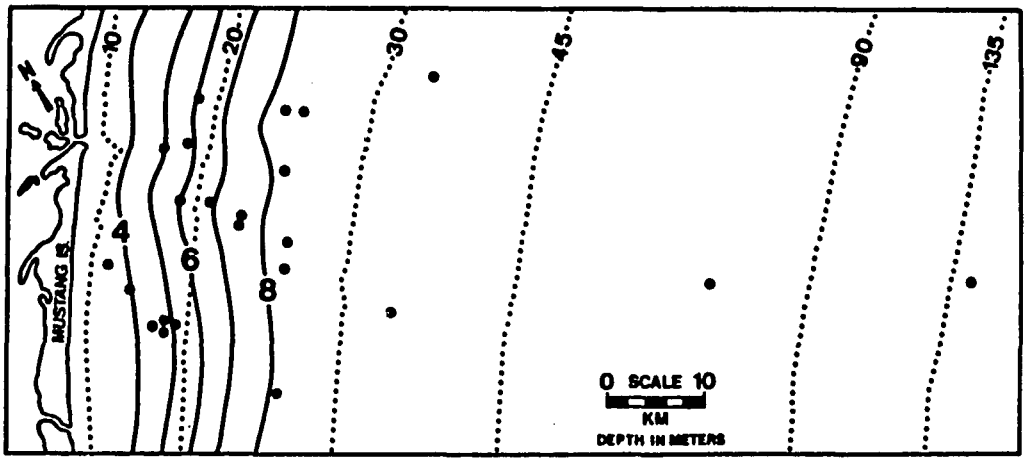

Fig. 27.--Trend of modal grain sizes (phi scale) in surficial sediments across the study area.

seaward grading in the "sub-surface" sediments may also be depth-sensitive, reflecting an offshore gradient in combined flow power. In addition, the well-sorted nature of the sand fraction lends credence to the notions of progressive sorting away from a coastal source (Fig. 24).

Absolute Dating

In order to place interpretation of the discrete sand beds in light of recent observations of modern processes, several cores were selected for absolute dating. The two techniques used most often to date sediments deposited within the last 100 years are Cs-137 and Pb-210. The Cs-137 method involves gamma-counting of oven-dried samples using a lithium-drifted germanium detector. Cs-137 was introduced into the world atmosphere by atmospheric nuclear testing which began in 1954 and reached a peak in 1963 just prior to the open-air test ban treaty. Sedimentation rates are calculated by observing the depth of maximum activity which corresponds to the year 1963 (DeLaune et al., 1978). This technique has proven to be successful in freshwater, brackish and salt marsh environments of the Louisiana coast (Hatton et al, 1983) and estuaries of the Atlantic coast (Olsen et al., 1978). However, the technique has rarely been used in open marine shelf settings. Analysis of boxcores CB-3 (26 m) and CB-5 (25 m) show Cs-137 to be present in only low amounts, approximating what is considered background levels.

However, analysis by Pb-210 techniques yielded better results. Pb-210 is an unstable isotope of the U-238 natural radioactive series. It is introduced into the world environment by precipitation, runoff, and decay of its Ra-226 precursor (Nittrouer et al., 1979). It becomes

adsorbed to clay minerals and organics and generally has a short residence time in the water column of the ocean (< 1.0 year). Chemically immobile, it breaks down to Bi-210 by beta decay with a half-life of 22.3 y.

Several methods exist for deriving absolute dates with Pb-210. The most common and the technique used in analysis of boxcore CB-3 (Fig. 28) is a geochemical procedure which measures the Po-210 granddaughter product. The alpha decay of Po-210 is counted by a silicon barrier detector coupled to a pulse height analyzer. The units are given as disintegrations per minute per gram (DPM/G). It is generally assumed that secular equilibrium exists between the Pb-210 and Po-210: all the Po-210 present is supported by the decay of Pb-210. This seems to be valid since Po-210 produced by the decay of Bi-210 (h/l 138 days) should disappear by 4-5 half/lives or 1-2 y (Nittrouer et al., 1979).

The second procedure, the one used in analysis of boxcore CB-5 (Fig. 29), is a newer technique involving the direct measurement of Pb-210 with a germanium detector (Cutshall et al, 1983). Pb-214, a short-lived (h/l 27 minutes) daughter of Ra-226, is also counted. This facilitates the determination of supported levels of Pb-210 in the sample. Units are pico Curies/gram (pCi/G), similar to the Cs-137 measurement.

Both methods yield plots of total Pb-210 activity versus depth (Figs. 28 & 29). Analysis of marine samples on other shelves indicate that the total activity falls into three regions: a surface-mixed layer of high but homogeneous activity, a region of logarithmically decreasing activity with depth, and a region of constant but low activity approximating background levels (Nittrouer and Sternberg, 1981). The

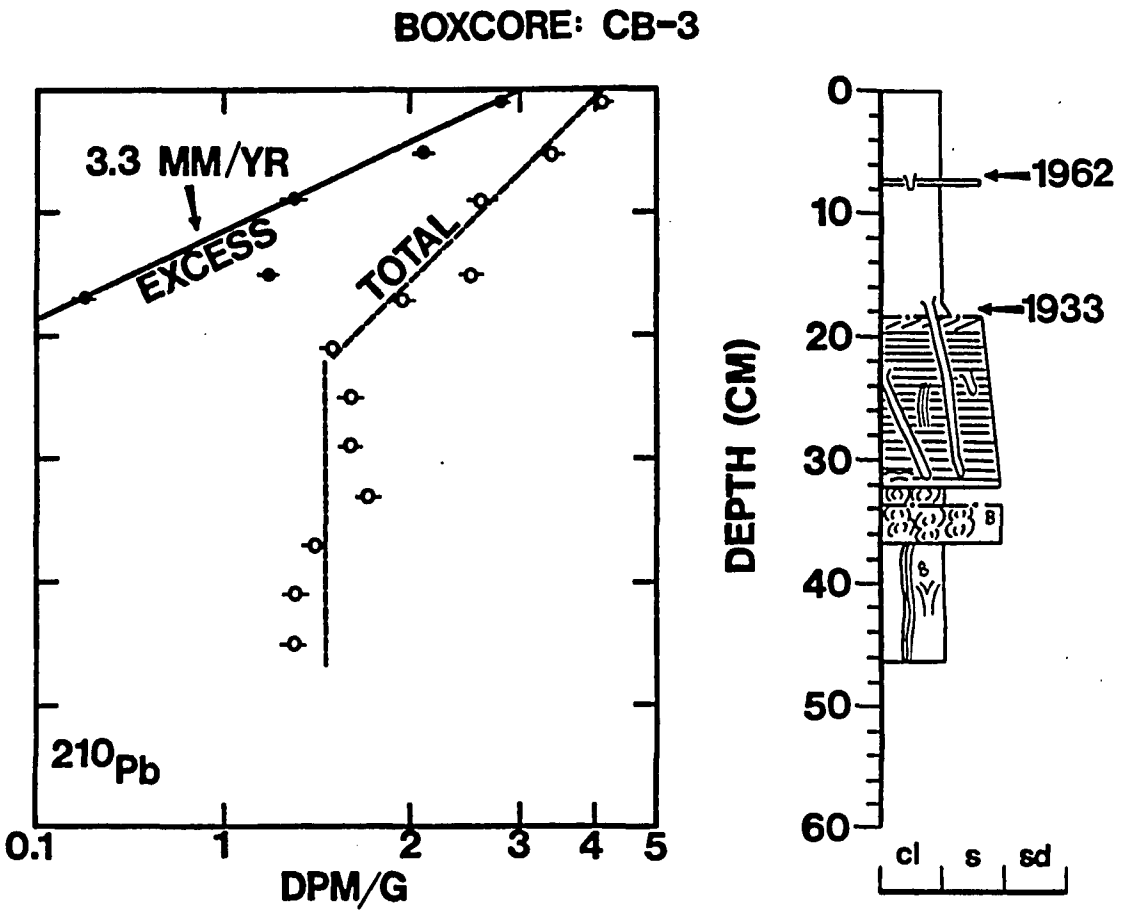

Fig. 28.--Distribution of total and excess Pb-210 in boxcore CB-3 (26 m water depth). Absolute dates and sediment accumulation rates from equation given by Faure (1977). Pb-210 dating courtesy C. Nittrouer, North Carolina State University.

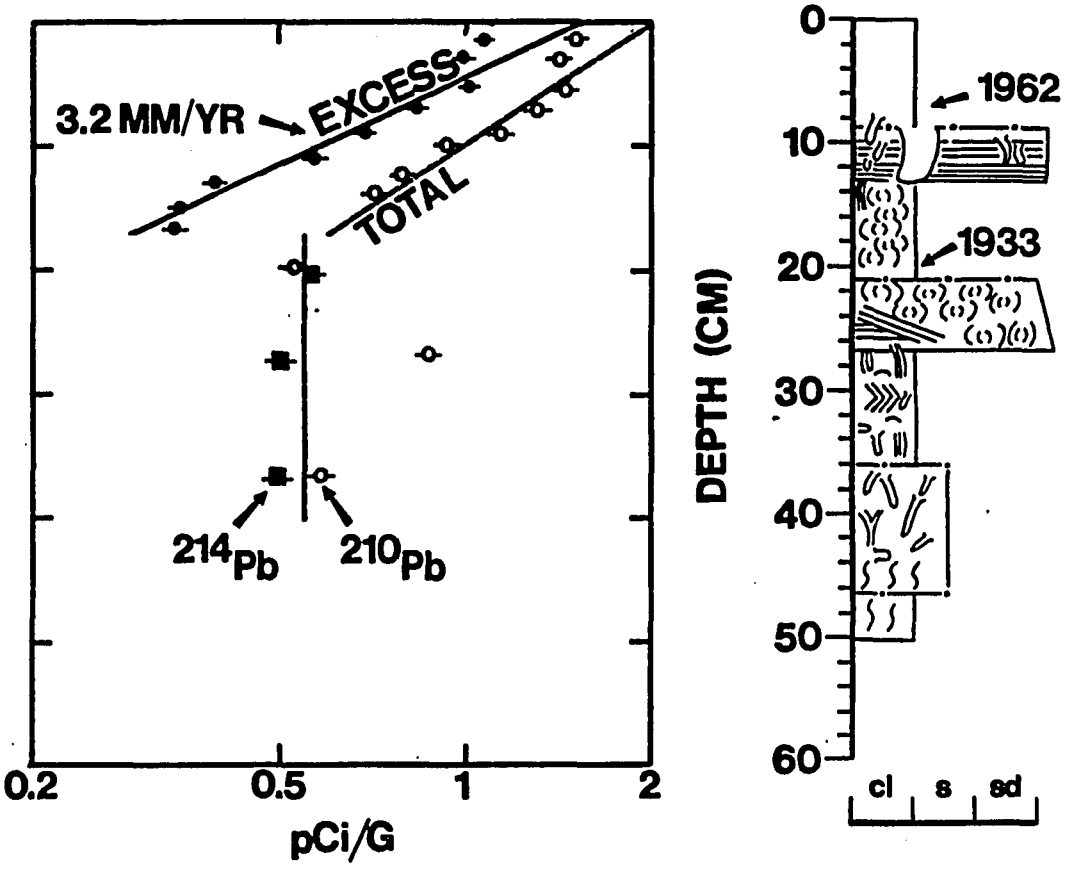

Fig. 29.--Distribution of total and excess Pb-210 in boxcore CB-5 (water depth 26 m). Absolute dates and sediment accumulation rates from equation of Faure (1977). Pb-210 dating courtesy K. Olsen, Oakridge National Laboratory.

background level is subtracted from the total values in the logarithmic zone to yield excess Pb-210. The absolute age of a sample can be calculated from the equation:

$$T = (2.303/L) \log (Pb\text{-}210_o/Pb\text{-}210_m)$$

where, T equals the age in years, L is the decay constant of Pb-210 ($3.11 * 10^{-2}$ y), $Pb\text{-}210_o$ the excess activity at the surface, and $Pb\text{-}210_m$ the excess activity of Pb-210 at a point of interest, generally the deepest value in the logarithmic layer (Faure, 1977). The sediment accumulation rate is found by dividing the depth by the age.

Previous work by Holmes and Martin (1977) on determination of sediment accumulation rates in the CTCS area yielded highly variable results, with a general decrease in sedimentation rates in shallow water (Table 3). The large discrepancy may be in part be due to the intense bioturbation in nearshore waters (<20 m) and the change in sediment texture to that of predominantly sand. To avoid these problems, cores were selected that were largely clay-rich and that appeared to have less than 30 % bioturbation (and did not show low scales and intensities of segregation (Hanor and Marshall, 1971; Fig. 18). The trend of total activity in the two cores illustrated in Figs. 28-29 indicates that a surface mixed layer was present only near the top of CB-5 (0-4 cm). The most of the first 20 cm in both samples appears to be a zone of logarithmically decreasing activities. Background values are attained in about 18-20 cm depth in the cores. This is supported by the measurements of Pb-214 in core CB-5. The two cores are about 30 km apart.

The sediment accumulation rates of 3.3 and 3.2 mm/year calculated

TABLE 3.--Previous Pb-210 work in CTCS area

Core	Water Depth	Calculated Sedimentation Rate[1]	% Bioturbation[2]
OCS-45	18 m	0.0 mm/yr	>60%
OCS-70	20 m	2.1 mm/yr	>60%
OCS-75	40 m	4.0 mm/yr	<30%
OCS-106	50 m	4.0 mm/yr	<30%

[1]From Holmes and Martin (1977).

[2]From Hill (1985).

from CB-3 and CB-5, respectively, are close to the value of 4.0 mm/year deduced from relatively unbioturbated mid-shelf cores by Holmes and Martin (1977) (Table 3). The general decrease in sedimentation rates away from the mid-shelf water depths (50-100 m) shown by Holmes and Martin (1977) appears to be supported here. However, their claim that rates fall to zero in the inner shelf (Table 3) is erroneous, in the author's opinion, and more likely an artifact of the the problems of bioturbation and sediment texture mentioned previously.

Absolute dates derived from this analysis suggest that the uppermost sand in the two cores formed just prior to the year 1962. As mentioned, Hurricane Carla made landfall upon the coast less than 100 km away from this location in September of 1961. It is well-known that this storm was responsible for the deposition of a 1-9 cm sand bed well to the south of this location (Hayes, 1967; Fig. 1).

What is less well-documented is the presence of a sand bed deposited just prior to 1933. Several hurricanes affected the coast around this time period (Morton and Pieper, 1977). Two were considered "major" hurricanes, with wind speeds in excess of 100 mph (45 m/sec). One made landfall near Freeport in the summer of 1932, the other near Brownsville in 1933. The latter produced a storm-surge tide of 2.5 m at Corpus Christi, Texas (Ellis, 1984).

One of the mid-shelf cores studied by Holmes and Martin (1977) was taken from a location close to where boxcore C-1 was obtained (Fig. 30). Like the two cores discussed previously, the top 20 cm is a logarithmic zone. Using the sediment accumulation rate yielded by this core, absolute dates can be inferred for boxcore C-1. This suggests that the sand deposited during 1961-1962 is present while the 1932-1933

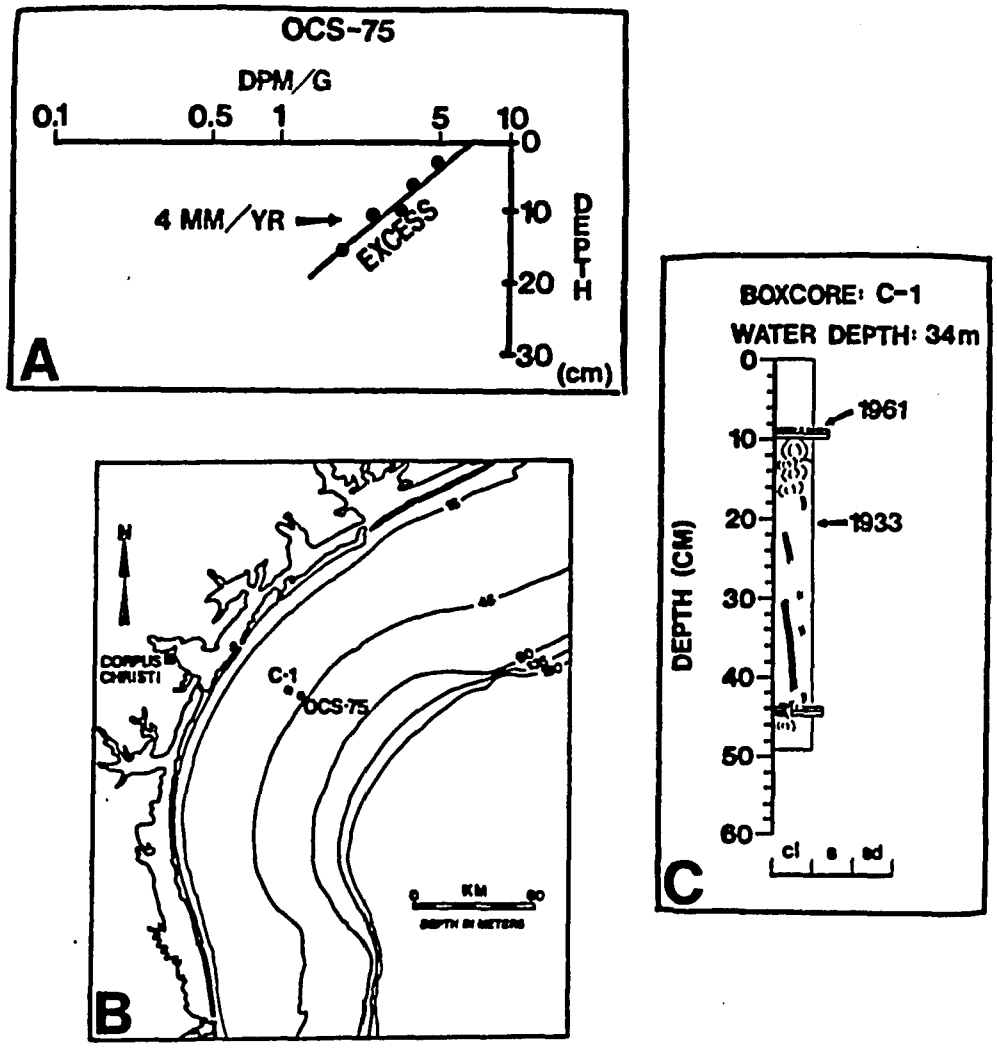

Fig. 30.--A) Distribution of excess Pb-210 in OCS-75 (from Holmes and Martin, 1977). B) Location of boxcore C-1 relative to OCS-75. C) Inferred absolute dates of beds in C-1 using sediment accumulation rates from OCS-75.

sand is not. Fig. 31 shows the radiograph of this core.

The sediment accumulation rates and absolute dates yielded by the Pb-210 procedure provide a direct answer to the question of the preservation potential of the discrete sand beds and the "Carla" sand bed in particular. As mentioned, there has been some suggestion that the sand deposited by Hurricane Carla in 1961 did not survive the successive years of infaunal activity (Dott, 1983). Yet the Pb-210 data indicate otherwise. However, correlation of the "Carla" bed in towards shore, where bioturbation is much higher, reveals that the Carla bed indeed may have have been destroyed. Again we see a depth-control upon the discrete sand layers and the sedimentary record of the CTCS area.

Discussion

Study of the sedimentary features of the discrete sand beds has revealed a number of findings which are relevant to the questions of sand source, transport pathway, transport mechanism, and preservation potential. These findings allow some inferences to be made.

Sand Source--Seaward fining is indicated by grain size analysis of a bed dated as forming in 1961-1962 (Fig. 26). This, plus the well-sorted nature of the sand faction, suggests that the coast is a likely source for the clastics found in this and other discrete sand beds. Indeed, the shoreline is the closest source. This is supported by shape analysis of sand grains from selected sand beds (Mazzullo, unpub. data, Table 4), which shows a predominance of grains from what is referred to as the "Texas Coast Province" (Mazzullo and Withers, 1984). These sands were originally derived from the drainage basins of the

Fig. 31.--Radiograph of boxcore C-1 (34 m water depth).

(next page)

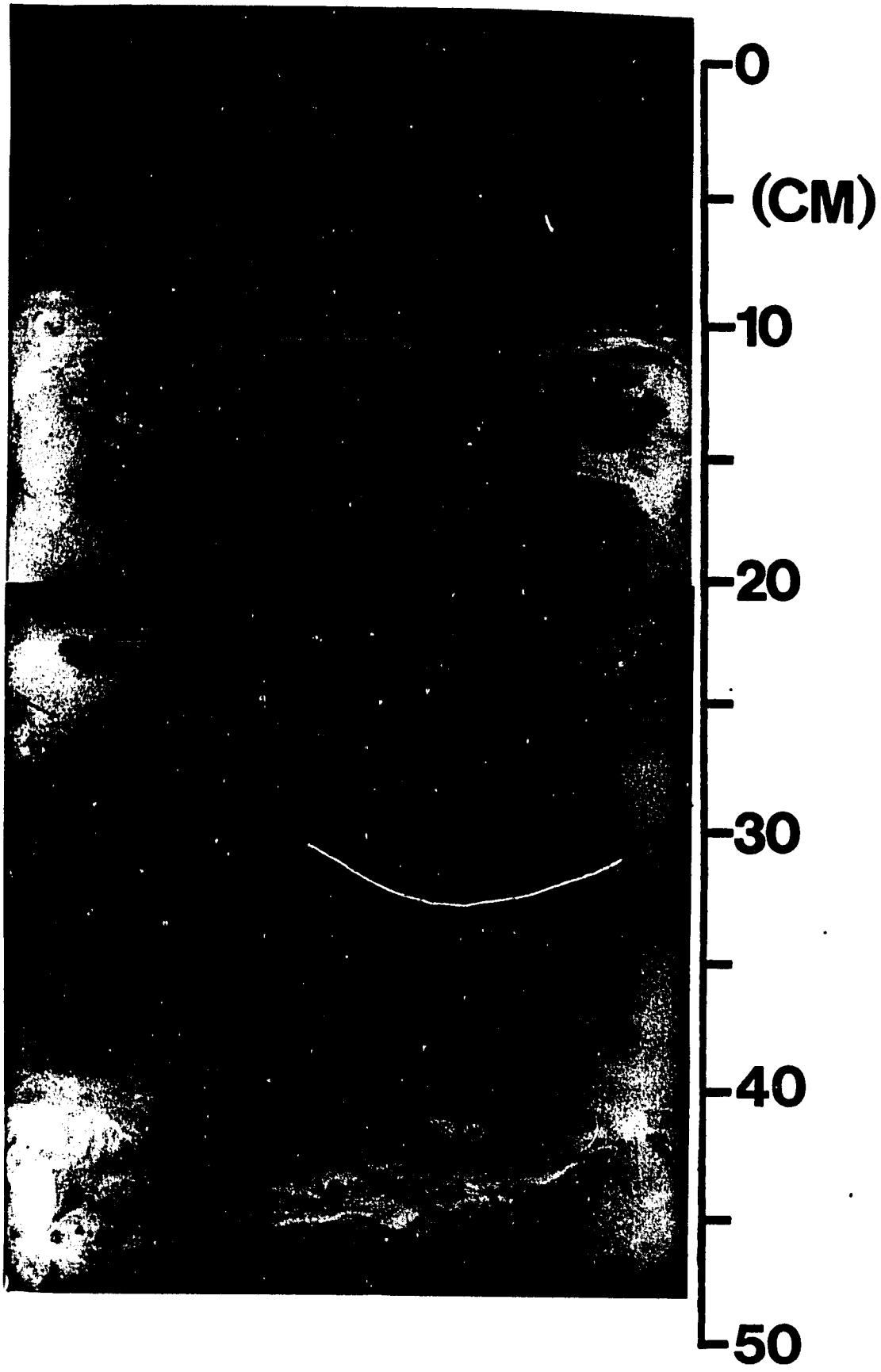
0
(CM)
10
20
30
40
50

TABLE 4.--Grain shape analysis of sand samples of selected cores[1]

Boxcore	Water Depth	Core Depth	Province
CB-8	24 m	9-10 cm	Texas Coast
CB-8	24 m	20-24 cm	Mixed Texas Coast/Brazos-Colorado
CB-6	25 m	9-10 cm	Texas Coast
CB-5	25 m	20-25 cm	Texas Coast
CB-5	25 m	34-35 cm	Texas Coast
AB-1	15 m	0-3 cm	Texas Coast
AB-1	15 m	7-8 cm	Texas Coast

[1]From Mazzullo, unpubl. data, 1985.

South Texas coastal plain rivers. The grain suite is typified by high percentages of multi-cyclic grains, a finding which is supported by SEM observation of inherited surface features (Fig. 21a). Only in one sample is there any indication of a Brazos-Colorado source and no samples contained any Rio Grande source material.

However, the category of the "Texas coast" is sufficiently broad to warrant further investigation. There are several possible sources of sand, including the shoreface, the beach, the ebb-tidal deltas associated with tidal inlets (specifically Aransas Pass), and the back-barrier environment. During a storm, the shoreface, ebb-tidal delta and the beach are all under attack by waves and currents. The back-barrier environment could yield sand to storm-surge ebb currents across the barrier (Hayes, 1967) or to ebb flow out of Aransas Pass. However, numerical calculations by Maynard and Suter (1983) indicate the flood currents across the Texas barrier islands during Hurricane Allen (1980) were far stronger than the ebb-currents. In addition, Maynard and Suter (1983) pointed out that high-profile barrier islands such as Mustang Island do not show the numerous hurricane-cut channels so typical of the low-profile barriers such as Padre Island; interdune fans, which are typical flood-oriented features, are the main geomorphic results of hurricanes. This leaves the ebb-flow out of Aransas Pass and the intermittantly active tidal inlets at the south end of Mustang Island as the only possible pathways of sand from the lagoon into the Gulf. The reactivated tidal inlets (Newport, Corpus Christi, and 1852 Pass) at the south end of the island were not considered in this analysis as Maynard and Suter (1983) and Jordan et al., (1981) found that the majority of the sedimentary features in that area asso-

ciated with Hurricane Allen to be flood-oriented.

Simple calculations were performed to identify which of the four sources was quantatively the most significant (Fig. 32). A 1080 km^2 area centered upon Aransas Pass was selected for analysis. The horizontal dimensions of the unvegetated areas listed by White et al., (1983) as containing >75 % sand were measured. This included the areas adjacent to the tidal pass and various channels. The available beach area was assumed to be the foreshore, back beach and a small portion of the dunes. The measured areas are shown in Table 5. Clearly, the 2 km wide shoreface is areally the most important, by nearly a factor of three over the back-barrier zone.

This finding is consistent with the modern view of the shoreface as a zone of critical importance in relation to the coastal sand budget (Swift et al., 1985). On the Atlantic coast, erosional shoreface retreat is thought to play an important role in the long term evolution of the shelf surface (Swift et al., 1976; Swift et al., 1978). It is also probable that the shoreface in the CTCS area is important in the shorter term development of the discrete sand beds.

Transport Pathway--A number of the boxcores were correlated in along-shelf and cross-shelf transects (Fig. 33). Fig. 34 shows an along-shelf cross-section which connects cores CB-5 and CB-3, the ones dated with PB-210. The dashed line traces the base of the bed deposited in 1961-1962, probably during Hurricane Carla. When one considers the relative sizes of the distances (31 km) and thicknesses (0-6 cm) involved, it is apparent that the "Carla" sand displays remarkable along-shelf continuity. However, it thins to the southwest in the area of CB-3.

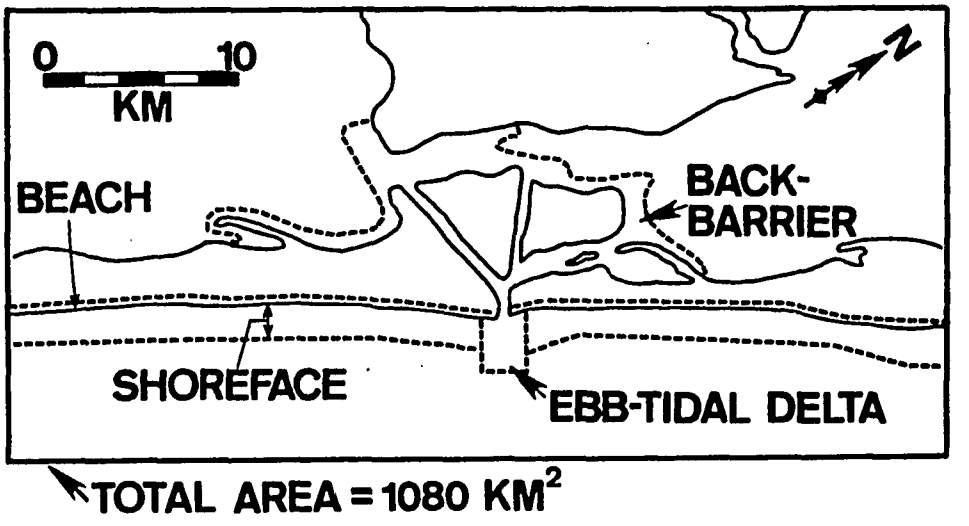

Fig. 32.—Location of areas specified in text as possible sand sources. (Table 5).

TABLE 5.--Comparison of Possible Coastal Source Areas

Environment	Area
Shoreface	90.0 km^2
Back-Barrier	37.5 km^2
Ebb-tidal Delta	6.0 km^2
Beach	4.5 km^2

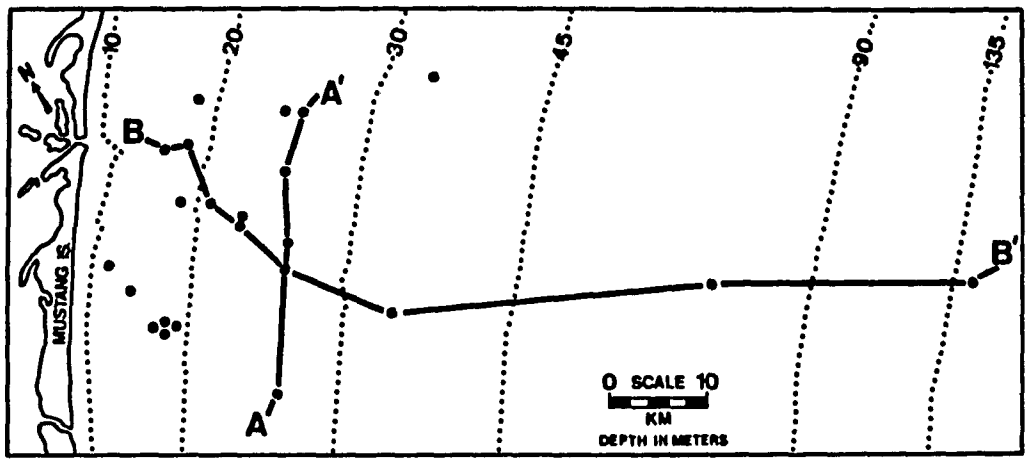

Fig. 33.--Location of cross-sections A-A' and B-B'.

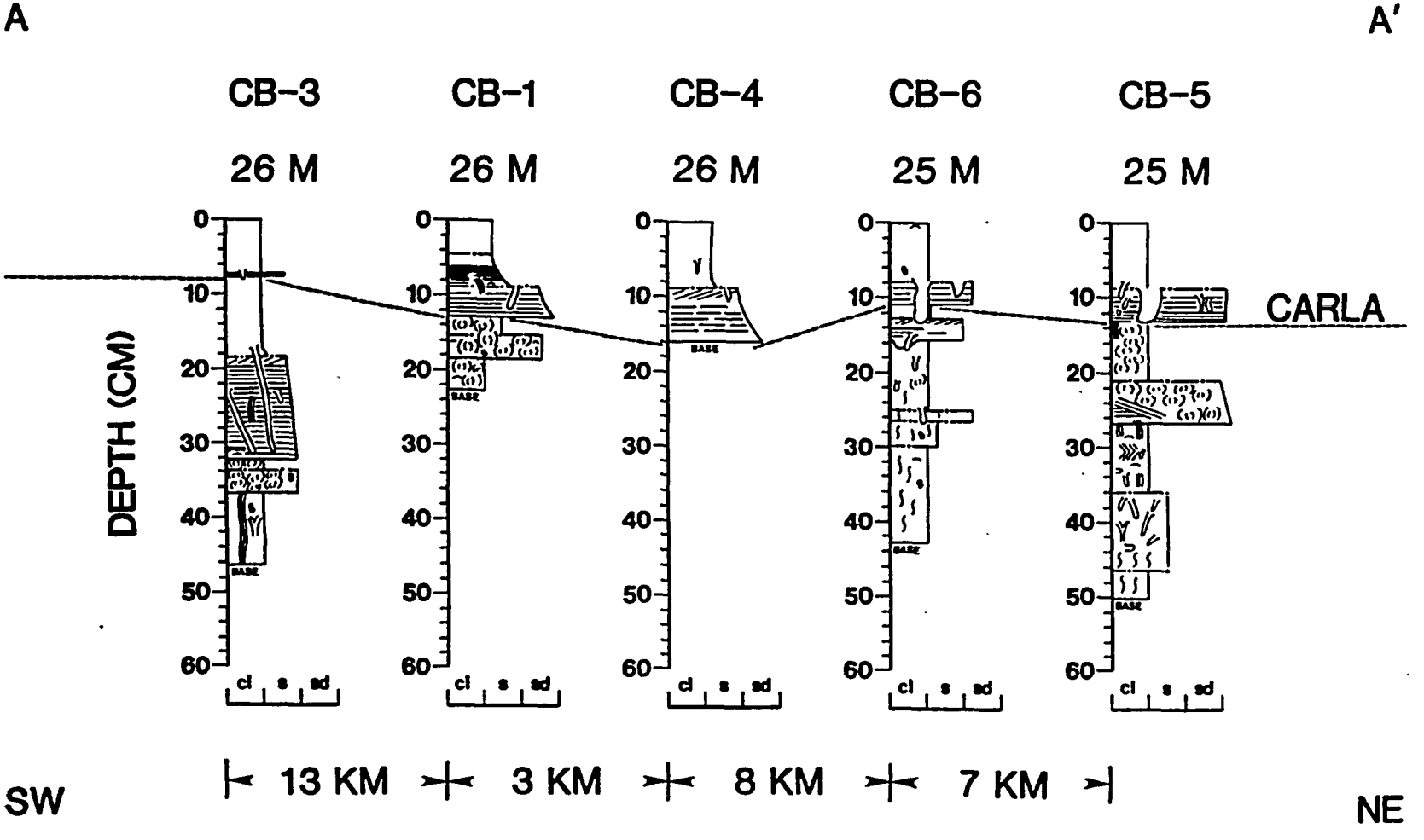

Fig. 34.--Along-shelf cross-section A-A´.

A cross-shelf section (Fig. 35) shows that the Carla sand generally decreases in thickness in an offshore direction, although there are some spatial differences in thickness. Correlation of this bed into water depths shallower than 20 m is tenuous, due to the intense bioturbation and increasing number of truncations in the sedimentary section.

An effort was made to correlate the Carla bed laterally along-shelf from the CTCS study area (Fig. 36). Forty km to the southwest is the area where Hayes (1967) discovered surficial sand deposits following the passage of Hurricane Carla in 1961 (Fig. 1). In between and overlapping the study site of Hayes (1967) were a number of gravity cores taken by the USGS and reported in Berryhill et al., (1976, 1977). Sand thicknesses reported by Hayes (1967) and Berryhill et al., (1976, 1977) (as well as sand thicknesses in cores taken in the same area by the author in 1985) were compared, allowing estimation of the amount of compaction that has occurred in the 13 years between the two studies. Using this as a guide, the thicknesses given by Hayes (1967) were adjusted in order to facilitate direct correlation with the boxcores taken in the CTCS study area. There is, of course, some degree of uncertainity when one compares measurements from three different coring devices (Phleger, gravity and boxcores) taken over a 22 year period. However, the zero isopach line (the presence or absence of sand) can be considered quite valid.

Isopach mapping of the net sand thickness further emphasizes the along-shelf continuity of the Carla sand (Fig. 36). Although the map shows noticeable variations in thickness (0-7 cm), these differences are relatively minor in the context of the large distances involved (120 km). The Carla bed appears to thin in the offshore direction

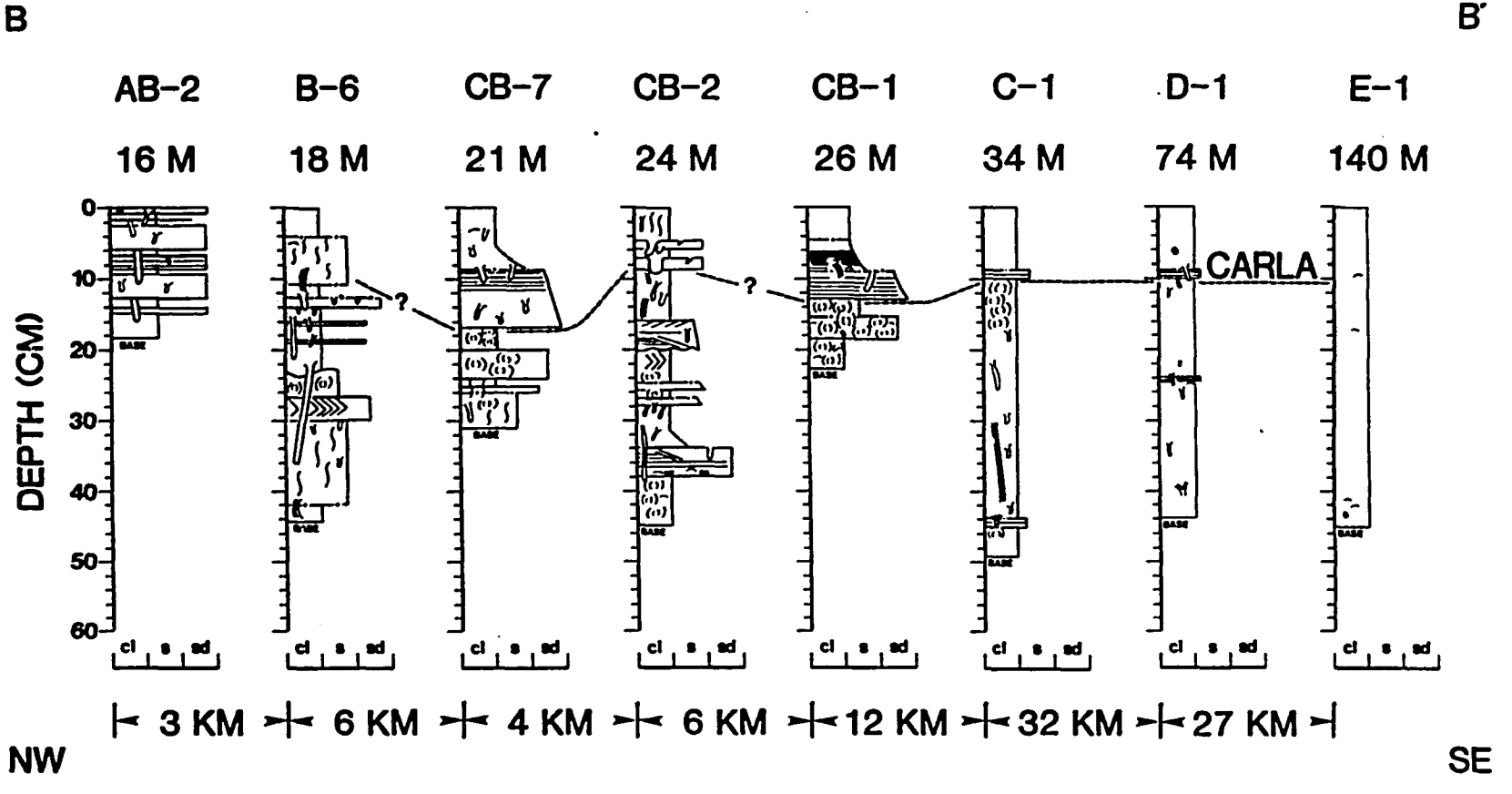

Fig. 35.--Cross-shelf cross-section B-B'.

Fig. 36.--Isopach map of net Carla sand. Contour interval equals 2 cm. Data of Hayes (1967) adjusted for changes in thickness due to compaction as determined by comparison with cores taken in the same area by Berryhill et al., (1976) and by the author in 1985.

(next page)

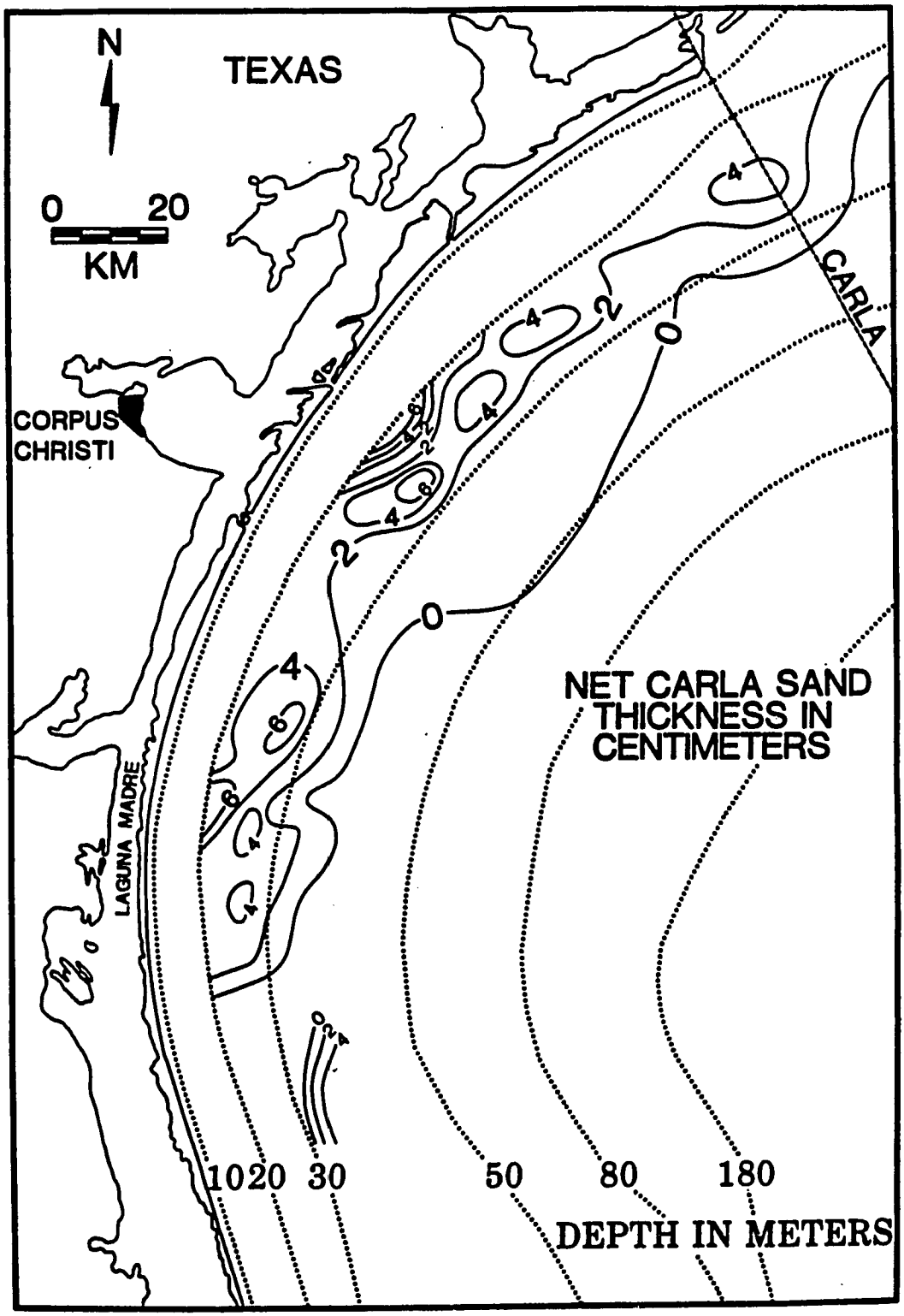
N
TEXAS
0 20
KM
CARLA
CORPUS
CHRISTI
LAGUNA MADRE
NET CARLA SAND
THICKNESS IN
CENTIMETERS
10 20 30 50 80 180
DEPTH IN METERS

(compare with Fig. 35). As mentioned, identification of the Carla sand landward of 20 m was hindered by the intense biological reworking and physical truncation of the sedimentary section.

Any transport pathway which is proposed for the Carla sand must take into account its seaward size-grading and tremendous along-shelf continuity. A purely shore-normal pathway does not satisfy the latter nor does an entirely along-shelf motion explain the former or the seaward thinning trend. However, a southerly path at an oblique angle to the bathymetric contours is consistent with these observations. This kinematic reconstruction for the Carla sand, to some degree, parallels the pathway suggested for surficial sediments by Shideler (1978) and Mazzullo and Withers (1978).

Transport Mechanism--As stated, the three mechanisms hypothesized to be responsible for the formation of the Carla sand are turbidity currents (Hayes, 1967), wind-forced currents (Morton, 1981), and geostrophic currents combined with wave orbital motion (this study). Many of the observed features, such as sharp basal and gradational upper contacts, asymmetrical ripples, plane beds, and vertical and offshore size-grading, are consistent with all three interpretations. However, the along-shelf continuity of the Carla sand (Figs. 34 & 36) does not fit the typical dip-trending pattern shown by deposits of turbidity currents (e.g. Berg and Tedford, 1977).

Hayes (1967) also inferred a close association between hurricane-cut channels on Padre Island and the thickest beds deposited after Hurricane Carla. As stated previously, barrier islands in and adjacent to the CTCS area possess a large, continuous foredune ridge which prevents the formation of numerous channels. The only areas where lagoonal

waters could return to the Gulf by a storm surge ebb is through the active tidal inlets (such as Aransas Pass) or the reactivated tidal inlets (such as 1852, Corpus Christi Pass, etc.). Isopach mapping of the net Carla sand thickness indicates that there is little relation ship between these shoreline features and offshore sand trends.

Thus, the available sedimentologic evidence suggests that the turbidity current hypothesis of Hayes (1967) is invalid. These findings agree with the morphological evidence provided by Morton (1981) that the storm-surge ebb flow after Hurricane Carla was not responsible for the discrete sand beds. Morton (1981) also proposed that wind-forced currents during Hurricane Carla were responsible for deposition of the sand. Specifically, Morton (1981) argued that during Carla the shelf waters comprised a single water layer driven solely by the wind. Unfortunately, the geologic information gathered from study of the box-cores is not precise enough to be able to differentiate between this mechanism and the working hypothesis of this study, which holds that the steady current flow (driven by the geostrophic balance of forces) and the oscillatory wave orbital motion interact near the sea bottom boundary to force sediment transport. For example, the asymmetrical ripple structures observed at the top of many of the beds could have originated under unidirectional current flow or under conditions of combined wave and current interaction (Reineck and Singh, 1975). Discrimination between the two requires detailed study of the kinematics and dynamics of fluid motion in the CTCS area. This encompasses the next chapter of this dissertation.

Preservation Potential--The absolute dating by Pb-210 techniques confirm that the sand deposited by Hurricane Carla in 1961 and described

by Hayes (1967) is present in varying degrees of preservation throughout the CTCS area. This contrasts with the opinion of Dott (1983) who felt that the "Carla sand" had not survived the infaunal activity so typical of the shelf area. The apparent relationship between the degree of bioturbation and the thickness of the bed suggests that thicker beds will be preferentially preserved over thinner beds (Fig. 34). The cross-shelf transect shows a decrease in the thickness of the beds with increasing water depth (Fig. 35). Beyond 50 m or so, it is debatable whether the bed could be recognized in an outcrop or core. This, combined with the landward increase in bioturbation, tend to result in a "window of preservation" between 20 to 50 m water depth. It is in this depth range that the typical sedimentary sequence and internal structures (Fig. 14b) of these discrete sand beds are so clearly visible.

CHAPTER 3

KINEMATICS AND DYNAMICS OF SEDIMENT TRANSPORT ON THE CENTRAL TEXAS CONTINENTAL SHELF

Continental shelves have often been categorized as either tide- or storm-dominated (Swift and Niedoroda, 1984). In the former, bottom sand transport can occur with nearly every tidal cycle. An example is the shelf off the coast of Holland (McCave, 1971). When wind-driven currents are present, however, they often augment the diurnal and semi-diurnal tidal flow (Caston, 1976).

However, the majority of the world's shelves fall into the latter category (Swift and Niedoroda, 1984). With tidal current speeds less than 20 cm/sec, sand transport generally occurs during infrequent, short duration storm events. An example is the Atlantic shelf offshore from New York where Lavelle et al., (1978) monitored sand movement with radio-isotope tracers. They found that the bulk of the sand transport during a 135 day period took place during a storm of two days duration. The kinematics of fairweather and storm transport can also differ considerably on these shelves; Adams et al., (1982) discovered that storm-driven motion on the central Louisiana shelf is eastward, in contrast to the westward "fairweather" current flow.

With typical tidal current amplitudes of less than 10 cm/sec, the Texas continental shelf is considered a storm-dominated shelf (McGrail and Carnes, 1983). Both cold-frontal passages and tropical storms affect the area. Cold-frontal passages are associated with the trailing margins of wave cyclones which migrate across the midwestern states (Lutgens and Tarbuck, 1979). Approximately 60 fronts pass through the CTCS area each year (Dimego et al., 1976). Wind speeds associated with

these frontal passages are variable but seldom exceed 15 m/sec (Crout, 1983). Tropical storms, which can originate in the Atlantic, Caribbean or the Gulf of Mexico itself, are more infrequent but are more intense. Wind speeds associated with hurricanes average at least 33 m/sec and are often greater than 56 m/sec (Nummedal, 1982). Hurricane frequency is highly dependent upon the sea surface temperature distribution, upper level winds, and other climatic factors (Wendland, 1977; Anthes, 1982). An average of 0.64 hurricanes per year affect the Texas-Louisiana coast (Nummedal, 1982).

Both tropical cyclones and cold fronts are impulsive forces whose winds provide momentum to the sea surface and ultimately to the sea bed in the form of elevated current velocities. In addition, the wind fields are responsible for dramatic increases in wave height and period. This in turn is applied to the sea bed in the form of oscillatory currents.

It seems intuitively obvious that the size of a storm should be inversely proportional to its frequency. This is supported by numerous storm wave hindcast studies in which wave parameters such as height and period are plotted against the probability of occurrence (e.g. Fig. 37a). But the semi-logarithmic plots for the Gulf of Mexico also tend to show a flattening-out of wave dimensions near 100 years. This flattening is due in part to the limits of the historical data upon which storm wind strength, duration, and central pressure are based (Bea, 1974). However, numerical modeling suggests that storm wave parameters may reach a maximum at 100 years because the storm magnitude, a function of its size, duration, wind speed, and other factors, may flatten out. This is thought to be due to certain environmental

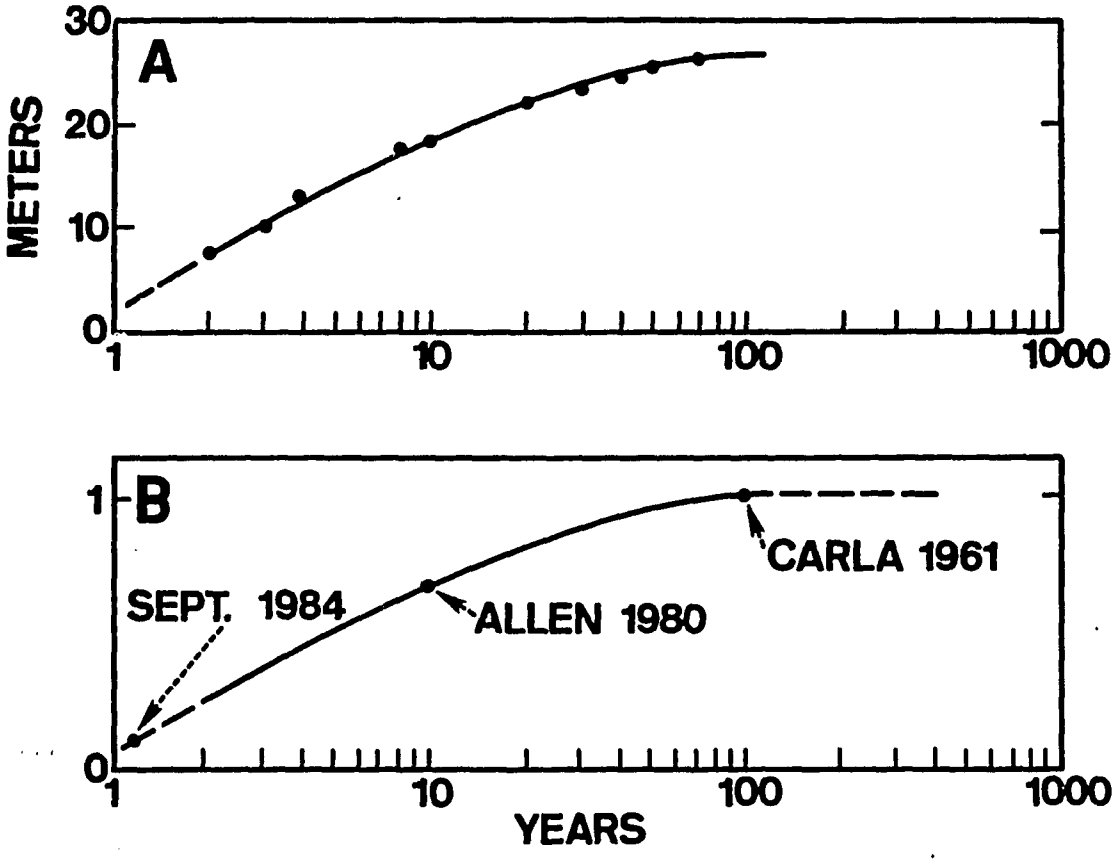

Fig. 37.--A) Hindcast maximum expected wave height for the Gulf of Mexico (modified after Bea, 1974). B) Hypothetical relative storm magnitude.

constraints such as the maximum surface water temperature, the size of the Gulf, atmospheric conditions, etc. (J.D. Smith, pers. comm.). Fig. 37b shows a hypothetical plot of storm magnitude versus recurrence interval. In the Gulf of Mexico, the long end of the spectrum tends to be occupied by hurricanes (Patterson, 1972).

Thus, it appears that there is a spectrum of storms running from those which can be observed once or twice a year to the largest occurring once every 100 years. After some introductory sections, this spectrum will be examined closely, beginning with a discussion of fairweather conditions in the CTCS area, followed by data from an extratropical storm of September of 1984, a typical once-a-year event. The succeeding section will involve Eulerian measurements made during Hurricane Allen, a larger storm, whose recurrence interval is likely to be 5-10 years. This data will allow extrapolation to hurricane Carla, a storm whose magnitude literally defines the 100 year storm. Particular emphasis will be placed upon the kinematics and dynamics of sand transport during these events. Study of the kinematics allows understanding of the transport pathway; analysis of the dynamics and timing of forcing during these storms facilitates discrimination between the transport mechanisms proposed by Hayes (1967), Morton (1981) and this study.

Relevant Oceanographic Principles

General concepts of fluid motion in the coastal ocean are founded upon Newtonian mechanics (Csanady, 1982). In particular, Newton's second law (in the case of a rotating coordinate system) provides a physical basis for a vector form of the equation of motion:

$$dV/dt = (-\alpha \nabla p) + (-2\Omega \times V) + G + F$$

where dV/dt is the acceleration of a unit mass due to the accumulated effects (per unit mass) of the pressure gradient force ($-\alpha \nabla p$), the Coriolis force ($-2\Omega \times V$), gravity (g) and frictional forces (F). α is the specific volume (reciprocal of the fluid density), ∇p is the gradient of pressure, and Ω the angular velocity of the earth (0.73×10^{-4} sec^{-1}) (Von Arx, 1962). The above form of the equation of motion can be further broken down into three component equations for the x, y, and z axes (Pond and Pickard, 1983). These Eulerian expressions are generally expanded into fixed (local) and moving (advective) parts (Von Arx, 1962).

In his study of wind-forced currents, Ekman (1905) neglected all the terms save that of the Coriolis and frictional forces (per unit mass). Further, by making a number of broad assumptions such as that of an unbounded, infinitely deep, homogeneous ocean, Ekman (1905) derived the now familiar spiral of currents (Fig. 38). Surface flow is 45^{o} to the right of the wind stress and currents decrease and rotate clockwise away from the air-sea boundary (in the northern hemisphere). The layer of fluid in which the spiral acts is known as the surface Ekman layer (McLelland, 1965). Representing a large portion of the upper boundary layer (Fig. 39, inset), the surface Ekman layer should be differentiated from what is known as the wind-mixed layer, a zone which depends more on the wind history and stratification in an area (Pollard et al., 1973).

Prior to Ekman's (1905) work, it was well known that the distribu-

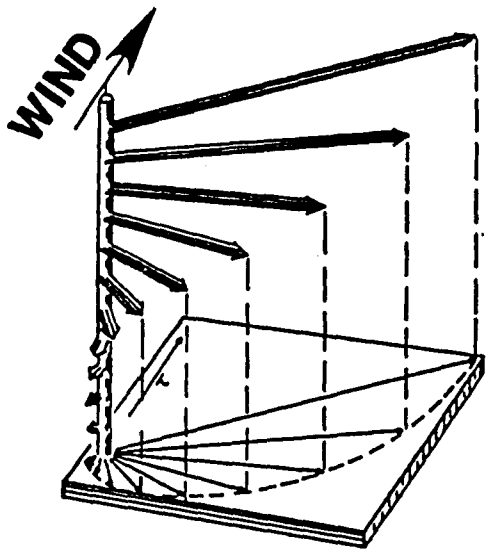

Fig. 38.--Vertical structure of horizontal velocity in a purely wind driven current according to Ekman (1905) (from McLellan (1965).

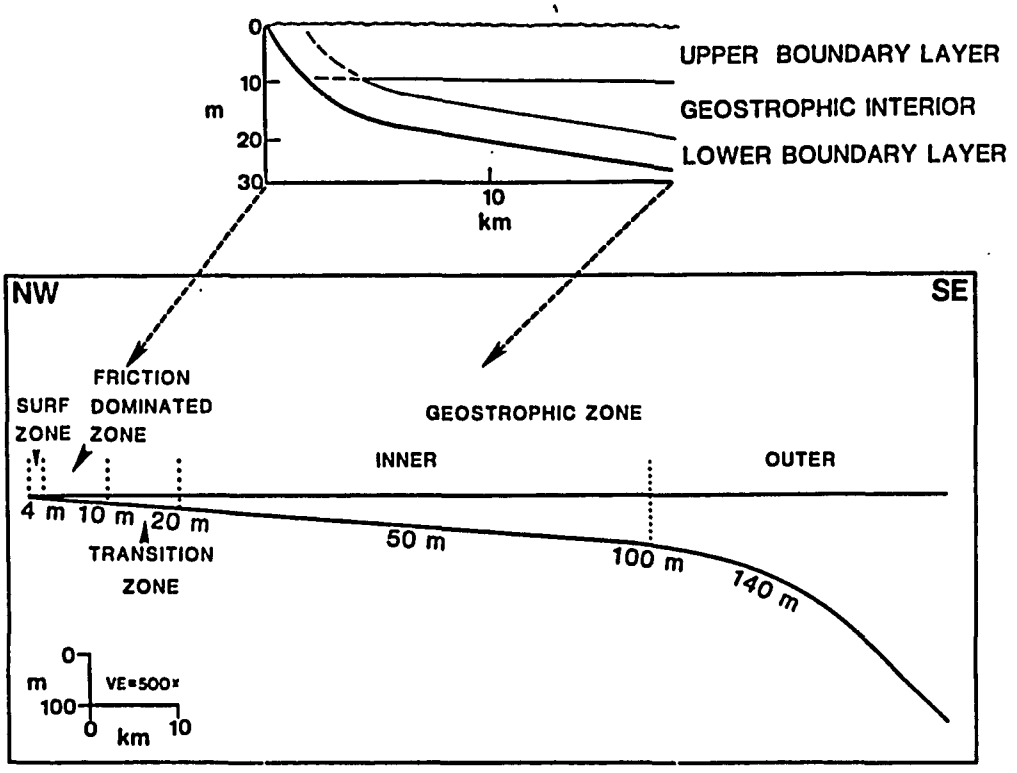

Fig. 39.--Coastal ocean dynamic zones in the CTCS area. Inset shows an expanded view with schematic representation of boundary layers and frictionless (geostrophic) interior described in text. It should be noted that depths and areal distributions are not fixed points in space but depend upon the dynamics of the coastal ocean during fairweather and storm conditions (from Mooers, 1976; Swift and Niederoda, 1984).

tion of mass within the ocean gave rise to motion. An important consideration in this distribution of mass is the sea surface slope and the ensuing pressure gradient. By making the assumption that the pressure gradient, gravitational, and the Coriolis accelerations are the only accelerations involved in fluid motion, the geostrophic motion was recognized (Beer, 1983). Although the geostrophic assumption is never more than approximately correct, it does adequately describe motion in portions of the water column distant from the boundaries, a region known as the geostrophic or frictionless interior (Fig. 39; McLelland, 1965).

However, the assumption that the frictional forces are negligible is invalid in geophysical fluid boundary layers. For example, in the boundary layer located at the base of the shelf water column (the benthic boundary layer), the no-slip condition requires that fluid motion halt in the vicinity of the bottom. This results in considerable shear, both in terms of current direction and speed (Pond and Pickard, 1983; Fig. 40A). The shearing of fluid past the boundary generates geophysical turbulence. Turbulent fluctuations become embedded in the larger-scale flow, draining the flow of energy and passing it to finer scales of motion where viscosity can act directly (Pedlosky, 1979). Turbulent stresses and the character of the boundary to some extent determine the structure of the benthic or lower boundary layer (Fig. 40B). A typical shelf lower boundary layer consists of an inner layer, which shows large velocity shear, and an Ekman-like outer layer (Adams and Weatherly, 1981). Under some conditions, a logarithmic profile in current speeds increasing upward from the boundary can occur in the inner layer (hence the name). The overlying Ekman layer

Fig. 40.--A) Schematic representation of veering of current vectors through the lower boundary layer. X-axis oriented along-shelf, positive to the southwest. Y-axis oriented cross-shelf, positive to the southeast. V_g is the geostrophic (interior) velocity vector and τ_c is the bottom stress vector. B) Idealized diagram of an oceanic benthic boundary layer (BBL) with a rough bottom. Z is height above bottom in meters, positive upwards. Log. layer is the logarithmic layer (modified from Pedlosky, 1979). It should be noted that layer thicknesses are approximate, in reality are a function of the dynamics of flow, water column stratification, and suspended sediment concentration gradients. A viscous sublayer may be present in cases of a smooth to transitional bottom.

(next page)

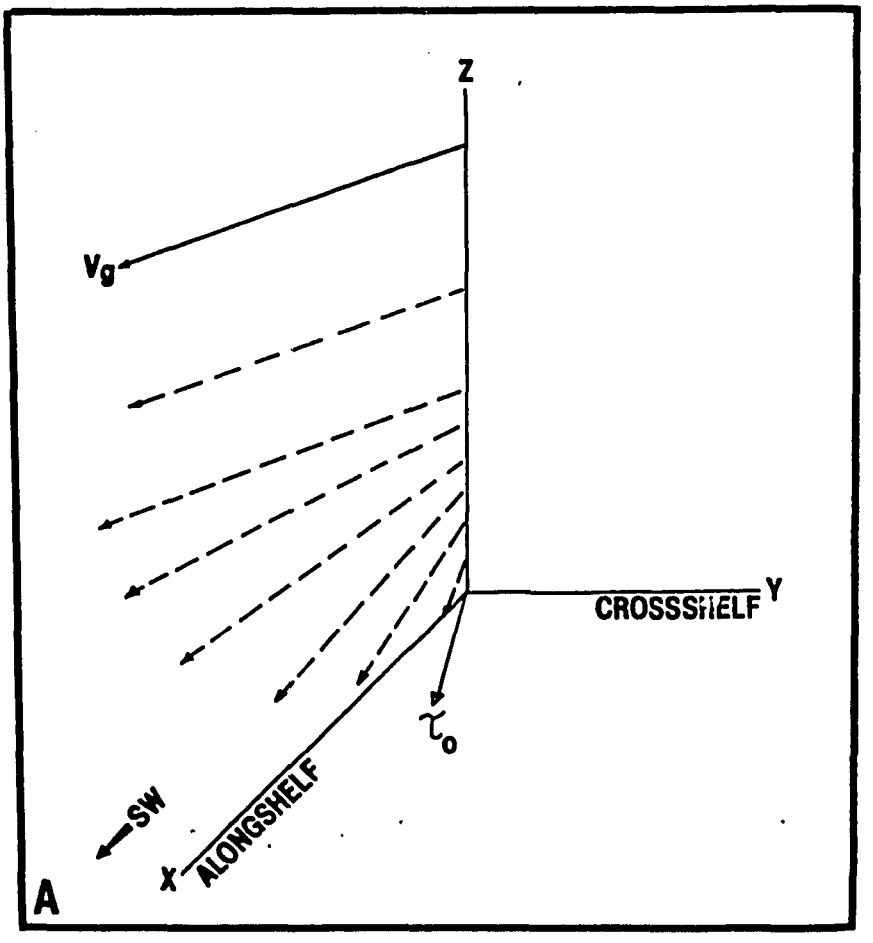
z
V_g
CROSSSHELF
Y
τ_o
SW
X
ALONGSHELF
A

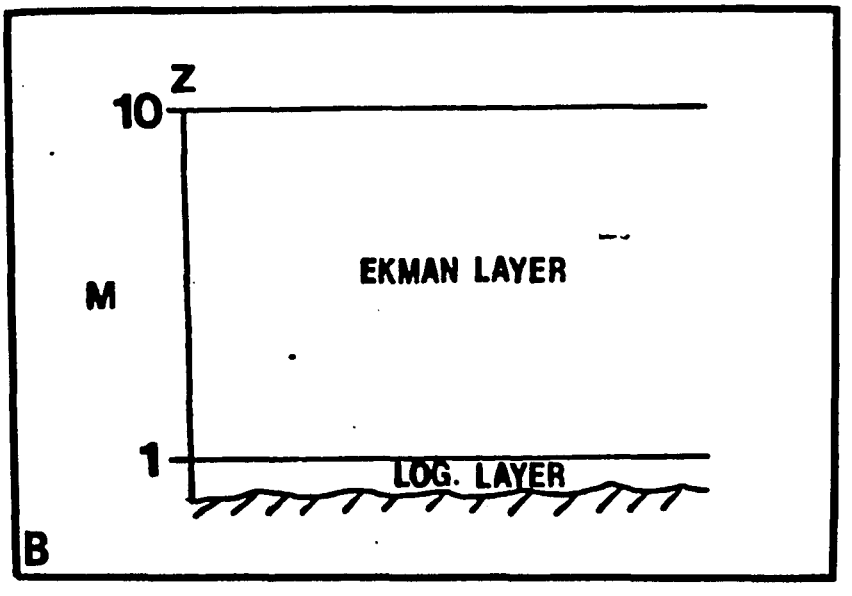
10
z
EKMAN LAYER
M
1
LOG. LAYER
B

often exhibits considerable directional shear, although there have been reports of veering in the logarithmic layer (e.g. Weatherly, 1972). The amount of turning in the Ekman layer (expressed as the angle between the geostrophic velocity vector, Vg, and the bottom stress vector) is known to be a function of a number of variables, including the geostrophic velocity, the water column stratification, and the suspended sediment concentration gradient (Weatherly, 1972; Kundu, 1976; Weatherly and Van Leer, 1972; Adams and Weatherly, 1981).

Mooers (1976) and Swift et al., (1985) present a qualitative framework for for the description of fluid motion on a storm-dominated continental shelf (Fig. 39). In this system, four shore-normal zones, the surf, friction-dominated, transition, and geostrophic zones, extend across the shelf. The surf zone, which will not be included in this dissertation, is the area where the radiation stress of shoaling and breaking waves generates littoral longshore currents. The friction-dominated zone can be considered to be an area where currents tend to flow parallel to the forcing mechanism (such as the driving wind stress). Due to the shallow depth, friction dominates and there is little directional shear. The lack of rotation has been attributed to the overlap of the upper and lower boundary layers (Swift and Niedoroda, 1984). During episodes of elevated wind stress the flow takes on the characteristics of a well-stirred, non-rotational "slab" driven by the wind (Csanady, 1982). In such situations, the majority of the velocity shear is concentrated near the bottom. This zone is confined to areas where the water depth is less than 1/10 the Ekman depth (Pond and Pickard, 1983). Near-bottom wave orbital motion is also important in this zone as waves feel bottom in both fairweather and storm condi-

tions (Madsen, 1976).

In the geostrophic zone (and to some degree the transition zone), there is significant separation between the surface and bottom boundary layers (Fig. 39). Momentum imparted to the sea surface is not directly expended against the bottom. Instead, motion in the frictionless interior is responsive to the sea surface slope, as manifested in the pressure gradient force. However, low frequency (long period) motion tends to be in geostrophic balance with the Coriolis force and flow is often directed along-shelf. As mentioned, flow near the sea bottom boundary departs from this balance (ageostrophic flow). The main difference between the inner and outer portions of the zone is that the outer areas are affected by oceanic circulation, such as western boundary currents and rings and eddies which spin off those currents (Kirwan et al., 1984).

The transition zone adjoins the friction-dominated and the geostrophic zones (Fig. 39). As the name suggests, it displays aspects of both zones. It can also be the site of interesting flow patterns set up by the convergence or divergence of bottom and surface flow from the adjacent zones (Swift and Niedoroda, 1984).

A qualitative description of the structure of fluid motion during cases of coastal downwelling and upwelling is presented in Swift and Niedoroda (1984) (Fig. 41). In the downwelling case, northerly along-shelf winds blow down a north-south trending coastline. Surface water transport in the upper boundary layer is driven to the right of the applied wind stress, up against the coastal boundary (Fig. 41A). Sea level set-up ensues, and a cross-shelf pressure gradient is formed

Fig. 41.--Idealized models for motion in surface boundary layer, geostrophic interior, and lower boundary layer as a function of wind-induced cross-shelf barotropic pressure gradient on a north-south coastline. A) North wind case (downwelling). B) Top, cross-section through coastal pressure field, showing reference level (dotted line) and bottom, balance of forces near bottom. C) South wind case (upwelling).

(next page)

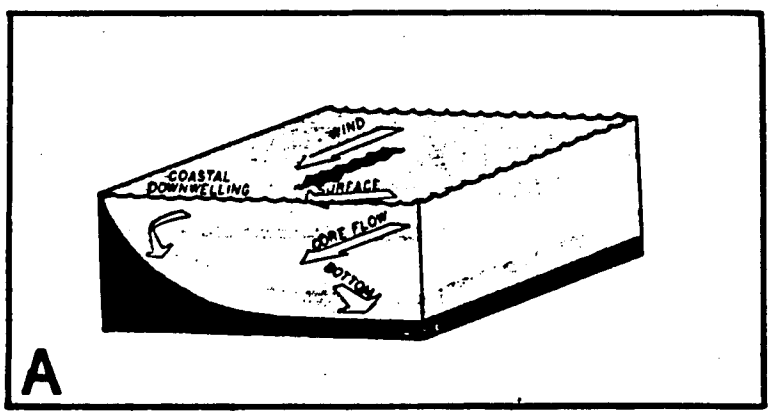
WIND
COASTAL DOWNWELLING
SURFACE
CORE FLOW
BOTTOM
A

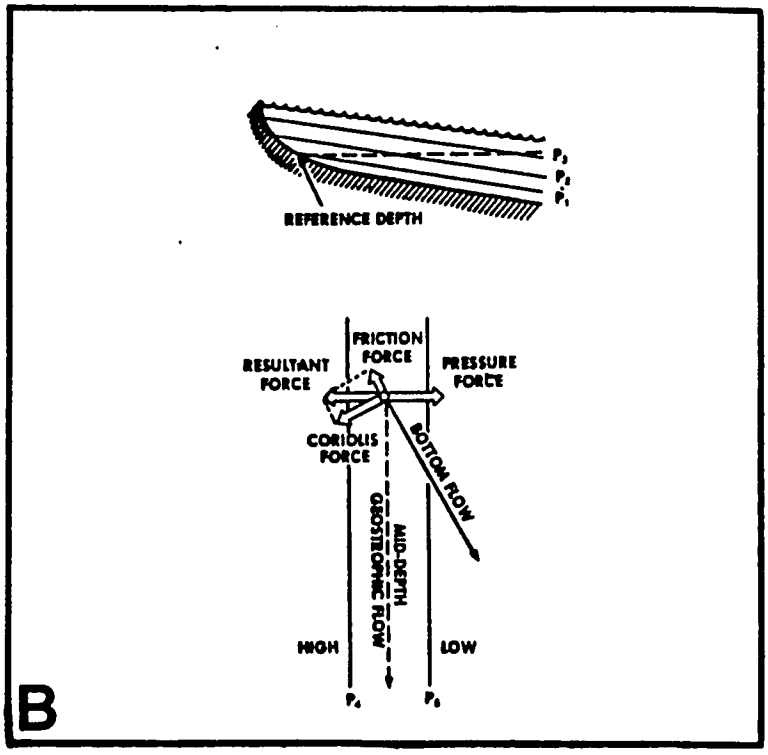
REFERENCE DEPTH
FRICTION FORCE
RESULTANT FORCE
PRESSURE FORCE
CORIOLIS FORCE
BOTTOM FLOW
GEOSTROPHIC FLOW
HIGH-HIGH
HIGH
LOW
B

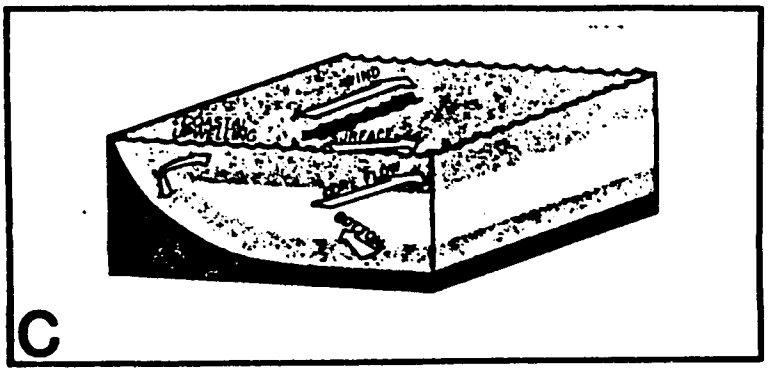
WIND
SURFACE
C

(Fig. 41B). Once the motion comes into geostrophic balance with the Coriolis force, motion in the frictionless interior is oriented alongshelf (Fig. 41B). However, in the ageostrophic lower boundary layer, directional veering of flow occurs. Turning is toward the left (as one looks toward boundary from above) or in this case in the offshore direction.

In contrast, the upwelling case is generated by southerly winds, surface flow away from the coastal boundary (sea level set-down), and core flow to the north (Fig. 41C). Bottom flow has a large onshore component, in part a compensation for the offshore surface flow (Swift and Niedoroda, 1984).

It should be remembered that these models are highly generalized. For example, winds are seldom linear as the models suggest (Lutgens and Tarbuck, 1979). However, when the scale of a storm matches the scale of the coastal boundary, this is correct to a first approximation. The degree of Ekman veering in the upper and lower boundary layers is dependent on a number of factors and under some conditions may be negligible (Weatherly, 1972; Beer, 1983). The low frequency motion presented in the models is strictly a function of the barotropic field of mass (where surfaces of equal water pressure, called isobars, are parallel to surfaces of equal water density, called isopycnals). In many cases, a baroclinic field of mass (where the isobaric and isopycnal surfaces are non-parallel) is superimposed upon the barotropic field (Csanady, 1976). However, it has been shown that during peak flow events in coastal settings distant from large freshwater influx centers (such as a delta), the barotropic field will dominate the baroclinic field (Lavelle et al., 1978). The models also do not discuss

along-shelf pressure gradients, which may augment or oppose the motion generated by the cross-shelf pressure gradient (Chase, 1979). Nonetheless, they do provide a convenient starting point for the discussion of fluid motion in the CTCS area.

General Oceanographic Setting

There appears to be a seasonal pattern to the wind stress and general circulation of the CTCS. Due to the almost year-round influence of the Bermuda High, the prevailing winds are southeasterly except for brief periods when during the fall and winter when the trailing edges of cold fronts intrude upon the area. Along the north-south trending portion of the Texas coast, the result is a general northerly flow (Smith, 1980a). Along the more east-west trending Louisiana and east Texas coasts the consequence is a westerly current. Clearly the two must converge somewhere. Drifter data suggest a convergence near 27° N latitude (Hill and Garrison, 1978). However, this convergence appears to be more of a net annual condition. What appears to be more typical of a specific area like that offshore from Mustang Island, Texas is a seasonal pattern where summer along-shelf current flow is to the north under the influence of southeast winds and to the south under more northerly winds associated with cold air outbreaks (Watson and Behrens, 1970; Smith, 1975). In fact, it is well-known that that the most important factors in the general circulation on this shelf are the magnitude and orientation of the wind (Sturgis and Blaha, 1976; Cochrane and Kelly, 1982).

Other forces to consider in relation to general shelf circulation in the CTCS area are the anti-cyclonic rings which are known to pinch off

the Loop current and migrate westward toward the CTCS area (Elliott, 1982). Surface velocities associated with these features can get as high as 50 cm/sec. However, most of these rings appear to dissipate their energy on the Mexican shelf, well south of the CTCS study area (Kirwan et al., 1984).

Fig. 42 illustrates the nature of water column stratification during late summer months in the CTCS area. Typically, shelf surface waters (A) have a higher temperature (and thus lower density in σ_t units, where γ_c equals the seawater density in kg m^{-3} minus 1000.00) than do shelf bottom waters (B). This stable stratification extends across much of the shelf, except for shallow nearshore areas which can be unstratified, even in summer months. Nearshore stratification is often related more to the magnitude and timing of the influx of light fresh water from coastal river point sources (Fig. 44). The highest river discharge rates occur typically in the late spring, although heavy rains during other periods can occasionally cause high discharges such as seen in the Brazos valley during Fall of 1981. The late spring peak discharges of Texas rivers occur somewhat later than the maximum outflow of the Mississippi and Atchafalaya rivers. Smith (1980) noted from hydrographic measurements that a salinity minimum occurs at approximately the same time in shelf waters of the CTCS. However, by midsummer, the minimum disappears and temperature becomes the dominant parameter controlling water density. However, a late summer freshening of surface waters in the mid-shelf area was also recognized in the data of Smith (1980). This same freshening is present as a very low density layer (C) in hydrographic measurements at 74 and 140 m depths (Fig. 42). Lewis (1980) attributed this salinity decrease to westward

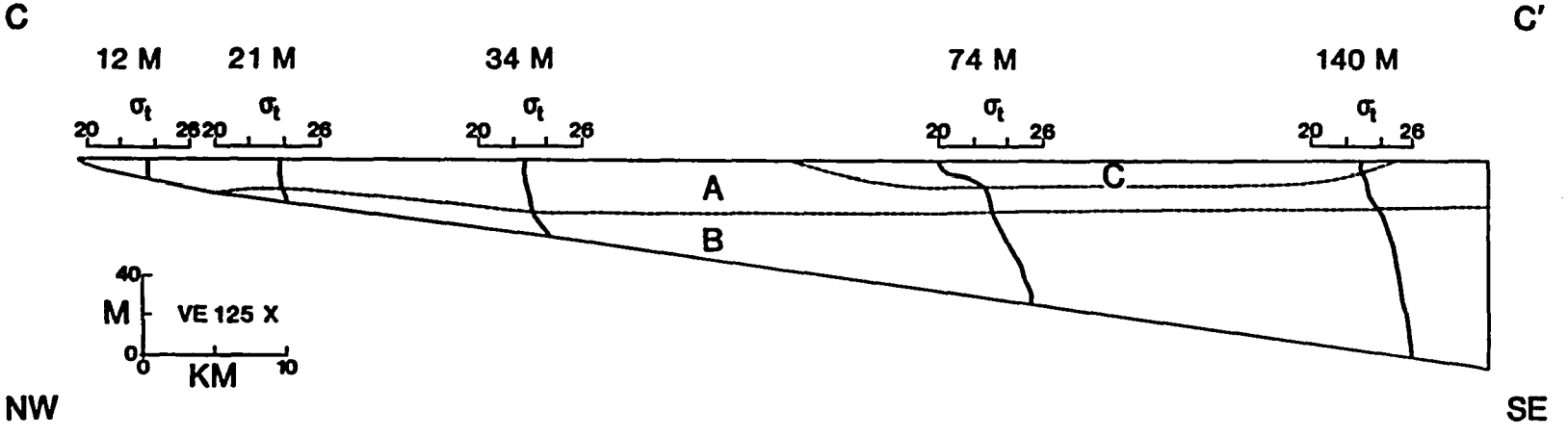

Fig. 42.--Water column density (in σ_t units) across the CTCS area as measured by a CTD probe from the R/V Longhorn July 16-17, 1984. A denotes low relative density shelf surface water, B is the denser shelf bottom water, and C the very light surface water advected from the Mississippi-Atachafalaya River deltas.

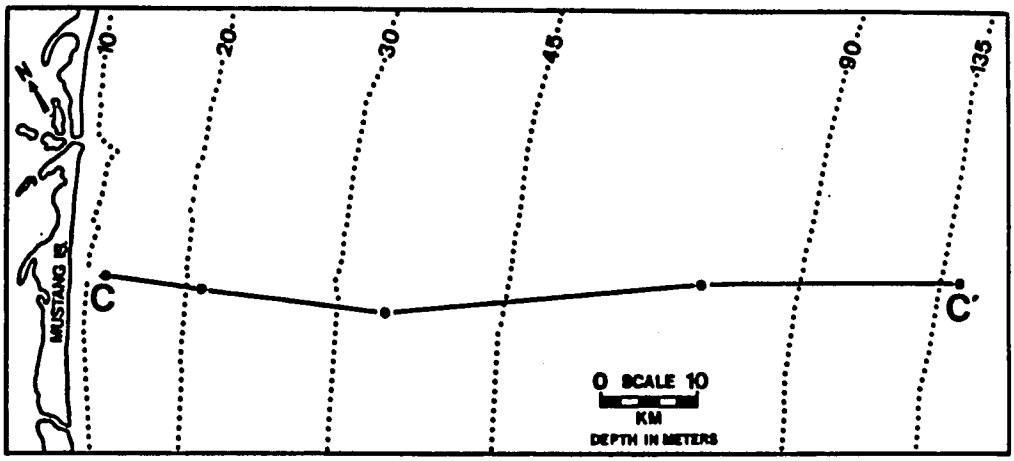

Fig. 43.--Location of CTD cross-section C-C′.

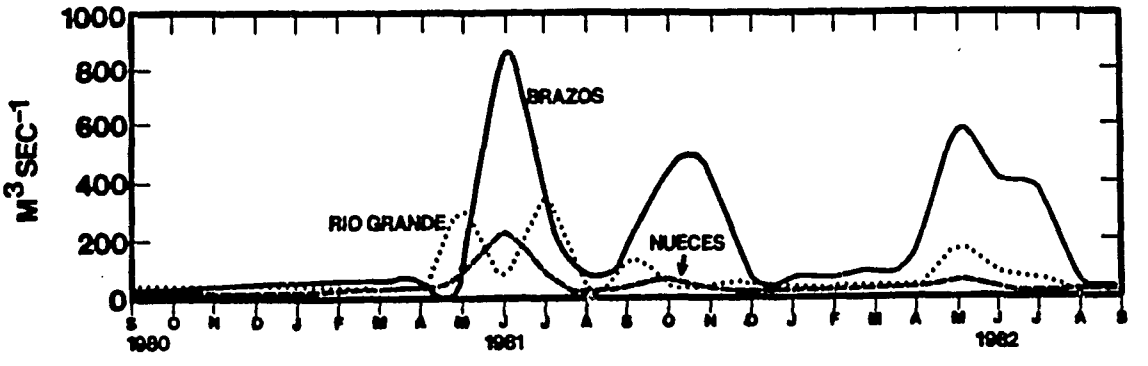

Fig. 44.--Monthly mean water discharges for the Brazos River near Richmond, Texas (solid line), the Nueces River at Mathis, Texas (dashed line), and the Rio Grande River at Brownsville, Texas (dotted line) from September, 1980 to September, 1982. Data from U.S. Dept. of Interior.

advection of the Mississippi-Atachafalaya river fresh water plume.

Summer Fairweather Conditions

In order to understand the kinematics and dynamics of shelf sediment transport during peak flow events, it is useful to study bottom water motion during fairweather periods. Toward this end, Eulerian data was collected during the summer of 1984 in the CTCS area.

Methods of Data Acquisition--The data from 1984 was collected by five ENDECO 105 current meters located in 12, 18, 34, 74, and 140 m water depths (Fig. 45, Table 6). The ENDECO current meter is an axial flow ducted impeller device which records the current speed and direction on 16 mm film every 30 to 60 minutes, dependent upon the setting. According to the manufacturer, the device has a accuracy of plus or minus 2.5 cm/sec and 7 degrees of direction.

The current meters were attached to free-standing taut line moorings (Fig. 46). At 74 and 140 m the arrays included an acoustic release. At the shallower locations (12, 18 and 34 m) the arrays were deployed and retrieved by divers and no releases were used. The shallow arrays were located next to oil company gas platforms to avoid the problems posed by commercial shrimping activity. In all cases, the current meters were mounted some 150 cm above the seabed.

Measurements of deep water wave height and period were recorded hourly by NODC Buoy 42002 (Fig. 45). Wind speed and direction were measured hourly at Horace Caldwell Pier, Port Aransas, Texas.

During the deployment period, current meter "C" (34 m) was pulled up by a shrimp boat on or about August 20th of 1984. It was then redeployed on the 23d of August by divers near a gas platform at location

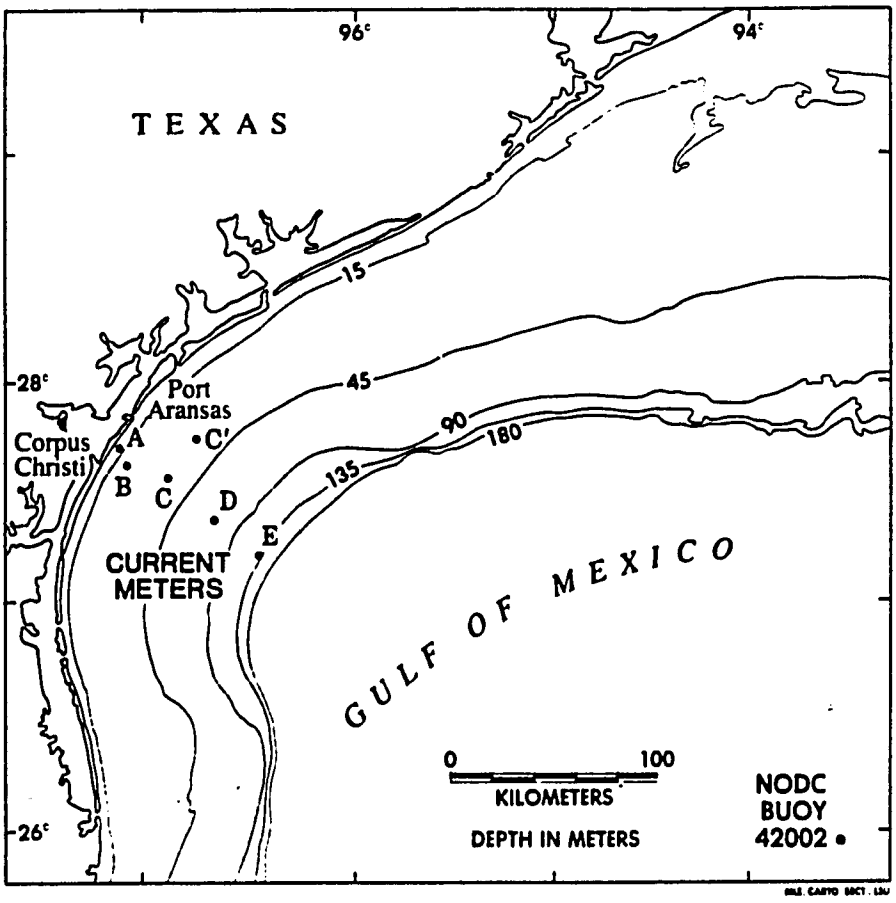

Fig. 45.--Location of current meters and NODC Buoy 42002.

TABLE 6.--Current Meter Locations

Current Meter	Location	Water Depth
A	Lat. 27°42.52′ N, Long. 97°06.20′ W	12 m
B	Lat. 27°37.81′ N, Long. 97°04.12′ W	18 m
C	Lat. 27°32.90′ N, Long. 96°52.70′ W	34 m
C′	Lat. 27°43.97′ N, Long. 96°42.78′ W	34 m
D	Lat. 27°22.40′ N, Long. 96°35.30′ W	74 m
E	Lat. 27°12.18′ N, Long. 96°23.61′ W	140 m

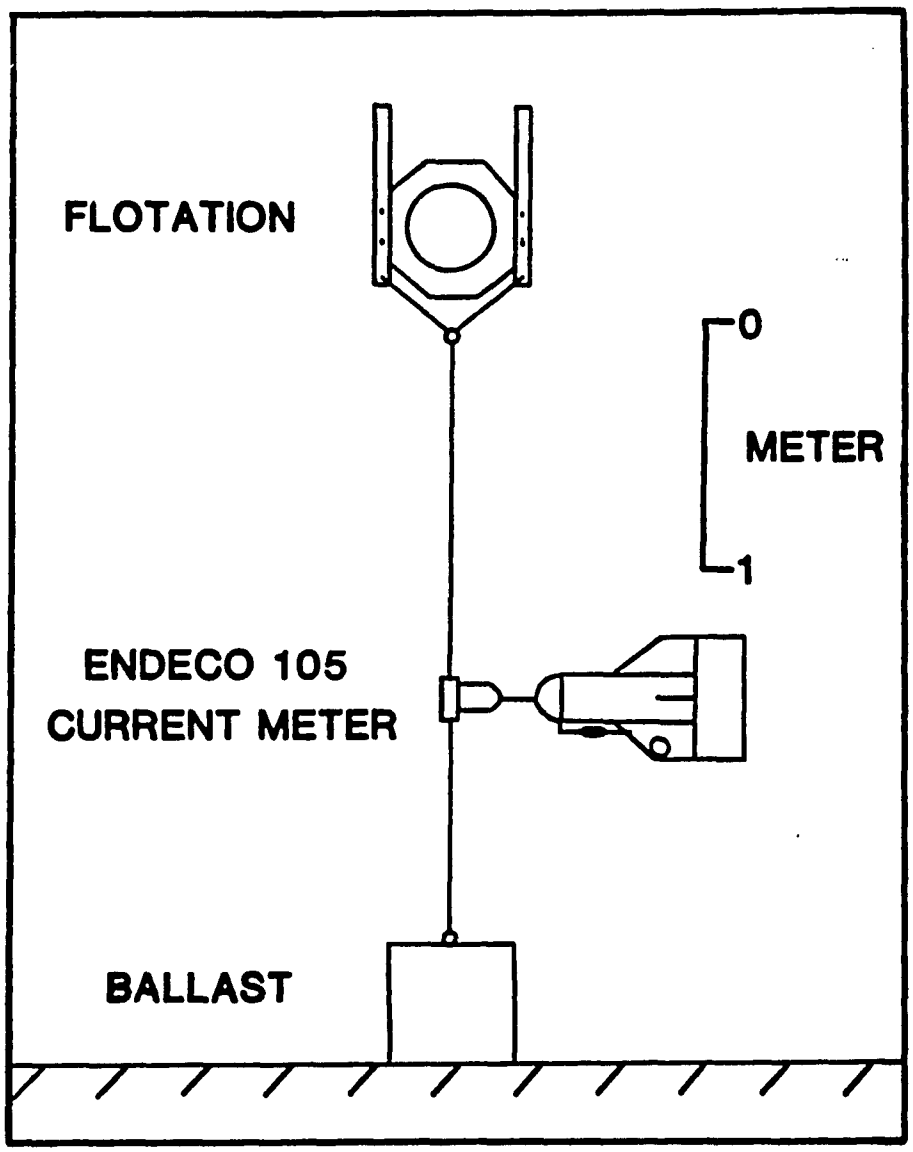

Fig. 46.--Schematic diagram of the current meter array.

C', also at 34 m water depth. Current meter D (74 m) was grabbed by a shrimper's nets around the 26th of September and was not redeployed due to extensive damage to the acoustic release. Current meters A and B (12 and 18 m) were set for 30 minute recording intervals and ran out of film near the end of September.

Spectral Analysis--Collection of Eulerian data, that is, measurements of flow past a stationary device (as opposed to sampling by a device which floats with a current--Lagrangian measurements) yields time series of motion with different time scales, cycle lengths, and recurrence intervals (Kinsman, 1965). The data collected by the ENDECO meters over the three month period of study represent a time series of some 2000 points at each meter. These time series contain motion ranging from what may be considered high frequency motion (such as diurnal and semi-diurnal tides) to that with a low frequency or long period of recurrence. One numerical technique that has proven valuable in the study of time series of currents, winds and waves is spectral analysis. As mentioned, it is the contention of this study that most sediment transport is associated with events of low frequency (long periods of recurrence). Spectral analysis facilitated examination of the spectrum and selection of an appropriate "filter" to separate the low frequency motion from the high frequency motion. It was also used to study the relationship between time series of the currents and that of the overlying wind field (coherence and phase spectra).

The specific procedures used in this study are those given by Fee (1969). First, the data was examined to determine if any instrumental effects (such as improper trim of the meters) were present. After

concluding that none were evident, the data was then studied to resolve any trend and then to take out that trend. The time series were then averaged and then subtracted from that average to yield the variance. The amplitude of that variance was then subjected to the fast Fourier transform using a Parzen spectral window (as described by Chatfield, 1980). Fig. 47 shows a typical power spectrum for the current meter data. Several points should be considered. First, there is a smooth decrease in energy levels with decreasing period (and increasing frequency). Secondly, there are only marginally significant increases in energy density at the inertial and tidal periods. The inertial period is the time scale of the long wave associated with the rotation of the earth (Beer, 1983). Because of the location of the CTCS at 27° N latitude, there is very little frequency separation between the inertial period (26.0 h) and the diurnal tidal periods. Thus, they are represented by one peak. The semi-diurnal tidal peak is less well-developed, an expected result on this portion of the coast which is dominated by the diurnal tide (Smith, 1974).

Spectral analysis of the wind records from Horace Caldwell Pier (HCP) at Port Aransas shows a similar decrease in energy level with decreasing period (Fig. 48). There is a well-pronounced peak near the diurnal frequency which probably corresponds to the sea-breeze effect. Another peak at 64 h has been not been previously recognized on the Texas coast to the author's knowledge.

From this and the spectra of the other meters it was decided to use a filter having a half-power point of 40 h. This effectively removed the high frequency components from the wind and current meter data. It was quite evident that in doing so, the majority of the variance in the

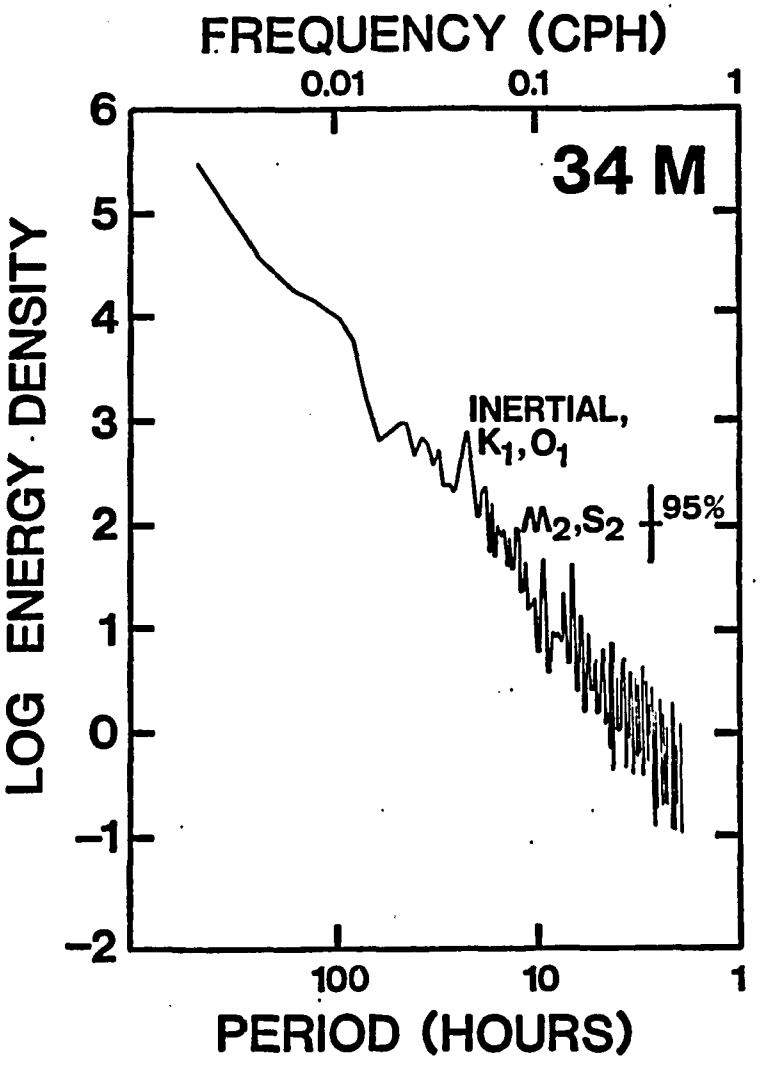

Fig. 47.--Energy density spectrum ($cm^2/sec^2/cpd$) of the alongshelf (v) component of the currents at location C (34 m water depth). Degrees of freedom equals 18.0.

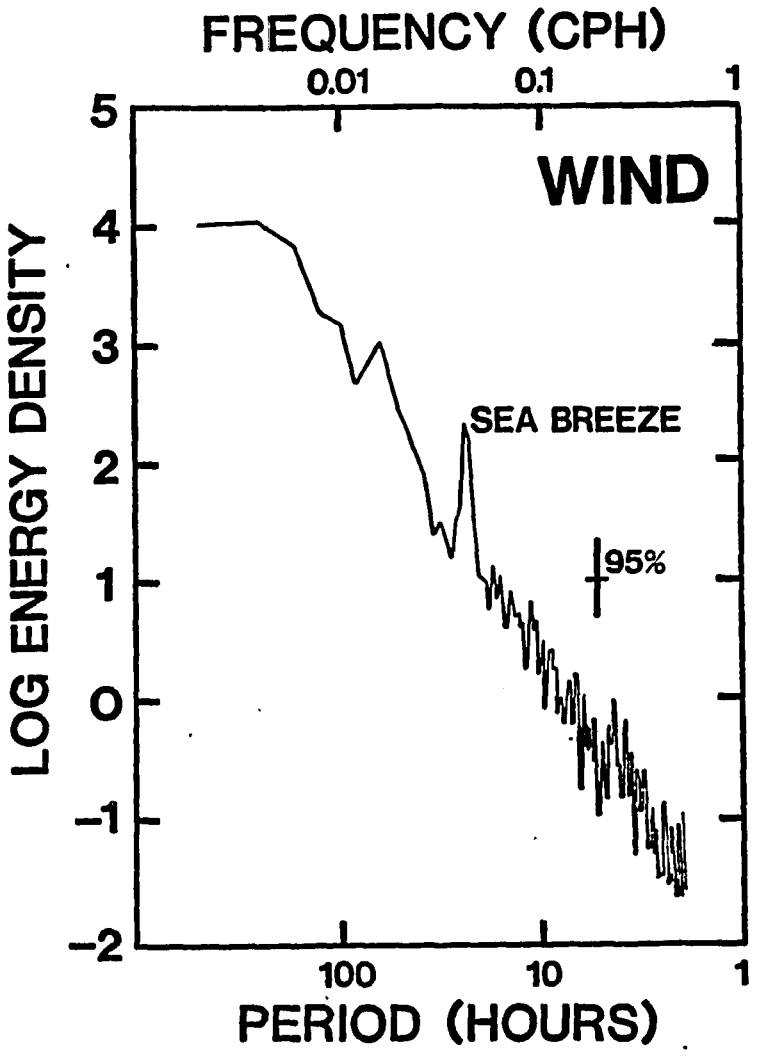

Fig. 48.--Energy density spectrum ($cm^2/sec^2/cpd$) of the alongshelf (v) component of the wind recorded at Horace Caldwell Pier, Port Aransas, Texas. Degrees of freedom equals 18.

wind and current time-series still remained. The use of the 40 hour low pass (HRLP) filter allows one to study the longer period forcing mechanisms, the mechanisms ultimately behind sediment transport on the CTCS.

Coherence and phase spectra between along-shelf (v) and cross-shelf (u) components of the wind and currents were also computed. Generally, values of coherence were statistically significant at only the lower frequencies. The highest degree of coherence for these longer periods was between the v-components of the wind and currents (Fig. 49). As expected, there is a steady decrease in coherence from A (12 m) to E (140 m). A slight increase between D and E may be attributed to the longer record length of E. Clearly, the coupling between the wind and bottom current fields decrease in an offshore direction. The phase spectra for the shallow locations (A, B, and C) show a slight lead for the wind, particularly at 100 h. At the deep locations (D, E) the phase spectra are highly variable, again suggestive of a poor coupling between the wind and the currents at these water depths.

The coherence spectra for the u-components of the wind and current are lower, the highest value 0.7 at 300 to 100 h at location A (12 m). Coherence between the v-component of the current and the u-component of the wind at long periods (> 100 h) is even lower at each station.

Low Frequency Currents, Winds, and Waves--The 40 HRLP data for the fairweather portion of the time series is characterized by typical summer wind conditions and alternating along-shelf flow (Fig. 50). In fact, these southeasterly winds persist through November (Fig. 51). Bottom current flow during the times of southerly winds is generally along-shelf to the northeast. Motion was fairly coherent across the

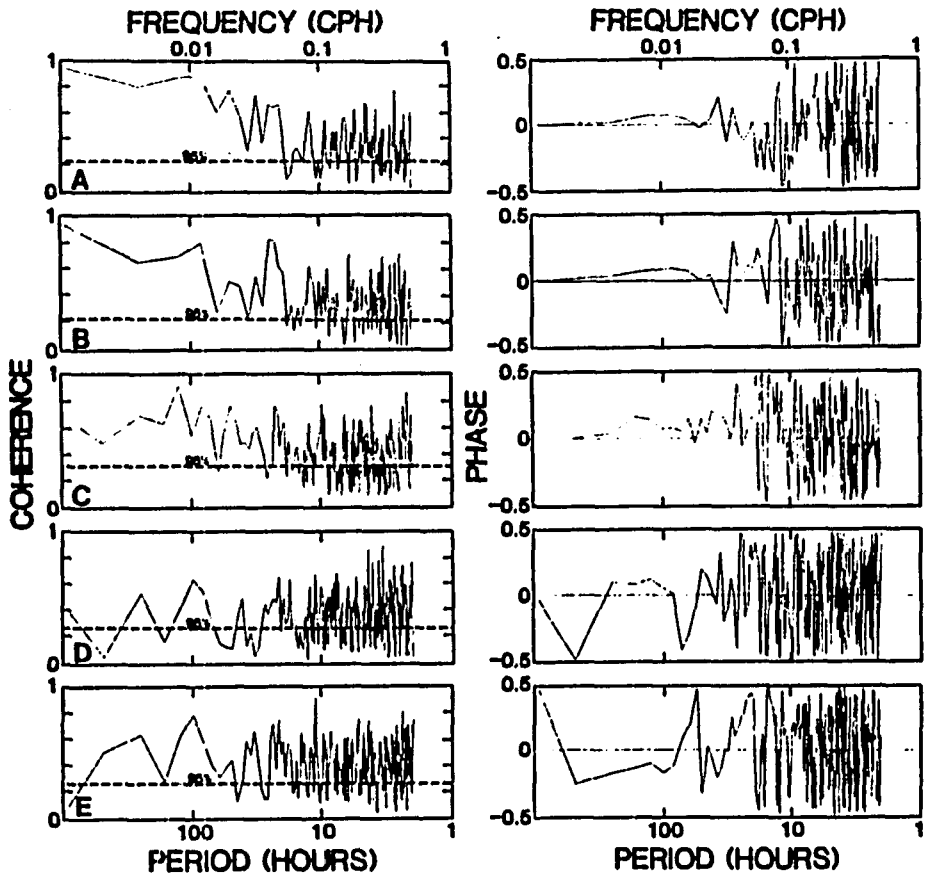

Fig. 49.--Coherence and phase spectra for alongshelf (v) component of the Port Aransas wind and alongshelf components of the motion at current meter A (12 m water depth), B (18 m), C (34 m), D (74 m), and E (140 m). Degrees of freedom range from 18 to 30.

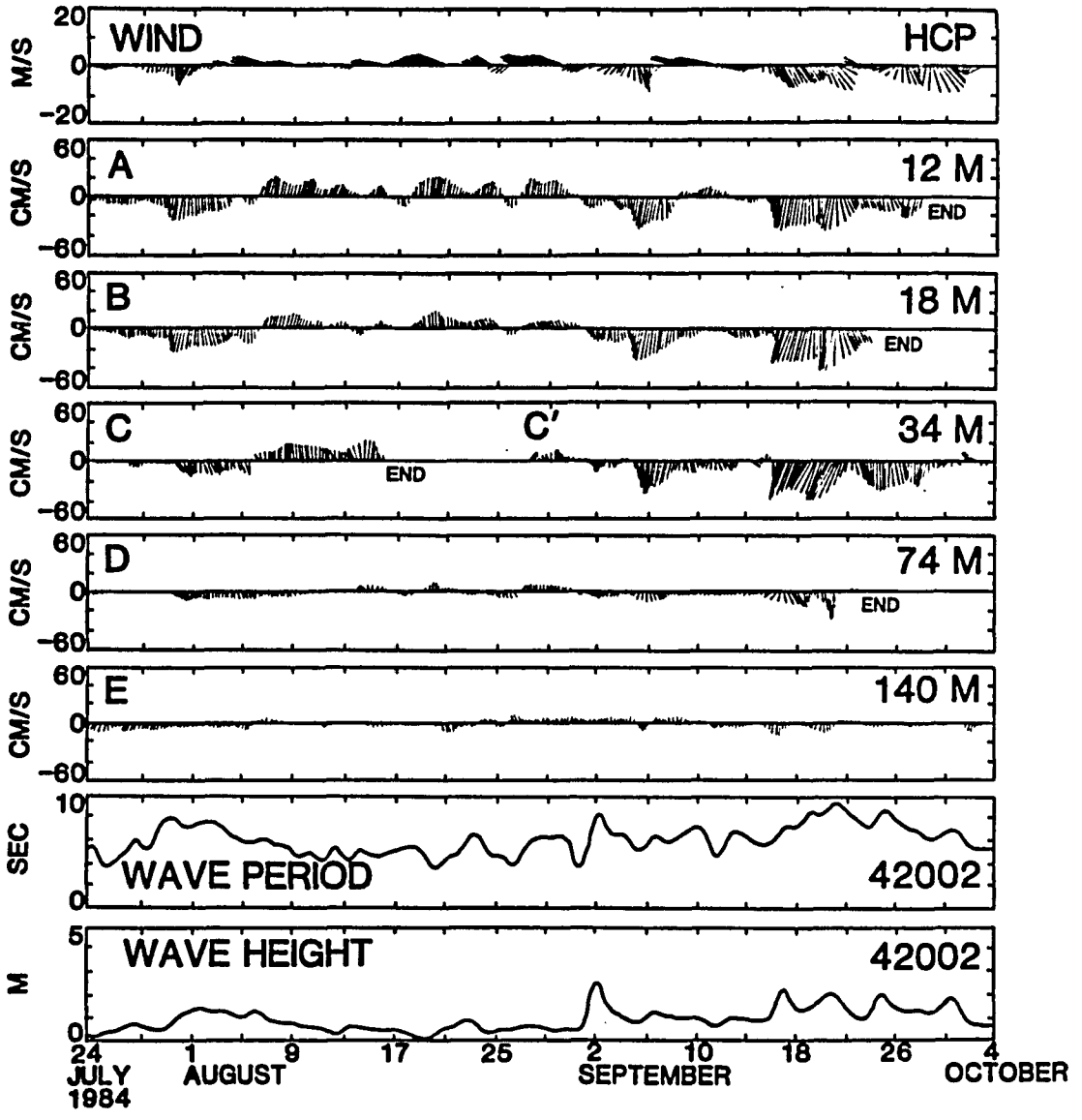

Fig. 50.--Forty-hour low-passed Eulerian data, July 24 to October 4, 1984. 40 HRLP wave data from NODC Buoy 42002 and 40 HRLP wind data from Horace Caldwell Pier (HCP) are also shown. Vertical axis is alongshelf (v) motion, positive toward the northeast. Cross-shelf (u) motion is positive offshore. Wind and currents are direction "towards".

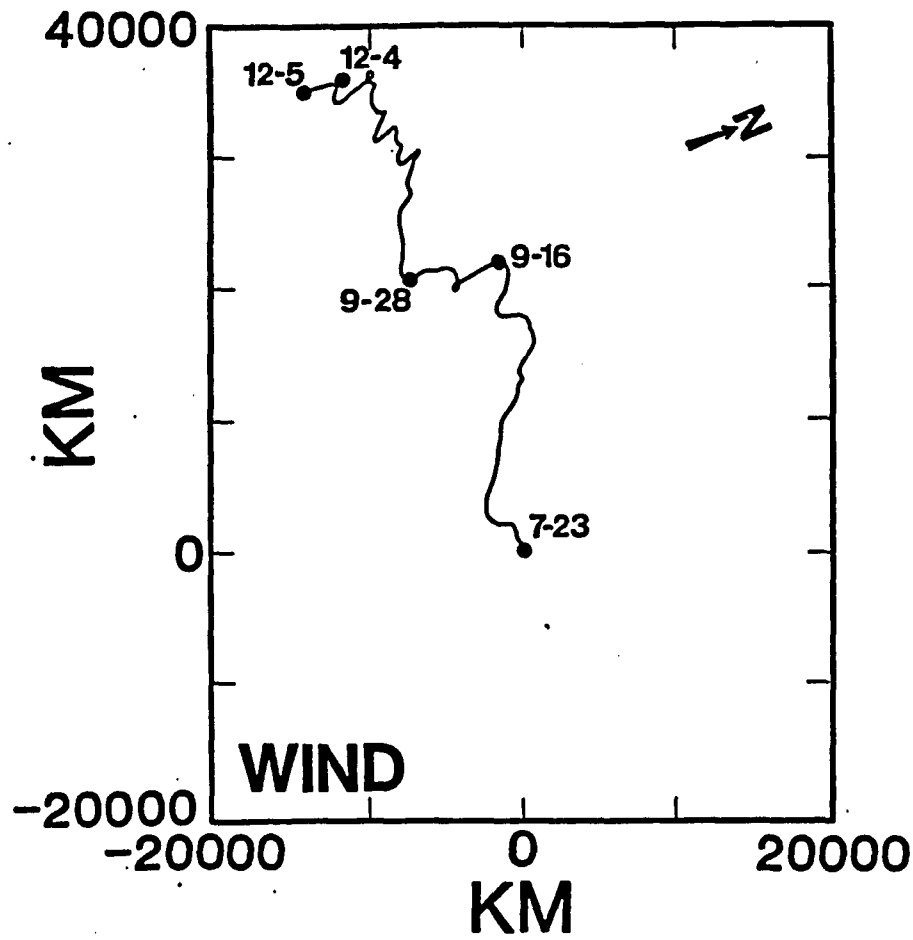

Fig. 51.--Inferred Lagrangian motion of low frequency wind, July 23 to December 5, 1984. Wind measured at Horace Caldwell Pier, Port Aransas, Texas. Vertical axis is cross-shelf (u) motion, positive towards the coast. Horizontal axis is alongshelf (v) motion, positive towards the northeast.

shelf, although at 140 m there are some differences. The strength of the flow generally decreases offshore, with some exceptions. Current speeds at the nearshore locations peak at 20 cm/sec. Deep water waves recorded by Buoy 42002 have periods of 5 to 6 seconds and heights of less than a meter.

Sturgis and Blaha (1976) recognized that such southerly winds constitute a negative wind curl and can give rise to a western boundary current which they called the Mexican current. Although there has been some question as to the exact origin of this northward current (e.g. Elliott, 1982), its presence has been well established. Indeed, this data set provides further evidence of its existence.

Discussion--Lagrangian descriptions of water motion can be inferred from Eulerian data such as this by connecting the heads and tails of the progressive displacement vectors (Von Schwind, 1980). During the fairweather period of southerly winds (e.g. 7-23 to 9-16-84), motion is weak, meandering, and often oriented towards deeper water (Fig. 52). This is similar to the weak bottom water return flow recognized by Smith (1977) to be a response to the onshore winds and presumably onshore-driven surface waters. Hydrographic data indicate that a well-developed pycnocline was present offshore of 20 m during this time which supports this notion of directional shear in the waters of the CTCS area (Fig. 42).

As mentioned, the areal distribution of the coastal ocean zones described by Mooers (1976) and Swift and Niedoroda (1984) is dependent upon the dynamics of the fully developed sea. In the case of the summer fairweather period, it appears that the response at all 5 current meter locations is consistent with what would be expected from the

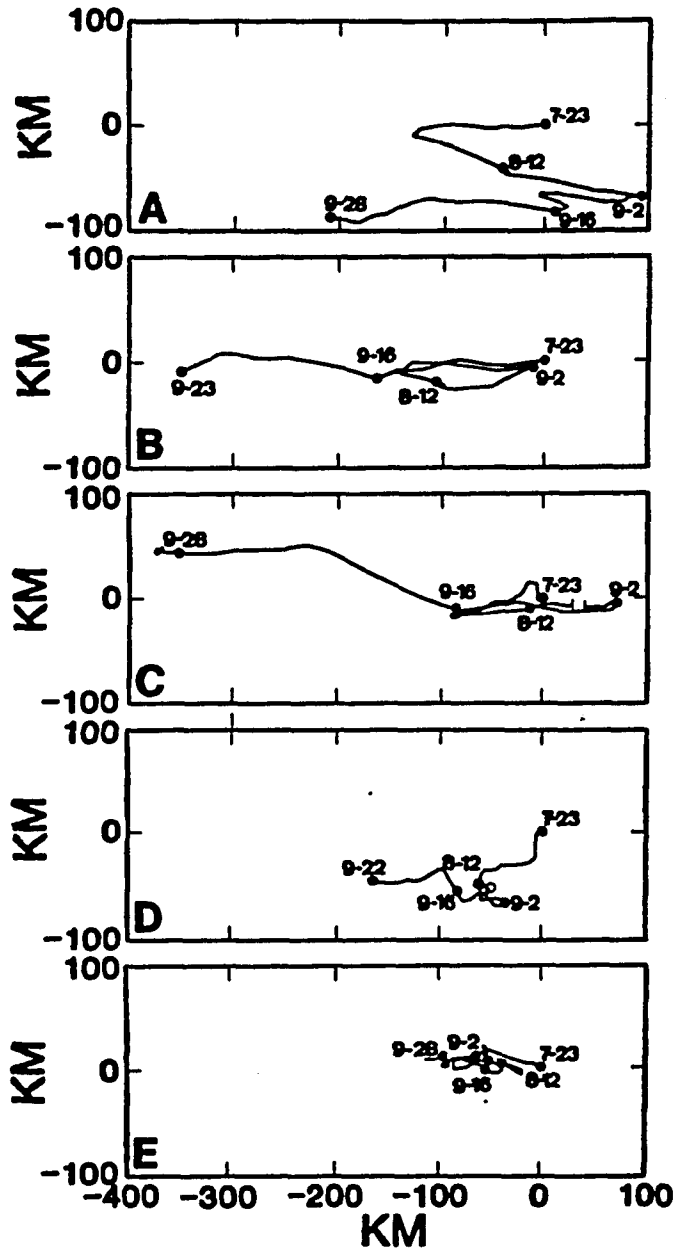

Fig. 52--Inferred low frequency Lagrangian motion at current meter A (12 m), B (18 m), C and C′ (34 m), D (74 m), and E (140 m), July 23 to October 4, 1984. Vertical and horizontal axes same as Fig. 51. Gap in motion at C (34 m) represents period when meter was out of water prior to redeployment.

geostrophic zone. There is a well-defined directional shear through the water column even at location A in 12 m of water (Fig. 52). In addition, there is a lack of coherence between the wind orientation and the bottom current direction. It is likely that the friction-dominated zone, where winds and currents show more coherence, is limited to inner most portion of the shoreface during this interval of low current speeds.

Extratropical Storm of September 1984

During the course of the deployment period, a flow event of moderate intensity and substantial duration (7 days) was recorded. Discussion of this event, an extratropical storm in September, provides an introduction to the nature of both fluid and sediment motion in the CTCS area. Although the episode is one of relatively small magnitude, the shelf response is similar to that observed during larger storms.

The departure from summer fairweather conditions is clearly evident in progressive displacement vectors of the low frequency wind (Fig. 51). The discrete period of northerly wind from on September 16 to 28 is quite distinctive. Synoptic weather maps indicate that beginning on the 16th of September, a stationary front became situated over the Gulf of Mexico midway between buoy 42002 and the Texas coast (Fig. 53). A low pressure center developed on its trailing edge at Lat. 27^{o} Long. 95^{o}. Although this center did not show any tropical characteristics, it did exhibit a cyclonic wind circulation pattern similar to that possessed by tropical storms. The north-northeasterly along-shelf winds produced a dramatic water level set-up at Mustang Island, with a rise of a meter and a half in 24 hours. Waves were observed breaking at the toe

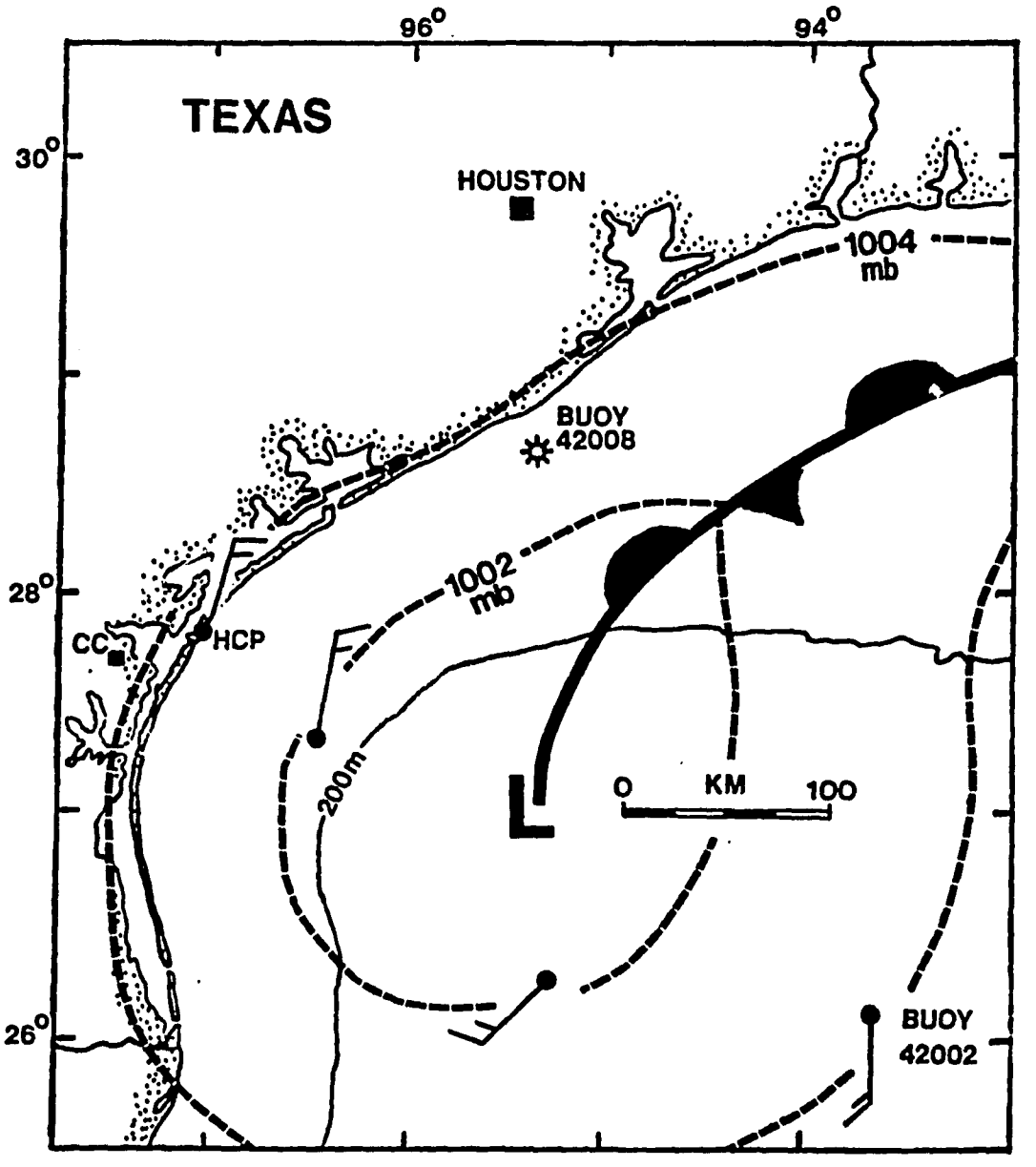

Fig. 53.--Wind field and atmospheric pressure distribution during the extratropical storm of September, 1984. From the U.S. Weather Bureau synoptic weather map September 21, 1984.

of the dune line (Anthony Amos, 1984, pers. comm.). The storm deepened and wandered to the north, eventually making landfall on the 22nd of September near Galveston, Texas. The highest tides recorded during September at Freeport, Texas (the nearest operative tide gauge) occurred at 0200 hours on the 21st. There was a dramatic change in the beach topography for some 200 miles along the Texas coast as a result of the superelevated tides. Wave period and height as measured at Buoy 42002 increased substantially during this storm (Fig. 50). Deep water wave period reached almost 10 seconds with wave heights up to 2.0 m. Current speeds recorded at the nearshore locations peaked at 40 cm/sec. Flow was highly coherent all the way out to 140 m. Near-bottom motion was to the southwest, along-shelf.

The well-defined motion imposed by the storm event of 16-24 September contrasts sharply with the weak offshore meandering of the fair-weather period (Fig. 52). Bottom flow is generally to the southwest, along-shelf. As will be discussed later, this displacement appears to be in phase with the northeasterly winds and the cross-shelf pressure gradient induced by those winds.

Boundary Shear Stress--Eulerian data such as this have often been used to make inferences concerning the nature of sediment transport in a given area (e.g. Adams et al, 1982). The flow of sea water past this sea bottom boundary generates a tangential (shear) stress. Early flume experiments have shown that the entrainment of clastic particles is related to the magnitude of this stress. Commonly, one can calculate the boundary shear stress by the use of the quadratic stress law:

$$\tau_o = c_d \rho (u_{100})^2$$

where τ_b is the boundary shear stress (measured in dynes/cm^2), C_d is the drag coefficient, ρ is the fluid density (1.027 g/cm^3) and U_{100} the velocity measured one meter above the bottom. The drag coefficient is used to relate the mean velocity at some height above the sea bed to the boundary shear stress (Nowell, Jumars, and Eckman, 1981). Experimentally, it has been found to be a function of the water depth, bed composition (grain size), and presence or absence of roughness elements such as bedforms (Soulsby, 1983). Adams et al., (1982) used a coefficient of 1.4×10^{-3} for substrates and water depths similar to the CTCS and for flow measured at 1 m off bottom. In the 1984 dataset, flow was measured slightly higher at 1.5 m above the boundary, necessitating a lower drag coefficient, in this case 1.0×10^{-3}.

However, in the coastal ocean, currents are not the sole source of shear stress. Surface gravity waves generated by the wind and other sources also exert force upon the boundary, particularly in shallow water (Madsen, 1976). It has also been shown that the non-linear interaction of waves and currents contributes to the total shear stress. This total may be greater than the simple addition of the shear stress due to the waves and currents alone (Grant and Madsen, 1979). The motion associated with interacting waves and currents has been termed "combined flow" (Harms, 1969; Swift et al., 1983).

With this in mind, the total boundary shear stress at each location was calculated for the study period (Fig. 54). The current meter data provided the input for the steady component of the combined flow. However, the wave data recorded at NODC Buoy in deep water had be to adjusted for phase velocity lag, bottom refraction, shoaling, bottom friction, and energy dissipation upon the muddy shelf bottom typical of

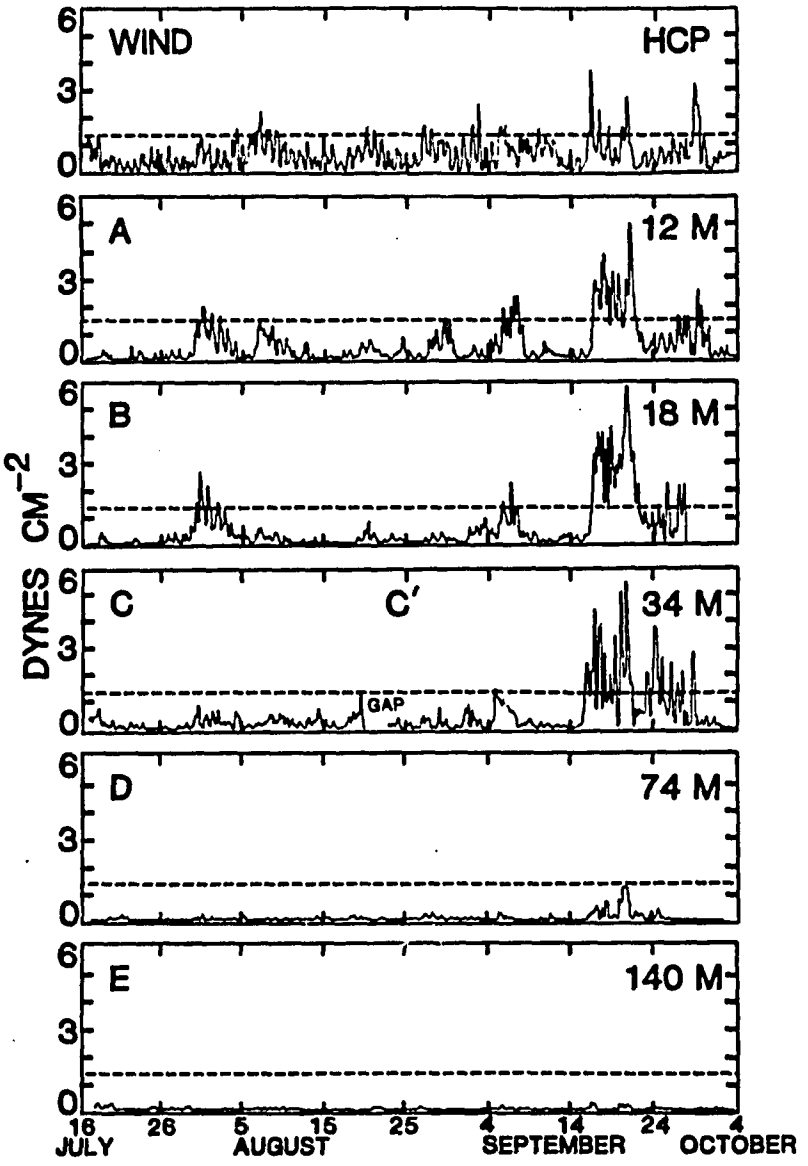

Fig. 54.--Boundary shear stress due to combined wave and current interaction at current meter locations on the CTCS July 16 to October 4, 1984. Wind stress is also shown. Dotted line is the critical threshold for the initiation of motion of 68 micron sand (based upon McCave, 1971; see Fig. 23).

the CTCS using the guidelines of Komar (1976), Madsen (1976), Tubman and Suhayda (1976), and Hsaio and Shemdin (1978,1980). The exact methods are described in Appendix B. Of particular importance was the energy dissipation in the muddy shelf bottom which can result in a considerable wave attentuation in some cases (Forristall and Reece, 1985).

Superimposed upon the shear stress diagram (Fig. 54) is a dotted line representing the critical threshold for 68 micron sand. As mentioned in the first chapter, analysis of the grain size distributions of discrete sand layers in boxcores taken on the shelf indicates that 68 microns is the modal peak of the size distributions (Fig. 22).

Flume experiments by Shields (1936) established the numerical conditions necessary for the initiation of sediment motion. In his work, he constructed diagrams of dimensionless fluid stress, Θ and grain Reynolds number. For a given grain size, the threshold shear stress can be calculated. Bagnold (1966) later revised this diagram, putting grain size on the horizontal axis. He also established criteria for determining the mode of sediment transport (i.e. suspension vs. bedload). These suspension criteria were later modified by McCave (1971), based upon measurements in the North Sea . This is shown in Fig. 23. Use of this diagram leads to the conclusion that 68 micron (.068 mm) sand will be transported entirely in suspension above a threshold shear stress of 1.4 dynes/cm^2. It should be mentioned that Shields (1936) did not actually have measurements of the threshold values for sand grains finer than 0.1 mm. Later work by Vanoni (1964) and White (1970) have suggested that Shields (1936) extrapolation is a little conserva-

tive in the fine sizes. However, the error is greatest at the finest sizes and for 68 micron sand is less than 10 %.

Fig. 54 indicates that the most important combined flow event in the time series occurred during the period September 16-24. However, even during this event, the threshold was not exceeded at locations D (74 m) and E (140 m). One reason is the fact that waves of 2 m heights and 9-10 second periods, typical of this storm, are incapable of contributing much shear stress in these water depths (see Appendix B). It is also important to note the boundary stress recorded at the shallower locations often exceeds the wind stress values, further emphasizing the contribution of other forces.

Adams et al., (1982) found that values calculated from the quadratic stress law tend to be 20 % higher than those actually present in a sediment-laden flow. This apparent reduction in boundary shear stress is related to the dynamics of sediment-current interaction. Without measurements at several different levels above the boundary, it is difficult to determine whether a flow has taken on such characteristics. However, as an adjustment for this phenomenon, a threshold of 1.68 dynes/cm^2 was superimposed upon periods when there appears to be just such a flow. As Fig. 54 suggests, the September storm is still an important event.

Once it is has been determined that threshold of sediment motion has been exceeded during an event, the most critical question concerns the kinematics of sediment transport. To answer this question, progressive displacement vectors were plotted for the periods during which the boundary shear stress was in excess of the threshold of motion (Fig. 55). Motion was assumed to continue until the shear stress values fell

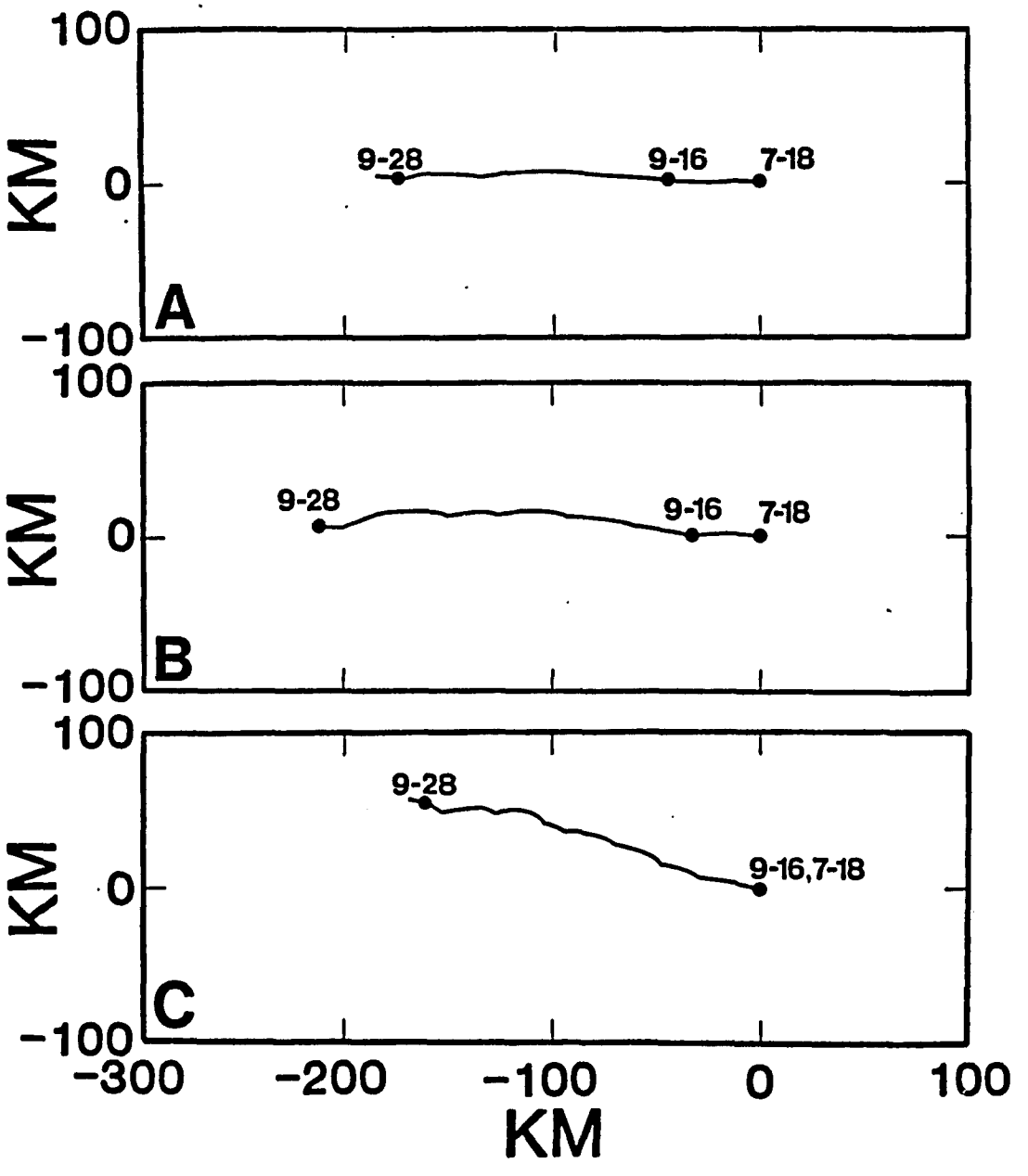

Fig. 55.--Inferred Lagrangian displacement of sand, July 16 to October 4, 1984. Orientation of axes same as Fig. 51. Relevant dates in 1984 are shown.

below 0.9 times the threshold. Because 68 micron sand is transported entirely in suspension, the progressive vectors are considered to represent the motion of this sand upon the CTCS during periods of elevated shear stress. During the September event, which makes up the bulk of the transport, sand motion is along-shelf to the southwest. There is a noticeable cross-shelf gradient in transport. Bottom sediment motion has more of an onshore trajectory as one moves towards deeper water.

Forcing Mechanisms--The importance of the wind stress in forcing motion during this time period is emphasized by the high degree of coherence between the long period along-shelf wind and current motion (Fig. 49). However, the high coherence does not extend to cross-shelf flow. This suggests that the bottom current motion is not a direct response to the applied wind stress as implied by Morton (1981).

Another means of deciphering the contribution of other forces is to compare directly the value of the wind stress and the magnitude of the boundary shear stress due simply to currents (e.g. Smith, 1978; Winant and Beardsley, 1979). Fig. 56 demonstrates that the unfiltered shear stress at C (34 m) and possibly B (18 m) is numerically greater than the wind stress. This points to an additional source of energy such as a wind-induced cross-shelf pressure gradient. Although caution should be exercised when making inferences of open shelf wind stresses from onshore wind measurements (e.g. Hsu, 1980), it should be pointed out that the winds during the mid-September event were along-shelf and were measured at a pier situated over water.

These along-shelf winds, related to the cyclonic circulation of the low pressure center, resulted in nearshore surface water being driven

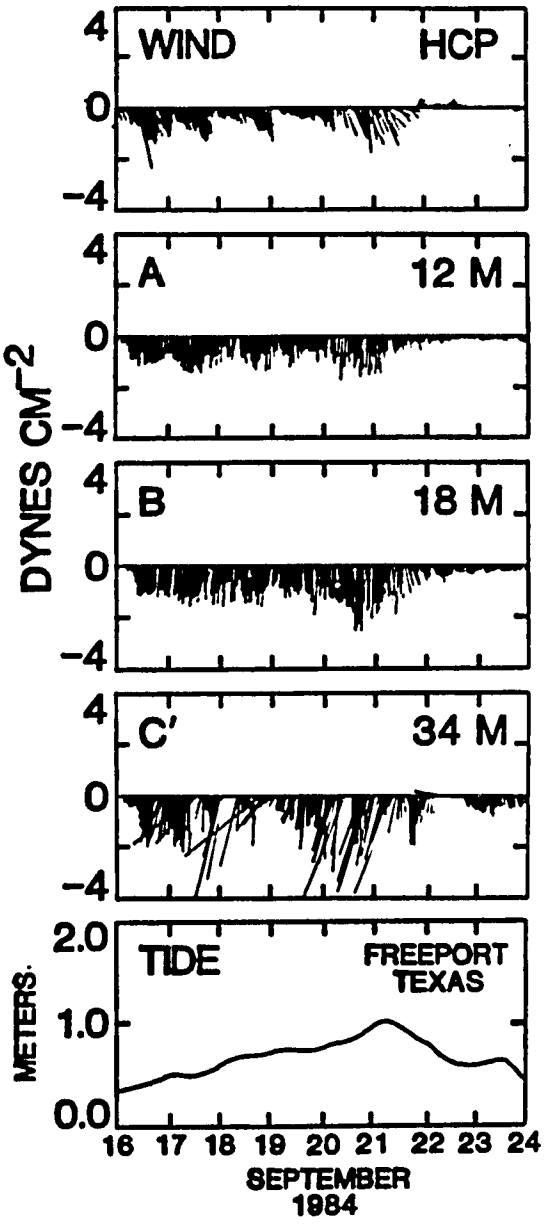

Fig. 56.--Shear stress from unfiltered current meter data at A (12 m), B (18 m), and C (34 m). Wind stress is also shown. 40 HRLP tidal record from Freeport, Texas. Height is distance above NGVD. Orientation of axes same as Fig. 50.

toward the coastal boundary (Figs. 44-46). Abnormally high tides, as illustrated by measurements at the nearest operative tide gauge at Freeport, Texas (200 km to the northeast of Port Aransas), were experienced all along the Texas coast (Anthony Amos, pers. comm., 1984). The highest water level occurred at 0200 CST on the 21st of September, slightly behind the peak of the current motion at meters A,B, and C (Fig. 56).

This elevated sea level probably lead to the formation of a cross-shelf pressure gradient and a pressure gradient force directed offshore (Fig. 41). Since the time-scale of the motion was greater than the inertial period (26 h), it is likely that the rotation of the earth played a role in deflecting flow to the southwest. In other words, motion was in geostrophic balance with the pressure gradient force and the Coriolis force. This observation is supported by calculation of the Rossby number (Ro), a non-dimensional term describing the ratio of the inertial and coriolis forces, which is given by:

$$R_o = U/fL$$

where U is the mean velocity scale, f is the Coriolis term ($2\Omega \sin \phi$ -- where Ω is $0.73 \times 10^{-4} s^{-1}$ and ϕ is the latitude), and L a representative length scale of motion. By using a current speed of 40 cm/sec and a length scale of 130 km (from Fig. 55), one finds that the Rossby number is quite small (.04). When the Rossby number is less than 1.0, the Coriolis force must be considered in any motion analysis (Pedlosky, 1979).

Bottom flow during the September event at current meters A (12 m) and B (18 m) was very similar to the presumed interior or core flow during a downwelling event (Fig. 41A). This suggests that the bottom

veering angle, the angle between the geostrophic velocity vector and the bottom stress vector, was smaller than that which could be measured by the ENDECO current meter (7^{o}) or was limited to the area below the meter. The former explanation is consistent with the magnitude of bottom turning commonly observed during downwelling episodes such as this (Weatherly and Van Leer, 1977).

The flow at current meter C (34 m) is similar but has a slight onshore component (Fig. 55). This "upwelling" is a departure from the idealized flow in the downwelling model presented by Swift and Niedoroda (1984) (Fig. 41). It may be linked to the rotary nature of winds associated with the low pressure cell (Fig. 53): further from the coast, winds have an offshore component which could bring about offshore surface flow and onshore bottom flow under the stratified conditions of the mid-shelf waters. The observed migration of the low pressure center to the north and ensuing rotation of the wind vector could also lead to the observed flow pattern at C (34 m).

Discussion--The 1984 data illustrates the shelf response to a small-scale storm event, an event which occurs approximately once a year. It is significant for several reasons. First, the data show clearly the difference between the weak, often meandering, offshore flow typical of fairweather conditions and the well-defined, intense southwesterly flow imposed by the storm event of September 16-24 (Figs. 47 & 49). Secondly, the along-shelf winds associated with this event are unusual. Low pressure centers of migrating cold fronts seldom pass this far south; The winds following frontal passage are more often from the northwest quadrant (Dimego et al., 1976). In fact, the cyclonic wind pattern shown by the extratropical low pressure center is similar to the pat-

tern of larger hurricanes and tropical storms. Like tropical storms, the along-shelf winds associated with the September event produced sea level set-up.

Third, the currents generated during this event are not simply wind-forced as Morton (1981) would suggest. There is a high degree of coherence between the wind and the bottom currents only when the wind has an along-shelf orientation. Shear stress analysis indicates that the cross-shelf pressure gradient force contributed significantly to the observed motion. The sea level set-up recorded along the coast during this event is one indication that a pressure gradient was present. The southwesterly flow recorded at the inshore stations is generally consistent with a multi-layered model of barotropic motion where there is a geostrophic balance between the cross-shelf pressure gradient force and the Coriolis force as given by Swift and Niedoroda (1984) and as shown in Fig. 41.

Fourth, there is a coincidence of elevated wave periods and heights and increased current strength (Fig. 50). At inshore stations, the threshold for sediment motion would not have been exceeded had the wave orbital motion not been present. In these water depths, the notion of "combined flow" is decidedly not academic. At mid-shelf, the wave motion is less significant but current strength increases. Outer shelf meters show little significant motion, either by waves or currents. Although there were no measurements of flow in the interior of the water column across the shelf, the observed mid-shelf peak of current speeds is consistent with the pattern show by geostrophically-balanced coastal jets that have been observed on the Atlantic shelf (Csanady, 1982).

Lastly, the Eulerian data suggests that the coastal ocean zones have expanded seaward from their fairweather positions. The bottom current response at current meter A (12 m) is typical of what Swift and Niedoroda (1984) describe as the friction-dominated zone: bottom current motion parallel to the forcing wind stress (Fig. 56). The numerical similarity of the values of wind stress and boundary shear stress lends support to the notion of a turbulent, non-rotating longshore flow in shallow water driven by the wind stress (Csanady, 1982). The response at 18 m depth (B) appears be to transitional to this and the more "geostrophic" pattern shown at 34 m (C).

Hurricane Allen, 1980

Unpublished current meter data from August of 1980 was acquired by the author from Continental Shelf Associates, Inc. (CSA). As part of a rig stability-monitoring program for Conoco, Inc., CSA maintained a tautline mooring of three current meters in 74 m of water in the CTCS area for a two-year period (Fig. 57). During this time, Hurricane Allen made landfall on the Texas coast north of Port Isabel.

The CSA array consisted of three ENDECO 105 current meters moored at 12 , 37, and 70 m depths (Fig. 58). The lowest meter was situated about 4 m off bottom. The meters recorded the current speed and direction every 30 minutes. Wave data was measured at NODC Buoy 42002 until late on the 8th of August when the device parted its mooring. With this device out of operation and NODC platform 42008 not yet installed, the nearest available wind data was from Corpus Christ Airport. Although the wind gauge was located some 20 km inland, the broad distribution of hurricane-associated winds makes the data quite relevant for

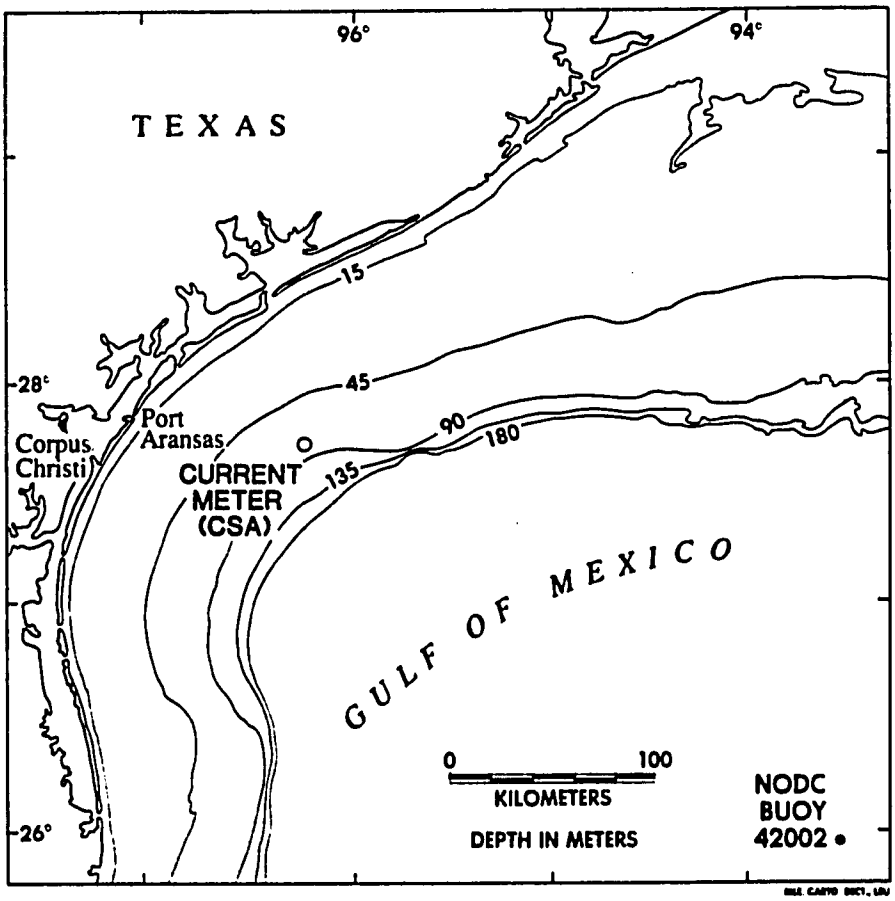

Fig. 57.--Location of CSA current meter mooring.

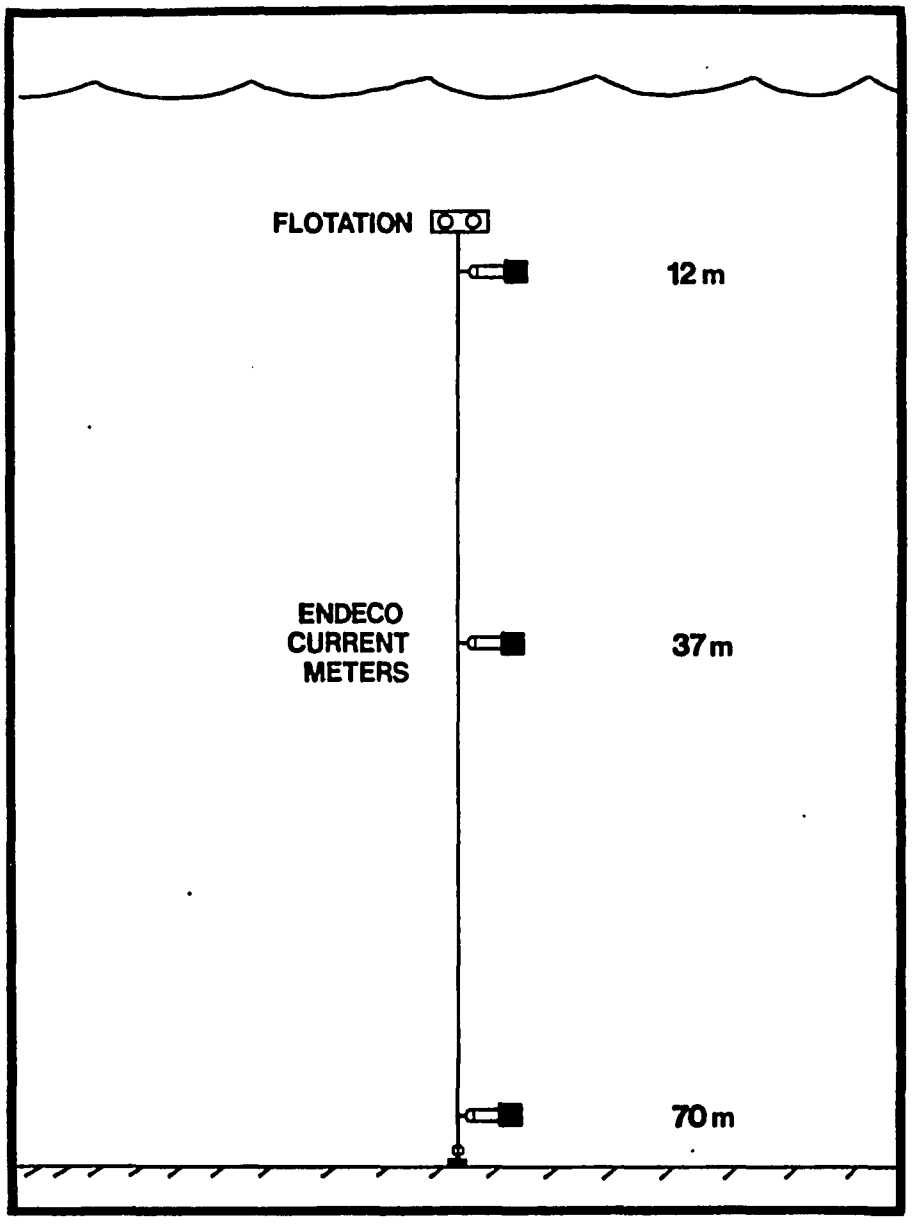

Fig. 58.--Idealized diagram of CSA array.

this study.

Winds--A detailed discussion of the origin, track and onshore geologic effects of Hurricane Allen is presented in Nummedal (1982). The eye of Hurricane Allen passed some 200 km south of the CSA array just prior to its landfall after midnight, August 10, 1980. (Fig. 59). However, during its approach toward the coast the hurricane's winds extended over much of the Texas shelf. The record from Corpus Christi Airport shows a general clockwise-rotating wind vector (Fig. 60). However, during the approach phase, the storm stalled and there was a significant period of along-shelf winds with speeds up to 20 m/sec. This represented a significant departure from the typical southerly winds before and after the storm.

Currents--Currents at the CSA array shifted and began to increase on the 9th of August (Figs. 55-56). Flow at the 12 m depth was generally onshore with speeds of 60-70 cm/sec. At 37 m, the currents were directed more along-shelf and were slightly weaker. Flow near-bottom at 70 m depth was purely along-shelf and significantly stronger (80-90 cm/sec). The intense flow at all levels during this period is quite distinct from the subsequent weak, rotating tidal-inertial motion.

It is probable that the CSA array was located in what Swift and Niedoroda (1984) describe as the "geostrophic zone". It is also reasonable to assume that at the beginning of the storm event, the water column consisted of a wind-influenced upper boundary layer, an interior or geostrophic layer, and a bottom-influenced lower boundary layer. It is likely that the one of three current meters (12, 37, 70 m) was located within each of the zones (Fig. 61b). The well-stratified nature of the water column during this period (e.g. Fig. 42) undoubted-

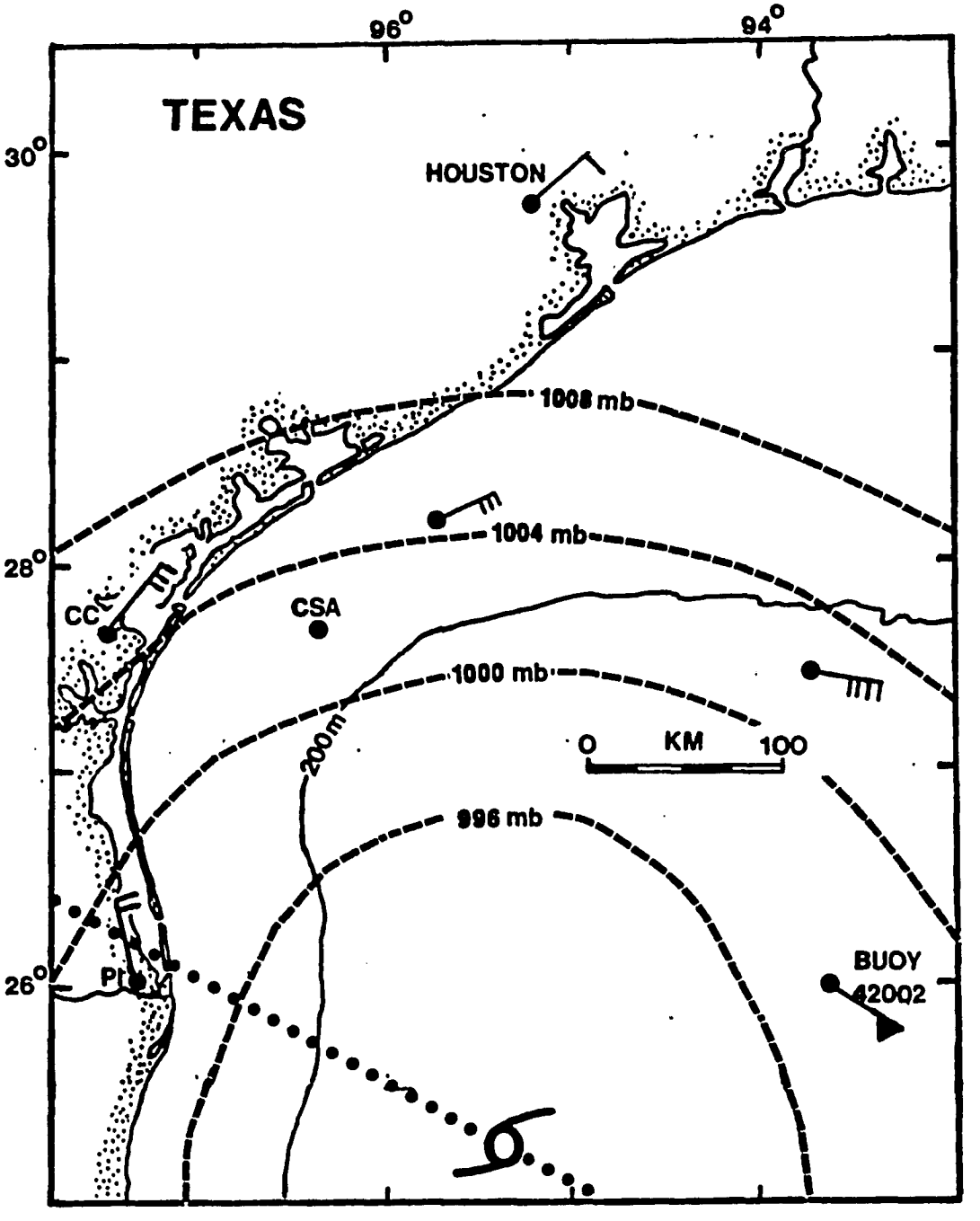

Fig. 59.--Synoptic meteorological map showing atmospheric pressure and wind circulation at 0600 CST 9 August 1980, 18 hours prior to landfall of Hurricane Allen. Contour interval equals 4 millebars (mb). Modified from U. S. Weather Bureau maps.

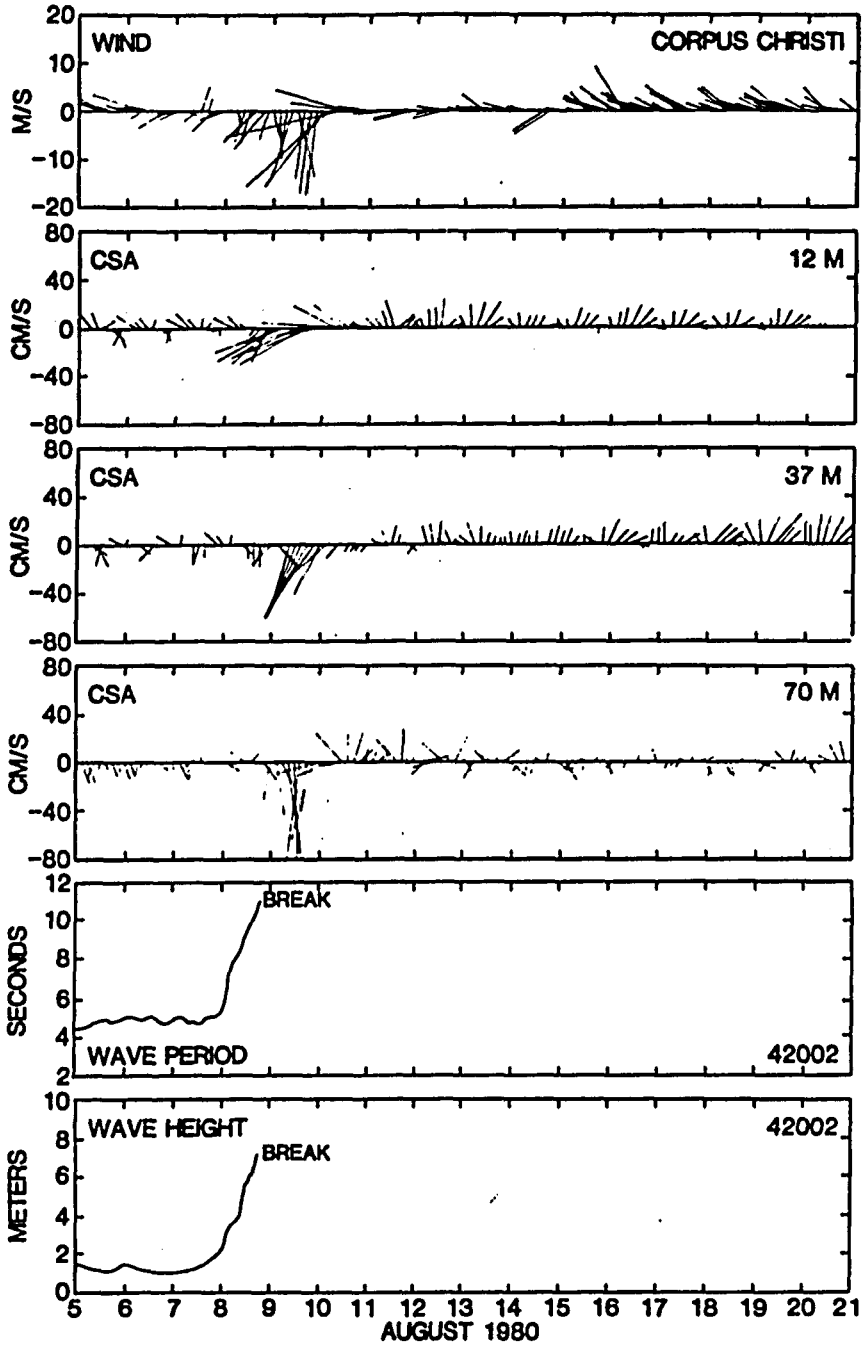

Fig. 60.--Unfiltered Eulerian data from CSA current meter array, August 5 to 21st, 1980. Wind velocity data from Corpus Christi Airport and wave measurements from NODC Buoy 42002 are also shown. Current meter and wind data subsampled at 3 hour intervals. Orientation of axes sames as Fig. 50. "Break" denotes point at which NODC Buoy 42002 parted its mooring near center of Hurricane Allen.

Fig. 61.--A) Unfiltered progressive vectors of inferred Lagrangian motion at 12, 37, and 70 m depths, August 8-11, 1980. B) Depth distribution of current meter motion within framework of three-layer model of downwelling flow (from Swift and Niederoda, 1984). C). Planar view of inferred bottom Ekman spiral. V_g equals the geostrophic velocity vector, τ_o is the bottom stress vector, and α is the total veering angle.

(next page)

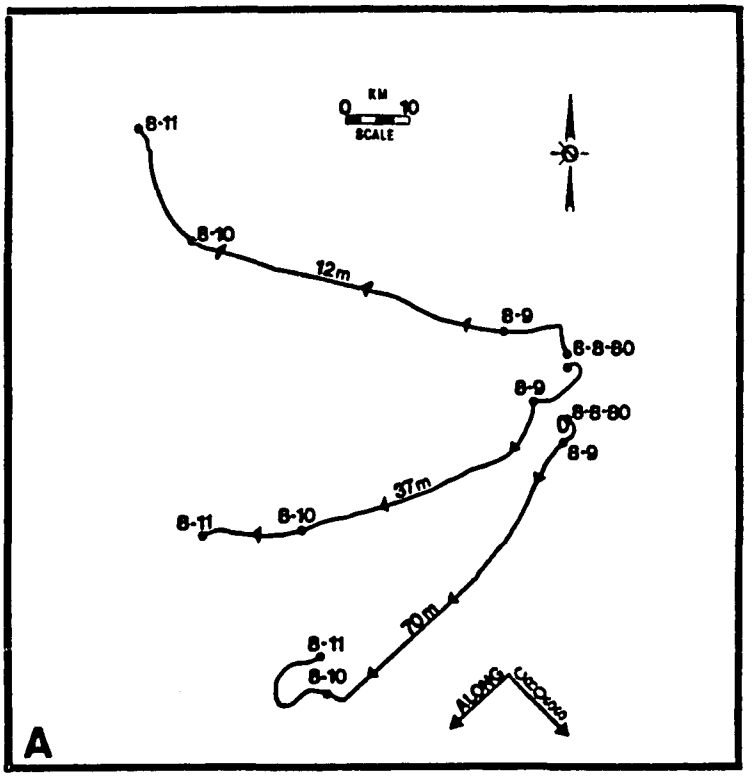
0 KM 10
SCALE
B-11
B-10
12m
B-9
B-8-80
B-9
B-8-80
B-9
37m
B-11
B-10
70m
B-11
B-10
ALONG
CROSS
A

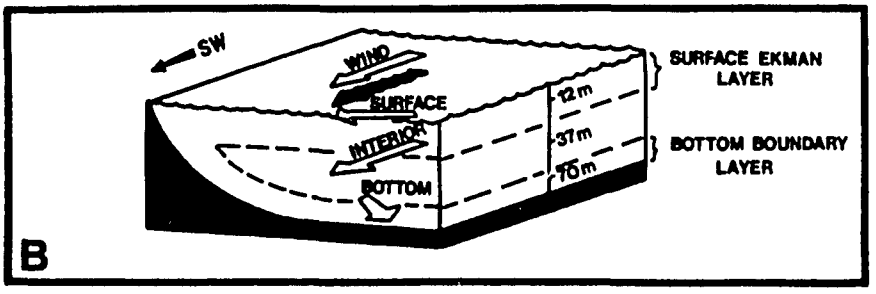
SW
WIND
SURFACE
INTERIOR
BOTTOM
12m
37m
70m
SURFACE EKMAN LAYER
BOTTOM BOUNDARY LAYER
B

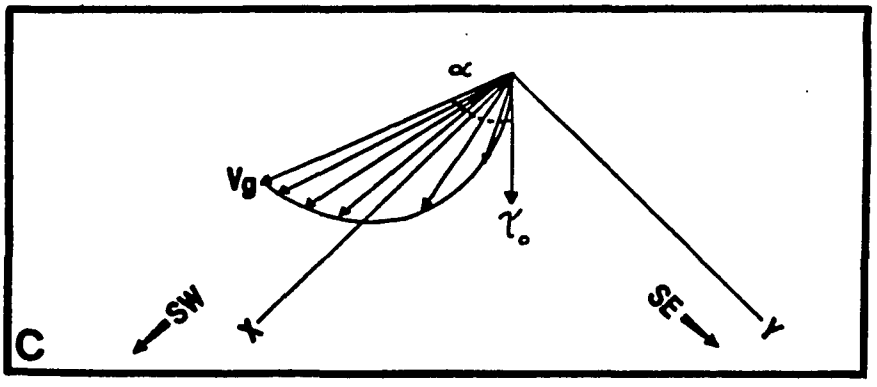
α
Vg
γo
SW
X
SE
Y
C

ly prevented significant deviations from this framework. Deepening of the surface (mixed) layer is known to occur during storms (Pollard et al., 1973) but is a function of the water column stratification and the duration of the forcing event (Daddio, 1977). Under well-stratified conditions such as this, the rate of deepening is initially high but later decreases with time (Kato and Phillips, 1969). Simple calculations using the formulation given by Daddio (1977) indicate that the base of the mixed layer did not quite extend to the 37 m depth of the second meter.

The thickness of the lower boundary layer is also related, among other things, to the degree of water column stratification. With velocities as high as these, the boundary layer in an unstratified fluid could expand upwards to include virtually the entire water column. However, turbulent kinetic energy produced by shearing of the flow near the sea bottom is dissipated by buoyancy forces associated with water column stratification (and suspended sediment concentrations) (Adams and Weatherly, 1981). In effect, the stratification acts to "cap" the benthic boundary layer. Although no salinity or temperature data was available from this time period, it is likely that the water column during early August of 1980 was highly stratified (e.g. Smith, 1980; Fig. 42). In this case the lower boundary layer probably had a thickness of 10-20 m.

However, there is some doubt as to whether the mid-depth current meter is representative of the geostrophic interior. Theoretically, the current speeds in the interior should be higher than the speeds in the benthic boundary layer (Pedlosky, 1979). Yet the velocities at 70 m depth are slightly higher, suggesting that the true interior velocities

occur somewhat below 37 m (Fig. 62). Nonetheless, the directional shearing between 37 and 70 m is the correct sense for a flow in frictional adjustment with the bottom (Fig. 61c). The observed turning angle (20-25 degrees) is compatible with near-bottom veering that has been observed under downwelling situations such as this (e.g. Weatherly and Van Leer, 1977). However, without additional measurements it is difficult to say whether the 37 m depth records truly represent the interior flow conditions.

Discussion--Although the measurements came from the fringe of Hurricane Allen, the data provide an opportunity to examine the hypotheses of Hayes (1967) and Morton (1981) concerning the timing of the shelf response to a hurricane. Central to Hayes's (1967) proposed mechanism of shelf turbidity currents is the runoff of lagoonal waters across Padre Island following the storm. On the other hand, Morton (1981) argued that the peak current flow should be associated with the peak of storm winds. Neither explanation appears to fit the shelf response to Hurricane Allen at the CSA location (Fig. 63). The maximum current flow near the bottom (and at all levels) occurred during the approach of Hurricane Allen toward the coast. This peak current flow preceded the fall of lagoonal water levels by about 24 hours, indicating that the storm surge ebb (either across the barrier or out through the tidal passes) contributed very little to the general shelf water motion. Secondly, the maximum wind stress at Corpus Christi was recorded after currents had fallen to background levels. In fact, the currents appear to be only in phase with the Gulf tide levels.

This phase relationship is no coincidence. During Hurricane Allen's approach toward the coast, the winds in the CTCS area had a substantial

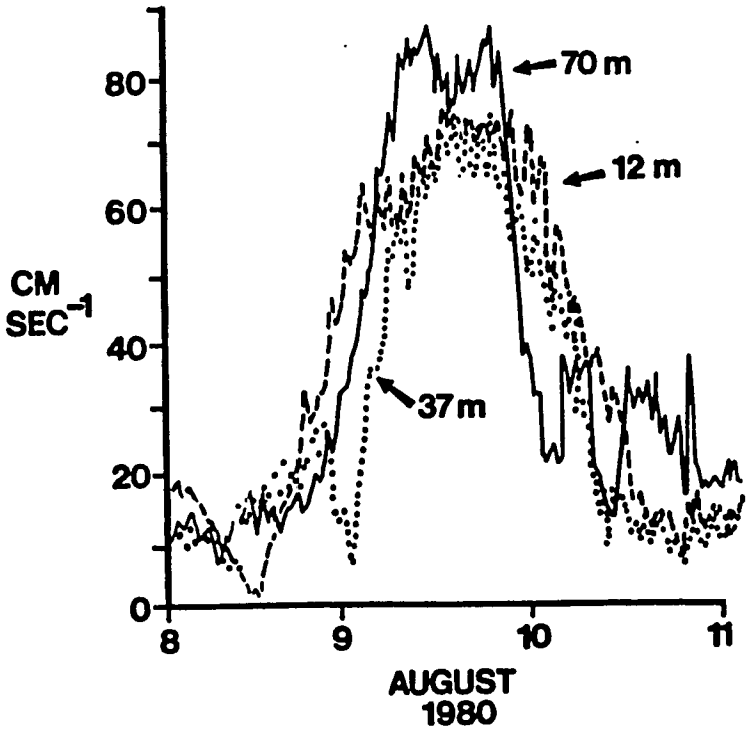

Fig. 62.--Comparison of unfiltered current speeds recorded at various depths by CSA array during Hurricane Allen.

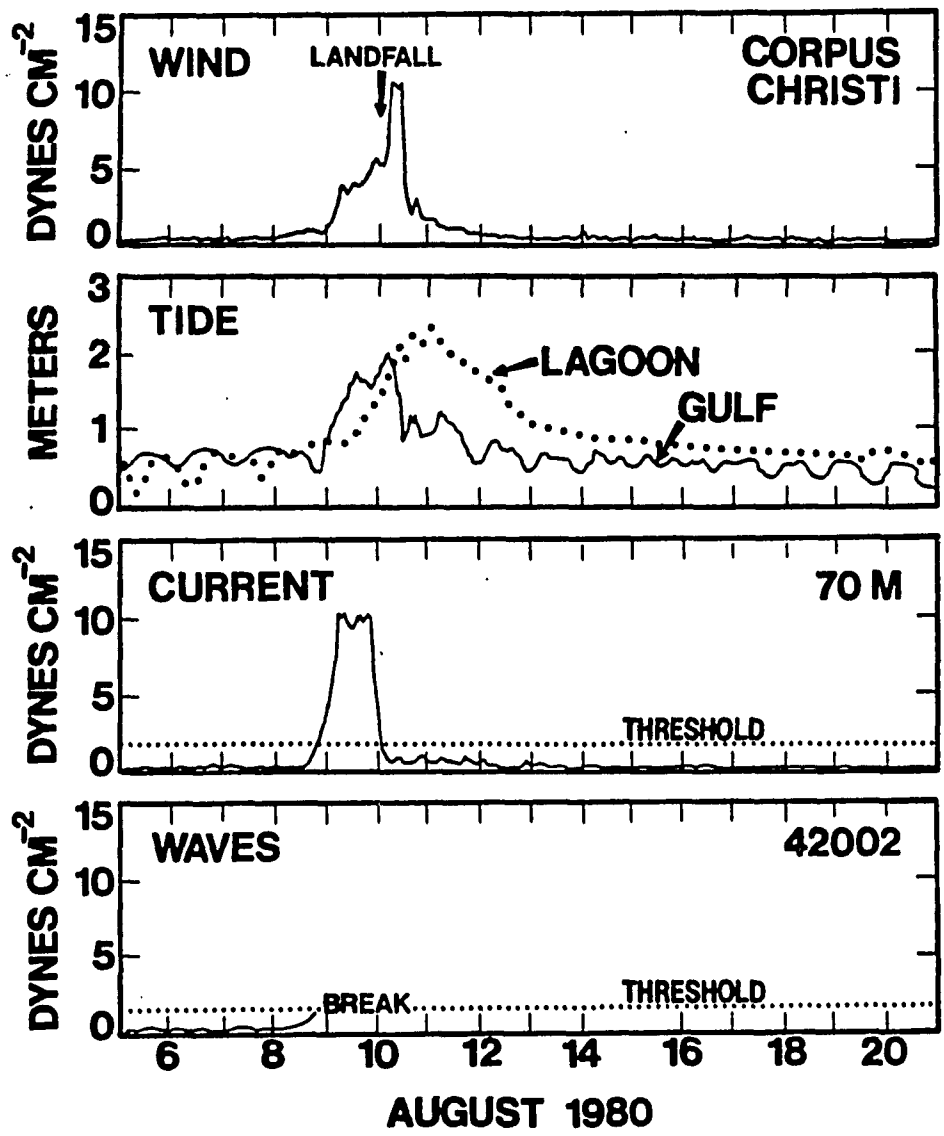

Fig. 63.--Unfiltered wind stress (Corpus Christ Airport), current- and wave-generated shear stress, August 5-21, 1980. Tide data from Jetty gauge at Port Aransas and Laguna Madre at Corpus Christi Naval Air Station. Dotted line is threshold of motion for 68 micron sand.

along-shelf component (Fig. 60). Because of the constraining influence of the coastal boundary, the result was a sea level set-up, as indicated by the Gulf tide gauge at Port Aransas. Because the storm stalled offshore from Port Isabel for over 24 hours, the flow induced by the along-shelf winds was of long enough duration to come into geostrophic balance with the wind-induced cross-shelf pressure gradient and the Coriolis force. Although interior motion has a slight onshore trajectory, the distribution of flow observed at the CSA array is consistent with the simple three-layer model advanced by Swift and Niedoroda (1984) (Fig. 41A).

Fig. 63 clearly demonstrates the importance of the wind orientation in driving shelf flow: wind stress on the 9th of August was actually lower than its magnitude on the 10th of August following landfall. The storm continued on land toward the north which took its winds closer to the CTCS area, resulting in higher values of wind stress. However, the wind at this point was directed from the south-southeast, a less favorable orientation for building the storm tide and cross-shelf pressure gradient. Hence, the Gulf tide level and near-bottom current velocity decreased.

It is also apparent that the current-generated shear stress easily exceeded the threshold of motion for the 68 micron sand mentioned earlier (Fig. 63). The waves measured prior to break-down of the NODC Buoy 42002 probably could not resuspend much material, however, in this water depth (74 m). Closer to shore, wave motion (and thus wave-current interaction) was probably quite significant. In fact, calculations of the wave-generated shear stress suggest that the waves measured during Allen could have resuspended 68 micron sand out to 68 m of

water depth (Fig. 64, Case C; Appendix B).

This data set provides a look at the current structure in the geostrophic zone during a hurricane. It is evident that similarities exist between the shelf response to this storm and the response recorded at the inshore current meters (12 m, 18 m, and 34 m) during the extratropical storm of September, 1984. In both cases, elevated tides were present, pointing to the presence of a wind-induced cross-shelf pressure gradient. This hypothesis is supported by the timing of current flow and by the fact that the wind stress in both cases was numerically smaller than the current-generated shear stress (compare Figs. 58 and 50).

Another similarity is the intense southwesterly flow recorded during the two events. This along-shelf transport direction appears to be in phase with the wind stress and the cross-shelf pressure gradient. Current flow during Hurricane Anita (Smith, 1978b) and Tropical Storm Delia (Forristall et al., 1977) was also primarily along-shelf to the southwest (and west in the case of Delia).

Hurricane Carla, 1961

Since 1957, eight major hurricanes have affected the Texas-Louisiana Coast (Fig. 65). Of these, five have made landfall along the Texas coast. Hurricane Carla, which struck the coast near Pass Cavallo on September 11, 1961, is generally considered the largest of these five and, in fact, is ranked as one of the largest storms in recorded meteorological history (Colon, 1966). Originating in the Caribbean, it displayed an unusually slow rate of forward progress which allowed the storm to build up to the point that its winds covered the entire

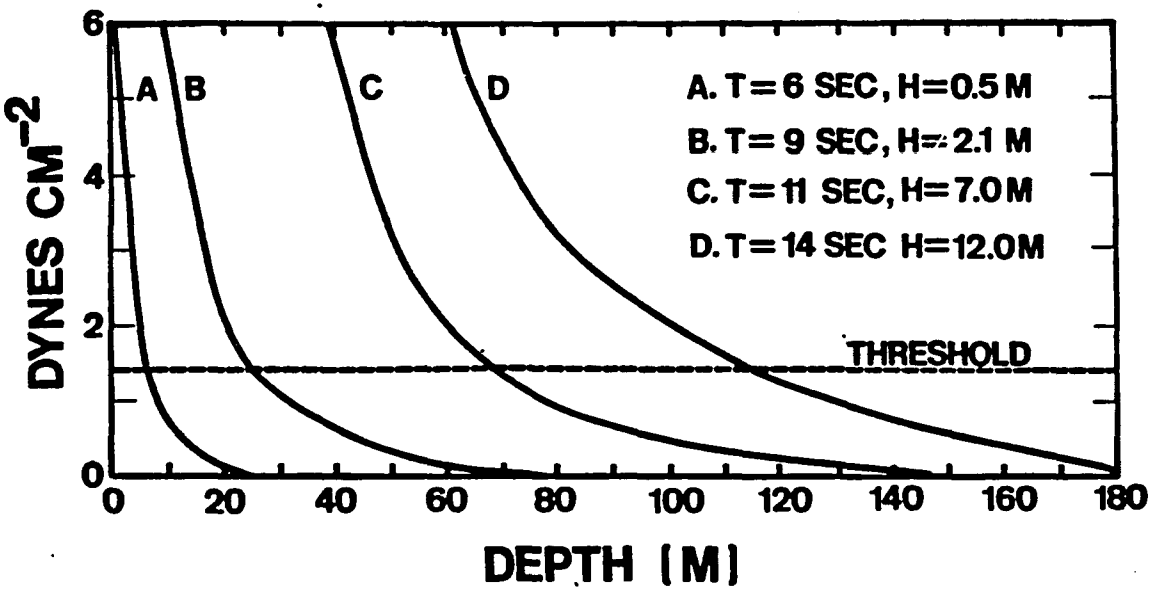

Fig. 64.--Boundary shear stress induced by wave orbital motion versus water depth for four different wave conditions (see Appendix B). Dashed line is threshold of motion for 68 micron sand.

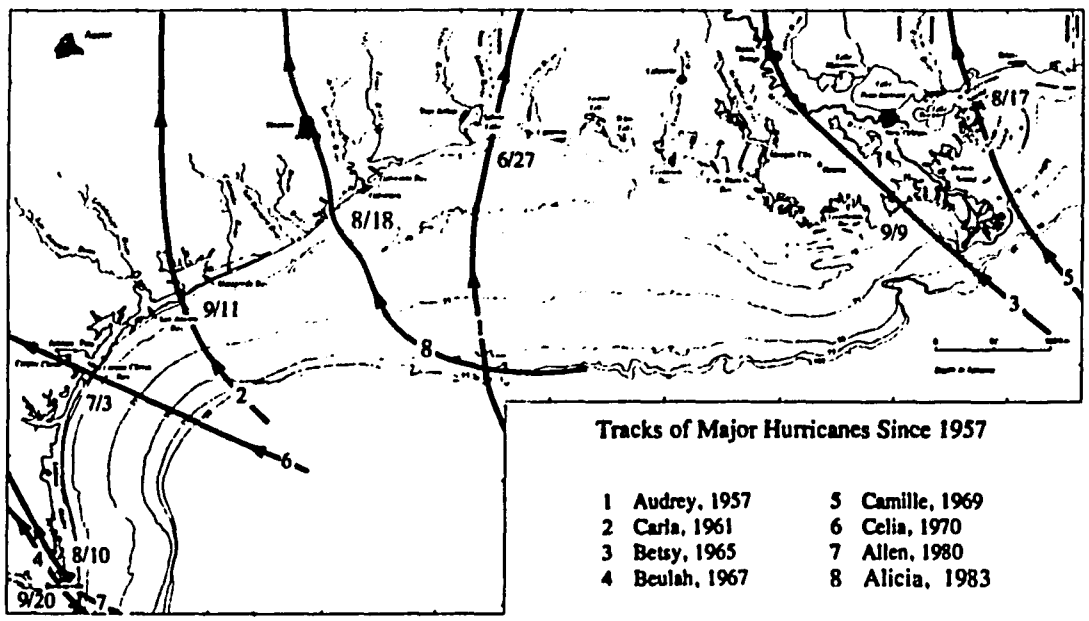

Fig. 65.--Tracks of the eight major hurricanes making landfall along the northwest coastline of the Gulf of Mexico since 1957. Date besides track is month and day of landfall (from Nummedal, 1982).

Gulf of Mexico (U.S. Army Corps of Engineers, 1962). Hurricane-force gusts (>33 m/sec) were reported from Brownsville to Port Arthur, Texas, a distance of 500 km (Ludlum, 1961). It made landfall near Pass Cavallo on the north end of Matagorda Island at 1600 hours September 11, 1961. Open coast storm tide peaked at 3.5 m just to the northeast of the point of landfall while tides in Matagorda Bay exceeded 7 m (Nummedal, 1982).

To the author's knowledge, there are no measurements of the shelf current field during hurricane Carla. However, it is important to extrapolate from known data and models to this storm. Carla comes very close to what is considered the 100 year storm (Colon, 1966; Nummedal, 1982), possibly the largest storm that can affect the Gulf of Mexico (Fig. 37b). Moreover, it is the storm upon which the models of Hayes (1967) and Morton (1981) were based. But most importantly, radiometric dating of the boxcores taken in the CTCS area indicate that this storm was responsible for the deposition of a discrete sand bed. This sand bed appears to have survived biological and physical reworking and it stands an excellent chance of becoming part of the permanent stratigraphic record of the Texas shelf.

Although no data exists on the bottom current structure during the storm, there is information available on the wind field, coastal sea level, and surface current flow during Hurricane Carla. Previous sections have established that there is a relationship between the wind field and resulting surface current kinematics, sea surface elevation, and bottom water flow. An effort was made to use the known information to infer the timing and magnitude of bottom current motion and resulting boundary shear stresses. The kinematics of fluid flow in various

coastal ocean dynamic zones was deduced from observations of surface current motion as well as data collected during other storms and from the results of numerical models.

Winds--It is enlightening to contrast the wind history of Hurricane Carla against the wind records of the other four major hurricanes which have affected the CTCS area since 1961 (Fig. 66). For the sake of comparison, the time series were chosen from stations located about 160 km (100 miles) north or northeast (to the right) of the point of landfall of the storms. The records are aligned on the time that the storms made landfall (dotted line). Wind speed was converted to wind stress using the quadratic stress law with an air density of 1.20×10^{-3} g/cm^3, and a drag coefficient of 1.20×10^{-3} for wind speeds below 11.0 m/sec and 1.50×10^{-3} above 11.0 m/sec (Large and Pond, 1981). Land-based wind measurements were converted to equivalent offshore speeds using the formulation of Hsu (1981). The time series emphasize the difference between large-scale hurricanes such as Carla and small but intense storms such as Celia (1970) and Alicia (1983). The high wind stress shown by Hurricanes Beulah (1967) and Allen (1980) following landfall can be attributed to the northerly path which they took after coming on land (Fig. 65). What is critical to shelf sedimentation, however, is the magnitude and duration of sustained winds prior to landfall. The data from Hurricane Allen demonstrated the importance of the along-shelf winds during the storm's approach toward the coast. Carla's wind record shows a longer duration and greater overall magnitude than any of the other hurricanes during this approach phase. This may be one reason why Hurricane Carla produced the largest storm tide of the five.

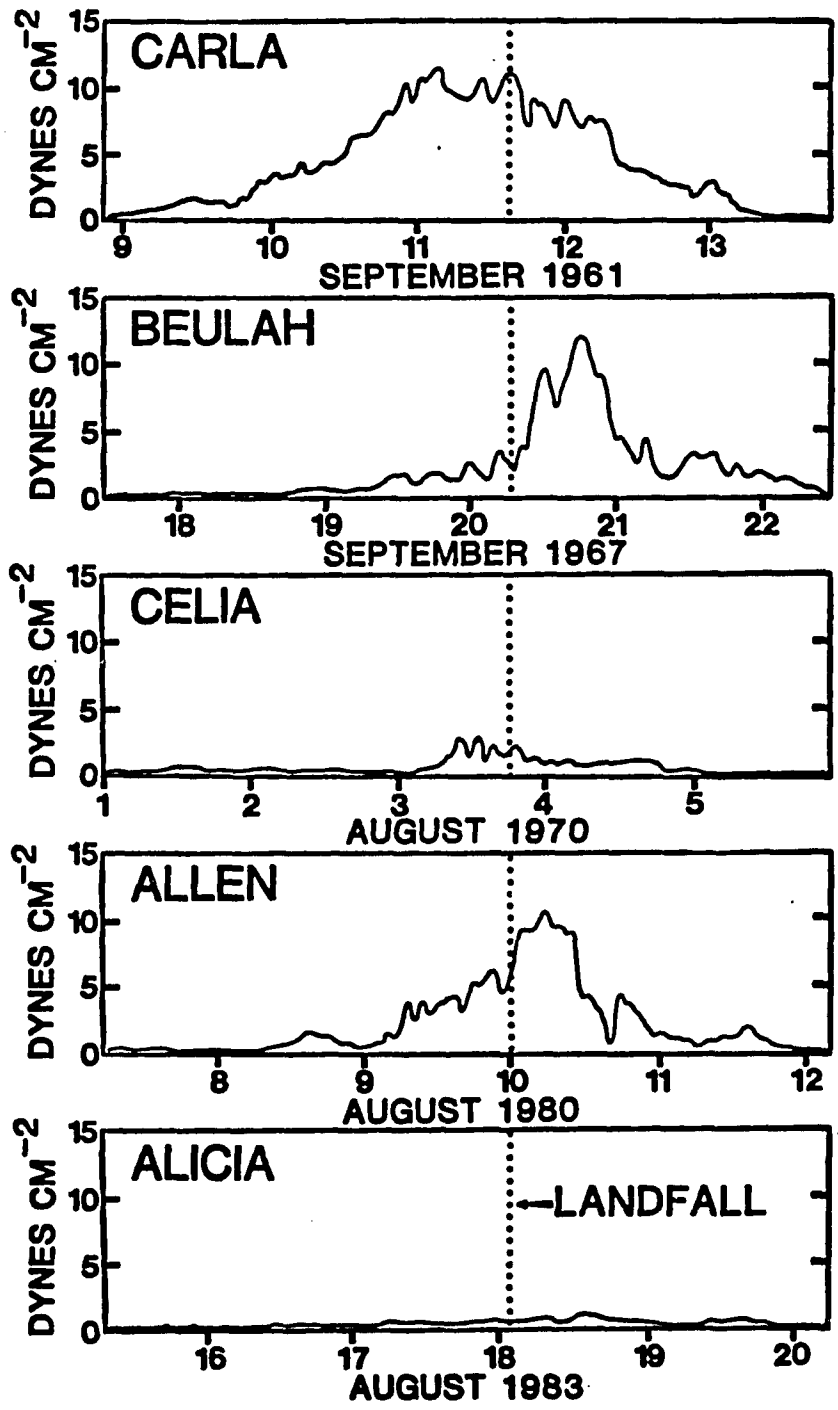

Fig. 66.--Comparison of wind stress time series of the five major hurricanes which have affected the CTCS area since 1957. Hurricane Carla measured at Galveston, Texas. Hurricanes Allen and Beulah recorded at Corpus Christi, Texas. Hurricane Celia at Palacios, Texas and Hurricane Alicia at Lake Charles, La. Data from U.S. Weather Bureau.

Storm Tide--The magnitude of the superelevated coastal water levels associated with storms such as Carla depends upon a large number of factors, including the central pressure index (the difference in the atmospheric pressure within the eye and that at the periphery of the storm), the storm's forward speed, the angle of the storm track relative to the local coastline, the storm radius to maximum winds, the size of the forerunners (long period waves which precede a storm), storm waves, normal tide levels, and the magnitude and orientation of the storm winds (Nummedal, 1982). It has been shown numerically that the most important factors of these are the magnitude, orientation, and duration of the wind stress (Jelesnianski, 1970). The inverse barometer effect (the sea surface bulge caused by the storm's atmospheric pressure gradient) represents 10-20 % of the overall storm surge (Simpson and Riehl, 1981).

Fig. 67 shows tidal records from three Gulf gauges along the coast affected by Carla. Predicted lunar-solar tides were subtracted off the observed measurements to yield the residual sea level elevations. The gauges were of the type that effectively filtered out surface gravity wave motion. It should be remembered that the water levels were referenced to mean sea level and not to a common vertical datum. In spite of the possibility of slight leveling differences between the gauges, there is clear evidence that sea level rose significantly at all three stations. The largest tides were at Matagorda, just to the right of the landfall point of the eye of Carla. The right-skewed storm tide pattern is typical of most hurricanes (Simpson and Riehl, 1981; Nummedal, 1982). This is partly due to the asymmetric distribution of wind speeds, the strongest in the northeast quadrant of the storm, and gene-

Fig. 67.--a) Location of tide gauges and track of Hurricane Carla. b) Comparison of residual (observed minus predicted) tidal heights from seaside tide gauges at Matagorda, Galveston, and Port Aransas, Texas. Height above mean sea level. Break indicates point at which tide gauge at Port Aransas became inoperative. From data of U.S. Army Corps of Engineers (1962).

(next page)

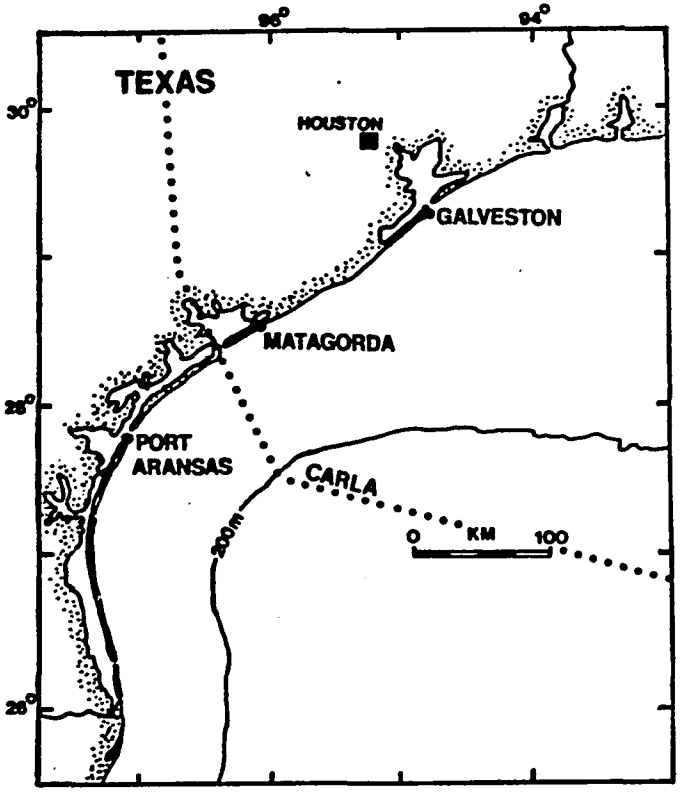
96°
94°
TEXAS
30°
HOUSTON
GALVESTON
MATAGORDA
28°
PORT
ARANSAS
CARLA
200m
0 KM 100
26°

a

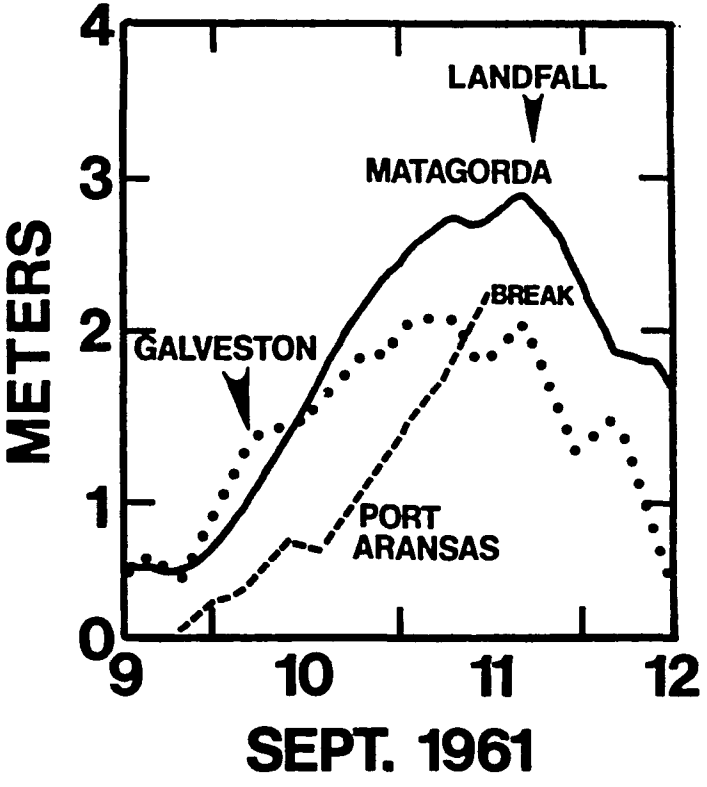
4
3
2
1
0
METERS
LANDFALL
MATAGORDA
BREAK
GALVESTON
PORT
ARANSAS
9
10
11
12
SEPT. 1961

b

ral along-shelf and onshore winds in this area during storm approach (Crutcher and Quale, 1974; Chow, 1971; Fig. 68). Offshore winds on the left side of the storm track oppose the storm-driven water bulge, thereby decreasing the overall heights.

Assuming the sea surface in the eastern Gulf of Mexico (distant from Hurricane Carla) to be largely invariant during this time, the large changes in absolute height at the Texas coast suggest a wind-induced sea level set-up and cross-shelf pressure gradient. The presence of such coastal pressure fields and their influence upon shelf flow is well documented (e.g. Beardsley and Butman, 1974). In addition, significant differences in sea level elevation at the three gauges are symptomatic of oppositely directed along-shelf pressure gradients on either side of the storm track.

This interpretation is supported by a numerical model study of the storm surge of Hurricane Carla by Miyazaki (1965). Based upon Ekman's (1905) equations for wind-driven transport, a finite-difference scheme was employed to derive the areal distribution of the storm surge upon the Texas shelf just prior to landfall (Fig. 69). Bottom and surface friction was included in the calculations. The model results fit well with the observed magnitude and timing of the surge at several coastal locations.

Magnitude of Current Flow--Previous sections of this dissertation have illustrated that the primary mechanisms forcing fluid flow during peak flow events in the CTCS area are the wind-induced pressure gradient and the wind stress. Rough estimates of the magnitude of current strength during Carla were made by use of the general relations describing motion due to simple wind forcing and geostrophic motion due to sea

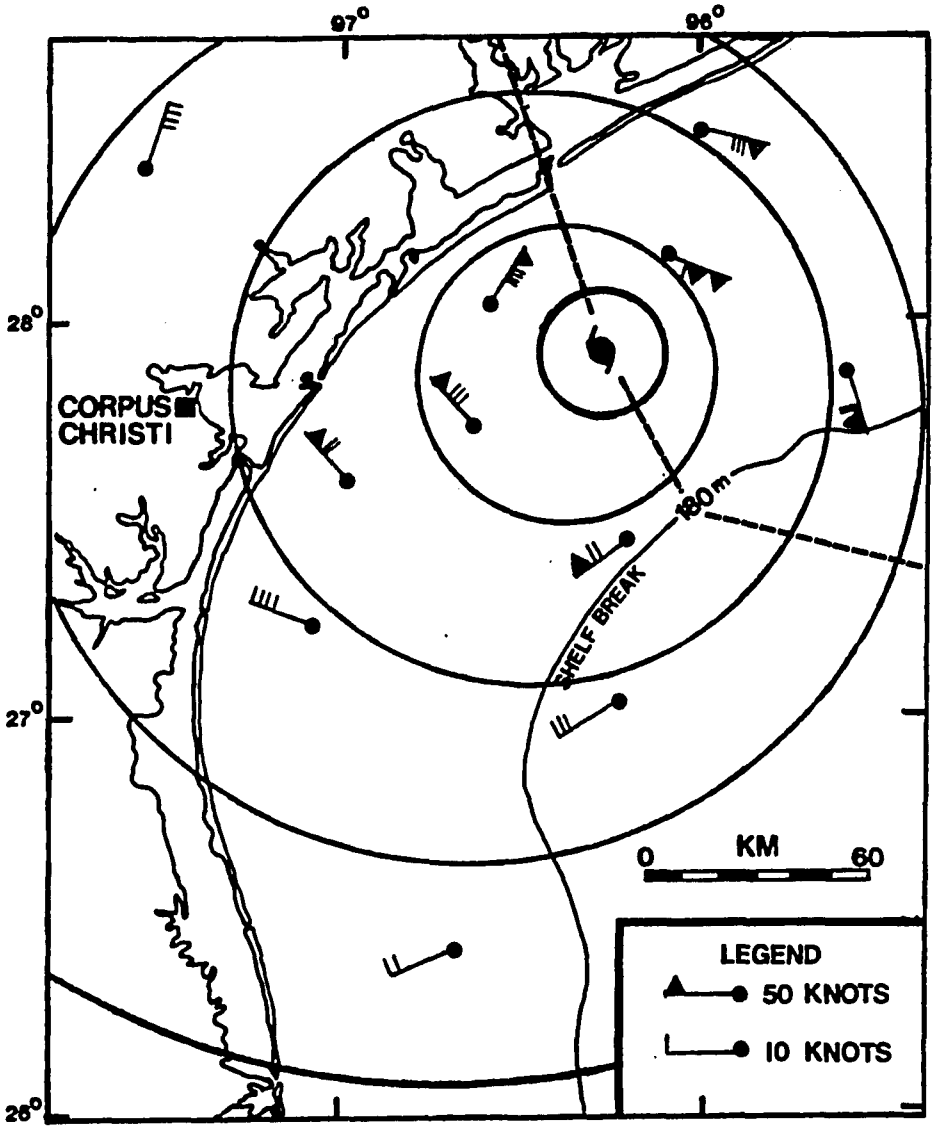

Fig. 68.--Surface wind field, 1000 CST 11 September 1961. Dashed line is path taken by eye of Hurricane Carla. Landfall of eye occurred at 1600 CST 11 September. Wind velocities are hourly sustained averages. Based upon data of Cardone et al., (1976), Ludlum (1961), and U.S. Army Corps of Engineers (1962).

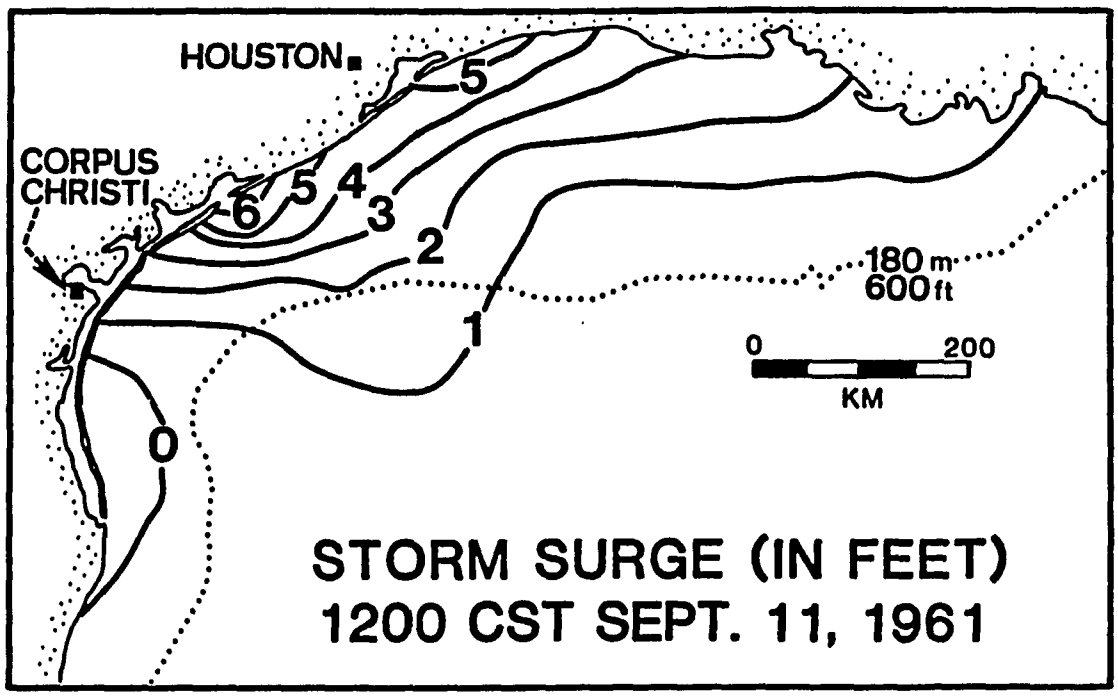

Fig. 69.--Hypothetical storm surge (in feet) during the approach of Hurricane Carla, 1200 CST Sept. 11, 1961 (From Miyazaki, 1965). Numerical model is based upon Ekman's (1905) equations and the quadratic stress law (for bottom and surface stress).

surface slope. This is shown in Fig. 70. The wind-driven surface current speed, V_o, was derived from the empirical relationship presented by Ekman (1905):

$$V_o = 0.0127\ W\ /\ (\sin\phi)^{1/2}$$

where W is the wind speed (m/sec) and ϕ is the latitude in degrees. It is understood that this expression is valid only outside 10 degrees north or south latitude and that it assumes a drag coefficient of 1.4 X 10^{-3} (Pond and Pickard, 1983). In addition, time dependent effects and the mixed layer depth are not considered. Nonetheless, the relationship has proven satisfactory for calculating speeds of surface currents driven strictly by the wind (McLelland, 1965).

The geostrophic or interior flow speed, U, was derived from the simple relationship given by Beer (1983):

$$U = g\ D\ /\ f\ L$$

where g is the gravitational acceleration, D is the sea surface elevation above the geopotential or level surface (such as mean sea level), f is the Coriolis parameter (at this latitude 6.6 X 10^{-5} s^{-1}), and L is the length scale across which the slope is present. Implicit in the use of this expression is the assumptions that the Coriolis and pressure gradient accelerations are the only accelerations present and that they are in balance (Pond and Pickard, 1983). Hence, frictional forces and accelerations are neglected. Nevertheless, the equation does give insight into the magnitude of current speed in the frictionless interior away from the upper and lower boundary layers (McLellan, 1965).

The numerical model results of Miyazaki (1965) were used to derive

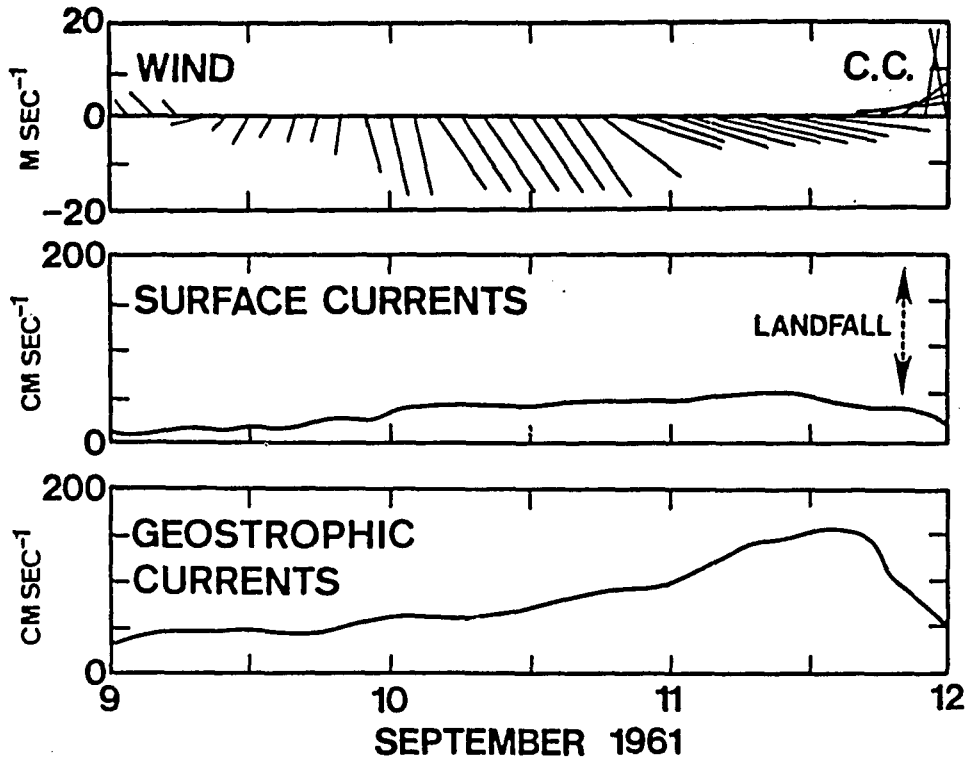

Fig. 70.--Time series of wind measured at Corpus Christi Naval Air Station, calculated wind-driven surface currents, and calculated geostrophic currents during Hurricane Carla. Orientation of axes for wind such that vertical axis is alongshelf (v) component, positive to the northeast and horizontal axis cross-shelf (u) component, positive offshore. Surface current velocity based upon Ekman's (1905) empirical expression. Geostrophic calculations use sea surface heights and slopes from numerical model of Miyazaki (1965).

the proper sea surface slope for calculation of the geostrophic speeds during Carla's approach. Interestingly, Miyazaki (1965) found that the slight undulations in the sloping surface due to atmospheric pressure gradients became essentially submerged in the high surge area of the shelf (Fig. 69). The simulated tidal record form Pass Cavallo, the landfall point of the storm, was used in the calculations.

The calculated magnitude of geostrophic currents during Hurricane Carla are substantial, nearly 150 cm/sec. This exceeds the wind-forced surface current strength by a factor of three, further emphasing the importance of the barotropic distribution of mass (and resulting cross-shelf pressure gradient forces) in driving flow during the storm. Currents of this magnitude and the resulting boundary shear stresses (probably on the order of 15 dynes/cm^2, assuming lower velocities near the boundary) easily exceed the threshold of motion for 68 micron sand or any sand size available for transport in the CTCS area.

Superimposed upon this current-generated stress during the storm is the shear stress arising from wave orbital motion. Simple calculations of the wave-induced shear stress based upon significant wave heights and periods actually recorded during the Carla suggest that the threshold for the initation of motion was exceeded across much of the shelf (Fig. 64, Appendix B). Current-induced and wave-generated shear stresses will often interact in a non-linear fashion to produce a total boundary shear stress greater than the simple sum of the two (Grant and Madsen, 1979). This leads to the inference that the wave and current conditions were sufficient for sand transport in the CTCS area during Hurricane Carla.

A general statement about the timing of sand transport can also be

made, given the relative magnitudes of the geostrophic and wind-forced current components of motion. Data from Hurricane Allen suggested that the peak flow was essentially in phase with the storm tide, as would be expected with a geostrophically-balanced flow (Fig. 63). Like Hurricane Allen, gulf tide gauges northeast of the point of landfall of Carla show peak water levels occurring just prior to the landfall of the eye of the storm. This is due in part to the strong along-shelf component of the hurricane winds as the storm approached the coast (Fig. 68). Net surface water transport, of course, is at 90° to the right of the wind. Unfortunately, this can not be verified in the CTCS area south of the storm track as the gauge at Port Aransas area failed late on the 10th as water was still rising (U. S. Army Corps of Engineers, 1962; Fig. 67). Nonetheless, observed data from Hurricane Allen (Fig. 63) and rough calculations of the contributions of wind stress and pressure gradient forces during Carla (Fig. 70) indicate that the majority of sand transport probably took place in the 24 hour period prior to hurricane landfall.

Kinematics of Sand Transport--Reconstruction of the sand transport pathway during the approach of Hurricane Carla is difficult, given the lack of Eulerian measurements of fluid motion. Deductions can be made, however, based upon inferences of surface current flow made during Carla, analysis of bottom current motion during other storms, numerical models, and a general knowledge of the characteristics of fluid motion in the coastal ocean dynamic zones.

Friction-Dominated Zone--Studies of the Atlantic shelf suggest that during yearly peak flow events, the friction-dominated, transition, and geostrophic zones correspond to morphologic zones of the shoreface,

inner and outer shelf, respectively. However, it is possible that during a storm of the size of Hurricane Carla, these dynamic zones expanded even further seaward. The shore-normal distribution of the zones was probably a function of the magnitude of the driving forces, water column stratification and time-dependent processes such as mixed-layer deepening. Analysis of available information about Carla suggests that the friction-dominated zone may have extended out into the inner shelf (Fig. 71a). As mentioned, the non-rotational flow typical of this zone is most prevalent in situations where the water depth is less than 10 % of the surface Ekman layer depth. Given the 25-35 m/sec sustained wind speeds experienced over the CTCS area during the approach of Hurricane Carla toward the coast (Fig. 68) and calculated surface Ekman depths of 220-250 m, it is theoretically possible that the friction-dominated could expand out to water depths of 22-25 m. However, it is likely that the physical process of Ekman layer deepening is similar to mixed layer deepening which in turn is dependent upon the water column stratification and the duration of applied wind stress (Daddio, 1977; Pollard et al., 1973). In the CTCS area during the summer season, shelf waters shoreward of 18 m are generally unstratified (Fig. 42). Stratification in the 20-25 m depth range present during Carla probably was broken down in the midst of the intense wind and wave mixing during the 24 hour period in which Carla slowly approached the coast.

Thus, one may start with the presumption that bottom current flow (and sand transport) in the 0-25 m depth range (friction-dominated zone) was similar to surface current flow direction. Analysis of the wind field present during this period suggests that surface water in

Fig. 71.--a) Hypothetical distribution of coastal ocean dynamic zones during approach of Hurricane Carla toward the Texas coast. b) Surface currents (1 m below surface) generated by wind field of Hurricane Carla. Dotted line is the track of the eye of Carla. c) Hypothetical bottom current patterns for flow 1 m off bottom. d) Near-bottom combined flow transport patterns during approach of Hurricane Carla. u_c is the steady current flow, $+u_w$ the onshore component of the oscillatory flow, and $-u_w$ the offshore component. Format from Swift et al., (1985). Wave kinematics based upon observations of King and Shemdin (1978).

(next page)

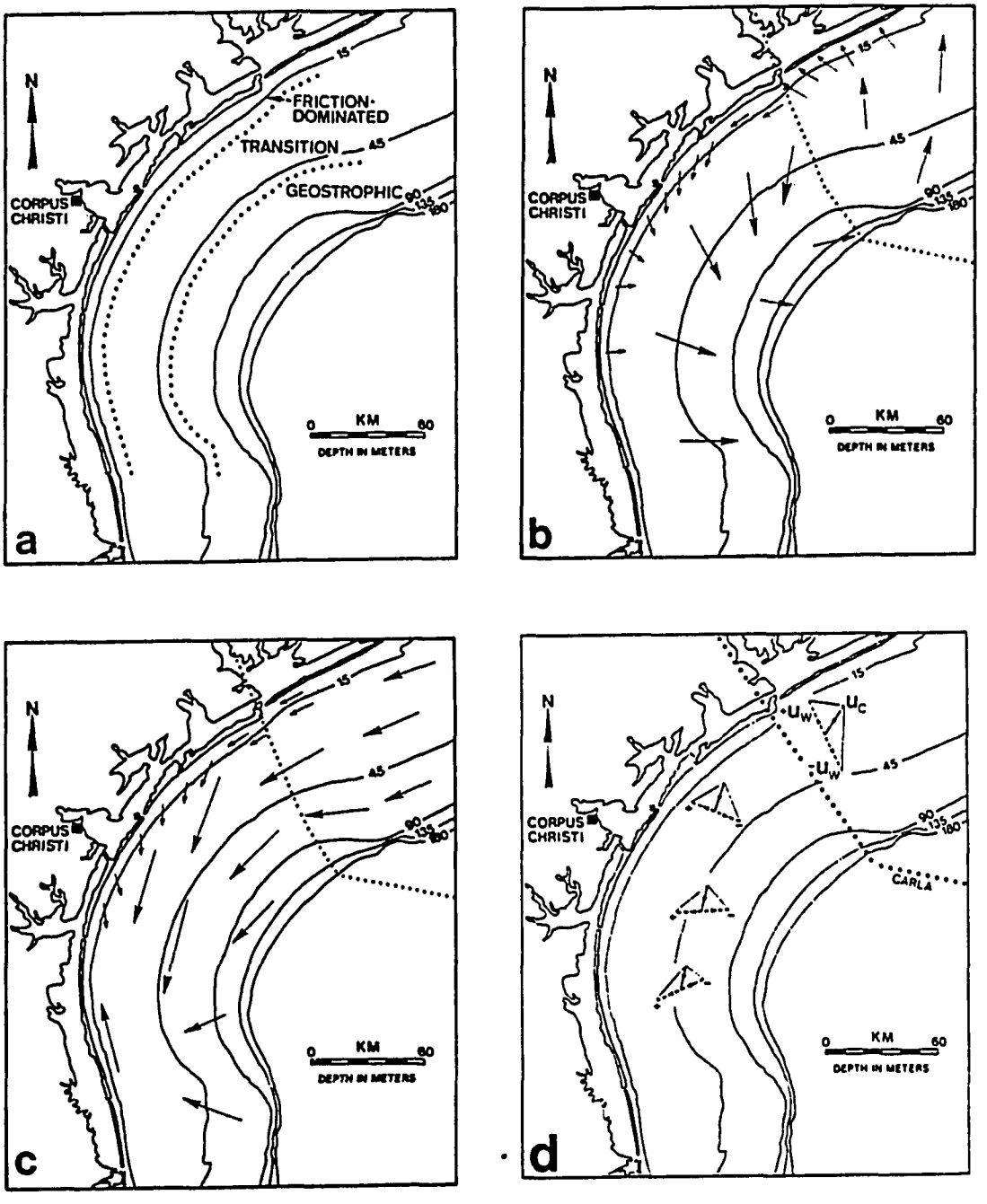
N
FRICTION-
DOMINATED
TRANSITION
GEOSTROPHIC
15
45
90
135
180
CORPUS
CHRISTI
0 KM 60
DEPTH IN METERS
a
b
c
d
U_W
U_C
CARLA

this area was driven onshore to the right of the storm track and offshore to the left of the storm track (Fig. 68 and 71b). This is supported by the pattern of surface drifter returns reported by Chew et al., (1962). They found a larger number of returns (normalized for coastal population density) and earlier returns on the right side of the storm track than the left, suggesting onshore surface flow to the right and offshore surface currents to the left of the storm track (Fig. 72).

The concept of a nearshore flow with little directional shear has been discussed previously by Gordon (1982) and Csanady (1982). Forristall et al., (1977) observed currents in 21 m water depth near Galveston, Texas during the passage of Tropical Storm Delia in 1973 (Fig. 73). The current meter array was located on the left side of the storm track until 1530 hours (dashed line) when it passed to the southwest, and headed toward landfall near Freeport, Texas at 2000 hours (arrow). Interestingly, there was very little change in current flow direction throughout the water column and bottom current speeds were within 75 % of the surface speeds. Flow was along-shelf and slightly offshore at an angle of 14^{o} to the isobaths. Although this record has been interpreted by others to represent strictly wind-forced flow (i.e. Morton, 1981; Hobday and Morton, 1984), Forristall et al., (1977) acknowledged that the observed motion was certainly in geostrophic balance with the wind-induced pressure gradients. This conclusion is supported by two observations: 1) The current-generated boundary shear stress has twice the magnitude of the wind stress; and 2) The current flow does not respond to significant changes in the wind speed or direction (Fig. 73).

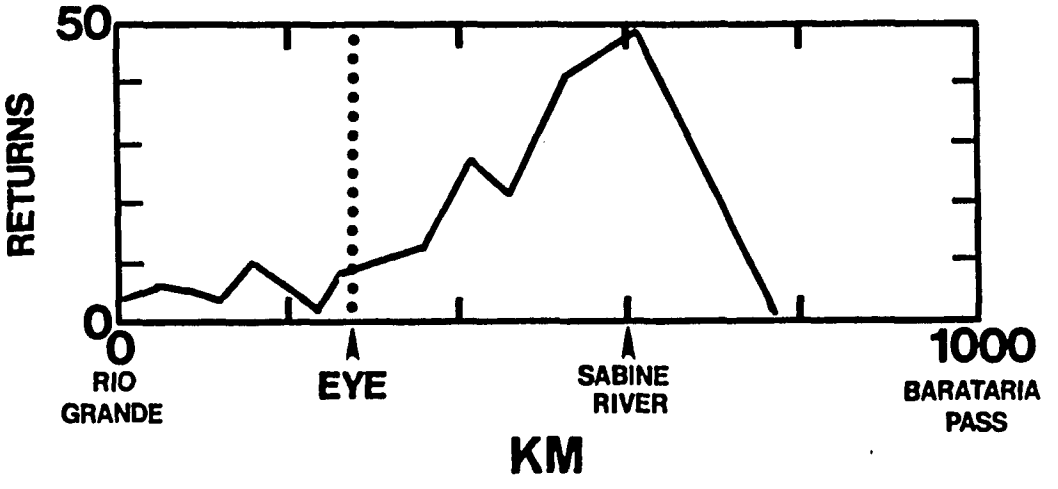

Fig. 72.--Distribution of surface drifter returns along the Texas and Louisiana Coast, normalized for population density (adapted from Chew et al., 1962). Drifters were released August 20, 1961, (three weeks prior to passage of Hurricane Carla) just seaward of the Mississippi delta.

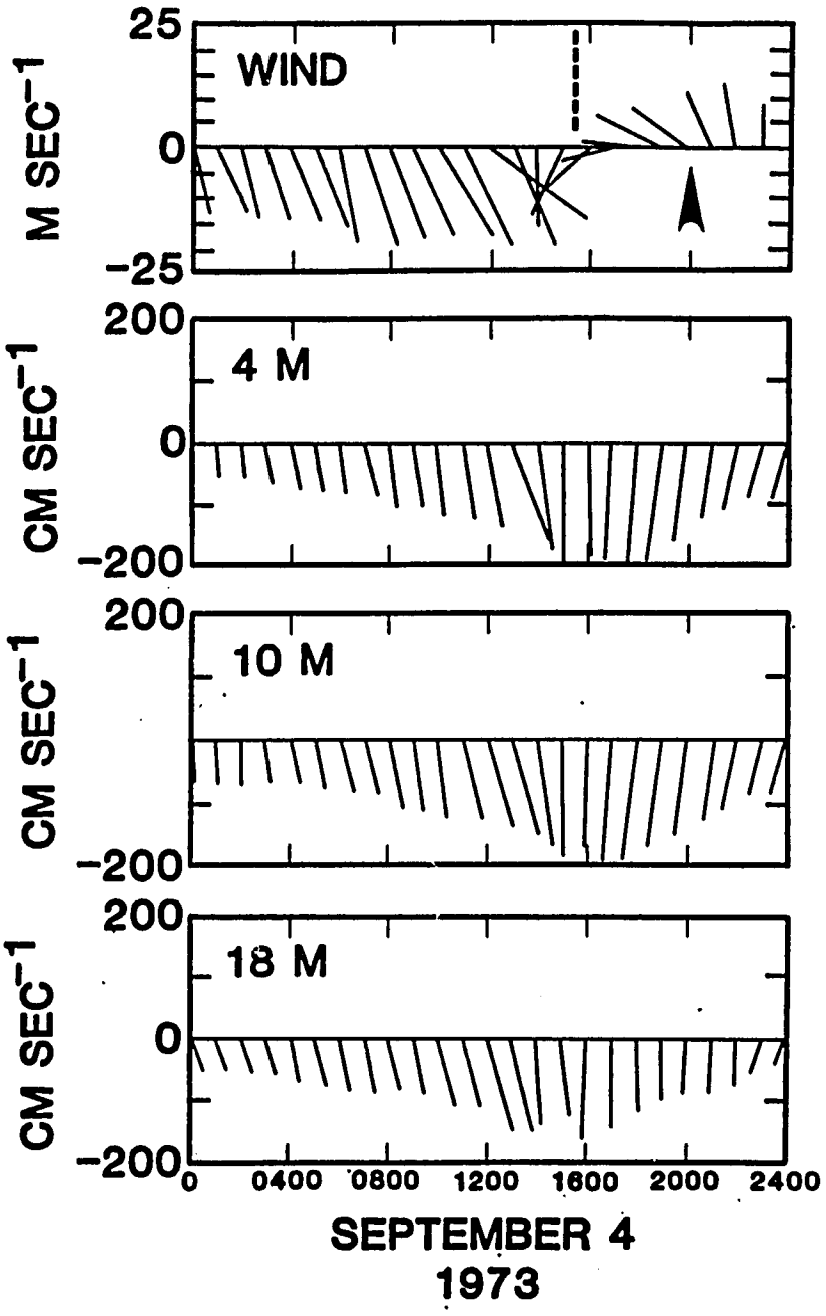

Fig. 73.—Wind and current vectors at 4, 10, and 18 m levels in 21 m of water offshore from Galveston Island, Texas during passage of Tropical Storm Delia in 1973 (adapted from Forristall et. al., 1977). Orientation of axes same as in Fig. 70.

An alternative explanation for the lack of directional shear observed by Forristall et al, (1977) is that the entire water column was the logarithmic zone of a lower boundary layer. It has been noted that very little directional shear occurs in the logarithmic layer in contrast to the overlying Ekman layer (Kundu, 1976). However, the velocity profiles recorded during the storm do not plot as straight-lines in log-linear coordinates, invalidating this hypothesis.

The assumption of a surface to bottom non-rotating flow pattern, however, does create problems in the friction-dominated zone if one considers the continuity of water volume. On the right side of the storm track, the onshore flow of surface waters cannot continue for a long period of time (such as the nearly 24 hours that Carla affected the coast during its approach) without some time of bottom flow compensation (Gorden, 1982). The kinematics of this flow depend to some degree upon the water column stratification. In the case where a well-developed pycnocline is present, it is expected that the onshore surface flow is complemented by a offshore bottom flow (Fig. 74,A). It has been suggested that the offshore-directed motion observed on the right side of the track of Hurricane Camille during its approach toward the northern Gulf Coast is evidence for this phenomenon (Murray, 1970; Fig 75). However, there are several points to consider with regard to this concept of a two layer flow, which by the way has received considerable attention (e.g. Walker, 1984) . One is the fact that the offshore flow, presumably driven solely by the cross-shelf pressure gradient, must eventually (once the flow has a time scale comparable to the inertial period) come into balance with the Coriolis force and turn along-shelf (in this case, to the southwest). Secondly, there is

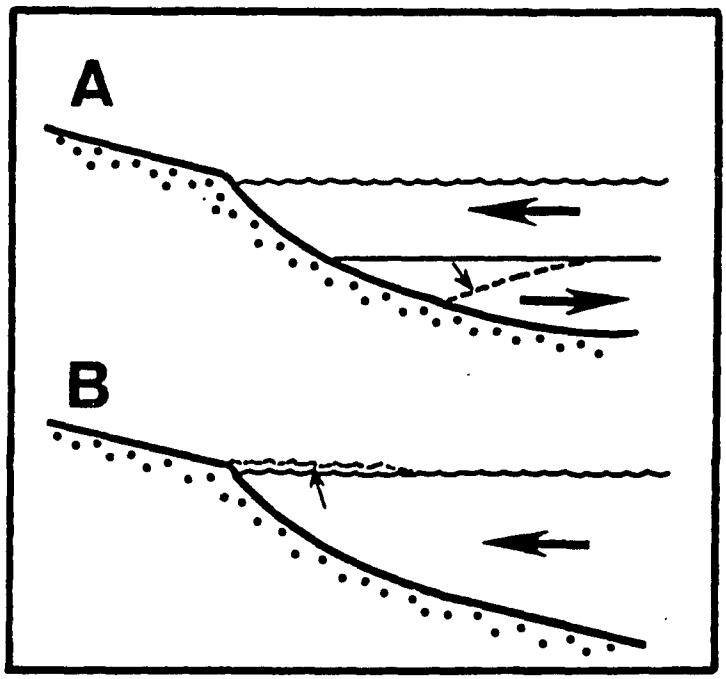

Fig. 74.--Possible responses to onshore flow in the friction-dominated zone: A) Thermocline is present and onshore flow is compensated by deeper return flow. B) No thermocline is present and change in surface elevation opposes further onshore flow; Hence, only alongshelf flow is allowed (From Gorden, 1982).

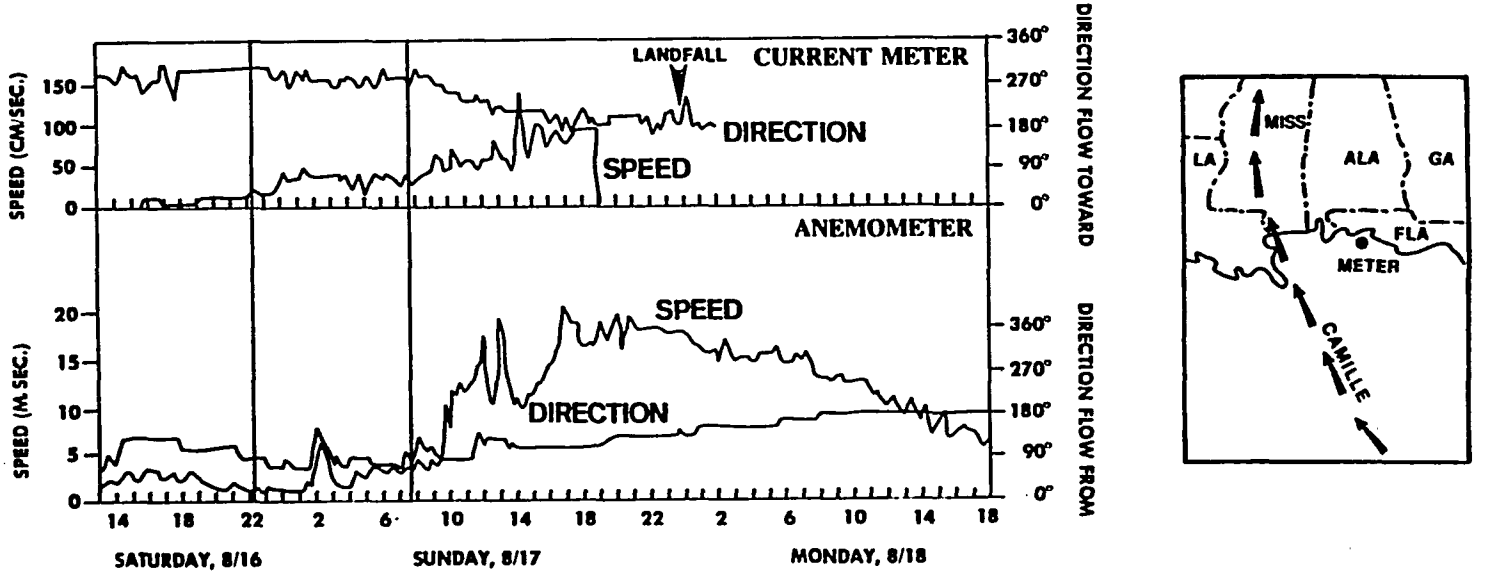

Fig. 75.—Onshore wind and offshore current meter data collected during Hurricane Camille. Inset shows location of MARINE ADVISORS Q16 current meter in 6.3 m of water 160 km east of the path of the eye of Hurricane Camille (from Murray, 1970).

evidence which suggests that the water column was unstratified in the friction-dominated zone on the right side of Carla's track: Stevenson and Armstrong (1965) found in surveys following the storm that the thermocline was absent in water shallower than 50 m to the east of the storm track (Fig. 76). In the case of an unstratified nearshore setting, the onshore flow is compensated by along-shelf flow (Gordon, 1982; Fig. 74, B).

On the left side of the storm track, water driven away from the coast must be replaced. Otherwise, adverse pressure gradients opposing this flow will result. This same problem was noted in a numerical model derived by Forristall (1974) to simulate the shelf response to Hurricane Camille, which made landfall on the Louisiana Coast on August 17, 1969 (Fig. 77). Forristall (1974) deduced that vertically averaged transport on the left side of the storm track was obliquely offshore and to the west. However, in this case, continuity of water volume was preserved by lateral advection of water along-shelf from the east. It is presumed that such a situation occurred on the Texas shelf during Carla, with along-shelf motion on the fringe of the storm and along-shelf flow from the friction-dominated zone on the right side of the storm (Fig. 71c).

Geostrophic Zone--Previous sections have shown that flow in the deeper waters of the CTCS area shows considerable directional shear. This is due in part to the well-established stratification in these waters (Fig. 42). Surface flow during the approach of Hurricane Carla was, as discussed, generally onshore on the right side of the track and offshore on the left (Fig. 71b). However, bottom current flow in the 50 to 180 m depths of the geostrophic zone (50 to 180 m) was probably

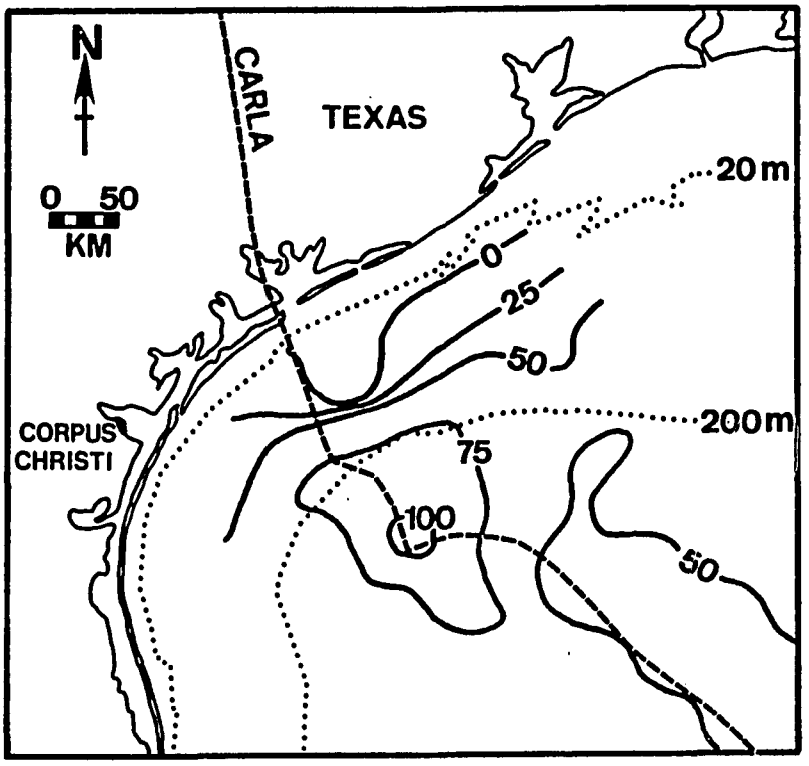

Fig. 76.--Depth to thermocline (25°C) as determined by thermistor measurements made one month after the passage of Hurricane Carla in 1961. Dashed line is path of the eye of Carla. From Stevenson and Armstrong (1965). Contour interval equals 25 meters water depth.

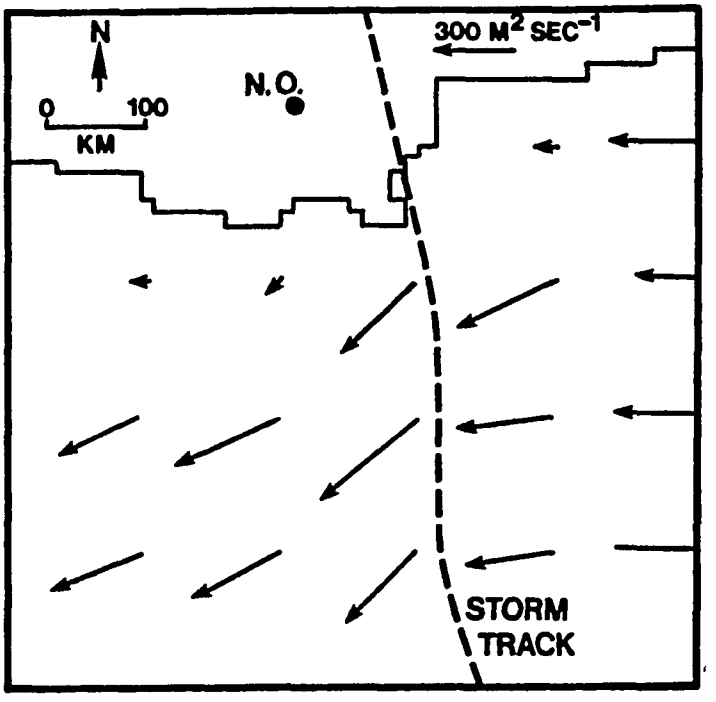

Fig. 77.--Predicted vertically averaged transport vectors at landfall of Hurricane Camille, 1900 hours, August 17, 1969 (from Forristall, 1974). Transport in m^2/second. Dotted line is track of the eye of Camille.

much different. If an analogy to the data collected during Hurricane Allen can be made, it is conceivable that bottom current motion on the right side of the storm track was along-shelf to the southwest (compare Figs. 61 and 71c). On the left side of the track it is probable that bottom motion was similar, perhaps with a slight onshore component to the flow in the outer most portion of the geostrophic zone, in areas where the pressure-gradient force and constraining influence of the coastal boundary was less important. This is consistent with the observations of Stevenson and Armstrong (1965) who noted decreases in bottom water temperature out in deep (>1000 m) water, suggestive of upwelling.

Transition--In between the friction-dominated and geostrophic zones lies a transitional realm where the flow described above must converge. In the 25-50 m depth range, the water column is generally stratified in the summer and unstratified during the winter (Fig. 42). Eulerian data collected during the September 1984 flow event indicate that mid-shelf current velocities were the highest. If this pattern was displayed during Carla, it is probable that the current velocities and current-generated boundary shear stresses were highest in this zone. Work upon other shelves has shown that the interior flows in this mid-shelf region approximate a geostrophically balanced coastal jet (Csanady, 1982). As shown previously, this geostrophic motion in the CTCS area tends to be southwesterly, along-shelf. However it is likely that flow in the lower boundary layer, below this point, departed significantly from this geostrophic balance due to the presence of friction and the condition that the velocity go to zero at the bottom (Pedlosky, 1979). This ageostrophic flow was characterized by the leftward rotation of

the current vectors looking downward (i.e. veering in the offshore direction). The degree of Ekman veering for downwelling episodes such as this is generally on the order of 20 to 30° (Weatherly and Van Leer, 1977; Kundu, 1976). Although the presence of suspended sediment, such as expected here, can increase the overall angle by several degrees, it appears that the most important effect of a sediment concentration gradient is related to the production of a more even distribution of turning through the Ekman layer (Adams and Weatherly, 1981).

Thus, it appears that bottom flow in the transition zone (25-50 m) was oriented obliquely along-shelf and offshore to the southwest on the left side of the storm track in the CTCS study area (Fig. 71c). Bottom water motion oriented obliquely offshore on the Washington continental shelf has also been ascribed to veering in the lower Ekman layer (Smith and Long, 1976). This motion probably converged upon and was modified by the along-shelf flow of the deeper geostrophic zone. This in turn may have given rise to secondary flow patterns with smaller spatial scales.

Another factor of consideration which is not explicit in the models of Swift et al., (1985) is the effect of the along-shelf pressure gradient. Along-coastal differences in sea level elevation during Hurricane Carla suggest the presence of gradients parallel to the coast (Fig. 67). It appears that a significant pressure-gradient was oriented to the west in the CTCS area and to the east in the area to the right of the storm track. The along-shelf gradients would tend to augment the general downwelling motion in the CTCS area and oppose motion in the areas to the east. Smith (1978b) inferred from tide

gauge measurements that the along-shelf slope generated by the passage of Hurricane Anita complemented the general southwesterly bottom motion in the Port O'Connor area.

Hurricane Waves and Combined Flow--The kinematics of sediment transport during large storms such as Carla is dependent upon both current and wave kinematics (Grant and Madsen, 1979). Often the directions of the steady current flow and wave orbital currents do not coincide (Swift et al., 1983). Hurricanes are no exception. The moving hurricane represents a translating wind field which produces waves of different frequencies, mean directions of travel, and directional spread (Forristall, Ward and Cardone, 1980). There is a marked radial asymmetry to hurricane wave patterns due to interaction with the local rotary wind patterns and the forward motion of the storm (Crutcher and Quayle, 1974). The dominant waves ahead of a storm are generated by a fetch system to the right of the eye which translates with the storm (Shemdin, 1980). This low frequency swell (wave periods of 10 seconds or greater) propagates along the storm track and shows a very narrow directional spread. The higher frequency waves show more spread and tend to follow more closely the changes in the local wind (Forristall et al., 1978). Synthetic Aperture Radar (SAR) images of the wave field during hurricanes has provided a look at the the wave patterns in different sectors of a tropical storm system (King and Shemdin, 1978).

The waves patterns for a translating hurricane can be superimposed upon the proposed bottom current kinematics to produce a view of the combined flow transport. This is illustrated in Fig. 71d using the format of Swift et al., (1985). the diagram shows the steady current velocity vector (u_c) and the oscillatory velocity vectors, separated

into the onshore motion ($+u_w$) and the offshore stroke ($-u_w$). In general, as one moves from the right side of the storm track toward the left, there is a change in the shape of the combined flow triangles: on the right side of the storm, the onshore portion of the wave stroke opposes the the downwelling current velocity vector while the offshore portion of the wave orbital motion augments that motion. In the CTCS area, the combined flow triangle is a right triangle, the bottom orbital motion neither opposing nor complementing the current flow. Further to the south, the wave-current angles are again non-perpendicular. In this case, it is the onshore wave motion which complements the steady current vector. This is the pattern that would occur during the approach of the Carla toward the coast. However, following landfall, the pattern shown on the far left side of the storm typifies all quadrants, suggesting that offshore sand transport occurred prior to landfall.

Discussion--The distribution of the Carla sand bed as reconstructed from the sedimentological data presented in the previous chapters is generally consistent with the hypothetical bottom current and combined flow patterns proposed by this study (compare Fig. 36 and Figs. 71c-d). In addition, the sand bed distribution is not inconsistent with evidence of sand transport driven by downwelling storm jets on the shorefaces of the Atlantic coast (Niedoroda et al., 1985). In fact, the flow pattern proposed here can be viewed in general as an extension of that downwelling pattern onto the shelf.

CHAPTER 4

SUMMARY AND CONCLUSIONS

Sedimentary Zones of the CTCS

The sedimentary character of the discrete sand beds is a function of the kinematics and dynamics of fluid motion on the shelf, particularly during storm events capable of entraining, transporting and depositing clastic sediments. It is the purpose of this section to compare relevant features of the sedimentological and oceanographic analyses performed in the preceding chapters.

Analysis of the boxcores taken across the study area reveals a number of shore-normal sedimentary zones (Fig. 78). In the inner shelf portion of the area (10-20 m), the cored section is composed of numerous thin (1-2 cm) sand beds with upper and lower erosional bedding contacts. Recognition of individual beds is difficult, particularly in the shallow parts of the zone, as the sequence borders on what might be called "amalgamated" (Fig. 17). As with other continental shelves, It is likely that the high degree of amalgamation parallels the high frequency of storm related erosion, transport and deposition events (Nittrouer and Sternberg, 1981). Numerical calculations of the boundary shear stress generated by wave orbital motion indicates that in these water depths, the sediment resuspension occurs on at least a yearly basis (Case B, Fig. 64). The presence of surficial sand in cores from this region supports this presumption (Figs. 12 & 17).

The middle shelf zone (20-50 m) is typified by muddy sections punctuated by a few thick (1-6 cm) discrete sand layers (Fig. 78). The surficial sediment is clay. The sand beds show sharp (presumably erosional) basal contacts, progressing upward from plane beds to ripples.

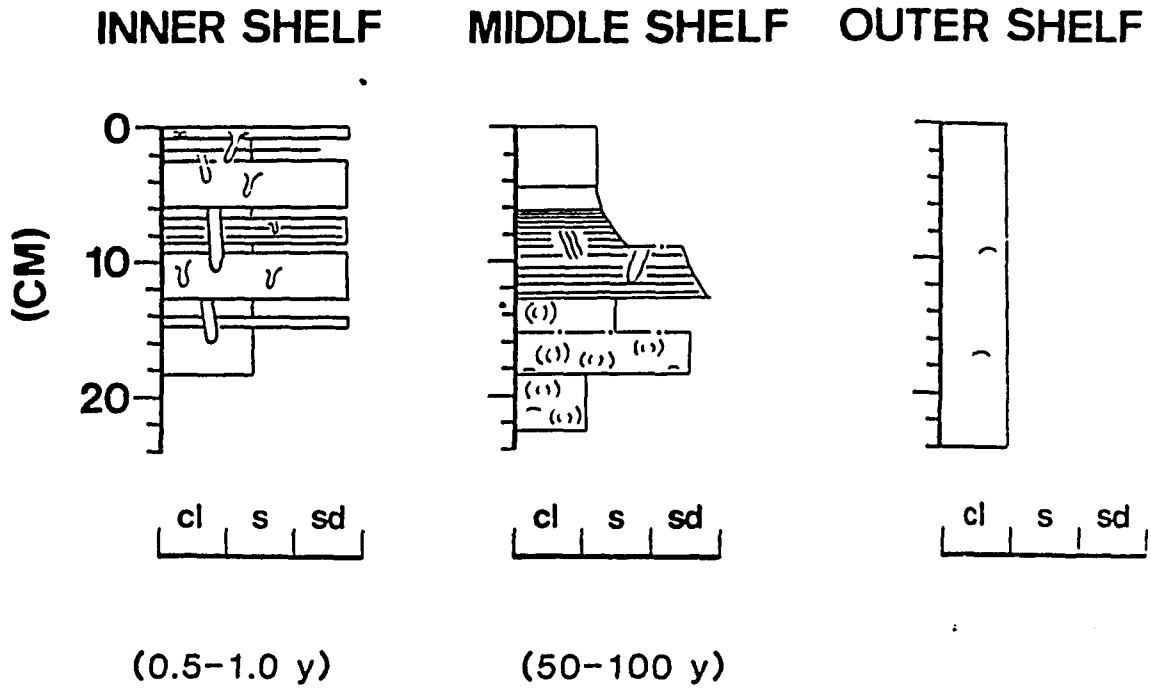

Fig. 78.--Typical cores from the inner, middle, and outer shelf sedimentary zones of the CTCS. Recurrence interval of sand bed deposition shown below in parentheses.

Upward fining trends are shown by grain size and sand-silt-clay percentages. Absolute dating of selected cores reveals that the sands were deposited quite infrequently, on the order of 1-2 times a century.

This does not quite agree with the calculated frequency of reworking based on analysis of the waves associated with storms whose reoccurrence interval ranges from 1 to 10 years (Fig. 64). This is best understood if one views the discrete sand beds as a product of sediment availability and fluid power expenditure (Swift and Ludwick, 1976). While it is possible to resuspend material on the middle shelf as often as once a year, it is not expected that sand will available for transport in each case; For example, the Eulerian data from the extratropical storm of 1984 showed a situation in which the combined flow boundary shear stress exceeded the threshold of motion for sand but the transport was onshore at 34 m water depth. Since the outer shelf in the CTCS region is composed of clay, it is not likely that additional sand beds were deposited during this event in the middle shelf depths. It appears that transport to the middle shelf zone is limited to the larger, Carla-sized storms in which downwelling flow extends across much of the shelf into the geostrophic and transition zones as well as the friction-dominated zone.

The tremendous along-shelf flow during Hurricane Allen at the CSA array might suggest that clastics from the sandy Brazos-Colorado shelf could be advance into the area through a series of discrete "hops" with successive small scale storms. Indeed, both Shideler (1978) and Mazzullo and Withers (1984) show Brazos-Colorado clastics encroaching upon the surficial sediments in the area immediately to the south. However, the formation of discrete sand beds is clearly tied to much more than

simple along-shelf flow from the East Texas shelf. Once sand is transported to the middle shelf zone, it soon is buried by clay deposited during the intervening fairweather period. This overlying clay may act as a "protective cap", preventing further transport: Flume experiments demonstrate that the transport threshold of cohesive clays can be as high as 100 dynes/cm^{-2} (Allen, 1984). It has also been shown that continued burial further increases the overall threshold (Southard et al., 1971).

Sediments of the outer shelf zone (50-180 m) are composed largely of clay (Fig. 78). Discrete sand beds are quite thin (<1 cm) out to 90 m. Beyond that point they are not present and there are few indications of wave or current activity. Even the largest waves observed in the Gulf are not capable of resuspending sand, should it be present, in these water depths beyond 100 m (Case C & D, Fig. 64). Bottom current motion in this "outer geostrophic zone" is weak and largely along-shelf (e.g. Fig. 50). In addition, the outer shelf zone is quite far removed from the sediment sources at the coast.

Thus, it appears that there is a shore-normal decrease in the frequency of sand beds (Fig. 79). Patterns such as these have been termed "proximality trends" (Aigner and Reineck, 1982). The offshore decrease in the number of sand beds in the CTCS area is slightly different than the trends shown in two other shelf settings, the Norton Sound of Alaska (Nelson, 1982) and the Helgoland Bight of Germany (Aigner and Reineck, 1982). This may be attributed to significant differences in the nature of fluid motion, basin configuration, wave climate, and sediment availability between the two areas and the CTCS area. The Helgoland Bight is a macrotidal funnel-shaped embayment which experien-

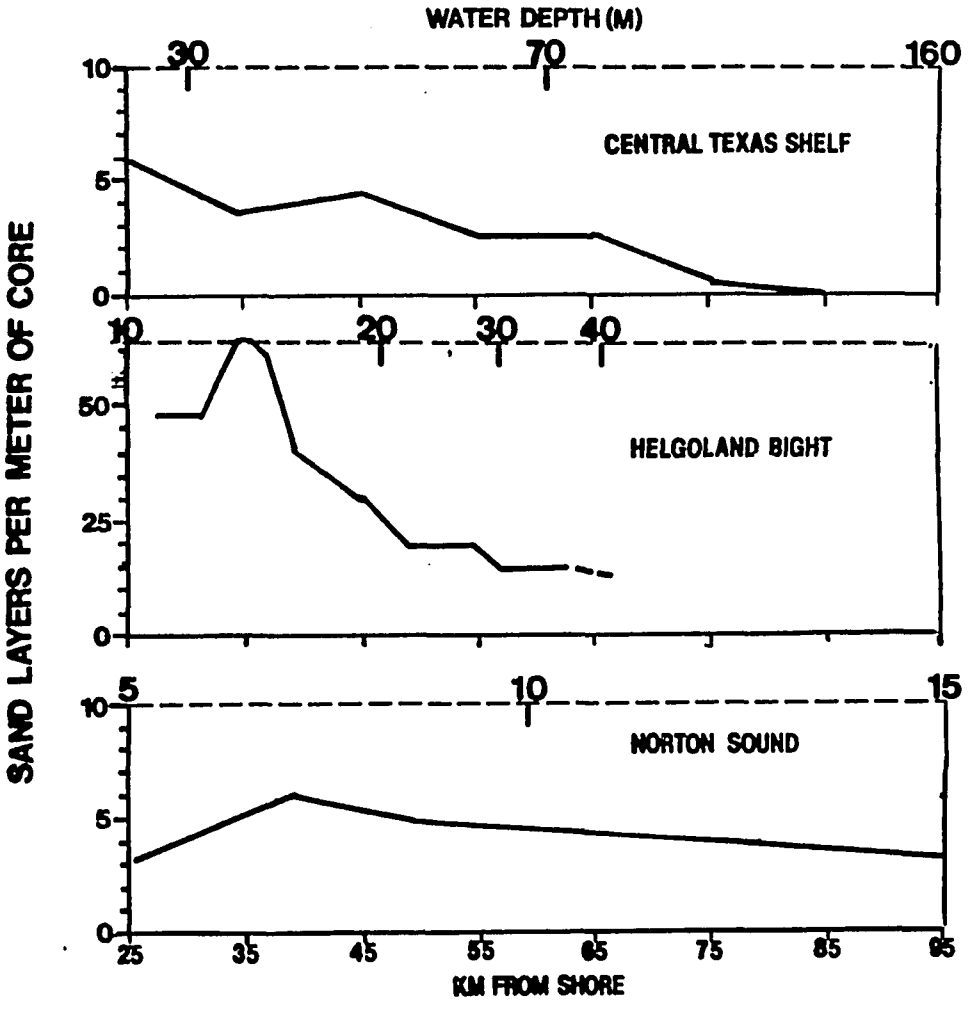

Fig. 79.--Proximality trends in sand bed frequency per meter of core in the CTCS area, the Helgoland Bight of Germany (Aigner and Reineck, 1982), and the Norton Sound of Alaska (Nelson, 1982).

ces frequent wind-induced sea-level set-up. There is an extremely high frequency of sand beds in a given meter of core, suggesting that transport may be augmented by tidal motion. The Norton Sound section is notable in the cross-shelf continuity of sand bed frequencies. However, the basin is quite shallow (<20 m) and it's rectangular shape probably enhances the storm surge and wind-induced pressure gradients.

In contrast, the CTCS shows a clear offshore decline in sand bed numbers. As was shown in the previous sections, this "proximality trend" is a direct function of the depth dependence of wave and current kinematics and dynamics. In addition, the seaward decline in sand bed frequency parallels the progressive sorting trends shown by the grain-size frequency distributions, a manifestation of the distance from the source as well as the offshore decline in combined flow power during storm events of varying magnitudes.

Conclusions

The origin of the discrete sand beds found in the modern sediments of the Texas shelf has been a source of controversy in the geologic literature for almost twenty years. Specific points of contention involve their clastic source, transport pathway, transport mechanism, and preservation potential. These questions were addressed in a two-phased approach involving study of the sedimentary characteristics of the sand beds and a step-wise analysis of the dynamics and kinematics of shelf bottom current motion during combined flow events of varying magnitude.

Boxcores taken from an area offshore from Mustang Island, Texas were examined to identify physical and biogenic sedimentary structures,

texture and composition, and the absolute age of discrete beds in the uppermost portion (0-60 cm depth) of the modern sedimentary section of the shelf. A seaward decrease in the size of sand and silt grains, accompanied by increases in clay content of the beds suggest a coastal source for the clastics found in the beds. This is consistent with grain shape analysis of sand from several of the beds as well as the evidence of a well-sorted sand population. Quantitative analysis of possible coastal sources as well as dynamic processes implies that the shoreface is the major source of the sand found in the discrete sand beds.

Correlation of a sand bed dated as having been deposited during the period 1961-1962 with surficial sand recognized by Hayes (1967) as a product of Hurricane Carla reveals that individual beds have a tremendous along-shelf continuity. This, combined with recognition of progressive sorting in the sand-silt frequency distributions as well as bed thinning trends suggest a transport pathway oriented obliquely across the shelf to the south-southwest.

Three mechanisms have been suggested to account for erosion, transport, and deposition of the Carla bed and other beds within the modern sedimentary section: turbidity currents (Hayes, 1967), wind-forced currents (Morton, 1981), and the concept of a steady current flow (driven by the geostrophic balance of forces) interacting with oscillatory wave orbital motion near the sea bottom boundary. Many of the sedimentary features recognized in the discrete beds are consistent with any of the above hypotheses. Yet the along-shelf continuity of the Carla bed, in particular, indicates that the turbidity current thesis of Hayes (1967) may not be valid.

Discrimination between the wind-forced current mechanism of Morton (1981) and the geostrophic current-combined flow hypothesis favored by this study was facilitated by study of the fairweather and storm current regime in the CTCS area. Time series analysis revealed that highest levels of coherence between bottom current motion and the wind are restricted to periods when the wind has an along-shelf orientation. These along-shelf winds often induce a cross-shelf pressure gradient, as indicated by tide gauge measurements. The resulting southwesterly flow is consistent with a multi-layered model of barotropic motion. During extratropical storms, shear stress generated by the flow of currents past the sea bottom boundary, combined with that supplied as a result of wave orbital motion, is responsible for the erosion, transport, and deposition of sediment on a yearly basis.

Less frequently, but in a similar fashion, sand transport occurs with the passage of hurricanes across the CTCS area. Data from Hurricane Allen indicates that bottom current motion is more in phase with tidal gauge measurements than wind gauges measurements, implying the influence of a cross-shelf pressure gradient in driving shelf flow. The coincidence of increased wave heights and periods and elevated current flow velocities during the approach of a hurricane lends support to the combined flow hypothesis advanced by this study.

Extrapolation to Hurricane Carla was made possible by knowledge gained from study of smaller storms and the measured shelf response. Calculation of the magnitude of the driving forces behind sand transport on the shelf reveals that simple wind-forced currents play a subordinate role to motion set-up by the cross-shelf and along-shelf pressure gradient forces. Transport occurs in different dynamic zones,

each subject to the constraints imposed by frictional boundaries and the continuity of water volume. A qualitative kinematic model for combined flow bottom motion during the approach of Hurricane Carla is consistent with the distribution of the Carla sand bed across the Texas shelf, as revealed by cores of the shelf sediments.

Preservation potential of the discrete sand beds is depth dependent. In the inner shelf setting (10-20 m water depth), beds undergo intense biological reworking and physical truncation. Analysis of trends in infaunal density as well as numerical calculations of the frequency of storm-related bottom agitation support this conclusion.

In the middle-shelf area (20-50 m), preservation potential of the beds is high, as biological reworking is less intense and physical truncation less frequent. The accumulation of cohesive clays in the intervening fairweather periods aids in the protection of the beds. In this water depth, the presence of a bed deposited during Hurricane Carla in 1961 was established with absolute dating techniques.

Further seaward (50-180 m), the recognition of discrete sand beds is hindered by the offshore thinning and lack of sandy material within the beds. Beyond 100 m, there are no discrete sand beds present in the sedimentary section.

There are numerous reported cases of thin-bedded sandstones of presumed storm origin in ancient shelf sequences. The discrete sand beds present in the modern sediments of the CTCS and the subject of this study stand as viable analogs to these ancient deposits.

REFERENCES CITED

Adams, C. E., and G. L. Weatherly, 1981, Suspended sediment transport and benthic boundary layer dynamics: Mar. Geol., vol. 42, p. 1-18.

Adams, C. E., J. T. Wells, and J. M. Coleman, 1982, Sediment transport on the central Louisiana continental shelf: Implications for the developing Atchafalaya River delta: Contrib. Mar. Sci., vol. 25, p.23-40.

Aigner, T. and H. E. Reineck, 1982, Proximality trends in modern storm sands from the Helgoland Bight (North Sea) and their implications for basin analysis: Senckenbergiana Marit., vol. 14, 5/6, p. 183-215.

Allen, J. R. L., 1984, Sedimentary Structures: Their Character and Physical Basis: New York, Elsevier, 663 p.

Anderson, J. B., et. al., 1982, Determination of depositional environments using vertical grain size progressions: Trans. Gulf Coast Assoc. Geol. Soc., vol. 32, p. 565-79.

Anthes, R. A., 1982, Tropical Cyclones: Their Evolution, Structure and Effects: Boston, Amer. Meteor. Soc., 202 p.

Bagnold, R. A., 1966, A approach to the sediment transport problem from general physics: U.S.G.S. Prof. Paper 422-I, 40 p.

Bea, R. G., 1974, Gulf of Mexico hurricane wave heights: Offshore Tech. Conf. paper no. 2110, p. 791-812.

Beardsley, R. C., and B. Butman, 1974, Circulation on the New England continental shelf: response to strong winter storms: Geop. Res. Letters, vol. 1, p. 181-84.

Beer, T., 1983, Environmental Oceanography: London, Pergamon Press, 262 p.

Berg, R. R., and R. Powell, 1976, Density-flow origin for Frio reservoir sandstones, Nine Mile Point Field, Aransas County, Texas: Trans. Gulf Coast Assoc. Geol. Soc., vol. 26, p. 310-319.

_____, and F. J. Tedford, 1977, Characteristics of Wilcox gas reservoir sandstones, Northeast Thompsonville Field, Texas: Trans. Gulf Coast Assoc. Geol. Soc., vol. 27, p. 6-19.

Berryhill, H. L., Jr., G. L. Shideler, C. W. Holmes, G. W. Hill, S. S. Barnes, and R. G. Martin, 1976, Environmental studies, south Texas outer continental shelf, Vol. 2, Geology: available only U.S. Dept. Commerce, Nat'l Tech. Inf. Serv., Springfield, Virg. Report PB-251-341, 273 p.

Berryhill, H. L. Jr., G. L. Shideler, C. W. Holmes, G. W. Hill, S. S. Barnes, and R. G. Martin, 1977, Environmental studies, south Texas outer continental shelf, Vol. 3, Geology: available only U. S. Dept. Commerce, Nat'l Tech, Inf. Serv., Springfield, Virg. Report PB-289-144/AS, 306 p.

Bouma, A. H., 1962, Sedimentology of Some Flysch Deposits: a Graphic Approach to Facies Interpretation: Amsterdam, Elsevier Publ. Co., 168 p.

Boyles, J. M., 1982, Origin and Significance of Hummocky Stratification: Cities Service Co., ERG Research Report #120, 76 p.

Brenchley, P. J., G. Newell, and I. Stantistreet, 1979, A storm surge origin for sandstone beds in an epicontinental platform sequence, Ordovician, Norway: Sed. Geol., vol. 22, p. 185-98.

Bridge, J. S., 1978, Origin of horizontal lamination under turbulent boundary layers: Sedim. Geol., vol. 20, p. 1-16.

Bullard, F. M., 1942, Source of beach and river sand on the Gulf coast of Texas: Geol. Soc. Amer. Bull., vol. 53, no. 7, p. 1021-1044.

Busby-Spera, C., 1985, A sand-rich submarine fan in the lower Mesozoic Mineral King Caldera Complex, Sierra Nevada, California: Jour. Sed. Pet., vol. 55, no. 3, p. 376-391.

Cacchione, D. A., and D. E. Drake, 1982, Measurements of storm-generated bottom stresses on the continental shelf: Jour. Geop. Res., vol. 87, no. C3, p. 1952-60.

Campbell, C. V., 1966, Truncated wave-ripple laminae: Jour. Sed. Pet., vol. 36, p. 825-828.

Cardone, V. J., W. J. Pierson, and E. G. Ward, 1976, Hindcasting the directional spectra of hurricane-generated waves: Jour. Pet. Tech., vol. 25, p. 385-94.

Caston, V. N. D., 1976, A wind-driven near-bottom current in the southern North Sea: Estuarine Coastal Mar. Sci., vol. 4, p. 23-32.

Chase, R. R. P., 1979, The coastal longshore pressure gradient: temporal variations and driving mechanisms: Jour. Geop. Res., vol., 84, no. C8, p. 4898-4904.

Chatfield, C., 1980, The Analysis of Time Series, Chapman and Hall, London, 270 p.

Chew, F., K. L. Drennan, and W. F. Demoran, 1962, Drift-bottle return in the wake of Hurricane Carla, 1961: Jour. Geop. Res., vol. 67, p. 2773-76.

Chow, S., 1971, A study of the windfield in the planetary boundary layer of a moving tropical cyclone: unpubl. M. S. thesis, Dept. of Meteor. and Oceanog., New York Univ., 58 p.

Cochrane, J. D. and F. J. Kelly, 1982, Proposed annual mean progression in the mean Texas-Louisiana shelf circulation: Trans. Am Geop. Union, vol. 63(45) p. 1012.

Coleman, J. M., 1966, Ecological changes in a massive freshwater clay sequence: Trans. Gulf Coast Assoc. Geol. Soc., vol. 16, p. 159-173.

Colon, J. A., 1966, Some aspects of hurricane Carla (1961): Hurricane Symposium, Amer. Soc. for Oceanog. Public. no. 1, p. 1-33.

Crout, R. L., 1983, Wind-driven, near-bottom currents over the western Louisiana inner continental shelf: unpub. Dissert., Louisiana State Univ., May, 1983, 117 p.

Crutcher, H. L., and R. G. Quayle, 1974, Mariners Worldwide Climatic Guide to Tropical Storms at Sea: Naval Weather Service Command,

Naval Weather Environmental Detachment, Asheville, N. C., 114 p.

Csanady, G.T., 1976, Mean circulation in shallow seas: Jour. Geop. Res., vol. 81, no. 30, p. 5389-99.

_____, 1982, Circulation in the Coastal Ocean, (Reidel Pub. Co., London) 280 p.

Curray, J. R., 1960, Sediments and history of Holocene transgression, continental shelf, Northwest Gulf of Mexico: In, F. P. Shepard, F. B. Phleger, and T. J. Van Andel, ed., Recent Sediments, Northwest Gulf of Mexico: Amer. Assoc. Pet. Geol. Spec. Publ., p. 221-66.

Cutshall, N. H., I. L. Larsen, and C. R. Olsen, 1983, Direct analysis of Pb-210 in sediment samples: self-absorption corrections: Nucl. Instrum. Methods, vol. 206, p. 309-312.

Daddio, E., 1977, Response of coastal waters to atmospheric frontal passage in the Mississippi delta region: Louisiana State Univ. Center for Wetland Res. Tech. Rep. no. 234, 38 p.

DeLaune, R. D., W. H. Patrick, and R. J. Buresh, 1978, Sedimentation rates determined by Cs-137 dating in a rapidly accreting salt marsh: Nature, vol., 275, p. 532-33.

Dimego, R. T., et al., 1976, An examination of the frequency and mean conditions surrounding frontal incursions into the Gulf of Mexico and Caribbean: Monthly Weather Review, no. 104, p. 709-18.

Dott, R. H., 1983, Episodic sedimentation - How normal is average ? How rare is rare ? Does it matter ?: Jour. Sed. Pet., vol. 53, p. 5-23.

_____, and J. Bourgeois, 1982, Hummocky stratification: significance of its variable bedding sequences: Geol. Soc. Bull., vol. 93, p. 663-680.

Drake, D. E., D. A. Cacchione, and H. A. Karl, 1985, Bottom currents and sediment transport on the San Pedro Shelf, California: Jour. Sed. Pet., vol. 55, no. 1, p. 15-28.

Eckart, C., 1952, The propagation of waves from deep to shallow water: In, Gravity Waves, Nat'l Bureau of Standards Circ. no. 521, p. 165-73.

Ekman, V. W., 1905, On the influence of the earth's rotation on ocean currents: Ark. F. Mat. Astr. Osh. Fysik. K. Sv. Vet. Ak. Stockholm, vol. 2, 11 p. (see McLellan, 1965 for discussion).

Ellis, M. J., 1984, Hurricane Almanac: Corpus Christi, Texas, Disaster Resources, 170 p.

Elliott, B. A., 1982, Anticyclonic rings in the Gulf Of Mexico: Jour. Phys. Ocn., v. 12, p. 1293-1309.

Englelund, F., 1970, Instability of erodible beds: Jour. Fluid Mech., vol. 42, part 2, p. 225-244.

Eriksson, K. A. and K. Soegaard, 1983, Storm-deposited outer shelf facies from Precambrian Ortega Group, New Mexico: Am. Assoc. Pet. Geol. Bull., vol. 67, p. 456 (abstr.).

Faure, G., 1977, Principles of Isotope Geology: New York, John Wiley and Sons, 465 p.

Fee, E., 1969, Digital computer programs for spectral analysis of time series: Univ. of Wisconsin Center for Great Lakes Studies, Special Report No. 6, 17 p.

Fisher, W. L., J. H. McGowen, L. F. Brown, and C. G. Groat, 1973, Environmental Atlas of the Texas Coastal Zone, Beaumont-Port Arthur area: Univ. Texas Bur. Econ. Geol., 93 p.

Folk, R. L., 1968, Petrology of Sedimentary Rocks: Austin, Texas, Hemphills, 170 p.

Forristall, G. Z., 1974, Three-dimensional structure of storm-generated currents: Jour. Geop. Res., vol. 79, no. 8, p. 2721-29.

_____, R. C. Hamilton, and V. J. Cardone, 1977, Continental shelf currents in tropical storm Delia: observations and theory: Jour. Phys. Ocn., vol. 7, p. 532-4.

_____, E. G. Ward, V. J. Cardone, and L. E. Borgmann, 1978, The directional spectra and kinematics of surface gravity waves in tropical storm Delia: Jour. Phys. Ocean., vol. 8, p. 888-909.

_____, E. G. Ward, and V. J. Cardone, 1980, Directional wave spectra and wave kinematics in hurricanes Carmen and Eloise: Proc. Coastal Engin. Conf., p. 567-585.

_____, and A. M. Reece, 1985, Measurements of wave attenuation due to a soft bottom: the SWAMP experiment: Jour. Geop. Res., v. 90 (C2), p. 3367-3380.

Friedman, G. M., 1961, Distinction between dune, beach, and river sands from their textural characteristics: Jour. Sed. Pet., vol. 31, p. 514-529.

_____, 1971, Staining: In, R. E. Carver, ed., Procedures in Sedimentary Petrology: New York, Wiley and Sons, p. 511-530.

_____ and J. E. Sanders, 1978, Principles of Sedimentology, New York, John Wiley and Sons, 790 p.

Gordon, R. L., 1982, Coastal ocean current response to storm winds: Jour. Geop. Research, vol. 87, p. 1939-1951.

Grant, W. D. and O. S. Madsen, 1979, Combined wave and current interaction with a rough bottom: Jour. Geop. Res., v. 84 (C4), p. 1797-1808.

Hamblin, W. K., 1962, X-ray radiography in the study of structures in homogeneous sediments: Jour. Sed. Pet., vol. 32, no. 2, p. 201-10.

Handin, J., and R. V. Hager, 1957, Experimental deformation of sedimentary rocks under confining pressure: Tests at room temperature on dry samples: Amer. Assoc. Pet. Geol. Bull., vol. 41, no. 1, p. 1-50.

Hanor, J. S., and N. F. Marshall, 1971, Mixing of sediments by organisms: In, B. F. Perkins, ed., Trace Fossils: A field guide to selected localities in Pennsylvanian, Permian, Cretaceous, and Tertiary rocks of Texas and related papers: Soc. Econ Paleo. Min. Field Trip Guidebook, p. 127-134.

Harms, J. C., 1969, Hydraulic significance of some sand ripples: Geol. Soc. Amer. Bull., vol. 80, p. 363-396.

_____, J. B. Southard, D. R. Spearing, and R. G. Walker, 1975, Depositional environments as interpreted from primary sedimentary structures and stratification sequences: Soc. Econ. Paleo. Min. Short Course Notes, no. 2, 161 p.

_____, J. B. Southard, and R. G. Walker, 1982, Structures and sequences in clastic rocks: Soc. Econ. Paleo. Min. short course lecture notes, no. 9, 200 p.

Hatton, R. S., R. D. DeLaune and W. H. Patrick, 1983, Sedimentation, accretion, and subsidence in marshes of Barataria basin, Louisiana: Limnology and Oceanography, vol. 28, no. 3, p. 494-502.

Hayes, M. O., 1967, Hurricanes as geologic agents; case studies of Hurricane Carla, 1961 and Cindy, 1963: Univ. Tex. Bur. Econ. Geol. Rept. Inv. no. 61, 56 p.

Hill, G. W., and L. E. Garrison, 1978, Maps showing seasonal drift patterns along the Texas coast, 1970-1975: U.S.G.S. Misc. Field Inv. Map MF-982.

_____, 1985, Ichnofacies of a modern size-graded shelf, Northwest Gulf of Mexico: In, H. A. Curran, ed., Biogenic Structures: Their Use in Interpreting Depositional Environments: Soc. Econ. Paleo. Min. Spec. Publ. no. 35, p. 195-211.

Hobday, D. K., and R. A. Morton, 1984, Lower Cretaceous shelf storm deposits, Northeast Texas: in, R. W. Tillman and C. T. Siemers, eds., Siliclastic Shelf Sediments, Soc. Econ. Paleo. Min. Spec. Pub. no. 34, p. 205-214.

Holmes, C. W., and E. A. Martin, 1977, Rates of sedimentation: In, H. L. Berryhill et al., Environmental studies, south Texas continental shelf, Vol. 3, Geology: Available only U. S. Dept. Commerce, Nat'l Tech. Info. Serv., Springfield, Va., Report PB-289-144/AS, 306 p.

Howard, J. D., et al., 1974, Biogenic sedimentary structures formed by heart urchins: Senckenberg. Marit., vol. 6, p. 185-201.

Hsaio, S. V., and O. H. Shemdin, 1978, Bottom dissipation in finite-depth water waves: Proc. 16th Coastal Engin. Conf., ASCE, Hamburg, p. 434-448.

_____, 1980, Interaction of ocean waves with a soft bottom: Jour. Phys. Ocn., v. 10, p. 605-610.

Hsu, S. A., 1980, Models for estimating offshore winds from onshore meteorological measurements: Boundary Layer Meteorology, vol. 20, p.341-351

Jahns, H. O., and J. D. Wheeler, 1973, Long-term probabilities based on hindcasting of severe storms: Jour. Pet. Tech., vol. 25, p. 475-480.

Jelesnainski, C. P., 1965, A numerical calculation of storm tides induced by a tropical storm impinging on a continental shelf: Mon. Weather Review, vol. 93, no. 6, p. 343-358.

_____, 1970, Bottom stress time history in linearized equations of motion for storm surges: Mon. Weather Review, vol. 98, p. 462-78.

Jonsson, I. G., 1966, Wave boundary layers and friction factor: Proc. 10th Coastal Engin. Conf., vol. 1, p. 127-148.

Jopling, A. V., 1965, Hydraulic factors controlling the shape of laminae in laboratory deltas: Jour. Sed. Pet., vol. 35, no. 4, p. 777-791.

Jordan, D. W., K. P. Helmhold, and T. F. Moslow, 1981, Storm washover deposition on the Texas Gulf Coast by Hurricane Allen, 1980 and Application to Stratigraphic Traps: Cities Service Co. Exp. Prod. Res. Report #94, 59 p.

Kato, H., and O. Phillips, 1969, On the penetration of a turbulent layer into stratified fluid: Jour. Fluid Mech., vol. 37, p. 643-55.

Kerr, P. F., 1977, Optical Mineralogy: New York, McGraw-Hill, 492 p.

King, D. B., and O. H. Shemdin, 1978, Radar observations of hurricane wave directions: Proc. 16th Int. Conf. Coastal Engineering, Hamburg, Germany, p. 209-226.

Kinsman, B., 1965, Wind Waves: New Jersey, Prentice-Hall, 676 p.

Kirwan, A. D., Jr., W. J. Merrell, Jr., J. K. Lewis, and R. E. Whitaker, 1984, Lagrangian observations of an anticyclonic ring in the western Gulf of Mexico: Jour. Geop. Ocn., v. 89 (C3), p. 3417-3424.

Komar, P. D., 1974, Oscillatory ripple marks and the evaluation of ancient wave conditions and environments: Jour. Sed. Pet., vol. 44, p. 169-80.

_____, 1976, Beach Processes and Sedimentation: Prentice-Hall, New Jersey, 426 p.

_____, 1985, The hydraulic interpretation of turbidities from their grain sizes and sedimentary structures: Sedimentology, vol. 32, p. 395-407.

Kriesa, R. D., 1981, Storm-generated sedimentary structures in subtidal marine facies with examples from the Middle and Upper Ordovician of Southwestern Virginia: Jour. Sed. Pet., vol. 51, no. 3, p. 823-848.

Kuenen, P. H., 1966, Experimental turbidite lamination in a circular flume: Jour. Geol., vol. 74, no. 5, part I, p. 523-545.

Large, W. G. and S. Pond, 1981, Open ocean momentum flux measurements in moderate to strong winds: Jour. Phys. Ocn., vol. 11, p. 324-36.

Larsen, L. H., R. W. Sternberg, N. C. Shi, M. A. H. Marsden, and L. Thomas, 1981, Field investigations of the threshold of grain motion by ocean waves and currents: Mar. Geol., vol. 42, no. 1/4, p. 105-132.

Lavelle, J. W., et al., 1978, Fair weather and storm sand transport on the Long Island inner shelf: Sedimentology, vol. 25, p. 823-42.

Ludlum, D. A., 1961, Hurricane Carla: Weatherwise, vol. 10, p. 193-96.

Lewis, J. K., 1980, Comments on "The hydrography of shelf waters off the central Texas Gulf coast": Jour. Phys. Ocn., v. 10, p. 2121-2.

Lutgens, F. K., and E. J. Tarbuck, 1979, The Atmosphere: An Introduction to Meteorology: New Jersey, Prentice-Hall, 412 p.

Madsen, O. S., 1976, Wave climate of the continental margin: elements of its mathematical description: In, D.J. Stanley and D.J.P. Swift, eds., Marine Sediment Transport and Environmental Management: John Wiley and Sons, New York, p. 255-310.

Mantz, P. A., 1978, Bedforms produced by fine, cohesionless, granular and flakey sediments under subcritical water flows: Sedimentology, vol. 25, p. 83-103.

Maynard, A. K., and J. R. Suter, 1983, Regional variability of washover deposits on the South Texas Coast: Trans. Gulf Coast Assoc. Geol. Soc., vol. 33, p. 339-346.

Mazzullo, J. M. and K. D. Withers, 1984, Sources, distribution, and mixing of Late Pleistocene and Holocene sands on the south Texas continental shelf: Jour. Sed. Pet., vol. 54, no. 4, p. 1319-1334.

McCave, I. N., 1971, Sand waves in the North Sea off the coast of Holland: Marine Geol., v. 10, p. 199-225.

McGrail, D. W., and M. Carnes, 1983, Shelf edge dynamics and the nepheloid layer in the northwest Gulf of Mexico: In, D.J. Stanley and G.T. Moore, eds., The ShelfBreak: Critical Interface on Continental Margins: Soc. Econ. Paleo. Min. Spec. Pub. no. 33, p. 251-264.

McLellan, H. J., 1965, Elements of Physical Oceanography: London, Pergamon Press, Inc., 150 p.

Miyazaki, M., 1965, A numerical computation of the storm surge of Hurricane Carla 1961 in the Gulf of Mexico: The Oceanographical Magazine, vol. 17, no. 1-2, p. 109-140.

Moiola, R. J., and A. B. Spencer, 1973, Sedimentary structures and grain-size distribution, Mustang Island, Texas: Trans. Gulf Coast Assoc. Geol. Soc., vol. 23, p. 324-332.

Montz, M. J., D. Nummedal, and D. J. P. Swift, 1985, Shelf storm-deposited sandstones, Upper Mancos Shale, San Juan Basin, New Mexico: Amer. Assoc. Pet. Geol., vol. 69, no. 2, p. 289 (abst.).

Mooers, C. N. K., 1976, Introduction to the physical oceanography and fluid dynamics of continental margins: In, D. J. Stanley and D. J. P. Swift, eds., Marine Sediment Transport and Environmental Management: New York, John Wiley and Sons, p. 7-22.

Morton, R. A., and M. J. Pieper, 1977, Shoreline changes on Mustang Island and North Padre Island (Aransas Pass to Yarborough Pass): Univ. Texas Bur. Econ. Geol. Geol. Circ. no. 77-1, 45 p.

_____, 1981, Formation of storm deposits by wind-forced currents in the Gulf of Mexico and the North sea: In, S.D. Nio et al., eds., Holocene Marine Sedimentation in the North Sea Basin: Int. Assoc. Sed. Spec. Publ. no. 5, p. 385-96.

Murray, S. P., 1970, Bottom currents near the coast during Hurricane Camille: Jour. Geop. Res., vol. 75, no. 24, p. 4579-82.

Nelson, C. H., 1982, Modern shallow-water graded sand layers from storm surges, Bering shelf; a mimic of Bouma sequences and turbidite systems: Jour. Sed. Petrol., vol. 52, p. 537-546.

Niedoroda, A. W., and D. J. P. Swift, 1981, Maintenance of the shoreface by wave orbital currents and mean flow: observations from the Long Island Coast: Geop. Res. Letters: vol. 8, no. 4, p. 337-40.

_____, D. J. P. Swift, A. G. Figueiredo, Jr., and G. L. Freeland, 1985, Barrier island evolution, Middle Atlantic shelf, U. S. A., Part II: Evidence from the shelf floor: Mar. Geol., vol. 63, p. 363-396.

Nittrouer, C. A., R. W. Sternberg, R. Carpenter, and J. T. Bennett, 1979, The use of Pb-210 geochronology as a sedimentological tool; application to the Washington continental shelf: Mar. Geol., vol. 31, p. 297-316.

_____, and R. W. Sternberg, 1981, The formation of sedimentary strata in an allochtonous shelf environment: The Washington continental shelf: Mar. Geol., vol. 42, no. 1/4, p. 201-232.

Nowell, A. R. M., P. A. Jumars, and J. E. Eckman, 1981, Effects of biological activity on the entrainment of marine sediments: Mar. Geol., vol. 42, no. 1/4, p. 133-155.

Nowlin, W. D., and C. A. Parker, 1974, Effects of a cold-air outbreak on shelf waters of the Gulf of Mexico: Jour. Phys. Ocn., v. 4, p. 467-486.

Nummedal, D., 1982, Hurricane landfalls along the Northwest Gulf Coast: In, D. Nummedal, ed., Sedimentary processes and environments along the Louisiana-Texas coast: Geol. Soc. Amer. Field Trip Guidebook, 90 p.

Olsen, C. R., et al., 1978, A geochemical analysis of the sediments and sedimentation in the Hudson Estuary: Jour. Sed. Pet., vol. 48, no. 2, p. 401-418

Patterson, M. M., 1972, Hindcasting hurricane waves in the Gulf of Mexico: Soc. Pet. Engin. Jour., p. 321-328.

Pedlosky, J., 1979, Geophysical Fluid Dynamics, Springer-Verlag, New York, 624 p.

Pettijohn, F. J., P. E. Potter, and R. Siever, 1973, Sand and Sandstone: New York, Springer-Verlag, 618 p.

Pollard, R. T., P. B. Rhines, and R. O. R. Y. Thompson, 1973, The deepening of the wind-mixed layer: Geop. Fluid Dynamics, vol. 3, p.381-404.

Pond, S., and G. L. Pickard, 1978, Introductory Dynamical Oceanography: Oxford, Pergamon Press, 329 p.

Reineck, H. E. and I. B. Singh, 1972, Genesis of laminated sand and graded rhythmites in storm sand layers of shelf mud: Sedimentology, vol. 18, p 123-8

_____, 1975, Depositional Sedimentary Environments: New York, Springer-Verlag, 439 p.

Russell, R. D., 1939, Effects of transportation on sedimentary particles: in, P. P. Trask, ed., Recent Marine Sediments, London, Thomas Murphy, p. 32-47.

Sanders, J. E., Primary sedimentary structures formed by turbidity currents and related resedimentation mechanisms: In, G. V. Middleton, ed., Sedimentary Processes: Hydraulic Interpretation of Primary Sedimentary Structures: Soc. Econ Paleo. Min. Reprint Ser. no. 3, p. 194-223.

Sheldon, R. W., and T. R. Parsons, 1967, A Practical Manual on the Use of the Coulter Counter in Marine Science: Coulter Counter Electronics, Inc., Toronto, 66 p.

Shemdin, O. H., 1980, Prediction of dominant wave properties ahead of hurricanes: Proc. 17th Int. Conf. Coastal Engin., p. 600-609.

_____, S. V. Hsaio, H. E. Carlson, K. Hasselmann, and K. Schulze, 1980, Mechanisms of wave transformation in finite-depth water: Jour. Geop. Res., vol. 85, p. 5012-5018.

Shepard, F. P., 1948, Submarine Geology: New York, Harper and Bros. Publ Co., 348 p.

Shideler, G. L., 1978, A sediment-dispersal model for the south Texas continental shelf, Northwest Gulf of Mexico: Mar. Geol., vol. 26 p. 289-313.

Shields, A., 1936, "Anwendung der Aehnlichkeitsmechanik und der turbulenzforschung auf die Geschiebebewung," Mitt. der Preuss., Versuchsanstalt fur Wasserbau and Schiffbau, Berlin, (see Vanoni, 1964 for brief description of work).

Simons, D. B., E. V. Richardson, and C. F. Nordin, 1977, Sedimentary structures generated by flow in alluvial channels: In, G. V. Middleton, ed., Sedimentary Processes: Hydraulic Interpretation of Primary Sedimentary Structures: Soc. Econ. Paleo. Min. Reprint Ser., no. 3

Simpson, R. H., and H. Riehl, 1981, The Hurricane and Its Impact, LSU Press, Baton Rouge, 300 p.

Smith, J. D., 1970, Stability of a sand bed subjected to a shear flow of Low Froude number: Jour. Geop. Res., vol. 75, p. 5928-40.

_____, and C. E. Long, 1976, Effect of turning in the benthic boundary layer on continental shelf transport: Mem. Soc. R. Leige, vol. 6, no. 10, p. 369-396.

Smith, N. P., 1974, Intracoastal tides of Corpus Christi bay: Contrib. Mar. Sci., v. 18, p. 205-219.

_____, 1975, Seasonal variations in nearshore circulation in the northwestern Gulf of Mexico: Contrib. Mar. Sci. v. 19, p. 49-65,

_____, 1977, Near-bottom cross-shelf currents in the northwestern Gulf of Mexico: a response to wind-forcing; Jour. Phys. Ocn., v. 7, p. 615-620.

_____, 1978a, Low-frequency reversals of nearshore currents in the northwestern Gulf of Mexico: Contrib. Mar. Sci., vol. 21, p. 104-115.

_____, 1978b, Longshore Currents on the fringe of Hurricane Anita: Jour. Geop. Res., vol. 83, no. C12, p. 6047-51.

_____, 1979, An investigation of the vertical structure in shelf circulation: Jour. Phys. Ocn., v. 9, p. 624-630.

_____, 1980a, Temporal and spatial variability in longshore motion along the Texas Gulf coast: Jour. Geop. Res., v. 85 (C3) p. 1531-36.

_____, 1980b, On the hydrography of shelf waters off the central Texas Gulf coast: Jour. Geop. Ocn., v. 10, p. 806-813.

Snedden, J. W., and D. G. Kersey, 1982, Depositional environments and gas production trends, Olmos Sandstone, Upper Cretaceous, Webb County, Texas: Trans. Gulf Coast Assoc. Geol. Soc., vol. 32, p. 497-518.

_____, A. F. Amos, and D. Nummedal, 1985, Bottom currents during early winter on the south Texas continental shelf: implications for shelf sediment transport: Amer. Assoc. Pet. Geol. Bull., vol. 69, no. 2, p. 308 (abstr.).

Soulsby, R. L., 1983, The bottom boundary layer of shelf seas: In, B. Johns, ed., Physical Oceanography of Coastal and Shelf Seas, New York, Elsevier, p. 189-266.

Sowers, G. F., 1970, Introductory Soil Mechanics and Foundations: Geotechnical Engineering: New York, MacMillan Ltd., 615 p.

Stevenson, R. E., and R. S. Armstrong, 1965, Heat loss from the waters of the Northwest Gulf of Mexico during Hurricane Carla: Geofis. Intern. Tech. Conf. on Hurricanes and Tropical Meteorology, 7th session, Mexico City, p. 49-57.

Stow, D. A. V., and A. J. Bowen, 1980, A physical model for transport and sorting of fine-grained sediment by turbidity currents: Sedimentology, vol. 27, p. 31-46.

Sturgis, W. and J. P. Blaha, 1976, A western boundary current in the Gulf of Mexico: Science, v. 192, p. 367-69.

Suter, J. R. and H. F. Berryhill, 1985, Late Quaternary shelf-margin deltas, northwest Gulf of Mexico: Bull. Am Assoc. Pet. Geol., v. 69, no. 1, p. 77-91.

Swift, D. J. P., and J. C. Ludwick, 1976, Substrate response to hydraulic process; grain size frequency distributions and bedforms: In, D. J. Stanley and D. J. P. Swift, eds., Marine Sediment Transport and Environmental Management: New York, John Wiley and Sons, p. 159-161

_____, et al., 1976, Morphologic evolution and coastal sand transport, New York-New Jersey shelf: in, M.G. Gross, ed., Middle Atlantic Shelf and the New York Bight: Spec. Symp. Amer. Soc. Limn. and Ocean., p. 23-41.

_____, P. C. Sears, B. Bohlke, B. and R. Hunt, 1978, Evolution of a shoal retreat massif, North Carolina Shelf: inferences from areal geology: Marine Geology, vol. 27, p. 19-42.

_____, A. G. Figueiredo, Jr., G. L. Freeland, and G. F. Oertel, 1983, Hummocky cross-stratification and mega-ripples--A geologic double standard ? : Jour. Sed. Pet., vol. 53, no. 4, p. 1295-1318.

_____, and D. D. Rice, 1984, Sand bodies on muddy shelves; a model for sedimentation in the western interior seaway, North America: in R. W. Tillman and C. T. Siemers, eds., Siliclastic Shelf Sediments, Soc. Econ. Paleo. Min. Spec. Pub. no. 34, p. 43-63.

_____, and A. W. Niedoroda, 1984, Fluid and sediment dynamics on continental shelves: Soc. Econ. Paleo. Min. short course notes, p. 1-1 to 1-49.

_____, A. W. Niedoroda, C. E. Vincent, and T. S. Hopkins, 1985, Barrier island evolution, middle Atlantic shelf, U. S. A., Part I: Shoreface dynamics: Mar. Geol., vol. 63, p. 331-361.

Thrasher, L. W. and P. M. Aagaard, 1970, Measured wave force on offshore platforms: Jour. Pet. Tech., vol. 22, p. 339-346.

Tubman, M. W.,and J. N. Suhayda, 1976, Wave action and bottom movements in fine sediments: Proc. 15th Coastal Engin. Conf. ASCE, Honolulu, p. 1168-1183.

U. S. Army Corps. of Engineers, 1962, Hurricane Carla, September 9 -12, 1961: Corps. of Engineers, Galveston District, 30 p.

Vanoni, V. A., 1964, Measurements of of critical shear stress for entraining fine sediments in a boundary layer: W. M. Keck Lab. Hydraulics, Calif. Inst. Tech., Report KH-R-7, 47 p.

Von Arx, W. S., 1962, An Introduction to Physical Oceanography, London, Addison-Wesley, 422 p.

Walker, R. G., 1984, Geological evidence for storm transportation and deposition on ancient shelves: Soc. Econ. Paleo. Min. short course notes, p. 7-1 to 7-58.

Watson, R. L., and E. W. Behrens, 1970, Nearshore surface currents, southeastern Texas Gulf coast: Contrib. Mar. Sci., v. 15, p. 133-143.

Weatherly, G. L., 1972, a study of the bottom boundary layer of the Florida current: Jour. Phys. Ocn., v. 2, p. 54-72.

_____, and Van Leer, 1977, On the importance of stable stratification to the structure of the benthic boundary layer on the Western Florida shelf: In, J. Nihoul, ed., Bottom Turbulence: Amsterdam, Elsevier, p. 103-122.

Weigel, R. L., 1964, Oceanographic Engineering: New Jersey, Prentice-Hall, Inc., 532 p.

Wendland, W. M., 1977, Tropical storm frequencies applied to sea surface temperatures: Jour. Appl. Meteorology, vol. 16, p. 477-481.

White, S. J., 1970, Plane bed thresholds of fine-grained sediments: Nature, v. 228, p. 152-3.

White, W. A., et al., 1983 Submerged lands of Texas, Corpus Christi Area: Univ. Texas Austin Bur. Econ. Geol., 153 p.

Winant, C. D., and R. C. Beardsley, 1979, A comparison of some shallow wind-driven currents: Jour. Phys. Ocn., vol. 9, p. 218-220.

APPENDIX A
COLUMNAR SECTIONS OF BOXCORES

(Legend of symbols used is shown in Figure 9)

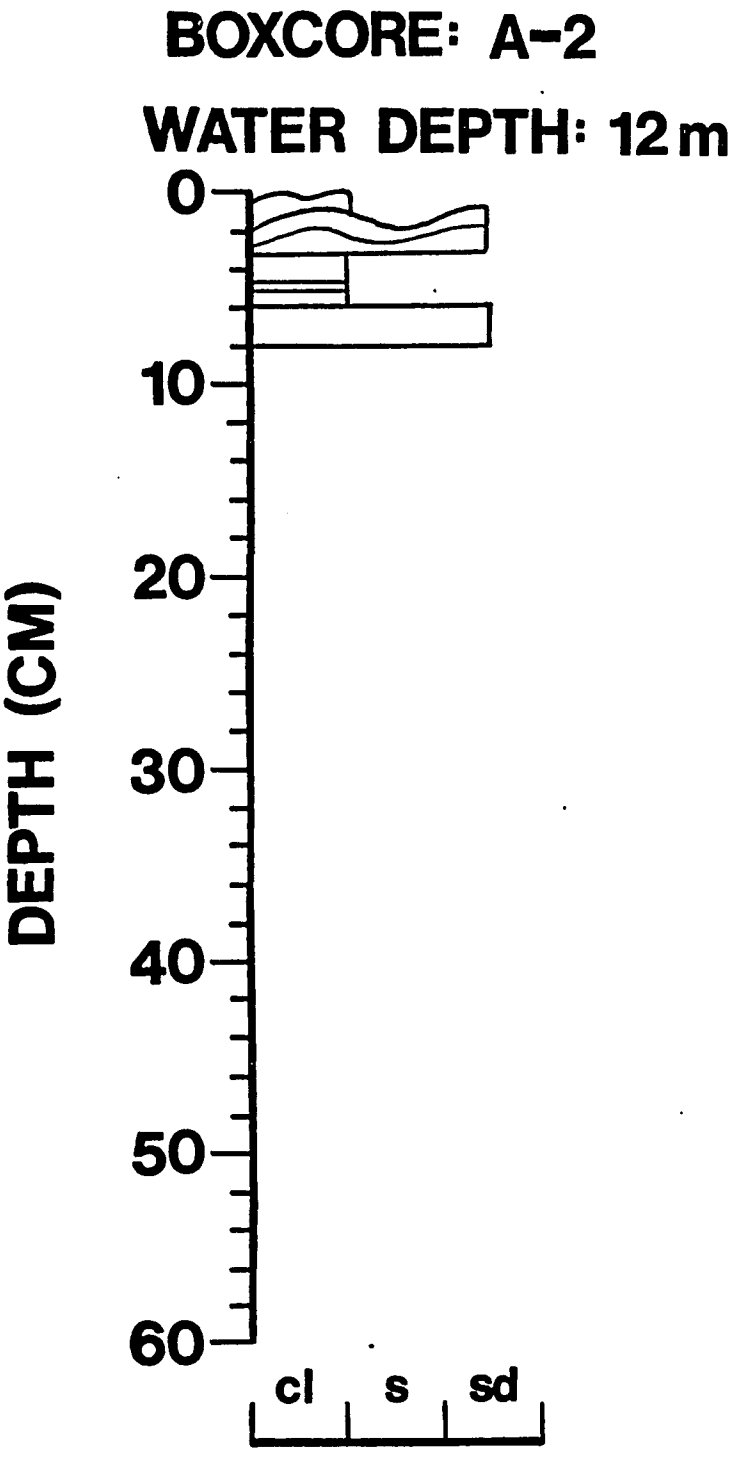
BOXCORE: A-2
WATER DEPTH: 12 m
DEPTH (CM)
0
10
20
30
40
50
60
cl
s
sd

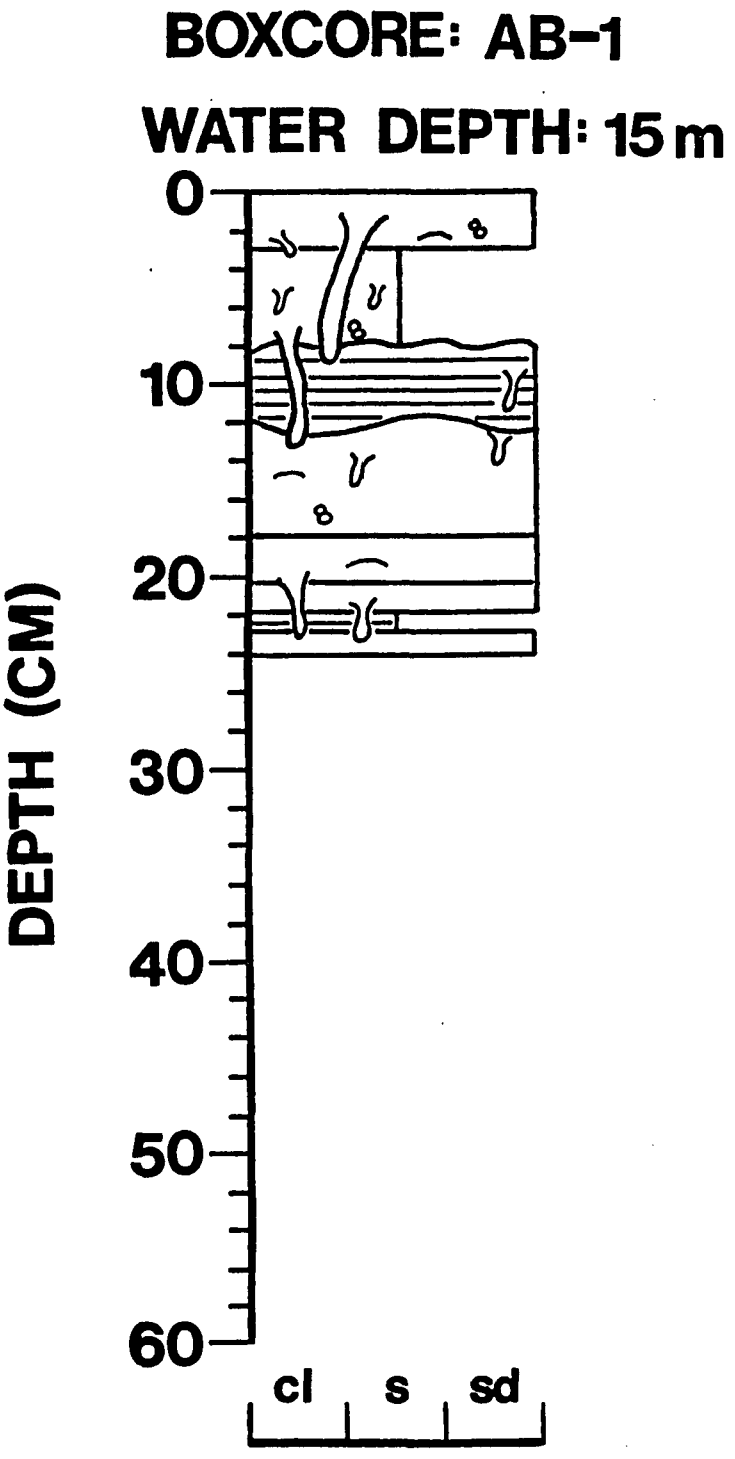
BOXCORE: AB-1
WATER DEPTH: 15 m
DEPTH (CM)
0
10
20
30
40
50
60
cl
s
sd

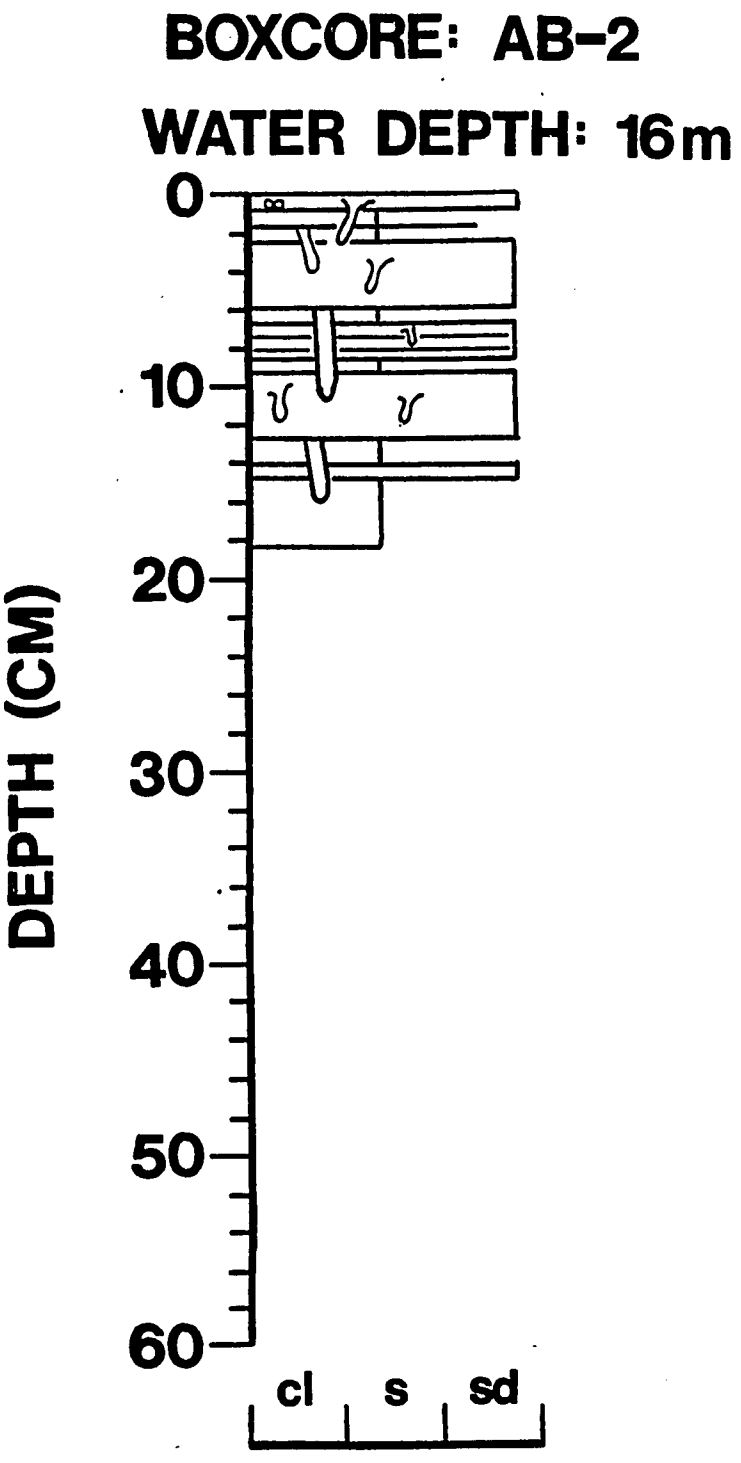
BOXCORE: AB-2
WATER DEPTH: 16m
DEPTH (CM)
0
10
20
30
40
50
60
cl
s
sd

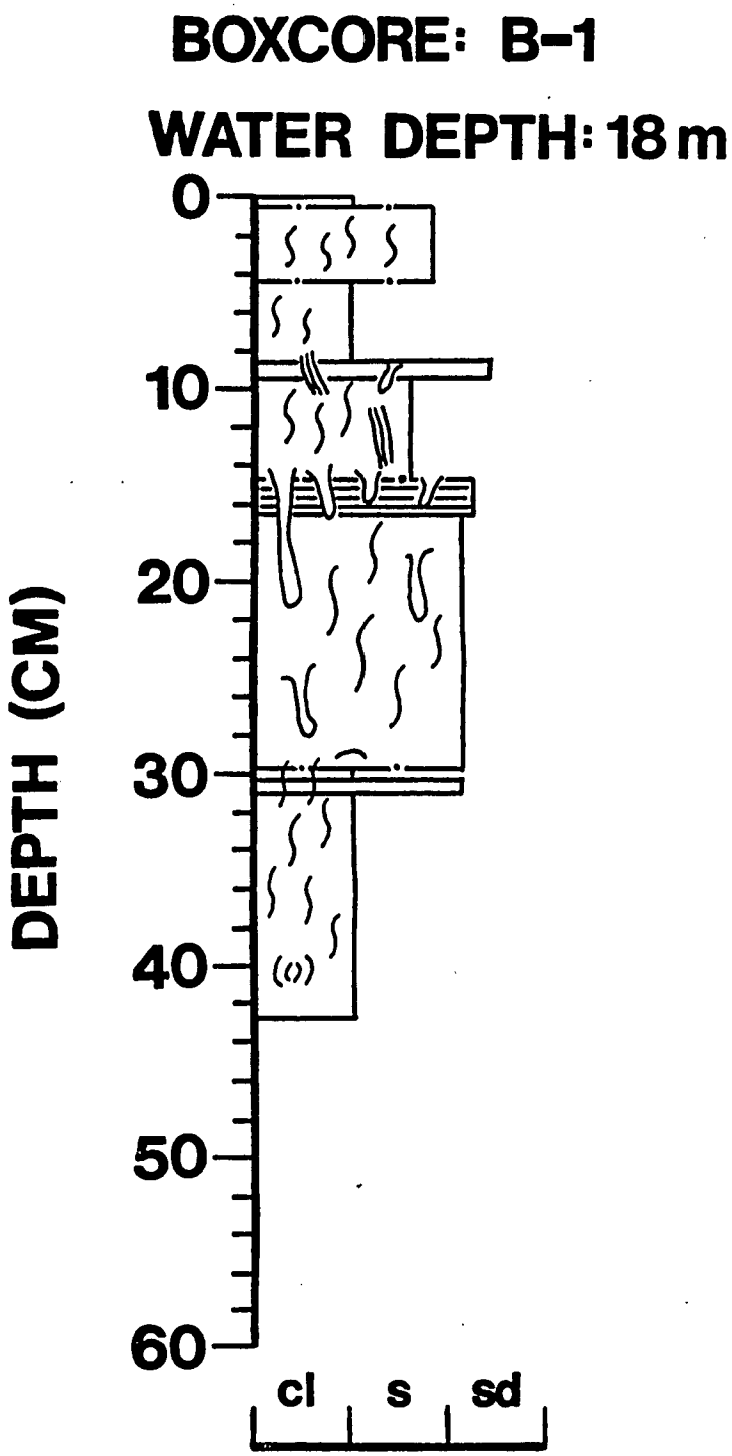
BOXCORE: B-1
WATER DEPTH: 18 m
DEPTH (CM)
0
10
20
30
40
50
60
cl
s
sd

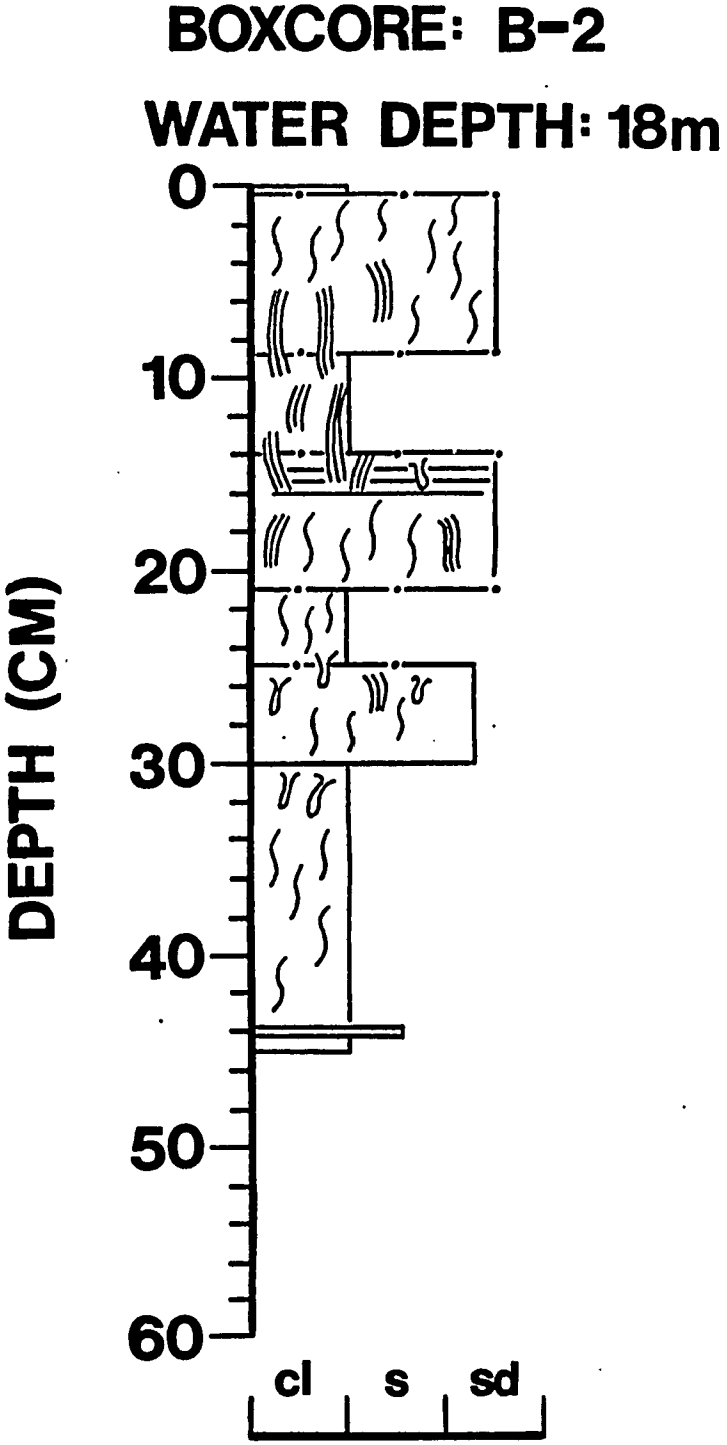
BOXCORE: B-2
WATER DEPTH: 18m
DEPTH (CM)
0
10
20
30
40
50
60
cl
s
sd

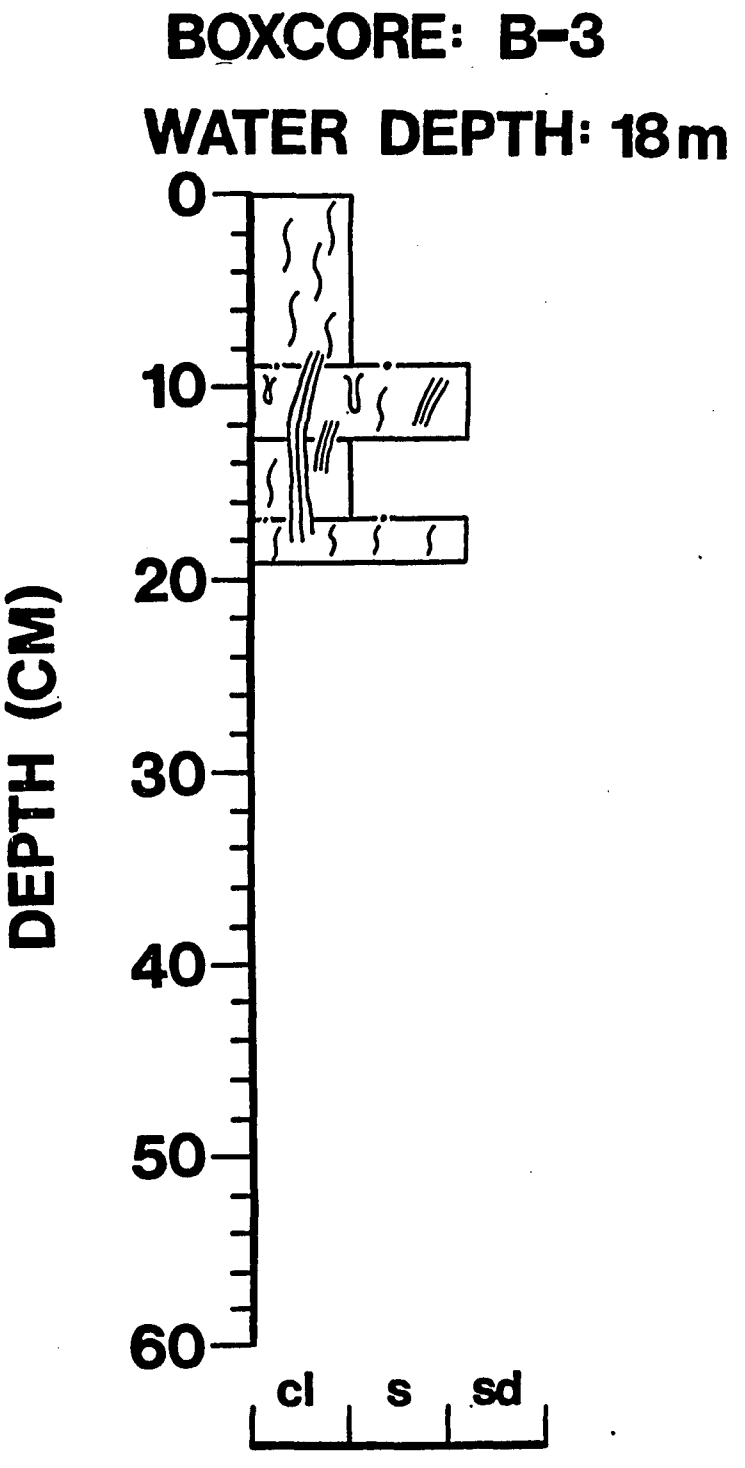
BOXCORE: B-3
WATER DEPTH: 18m
DEPTH (CM)
0
10
20
30
40
50
60
cl
s
sd

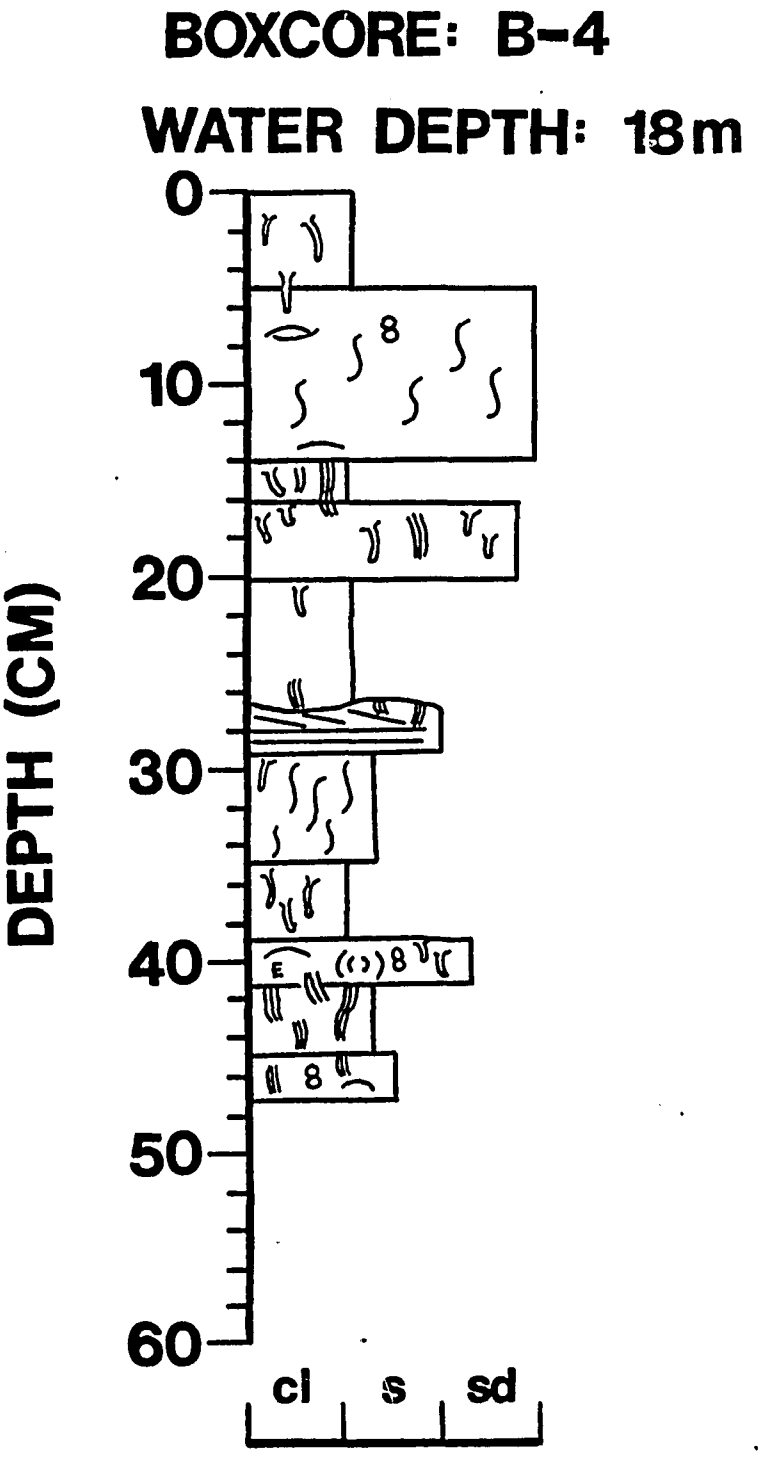
BOXCORE: B-4
WATER DEPTH: 18m
DEPTH (CM)
0
10
20
30
40
50
60
cl
s
sd

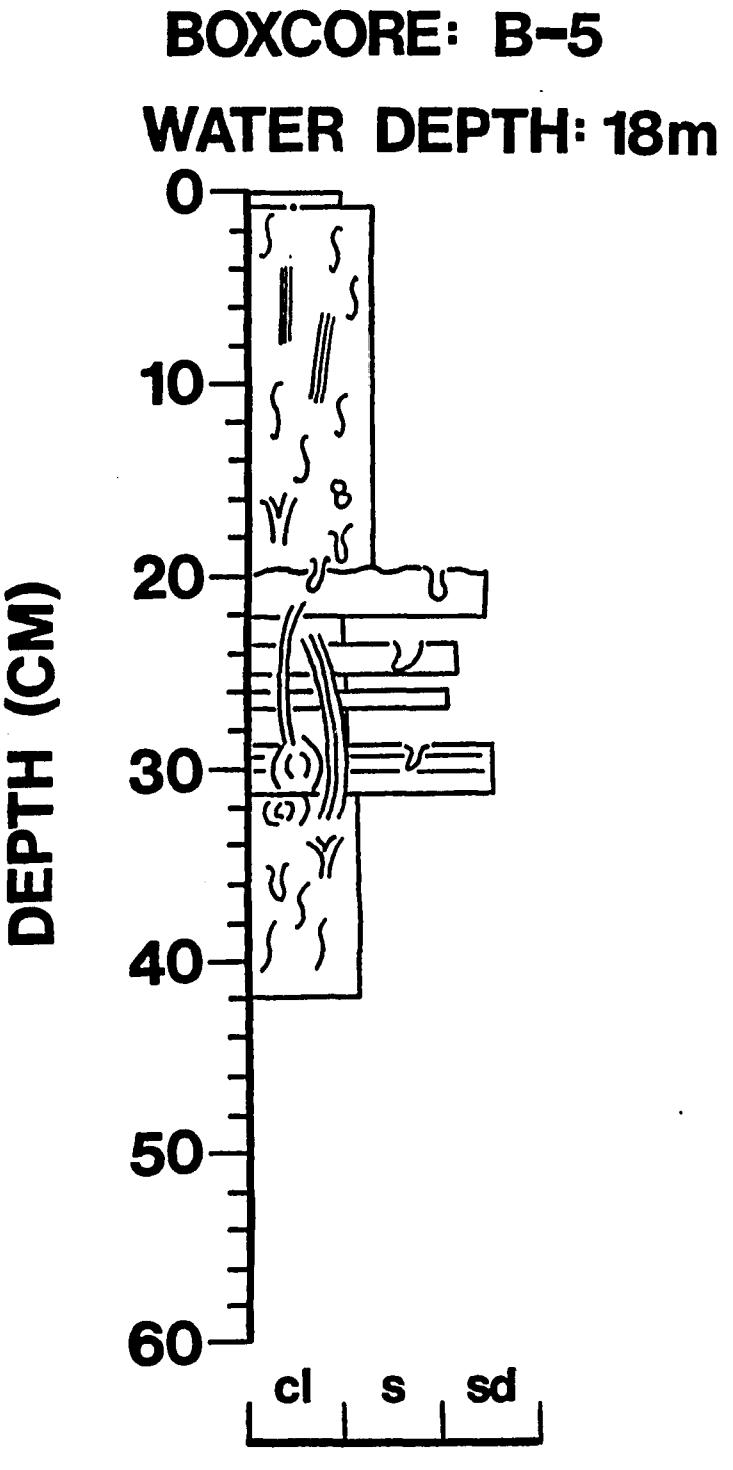
BOXCORE: B-5
WATER DEPTH: 18m
DEPTH (CM)
0
10
20
30
40
50
60
cl
s
sd

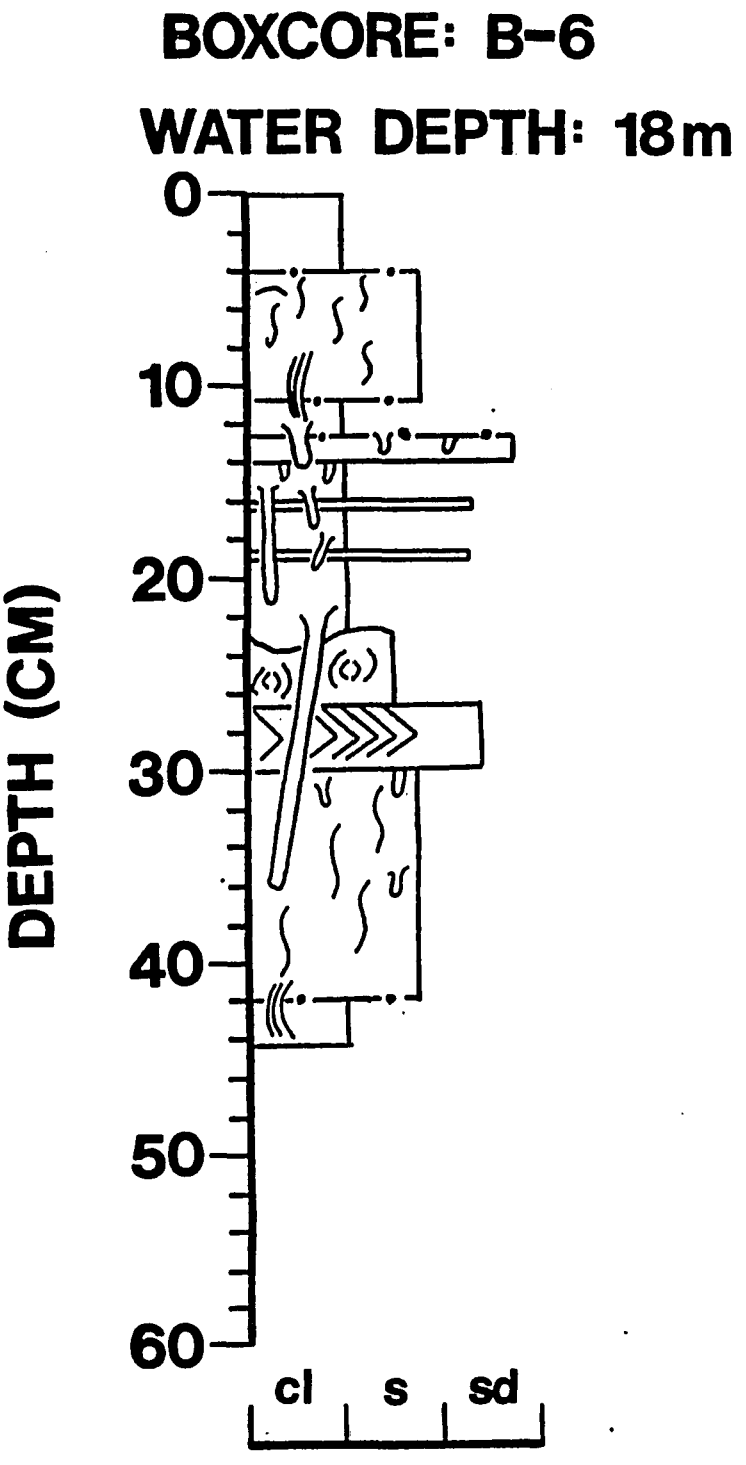
BOXCORE: B-6
WATER DEPTH: 18m
DEPTH (CM)
0
10
20
30
40
50
60
cl
s
sd

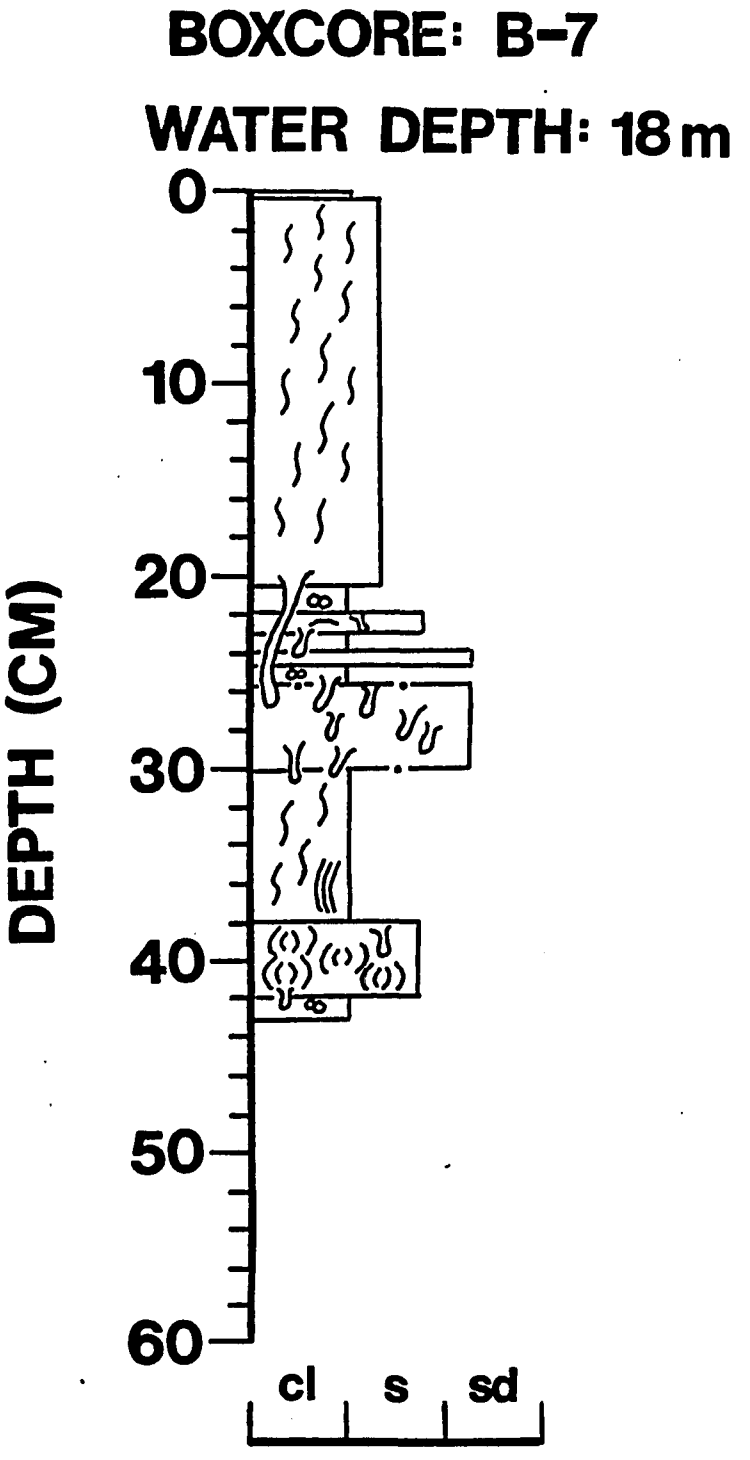
BOXCORE: B-7
WATER DEPTH: 18 m
DEPTH (CM)
0
10
20
30
40
50
60
cl
s
sd

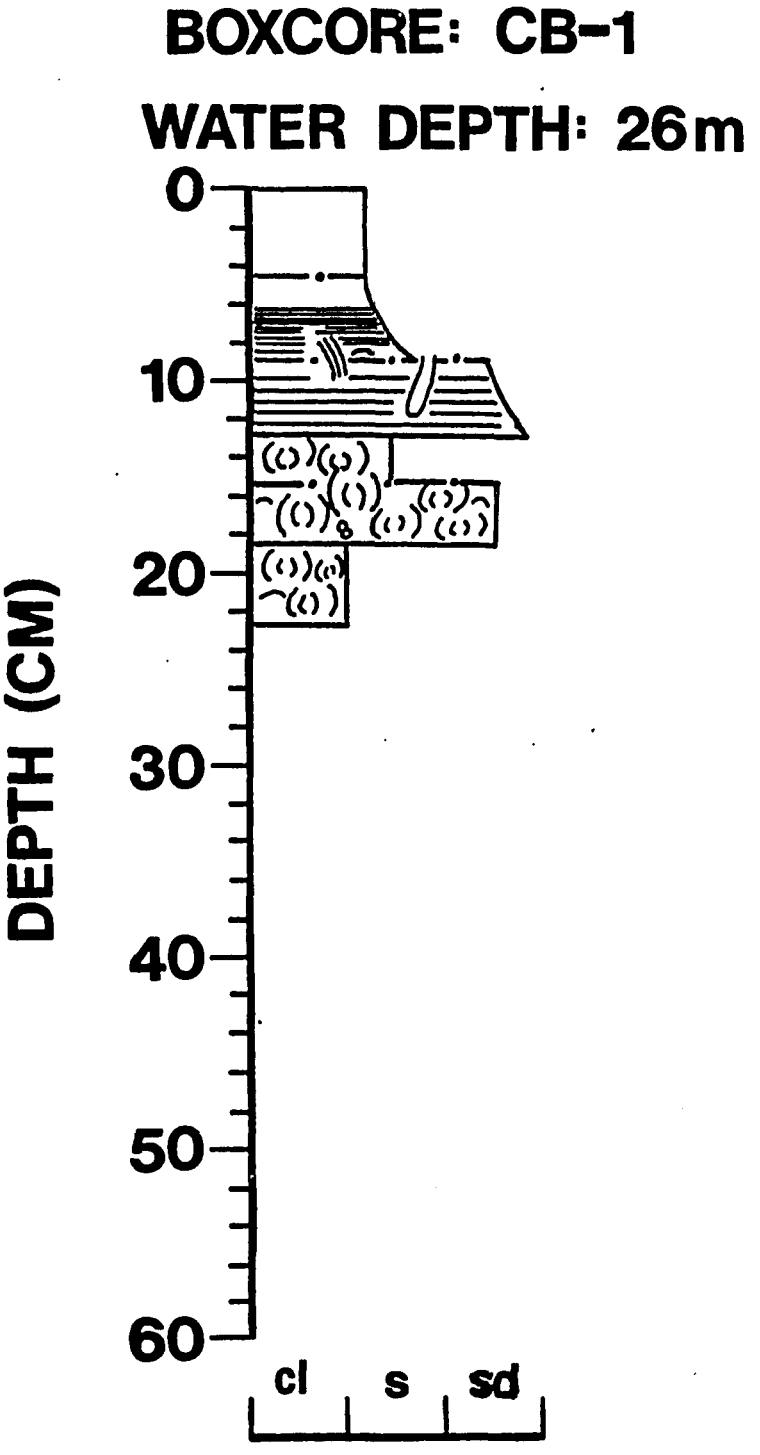
BOXCORE: CB-1
WATER DEPTH: 26m
DEPTH (CM)
0
10
20
30
40
50
60
cl
s
sd

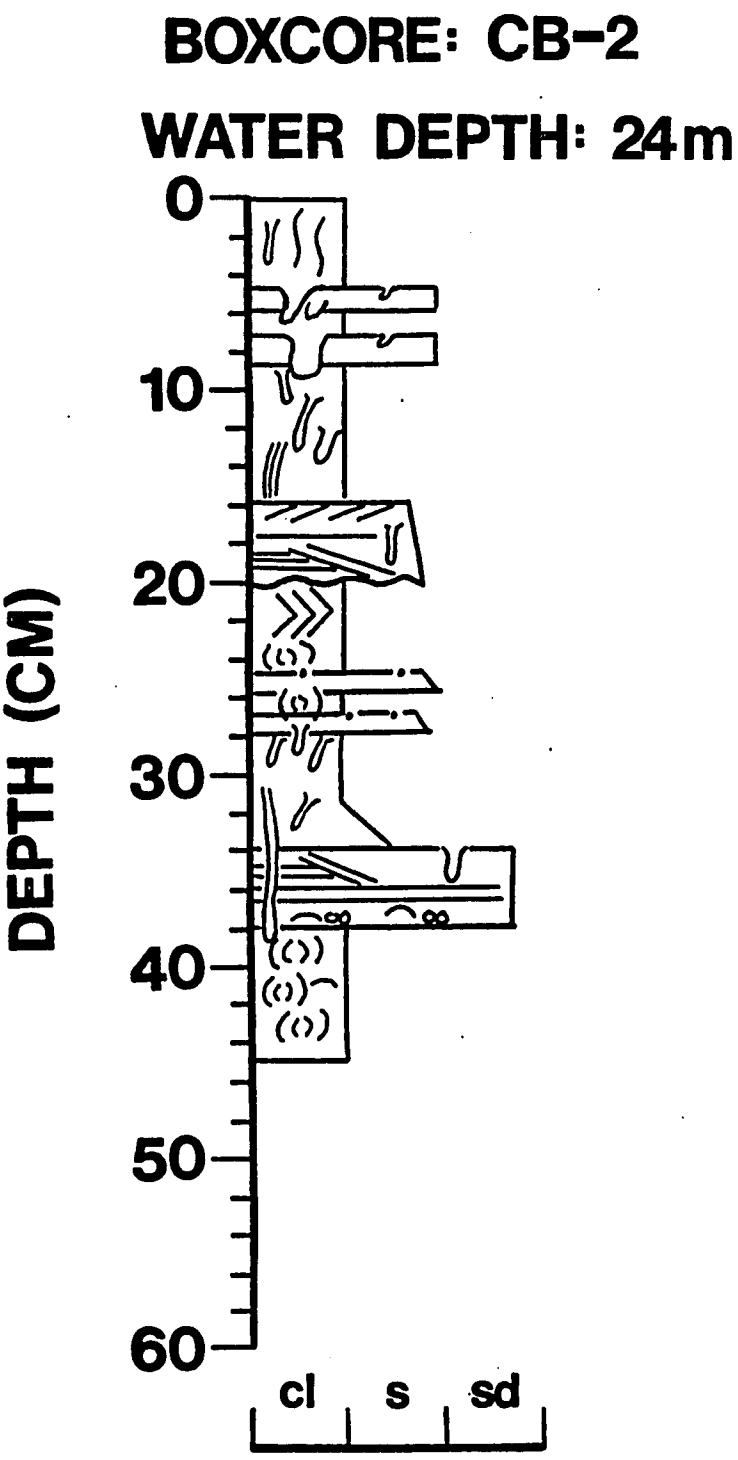
BOXCORE: CB-2
WATER DEPTH: 24m
DEPTH (CM)
0
10
20
30
40
50
60
cl
s
sd

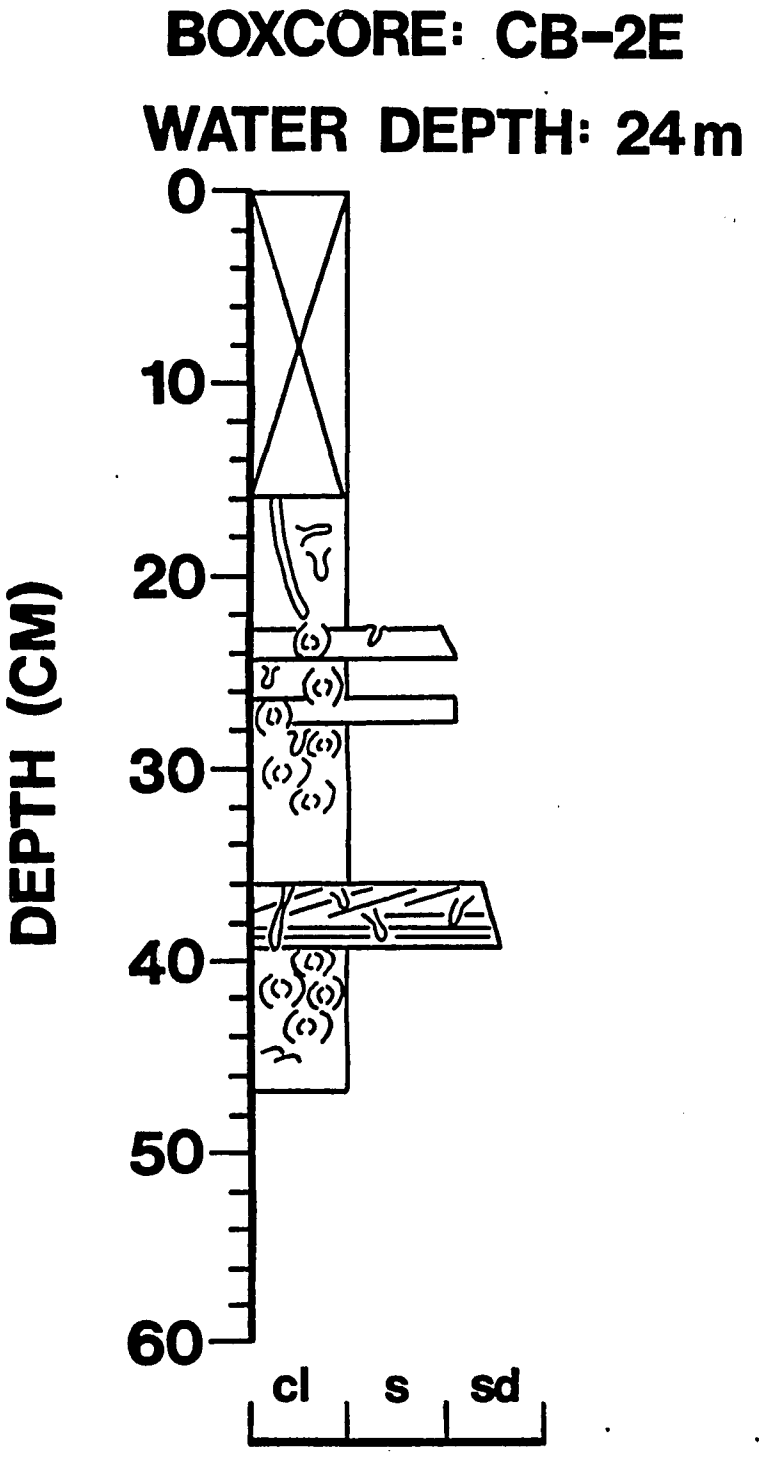
BOXCORE: CB-2E
WATER DEPTH: 24m
DEPTH (CM)
0
10
20
30
40
50
60
cl
s
sd

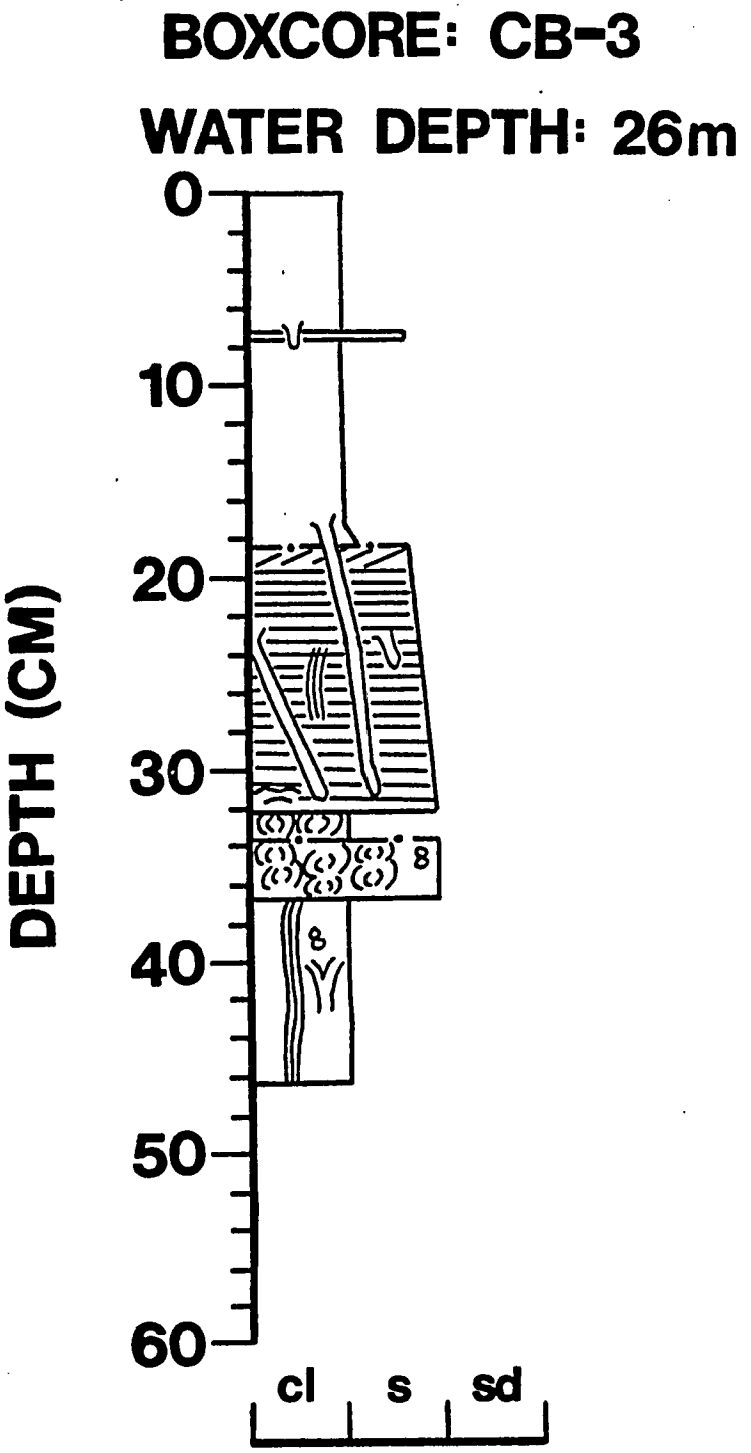
BOXCORE: CB-3
WATER DEPTH: 26m
DEPTH (CM)
0
10
20
30
40
50
60
cl
s
sd
8
8

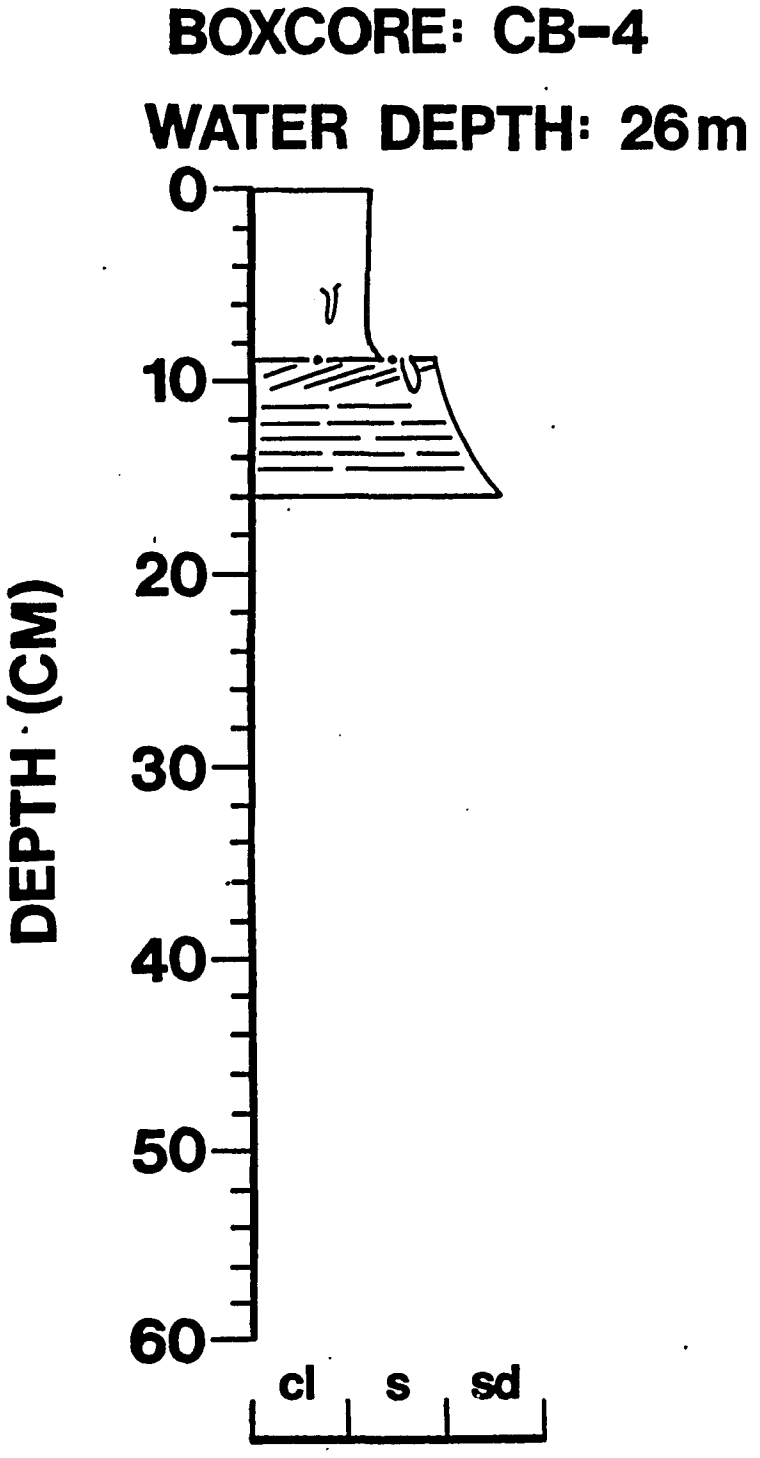
BOXCORE: CB-4
WATER DEPTH: 26m
DEPTH (CM)
0
10
20
30
40
50
60
cl
s
sd

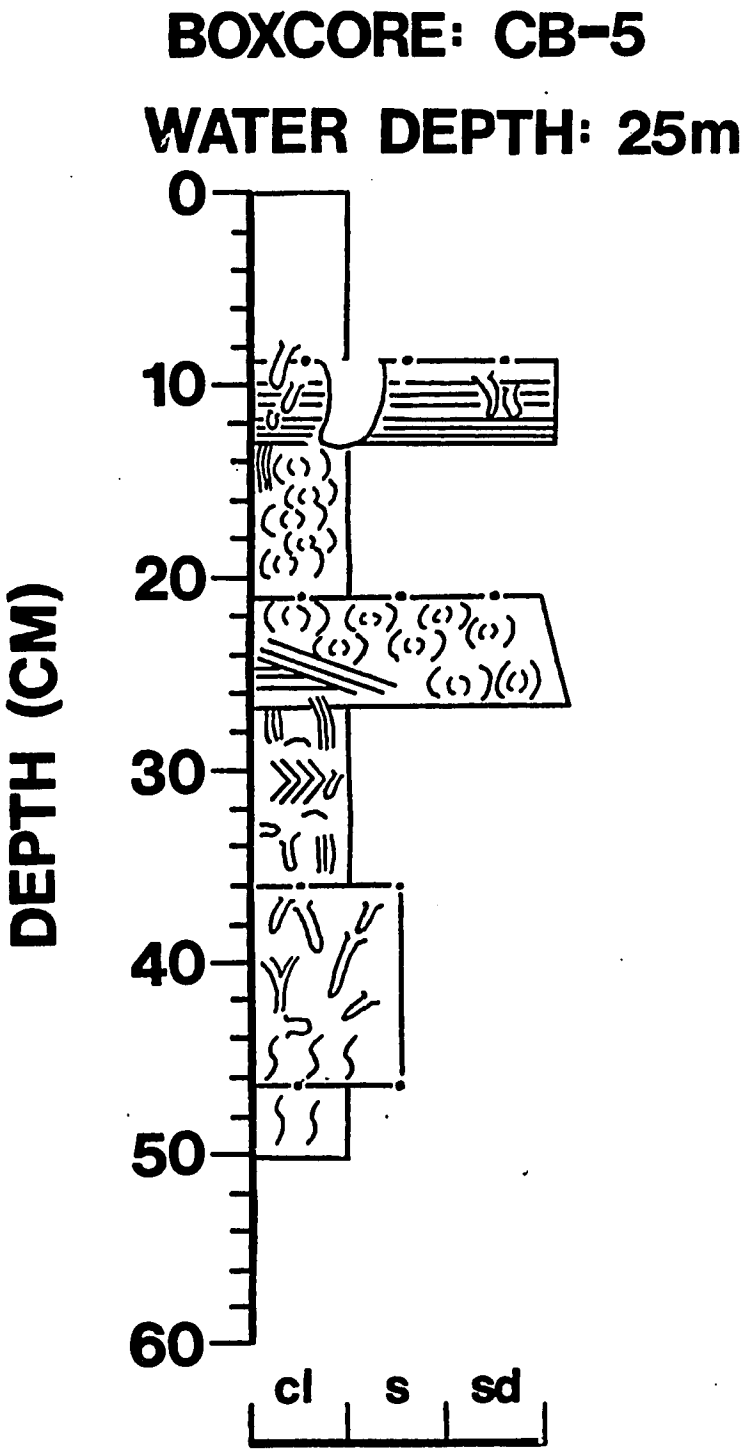
BOXCORE: CB-5
WATER DEPTH: 25m
DEPTH (CM)
0
10
20
30
40
50
60
cl
s
sd

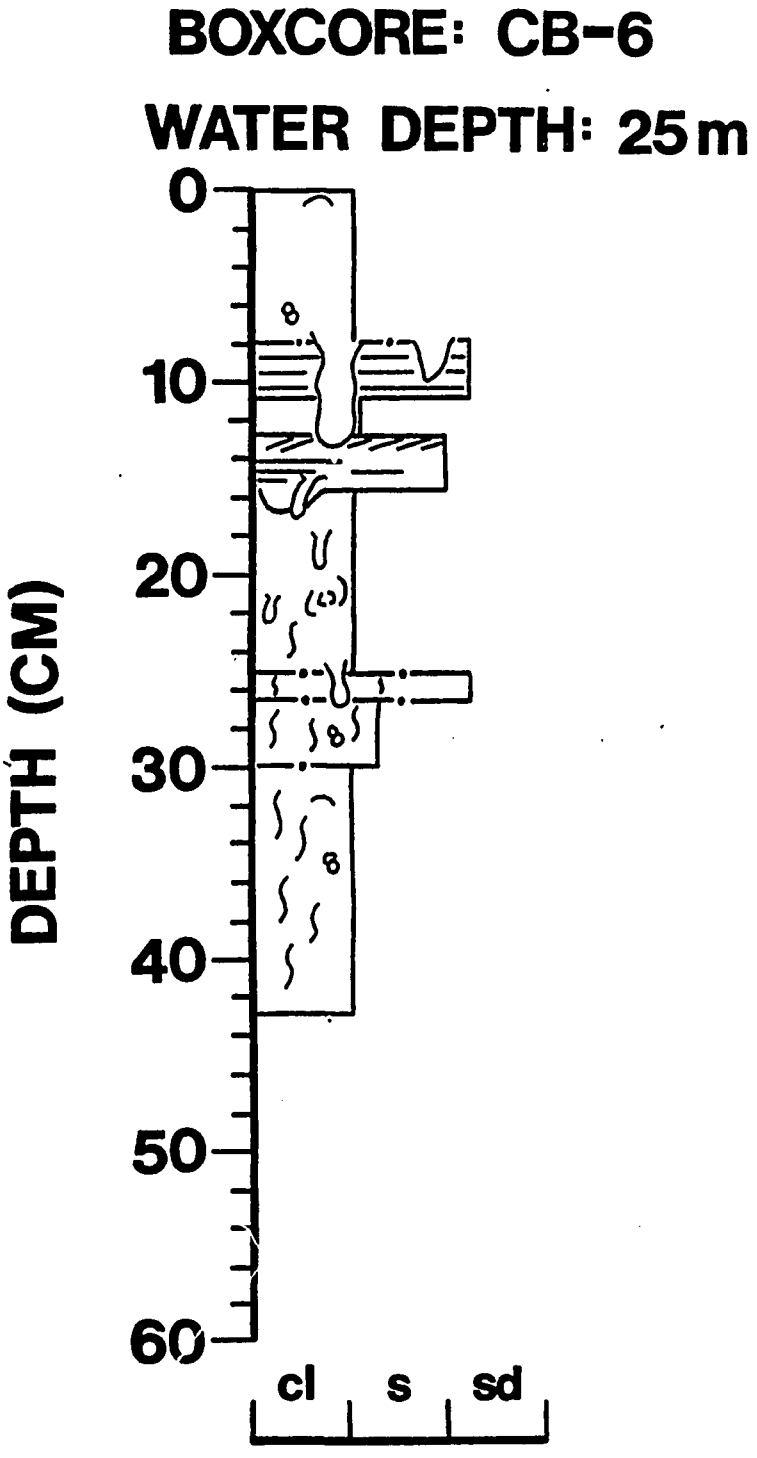
BOXCORE: CB-6
WATER DEPTH: 25m
DEPTH (CM)
0
10
20
30
40
50
60
cl
s
sd

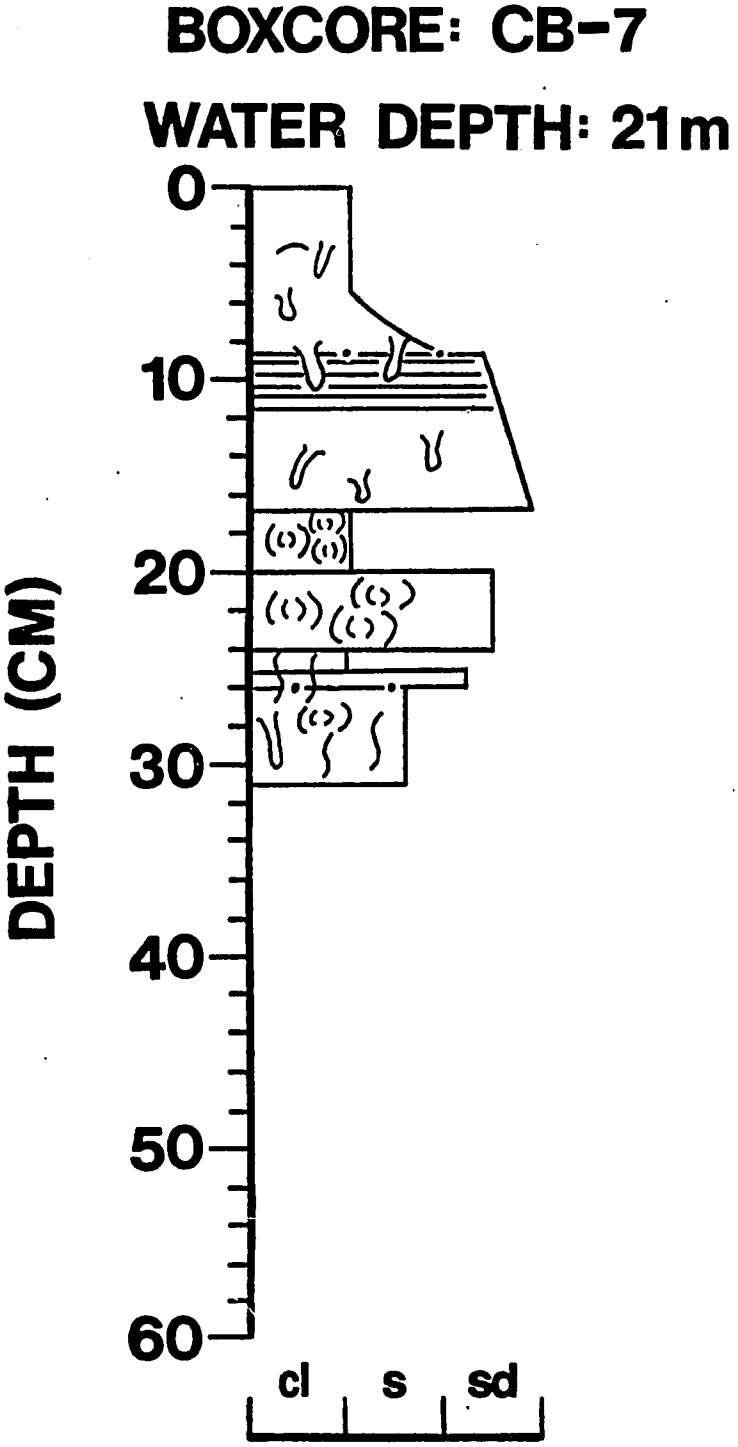
BOXCORE: CB-7
WATER DEPTH: 21m
DEPTH (CM)
0
10
20
30
40
50
60
cl
s
sd

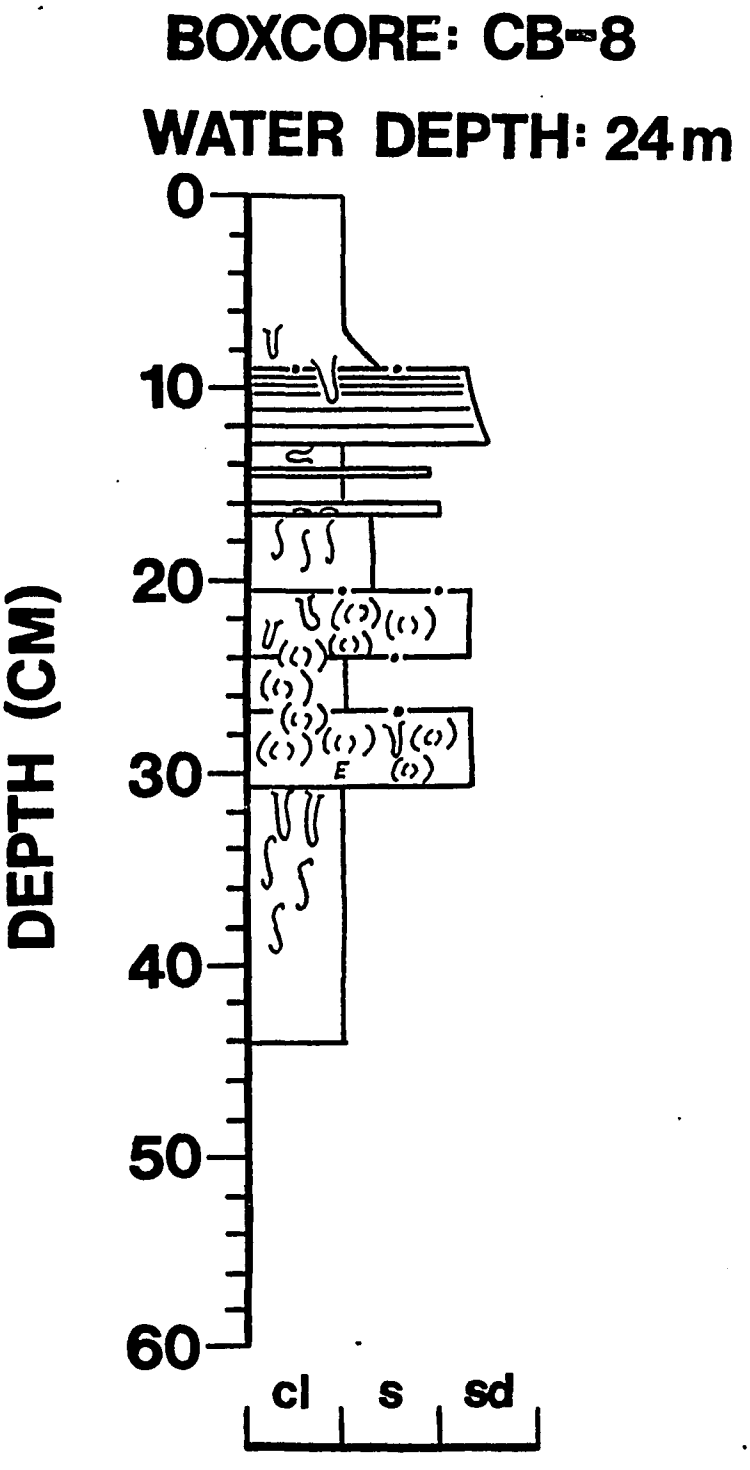
BOXCORE: CB-8
WATER DEPTH: 24m
DEPTH (CM)
0
10
20
30
40
50
60
E
cl
s
sd

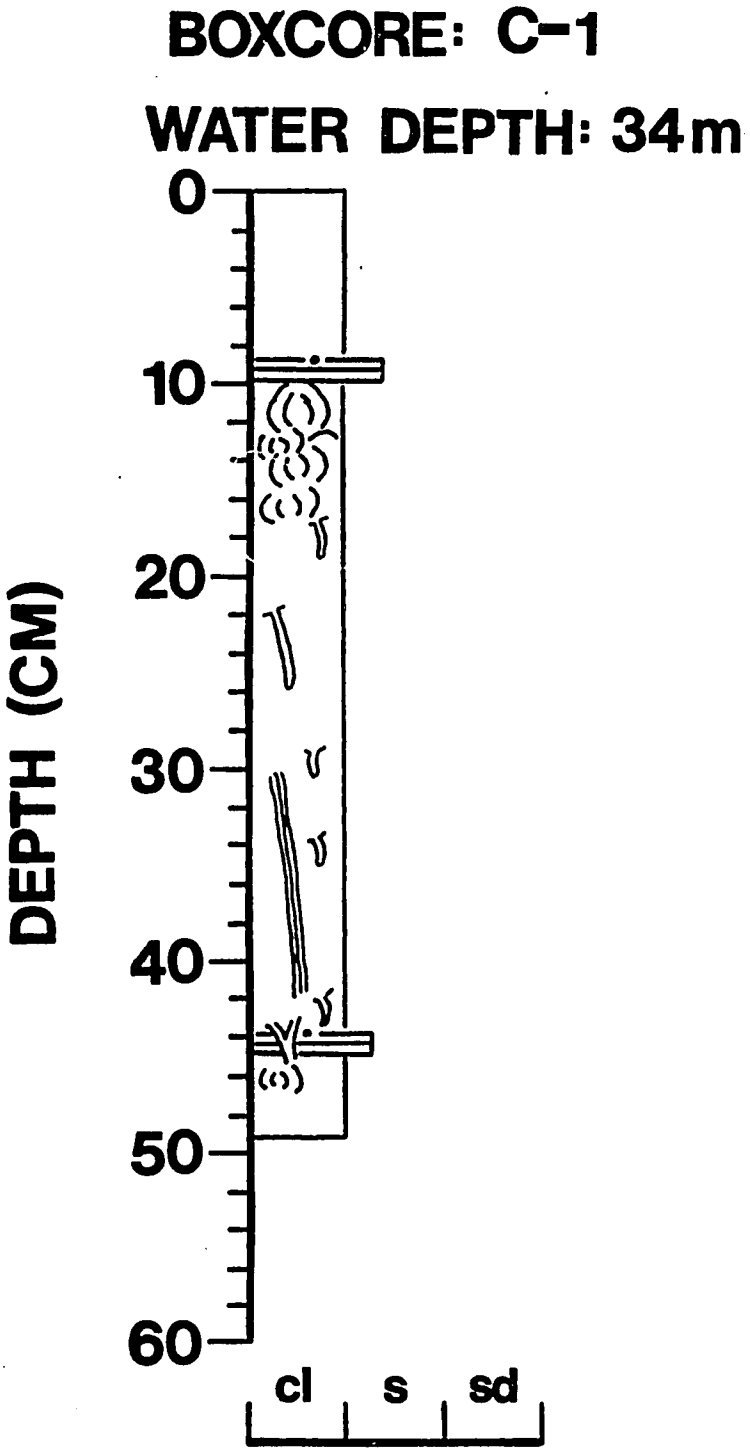
BOXCORE: C-1
WATER DEPTH: 34m
DEPTH (CM)
0
10
20
30
40
50
60
cl
s
sd

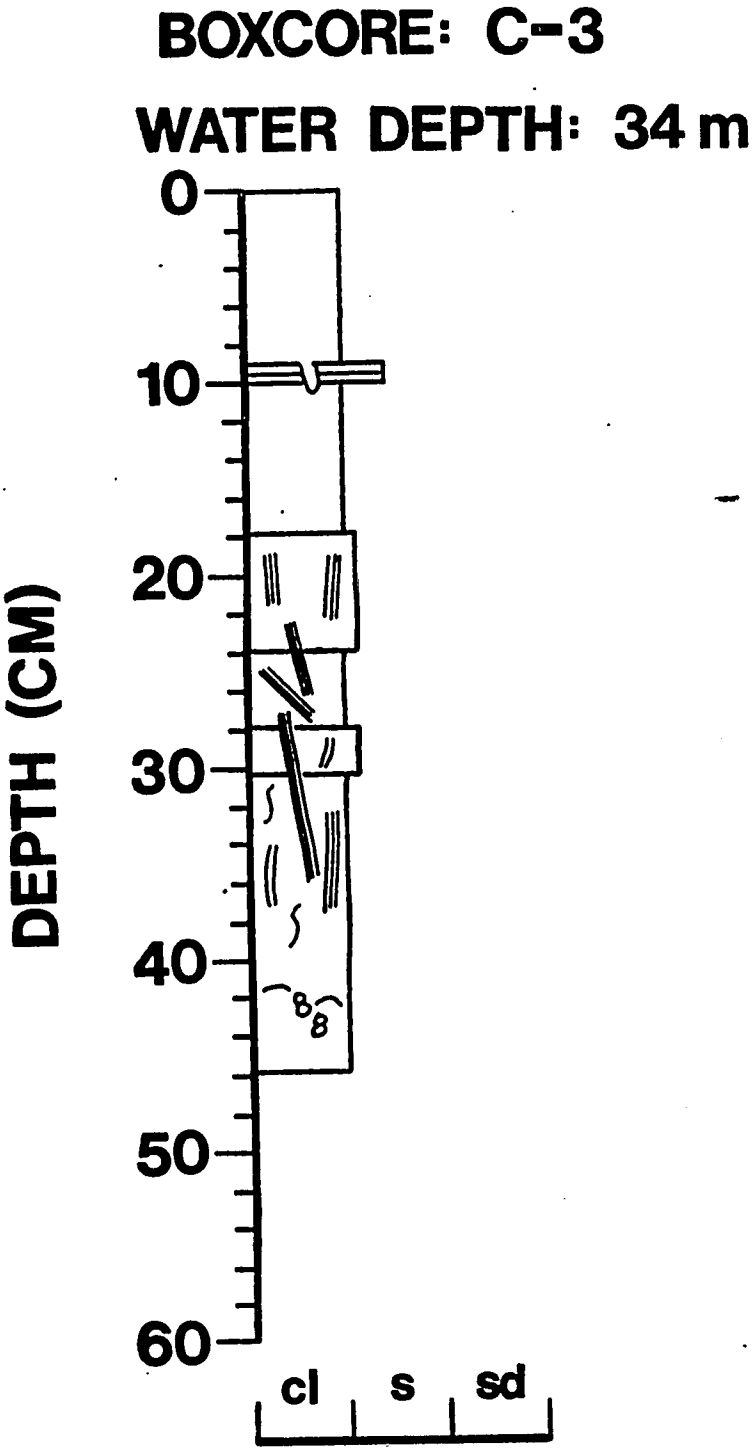
BOXCORE: C-3
WATER DEPTH: 34 m
DEPTH (CM)
0
10
20
30
40
50
60
cl
s
sd

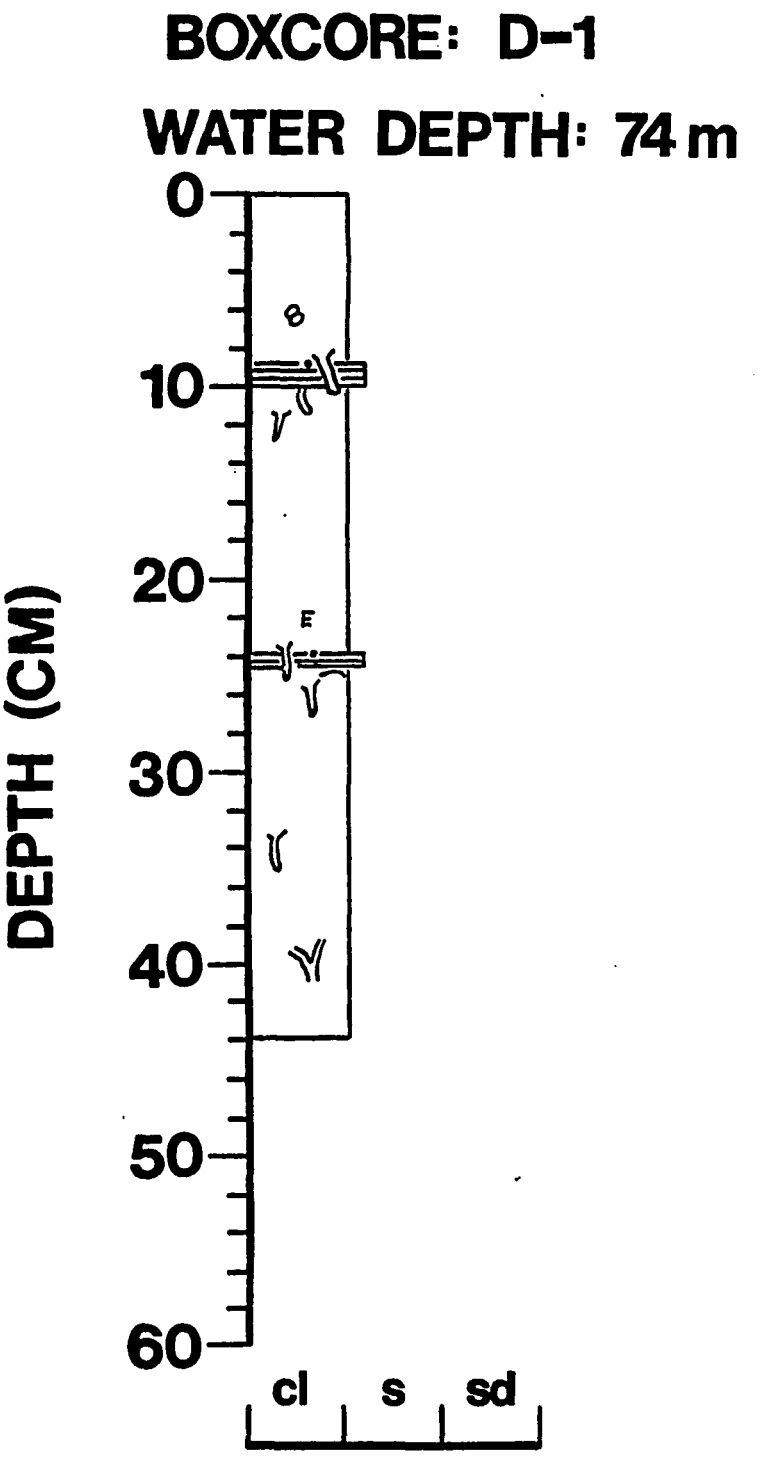
BOXCORE: D-1
WATER DEPTH: 74 m
DEPTH (CM)
0
10
20
30
40
50
60
B
E
cl
s
sd

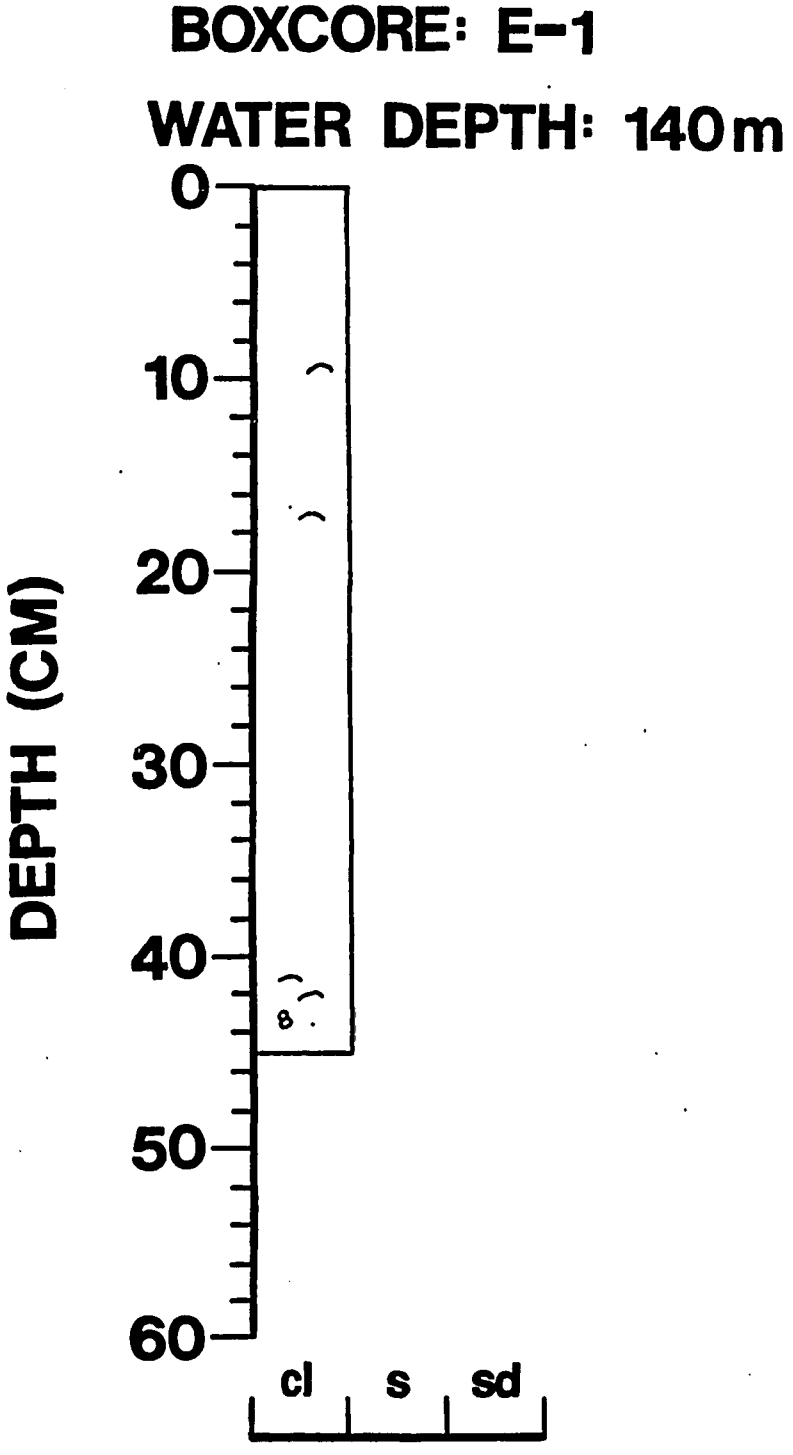
BOXCORE: E-1
WATER DEPTH: 140m
DEPTH (CM)
0
10
20
30
40
50
60
cl
s
sd

APPENDIX B

CALCULATION OF BOUNDARY SHEAR STRESS DUE TO WAVE-CURRENT INTERACTION AND DEEP WATER WAVE DATA ADJUSTMENT

The program used in this study to determine the total boundary shear stress is based upon Grant and Madsen (1979). The input data was near-bottom current measurements from the ENDECO meters and wave period and height from NODC Buoy 42002 (Fig. 45). Shear stress due to currents, waves and then the wave-current interaction were calculated in successive fashion. Shear stress due to currents was calculated from the quadratic stress law (cf Adams et al., 1982). Shear stress due to waves was derived from a equation given by Madsen (1976):

$$\tau_\omega = 1/2\ F_w \rho (U_m)^2$$

where τ_ω is the wave-generated shear stress, F_w is the wave friction factor (here 0.005), ρ is the fluid density (here 1.027 g/cm^3), and U_m is the bottom orbital velocity. The wave friction factor is derived from the graphs of Hsaio and Shemdin (1978). The procedure advanced by Madsen (1976) uses Airy (linear) theory for the derivation of the bottom orbital velocity. Linear wave theory assumes the waves to be sinusoidal, small in amplitude, and the bottom motion to be irrotational. It is valid for deep water wave calculations and has often been used in the calculation of boundary shear stress (Komar, 1976).

However, the location of NODC Buoy 42002 some 400 km southeast of the study site necessitated modifications of the measured wave parameters. It is well-known that waves undergo a marked transformation as they pass into shallow water (Kinsman, 1965). The wave phase velocity and length decrease, and there is often appreciable energy transfer due

to shoaling. These changes begin at a depth equal to one-half the wave length and become significant at one-quarter of the deepwater wave length. At a depth equal to 1/20th of the wavelength, Airy wave theory is no longer valid.

Shemdin et al, (1980) describe the mechanisms of energy transfer in finite-depth water waves. These include bottom percolation, wave refraction, wave-wave interaction, shoaling, bottom friction, and bottom dissipation. Each is discussed in order of increasing significance in the CTCS area:

1. Bottom Percolation--This was assumed to be negligible due to the low permeability of the muddy shelf sediments in the CTCS area.

2. Wave Refraction-- Winds in the CTCS area are dominantly from the southeast (Hill and Garrison, 1978). This includes hurricane-generated waves (eg. Nummedal, 1982). Waves associated with cold fronts can originate from the northeast, but the small fetch limits their size. Study of wave data from the fall of 1981 indicates that northwesterly winds can produce steeper waves but they do not significantly change the direction of wave motion (Snedden, Amos, and Nummedal, 1985). Waves generated by southeasterly winds encounter the shelf with angles of less than 12 degrees between the wave crest and the bathymetric contours. In addition, in the CTCS area, there are no large submarine topographic features to cause sudden changes in the amount of wave refraction. For these reasons, wave refraction was assumed to be negligible.

3. Wave-Wave Interaction--According to Shemdin et al., (1980), this phenomenon is only important in very shallow water depths where linear wave theory is invalid.

4. Shoaling--Changes in wave height and length occur as wave shoaling progresses. In intermediate depth waters there is a small decrease in wave height and an increase in shallower water. Komar (1976) recommends the use of Eckart's (1952) approximation:

$$L = L_o \, (\tanh \, ((2\pi h)/(L_o)))^{1/2}$$

where L equals the calculated wavelength, L_o is the deep water wave length, and h is the water depth. For changes in the wave height, the following relationships are recommended:

$$H/H_o = 1/2n((C_o/C))^{1/2}$$

and,

$$C = C_o(\tanh((2\pi h)/(L_o)))^{1/2}$$

where H and C are the wave heights and phase velocities, H_o and C_o are the deep water wave heights and phase velocities (Komar, 1976). Wave period does not change. The values generated by these equations were only used in water depths where the above expressions are applicable, as suggested by Weigel (1964).

5. Bottom Friction--Bottom frictional dissipation is the result of the work done by the wave orbital velocity against the sea bottom boundary It appears to be of less importance than energy dissipation on muddy bottoms except in very sandy substrates where roughness elements, such

as ripples, are present (Hsaio and Shemdin, 1978). This was accounted for in the wave friction factor term used here (0.005) which is used for muddy substrates, such as the CTCS.

6. Bottom Dissipation--Work by Tubman and Suhayda (1976) and Hsaio and Shemdin (1978) has shown that wave energy dissipation on muddy shelf bottoms is quite significant. Reduction in wave height is the primary consequence. The amount of reduction appears to increase with increasing wave heights (Forristall and Reece, 1985). Suhayda (1977) found a 46 % wave height decrease in the East Bay of the Mississippi delta from 19 to 5 m depths. Bea (1974) noted an 85 % attentuation in Hurricane Camille's waves as they passed into 12 m of water. However, the reductions recorded at the Mississippi delta probably exceed the attentuation actually occurring on the muddy CTCS. An empirical equation was adopted that compensated for this difference but took into account the relationship between wave height and the amount of attentuation observed by Forristall and Reece (1985).

As a further check on the validity of the output, ratios of significant wave parameters were generated to ensure that the waves dimensions were not unrealistic. These included the ratio of the depth to the deep water wave length, the shallow wave height to the depth, the shallow waveheight to the length and the depth to the shallow wavelength (after Komar, 1974). Generally, unrealistic wave dimensions only occurred in very shallow water (as defined by the wavelength/depth ratio) where Airy wave theory is not applicable.

Testing Against Real Conditions

In order to test the results of this program against actual condi-

tions, plots of wave generated boundary shear stress versus water depth were generated for several wave "cases" (Fig. 64). In doing so, an effort was made to derive the input wave periods and heights from actual experience or published statistics from the Gulf of Mexico. It was also decided to define wave parameters that characterize a storm, not simply the maximum or extreme. For this reason, the significant wave height and period (the average of the one third highest or longest waves) were chosen as input values.

Case A represents "fairweather conditions" as evidenced by wave statistics recorded during inter-storm periods in the 1984 data set and another data set from the NODC Buoy during fall of 1981 (Snedden, Amos, and Nummedal, 1985). A significant wave period of 6.0 seconds and a significant wave height of 0.5 meters appear to be characteristic of of year-round conditions. In the summer in the CTCS area, wave periods drop as low as 4-5 seconds and heights decrease to 0.25 m, calm seas. These values rise somewhat in the winter months (inter-frontal periods) to 6 seconds and 0.75 m respectively. The values chosen are known to be typical of more than 75 % of the year according to the Environmental Guide to the U. S. Gulf Coast.

Values of 9 seconds and 2.1 m were chosen as Case B. This was based upon analysis of the severest conditions recorded during the 1984 and 1981 data sets (Snedden, Amos, and Nummedal, 1985). This case is probably representative of the strongest storm that may be present during a given year. Wave height to length ratios reach 0.017 in contrast to the smaller amplitude fairweather waves whose ratio is more like 0.011.

Case C comes from data recorded by NODC Buoy 42002 during the pas-

sage of Hurricane Allen in 1980. Values of 11 seconds and 7.0 meters approximate what Jahns and Wheeler (1973) defined as the maximum significant wave height for a storm occurring once a decade. The values are also similar to estimates for Hurricane Hilda (1972). The wave height/length ratio is 0.037: the wave still can be considered to be of small amplitude.

The values of 14.0 seconds and 12.0 m for significant wave period and height are based upon actual recorded data for Hurricane Carla in 1961. Wave staffs in Louisiana waters during Hurricane Carla recorded typical wave heights of 6.1 to 9.1 m and wave periods of 8-12 seconds (Thrasher and Aagaard, 1970). However, these were recorded some 320 km from the actual point of landfall. Hindcast estimates, based upon wind speeds measured in the northeast quadrant of the storm, suggest higher values of 14-15 seconds and 14-15 m (Patterson, 1972). It was felt that while the hindcast wave periods were reasonable for the CTCS area (which was on the left side of the track), wave heights of 12 m were more appropriate than those hindcast. Wave dispersion allows long period waves to be experienced over a large distance, while wave height is much more dependent on the local wind field (Komar, 1976). No data exists in the U. S. Environmental Guide on the frequency of the chosen parameters in the CTCS area as the largest wave mentioned is 8 m in height. The wave height to length ratio of 0.039 is still below the theoretical steepness limit of 0.142 for deep water waves (Komar, 1977).

Superimposed upon the diagram (Fig. 64) is the threshold of sediment motion for 68 micron sand, the modal peak of the sand-size frequency distributions (Fig. 22). There are larger sand sizes available as one

moves landward on the shelf, but the difference is relatively minor. The intersection of the wave shear stress line and the threshold is the furthest seaward that a particular case's waves are capable of resuspending sand. This is analogous to what Drake et al., (1985) call the "wave threshold depth"--the maximum depth at which wave resuspension occurs.

Fig. 64 suggests that during fairweather conditions (Case A), resuspension of sand of this size (and virtually any size which may be present on this shelf) only occurs on the shoreface (<10 m depth). In Case B, the wave threshold depth expands to 24 m depths. The once-in-a-decade storm (Hurricane Allen) has a wave threshold depth of 69 m. In Case D, it appears that a storm the size of Hurricane Carla (1961) is capable of causing resuspension as far out as 115 m depth, nearly the entire width of the shelf.

The results of Case A, that fairweather waves feel bottom only on the shoreface, appears to fit with known conditions (Niedoroda and Swift, 1981). Verification of the other cases is more difficult but appears to fit with the sedimentological evidence of sand resuspension and transport as discussed in the second chapter.

Combined Wave-Current Interaction

Grant and Madsen (1979) defined the relationship between the instantaneous boundary shear stress τ_{wc}, and the combined wave and current velocity field as:

$$\tau_{wc} = 1/2\ \rho F_{wc}(u^2 + v^2)(u/(u^2+v^2)^{1/2}, v/u^2+v^2)^{1/2})$$

where ρ is the density of sea water (here 1.027 g/cm^3), F_{wc} is the

friction factor associated with the combined wave and current flow, and u and v are the x- and y-components, respectively of the horizontal wave-current velocity. By assuming a coordinate system in which wave propagation was always along the x-axis, Grant and Madsen (1979) further defined u and v as:

$$u = (\sin\Theta + (u_a/u_b)\cos\phi_c)(u_b)$$

and

$$v = (u_a/u_b)\sin\phi_c)(u_b)$$

where u_a is the magnitude of the steady current velocity vector at a height a above the bottom, ϕ_c is the angle between the direction of wave propagation and the steady current, u_b is the near-bottom orbital velocity (equivalent to U_m as discussed by Madsen, 1976), and Θ is the wave frequency factor, equivalent to $2\pi / T$ where T is the dominant wave period.

Several points should be noted with regard to the use of these equations. First, while the equations themselves are relatively straightforward, the derivation of values for the input parameters is quite complex. For example, Grant and Madsen (1979) demonstrated that the wave-current friction factor, F_{wc} is a function of a number of variables, including the ratio between the magnitude of the steady and oscillatory flow, the wave-current angle, and the ratio of K_b, a dimension related to the physical bottom roughness, and A_b, the maximum bottom excursion amplitude of the wave orbital. In keeping with the precedent set by Jonsson (1966), Grant and Madsen (1979) present this information in a diagram which allows interpolation between the wave-

current angle of 0^o and 90^o. In this study, a wave-friction factor of 0.005 was used, similar to that employed for the wave equation. This value is characteristic of smooth turbulent boundary conditions (Jonsson, 1966).

Secondly, Grant and Madsen (1979) indicate that the value of u_a is not directly equivalent to measurements of the steady current at a depth of 100 cm off bottom. Several iterative procedures are recommended to derive the proper value. In this study, the second method discussed by Grant and Madsen (1979) was employed, involving the dimensionless ratio u_{*c}/u_b.

Third, the wave data collected at NODC Buoy 42002 does not include measurements of wave direction, a necessary parameter to calculation of the wave-current angle, ϕ_c. As mentioned, the dominant wave direction (the azimuth of the wave orthogonal) throughout the year in the CTCS area is toward 315^o, paralleling the general southeasterly winds. Although winds shift during frontal passages, the most significant waves come out of the southeast in alignment with the largest fetch of the Gulf and Caribbean. For these reasons, ϕ_c was taken as the angle between the steady current and 315^o. Larsen et al., (1981) have shown that the combined flow boundary shear stress is just weakly dependent upon the wave-current angle.

Lastly, one of the assumptions of Grant and Madsen (1979) is that the boundary shear stress due to the wave orbital motion must be within an order of magnitude of the current shear stress. In calculations for the deeper water locations, where this condition was not always met, the program output was strictly the current-generated shear stress.

VITA

John W. Snedden was born 16 November 1954 in Hammond, Indiana. In 1973 he received his high school diploma from Culver Military Academy (Culver, Indiana). He then entered Trinity University (San Antonio, Texas) and graduated magna cum laude with a B.A. in geology and psychology in 1977. He continued studies in geology at Texas A&M University (College Station, Texas) which led to a M.S. degree in 1979. From 1979 to 1983, he was employed by Mobil Producing Texas and New Mexico, Inc., (Houston, Texas) as an exploration/production geologist. In the Fall of 1983, he took educational leave from Mobil to pursue the Ph.d degree in geology at Louisiana State University (Baton Rouge, Louisiana). Following graduation, he will be employed by Mobil Exploration and Producing Service, Inc. (Dallas, Texas).

DOCTORAL EXAMINATION AND DISSERTATION REPORT

Candidate: John W. Snedden

Major Field: Geology

Title of Dissertation: Origin and Sedimentary Characteristics of Discrete Sand Beds in Modern Sediments of the Central Texas Continental Shelf

Approved:

Major Professor and Chairman

Dean of the Graduate School

EXAMINING COMMITTEE:

Date of Examination:

November 25, 1985